INVESTIGATION OF ENZYMES FOR THE DEPOLYMERIZATION OF NYLON

Alana Rangaswamy

A Thesis Submitted to the University of Ottawa in Partial Fulfillment
of the Requirements for the Degree of

Doctorate of Philosophy in Chemistry

Department of Chemistry and Biomolecular Sciences

Faculty of Science

University of Ottawa

Supervisor:	Jeffrey W. Keillor
Examining Board:	Christopher N. Boddy, PhD, Chemistry and Biomolecular Sciences Adam J. Shuhendler, PhD, Chemistry and Biomolecular Sciences François-Xavier Campbell-Valois, PhD, Chemistry and Biomolecular Sciences
External Examiner:	David L. Zechel, PhD, Chemistry, Queen's University

Abstract

Plastic waste is ubiquitous in modern society, and a problem that every person interfaces with daily. As well as mismanagement of plastic waste posing a threat to ecosystems, the loss of plastic material to the environment or landfill represents loss of a valuable resource for new materials and other products. While current recycling practices are limited and produce lower-quality materials, biocatalysis offers a promising route to recover the value of plastic waste through generation of new materials through a more environmentally-compatible process. However, while enzymes have been identified and optimized to degrade ester-based polymers efficiently, other types of polymers pose a greater challenge.

Nylon is a useful and ubiquitous plastic, and forms a large component of ocean plastic waste in the form of discarded fishing equipment. Nylon is not easily recycled through traditional means, and is therefore an attractive target for biocatalytic degradation. In this thesis, we explore enzymes with the potential to degrade nylon, *via* two distinct approaches. First, we investigate *Bacillus subtilis* transglutaminase (bTG), which belongs to a class of enzymes known to be able to form and break aliphatic amide bonds. We discover that the activity of bTG is highly substrate-selective, and does not demonstrate the desired amide hydrolysis activity for this project. Second, we explore a known class of nylon oligomer hydrolases (NylCs) and develop assays to improve the efficiency of engineering campaigns for this and related enzymes. Our first class of substrate analogues are soluble, chromogenic substrates that can rapidly detect acyltransfer activity in NylC enzymes. Our second class of substrates are insoluble linear amide analogues which more closely resemble nylon, which are readily hydrolyzed by NylCs. We demonstrate the applicability of our assays to high-throughput screens, while exploring the substrate scope and specificity of this class of enzyme.

Dedication

For the Rangaswamy's,

Who always wanted another doctor;

And for the McInnis's

Who know that a PhD is not quite as impressive

As a 29-hand

Thank you all, for everything.

Acknowledgements

Reader, buckle in; this is going to be long.

To begin, I would like to thank my incredible supervisor, Dr. Jeffrey Keillor. Even before I officially joined the lab, you went out of your way to support me in the completion of my Master's degree and transition to this PhD program (not to mention, in the middle of a global pandemic). You have been with me every step of the way, willing and able to solve almost every problem I've brought to you, be it academic, administrative (pro tip –CC Jeff if you need something to happen) or personal. It takes an unprecedented amount of talent to Excel (lol) at every aspect of a professor's job, between teaching, mentoring, and coming up with research ideas; and every Keillor group member knows they are lucky to have you in their corner.

The Keillor group has played host to some of the best people I will ever meet. When I joined the lab, I was welcomed by veteran group members Eric Gates and Kelvin Tsao, who quickly taught me that the defining traits of a Keillor member are kindness, generosity, and a willingness to go out of one's way to help a lab member. These are qualities I have tried to embody throughout my time in the group, and pass along in turn. I would like to write a paragraph about every single Keillor member but I will instead be brief: thank you to: Nick Cundy (exceptional synthetic chemist), Sarah Watt (my first Keillor group contemporary) Sammir Shad (I still listen to your playlist) Daniel Wallace (one of the friendliest people I know) Bri Ryan (champion and leader of the movie crew), Thomas Grant (the other half of the legendary BL21s), and Sarah Tribe (a relentlessly positive presence). To all of the dynamic and static duos, everyone who supported and participated in anything in the folder on my laptop named "Keillor Group Shenanigans" (don't worry about it, Jeff) – you have all helped shape my time here into some of the best five years of my life.

That said, I have to call out some people in particular: thank you to Pauline Navals, an absolute force of nature and one of the most resilient and determined people I know. Your attitude of "let's do this!" is antithetical to my default state of "paralyzed by overthinking" in exactly the right way, and you inspire me constantly. You are the model of the kind of postdoc I hope to be, and if I do it half as well as you, I'll consider it a success. And thank you to Lavleen Mader, the coolest, smartest, most effective person, and best researcher I know. There is a reason we call you the unofficial PI – you've been there to add perspective, sanity, practicality, and humour to some of the hardest (and the best) times of my PhD. I am lucky to call you my friend, and to know that I'll still be able to 10 years from now.

I have been fortunate to work with some outstanding undergraduate students during my time here. Mégan Filiatrault joined our group for two summers, and proved to be talented, dedicated, and far more detail-oriented and rigorous than me, as well as kind and genuine and a joy to work with. Brenna Morgan did her honours with us during some of the most frustrating part of this project when (spoiler alert) nothing was working, but nonetheless brought patience and determination to her work.

Francis Roy, in lieu of being named a much-deserved co-author to this thesis, gets his own paragraph. When your summer student cheerfully agrees to a twelve-hour protein purification on his second day in the lab, you know you've got a good one. What I did not know then is that, over the next two years, you would end up being the greatest gift of my PhD career. Your enthusiasm, knowledge, talent, dogged determination, and exceptionally high standards for yourself (reminding me there is *always* better than "good") have made me a better scientist every day. People always say "I couldn't have done it without you" but here I would say instead: I *wouldn't* have done it without you constantly supporting me, always saying yes to my half-baked ideas, and working

overtime with me to turn them into reality. It has been the privilege of a lifetime to work with you, et je te remercie mille fois.

I owe all of my molecular biology skills to Jordan Brazeau-Henrie, an incredibly knowledgeable, patient, and diligent teacher. Thanks to you, I now confidently tell everyone that “DNA always works” and even though I have since learned it doesn’t, I still believe in your infallible protocols.

I would like to thank my examination committee, Dr. David Zechel, Dr. Chris Boddy, Dr. Adam Shuhendler, and Dr. F-X Campbell-Valois, for taking the time to evaluate my thesis. I hope you like it! I wanted to especially highlight my thesis advisory committee (Chris, Adam, F-X): in all of my PhD milestones, you have continued to challenge me while showing unwavering kindness and support. I’m sure I have come up to each of you at least once in the hallways of Marion, when you were probably very busy, to ask a random question and your enthusiasm for science and pedagogy always comes through in those moments.

I am fortunate to have an incredibly supportive network of family and friends. Thank you to my parents, who always listen to me rant about something or other going on in the lab, even though most of it probably doesn’t make sense, try their best to understand, and always send good vibes from afar. Thank you to my lifelong friends across Canada: our art night video chats help restore sanity to what is a fulfilling but admittedly very stressful and weird time in my life.

Finally, I need to thank my little Ottawa family: my partner Rob and my cat, Jack. Thank you to Jack for sitting vigil beside me all night for the last 3 months while I’ve been writing this thesis. And thank you to Rob for everything.

Statement of Contributions

Dr. Kelvin Tsao prepared the original expression plasmid for *Bacillus subtilis* transglutaminase (bTG).

Mégan Filiatrault performed the synthesis for some of the quenched fluorophore isopeptide substrates described in Section 2.2.3. She also collected data for the hydrolysis of ZFBC and analogues, as described in Section 2.2.4.

Brenna Morgan performed the Hydroxamate and GDH-coupled assays as described in Section 2.2.1.

Kian Mansour synthesized the peptide substrates evaluated in section 2.2.1.

Prof. Jeffrey Keillor, in addition to editing this document and advising on the entirety of the research presented herein, performed the modelling of NylC_A and ligands, as described in section 3.2.2.

Francis Roy performed the synthesis of the majority of compounds in Chapter 3, and contributed to performing assays (Chapters 3,4,5), protein expression (Chapters 3,4,5), mutagenesis (Chapter 5), preparing and screening lysate (Chapter 5) data interpretation (Chapters 3,4,5) and manuscript preparation (Chapters 3 and 4).

Table of Contents

List of Tables

List of Figures

List of Abbreviations

2×YT	2× Yeast extract Tryptone medium
Abs	Absorbance
Ac	Acetyl
ACN	Acetonitrile
AHX	Aminohexanoic acid
ALDFG	Abandoned, lost, or discarded fishing gear
AU	Absorbance units
Boc	Tert-butyloxycarbonyl
BSA	Bovine serum albumin
CAPS	3-(Cyclohexylamino)-1-propanesulfonic acid
Cbz	Benzyloxycarbonyl
DCM	Dichloromethane
δ	Chemical shift
DIPEA	*N,N*-diisopropylethylamine
DMAP	4-dimethylaminopyridine
DMC	*N,N*-dimethylcasein
DMSO	Dimethylsulfoxide
DSF	Differential scanning fluorimetry
E. coli	*Escherichia coli*
EDTA	Ethylene diamine tetraacetate
EIC	Extracted ion chromatogram
ESI	Electrospray ionization
$[E]_{TOT}$	Total enzyme concentration
FRET	Förster resonance energy transfer
g	gravitational force
GABA	Gamma-aminobutyric acid

GDH	Glutamate dehydrogenase
HBTU	2-(1H-Benzotriazole-1-yl)-1,1,3,3-tetramethyluronium hexafluorophosphate
HDPE	High-density polyethylene
HPLC	High-performance liquid chromatography
HRMS	High-resolution mass spectrometry
IPTG	Isopropyl β-D-1-thiogalactopyranoside
Kan	Kanamycin
k_{cat}	Catalytic constant
kDa	Kilodalton
K_M	Michaelis-Menten constant
λ_{Em}	Emission wavelength
λ_{Ex}	Excitation wavelength
LB	Lysogeny Broth
LCMS	Liquid chromatography-coupled mass spectrometry
MeOD	Per-deuterated methanol
MeOH	Methanol
Mol. Wt	Molecular weight
MOPS	3-(N-morpholino)propanesulfonic acid
MSA	Multiple Sequence Alignment
MWCO	Molecular weight cutoff
NADH	Nicotinamide adenine dinucleotide
NMI	N-methylimidazole
NMR	Nuclear Magnetic Resonance
OD_{600}	Optical density at 600 nm
PCR	Polymerase chain reaction
PDB	Protein databank
PET	Polyethylene terephthalate

PLA	Poly(lactic acid)
PMT	Photomultiplier tube
pNA	*para*-nitroaniline
pNBA	*para*-nitrobutyramide
pNP	*para*-nitrophenyl
qPCR	Quantitative PCR
R.T.	Room temperature
RFU	Relative fluorescence units
SDS-PAGE	Sodium dodecyl sulfate polyacrylamide gel electrophoresis
TAE	Tris-Acetate-EDTA
TCFH	(N,N,N',N'-tetramethylchloroformamidinium hexafluorophosphate
TG	Transglutaminase
THF	Tetrahydrofuran
TLC	Thin-layer Chromatography
TMS	Tetramethylsilane
TNBS	Trinitrobenzenesulfonic acid
Tris	Tris(hydroxymethyl)aminomethane
TS	Thermostable
U	Unit (of enzyme activity)
V_{max}	Maximum rate
w/v	Weight/volume
WT	Wild-type
ZQG	N-Cbz-glutaminyl glycine

Chapter 1. Introduction

1.1. Plastic Waste

I have always been a kind of environmentalist. When I was younger, my eco-conscious and community-oriented mother would bring my brothers and me along to pick up litter on the trails and teach us about the importance of minimizing waste through recycling and composting. In grade 4, my first independent study project was on climate change (then, "global warming"). Back then, at least from my perspective, the story was simple: pollution is bad, and it's our job as global citizens to clean up the planet by planting trees and adhering to the "3 R's" – reducing, reusing, and recycling.

As it transpires, the systems that propagate environmental damage are much more complex, and in some ways, more sinister than the narrative of one-dimensionally evil corporations who seek to clear-cut forests or choke cities in smog. Driven by economics, political inertia, lack of alternate infrastructure, and a certain amount of collective apathy, among many other factors, environmentally-damaging pollution prevails. And yet, in some ways, there's something to be said for the naïve perspective of my youth. Pollution is bad, and, specifically, in the context of this thesis: plastic waste is bad.

But, plastic waste is *necessary*, which is to say that waste is a natural consequence of necessary plastic use. While at first glance we may imagine that single-use plastics can be easily replaced by reusable alternatives like tote bags and metal straws (and while that is true for many plastic products), the reality is, once again, more complicated. Single-use plastics bring clean drinking water to communities without necessary water infrastructure. They keep medical equipment sterile, and food fresh. Plastic is used as the material of choice for these applications for a reason: defined as

synthetic carbon-based polymers, plastic is cheap, making it accessible, and morphologically diverse, making it versatile. With its universally bad reputation, plastic is a flawed solution to a flawed world, and is utterly irreplaceable. And correspondingly, plastic waste is a problem with which we will continually need to interface.

Much like the issue of plastic use and waste is not monolithically evil, it cannot be solved through an individual, vigilante-justice style effort: instead, it will involve the confluence of improved infrastructure, policy, and technology. While all are important, the work described herein focuses on the development of new technologies to mitigate plastic waste.

1.2. The Fate of Plastic Waste

In 2019, the Government of Canada released a report detailing the overall fate of plastic waste produced in Canada (See Figure 1.1).[1] While only one percent of plastic is reported to be "mismanaged" i.e. lost or dumped in the environment, another 86% is landfilled without recovery of material, allowing it to leach slowly into ground water in the form of microplastics.[2] Of the remaining 13%, four percent is incinerated to recover energy, and nine percent is recycled. Certain plastics are better suited for traditional recycling methods, particularly rigid plastics, where polyethylene terephthalate (PET) and high-density polyethylene (HDPE) have the highest recycling rates (29.1% and 29.3% respectively, as reported by the United States Environmental Protection Agency in 2018).[3] Conversely, most other resins lack the structural integrity to be recycled through traditional methods. Even successful recycling of plastics results in lower quality materials,[4] requiring the inclusion of virgin materials to increase the quality of the product. For this reason, plastic recycling is generally not economically viable, even considering the loss of value associated with landfilling.[1]

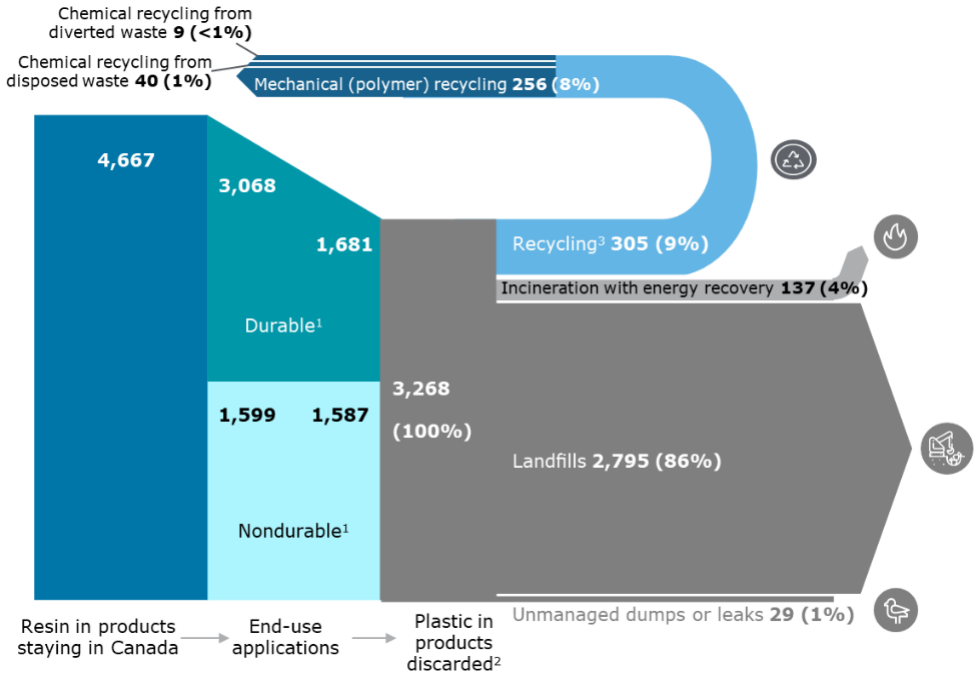

Figure 1.1. Flow of plastic resin in 2016, reported in thousands of tonnes per annum.[1]

Taken together, the reality is that even if all lost or discarded plastic was accounted for, we lack the necessary systems to manage it. This highlights the need for novel methods of plastic recycling, which can accommodate a larger variety of resin types and produce new materials without loss in quality. Development of a more circular plastic economy in this way would serve the dual goals of minimizing further resource extraction, and recovering the lost value of landfilled plastics, while mitigating environmental damage.

1.3. Biocatalysis for Plastic Recycling

One strategy, which is uniquely commensurate with the ideals of a circular economy, is bioremediation,[5] using organisms or the enzymes they produce to clean up environmental pollutants. In

the context of plastic waste, this can take on many forms, from metabolic engineering[6] to biocatalyst development.[7] For plastics, the goal is usually depolymerization: that is, converting a bulk, insoluble polymer into small molecules that can either be repolymerized into new plastics without loss of quality, or used as a chemical feedstock for other applications.

The use of biological catalysts (enzymes) to this end has huge advantages over traditional recycling methods, as aforementioned, or even depolymerization via chemical catalysis. While selective chemical depolymerization has been investigated and successfully applied to various plastic substrates, these processes generally need high temperatures (>100 °C), organic solvents, and expensive metal catalysts.[8,9] Conversely, biocatalysts are highly selective, and reactions are performed under benign, physiological conditions at significantly lower temperatures. Since biocatalysis is inherently biocompatible, production of ecologically harmful waste is also minimized.

Perhaps the best-known success story in the field of enzymatic plastic depolymerization is the use of protein engineering to develop highly efficient PET depolymerases.[7,10,11] PET falls into the category of "hydrolysable plastics" – those bearing heteroatoms in the polymer backbone, enabling disconnection at predictable points in the polymer. Among hydrolysable plastics, esters are among the easiest to depolymerize: an ester bond is relatively labile, and natural esterases are abundant in nature. For that reason, esterases have been identified with activity against poly(lactic acid) (PLA),[12] polycaprolactone and polyhydroxybutyrate[13] and even polyurethane *via* hydrolysis of the ester moiety of the carbamate linkage.[14] Thus, compared to polyesters, the enzymatic degradation of other plastic polymers poses a greater challenge.

1.4. Nylon

Nylon is a plastic defined by its aliphatic, linear polyamide structure (see Figure 1.2.). In industry and commercial applications, nylons are prized for their high tensile strength, flexibility, and resistance to both chemical and physical wear.[15] Because of this, nylon is often spun into fibres, which are in turn used for materials such as clothing, ropes, and tarps. Notably, nylon is the material of choice in the fishing industry, where it is used in cables, netting, and fishing line.[16] Unfortunately, due to its inherent stability, nylon waste is resistant to natural degradation and consequently accumulates in the environment. For instance, abandoned, lost, or discarded fishing gear (a source of plastic waste so prevalent, it has earned its own acronym, "ALDFG") constitutes over 40% of the Great Pacific Garbage Patch.[17] In addition to the shedding of microplastics and bioaccumulation risk inherent to all plastic waste, discarded fishing equipment is especially damaging in ocean environments, since they are specifically designed to entrap organisms, leading to uncontrolled death in marine populations.[18] Therefore, physical removal of nylon waste from the environment is a necessary first step to mitigate harm. Even so, recycling infrastructure for nylon is limited, and only 5% of nylon waste is recycled.[19]

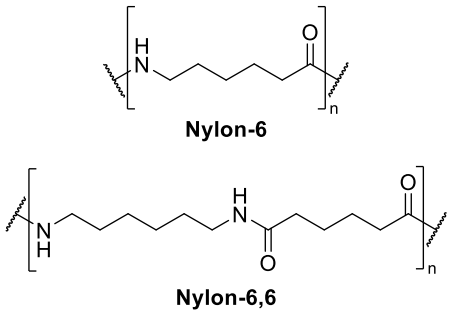

Figure 1.2 The two most industrially common architectures of nylon. Nylon-6 (above) is a polymer of caprolactam, and Nylon-66 (below) is a polymer of 1,6-hexanediamine and adipic acid.

Traditional recycling of nylon occurs through a thermomechanical process, where the plastic is shredded, washed, then melted and extruded into pellets or fibres.[20] This method has certain advantages, being simple, scalable, and producing only a small amount of waste. However, the melting step requires high temperatures, corresponding to a large input of energy at scale. Furthermore, while pure nylon can withstand several melt cycles, degradation of the polymer can occur more readily in the presence of impurities or especially water, which induces unwanted chain hydrolysis at the elevated temperatures during the melt step. To mitigate this, an extended drying step is incorporated, involving heating under vacuum to remove water,[21] corresponding to an additional input of energy. The process is further complicated by the presence of other polymers or additives which are often present in nylon-based materials such as carpets.[22] To address this, more specialized systems are necessary to separate these materials, since thermomechanical recycling is not a selective process. Due to these drawbacks, more efficient and selective strategies for nylon recycling are needed.

Chemical recycling of nylon – i.e. using chemical means to convert nylon polymers to the monomer (either caprolactam or aminohexanoic acid (AHX)) – has been of recent interest as an alternative to thermomechanical recycling. This general strategy encompasses several methods involving as acid- or base- catalyzed hydrolysis, or alcoholysis, to produce AHX or esters thereof, followed by heat-induced condensation to produce caprolactam.[23] Alternatively, the use of metal catalysts has shown to improve selectivity and yield of caprolactam (the industrial precursor to Nylon-6) in a solvent-free process.[24] However, high temperatures (>200 °C) and low pressures are still required to effect this conversion, corresponding to a significant input of energy. Most reports of chemical depolymerization are performed at lab scale[23] and while one company, Nylene, claims to perform industrial-scale chemical depolymerization of Nylon-6,[25] details of this process were

unavailable. Overall, as of 2020, less than 2% of Nylon was produced from chemically-recycled caprolactam, suggesting that the technology is not sufficiently cost-efficient for current demands.[26]

From a biocatalytic perspective, two main classes of enzymes have emerged as candidates for nylon degradation: oxidases and hydrolases.[27] In the former category, only a few enzymes, such as manganese peroxidases[28] and laccases[29] have been identified, but these reactions produce variable byproducts, making the process less amenable to upcycling or re-polymerization. Hydrolases are generally the preferred depolymerization catalysts as reactions occur predictably at the amide linkages, reliably returning useful byproducts. However, relatively few nylon-hydrolyzing enzymes have been identified, since amide bonds are chemically much more stable than the ester bonds that make resins such as PET and PLA attractive targets for depolymerization. Furthermore, while amidases are ubiquitous in nature in the form of proteases, far fewer *aliphatic* amidases are known compared to native long-chain esterases, further complicating the search for nylon-degrading enzymes. A more comprehensive overview of the existing nylon hydrolase literature will be provided in Chapter 3, as it more closely aligns with that section of this work.

1.5. Aims

In this work, we seek to identify enzymes capable of degrading nylon, and develop tools to facilitate engineering of nylon-degrading enzymes with improved amide hydrolysis activity. In the next chapters, we explore two classes of enzymes for their potential to catalyze the hydrolysis of Nylon plastic. In Chapter 2, we characterize the activity and substrate specificity of a bacterial transglutaminase with good biocatalytic properties and the potential to hydrolyze nylon-like isopeptide bonds. In Chapters 3-5 we perform a deeper investigation into the aminohexanoate oligomer hydrolases, enzymes with known albeit low nylon-degrading activity, as a basis for engineering. Chapter 6 presents a summary of this work, and perspectives for future directions of research.

Chapter 2. Investigation of the Substrate Scope and Reactivity of *Bacillus subtilis* Transglutaminase

2.1. Introduction

2.1.1. Transglutaminases

Transglutaminases (TGs) are most generally described as enzymes that perform modifications at glutamine residues of proteins. Usually, linkages are formed between glutamine and lysine residues as post-translational modifications, or in response to external stimuli: one salient example of this is transglutaminases' involvement in the blood clotting pathway in mammals.[30] Transglutaminases are found in animals, plants, and bacteria, where their structure and biological roles are correspondingly widely varied. Taken as a whole, transglutaminases have been referred to as "nature's biological glues",[31] where this unique cross-linking ability suggests their potential as biocatalysts.

All catalytic activity of transglutaminases follows the same general mechanism (Figure 2.1.).[32] Following substrate binding, TGs react with glutamines to form an acyl enzyme intermediate *via* its catalytic cysteine residue, releasing ammonia. Then, the thioester bond is cleaved either by an amine (acyl acceptor), forming a new amide linkage, or else by a water molecule, to release glutamate and regenerate the catalytic cysteine thiol.

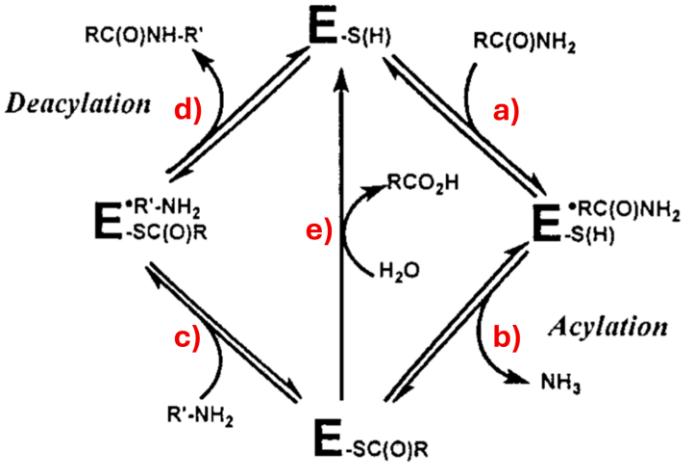

Figure 2.1. Mechanism of TG catalytic activity. A) non-covalent binding of acyl donor substrate; b) formation of acyl-enzyme intermediate through loss of ammonia; c) non-covalent binding of amine (acyl acceptor) substrate; d) formation of amide bond, regenerating the cysteine thiol(ate); e) hydrolysis of the acyl-enzyme intermediate to produce a carboxylic acid product. Figure adapted from Leblanc *et al.*[33]

Importantly, this general mechanism enables expanded reactivity with molecules bearing other carboxyl derivatives such as esters and secondary amides. One key example is the notable isopeptidase activity first identified in the enzyme Factor XIII[34] and later characterized in human tissue transglutaminase.[35] This reaction proceeds following steps d then c) (Figure 2.1) in reverse, binding the isopeptide followed by formation of the acyl-enzyme intermediate through loss of the amine group. The acyl-enzyme intermediate is then hydrolyzed (step e)) to give the free carboxylic acid.

Isopeptidase activity is relatively rare in nature, generally limited to highly specific enzymes such as the SUMO isopeptidases[36] or lasso peptide isopeptidases.[37] In the context of nylon degradation,

we noted that the isopeptidic ϵ-(γ-glutamyl)lysine bond recognized by transglutaminases is structurally similar to the amide bonds in nylon polymers (Figure 2.2.). We therefore considered that transglutaminases may be investigated and subsequently engineered as biocatalysts to recognize and hydrolyze nylon.

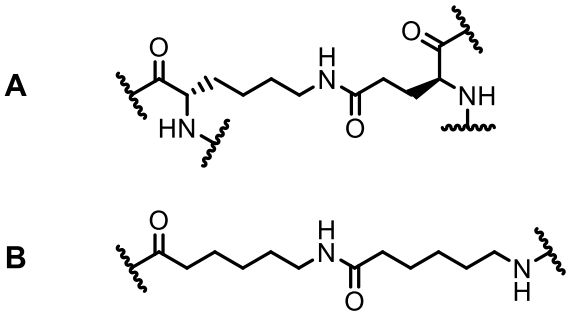

Figure 2.2.2. A) General structure of an isopeptidic linkage between glutamine and lysine residues. B) Structure of the polymer, Nylon-6.

2.1.2. Human Transglutaminases

Among the transglutaminases, the best studied have been the eight human transglutaminase isozymes, which are investigated largely for their potential as therapeutic targets. Of particular interest to our research group is human tissue transglutaminase (hTG2), a ubiquitous enzyme implicated in pathologies including cancer, fibrosis, and celiac disease. As such, an extensive catalogue of reactivity, substrate, and inhibitor scope has been developed for TG2, revealing several potential biocatalytic applications. Tissue transglutaminase accepts a variety of substrates, including those bearing small molecule,[33,38] peptidomimetic,[39] peptidic,[35] and protein[40] scaffolds. This substrate promiscuity and reactive versatility is perhaps reflective of its biological ubiquity in humans. However, TG2, and indeed all human isozymes, have features that are detrimental to their potential as

biocatalysts. Primary amongst these, and common among mammalian transglutaminases, is that their active conformation is dependent on a high concentration of calcium. Additionally, these enzymes are large, complex, flexible, and unwieldy: consequently, they have low thermal stability and are relatively challenging to express heterologously.

2.1.3. Microbial Transglutaminase

Microorganisms are common sources of practical biocatalysts. Usually small and structurally simpler than their multicellular -derived counterparts, these enzymes tend to express better in well-characterized systems like *E. coli* and naturally exhibit valuable properties such as enhanced solubility and thermal stability. Many bacterial transglutaminases exist. The best-characterized biocatalyst among these is *Streptomyces mobaraensis* transglutaminase, known commonly as mTG, the prototypical microbial transglutaminase.[41] The enzyme, mTG, has found a home in the food processing industry, where its cross-linking activity is used to improve food texture and stability. mTG is calcium-independent and expresses well in *E. coli*, allowing it to be studied extensively for its substrate scope and specificity, and mTG has been considered as a catalyst for site-specific labelling of proteins.[42,43] However, mTG is not well-suited to engineering to tailor its biocatalytic activity: at high levels it is toxic to its host cell, and thus it is expressed as an inactive proenzyme. The protein must be activated by thrombin prior to purification, restricting activity screens.

2.1.4. *Bacillus subtilis* Transglutaminase

In 1996, a transglutaminase was discovered in *Bacillus subtilis*, whose spores are unusually resistant to proteolytic degradation.[44] Subsequent analysis determined that the spore coat was highly stable due to ϵ-(γ-Glu)Lys cross-links formed by a transglutaminase,[44,45] sometimes called *Tgl*, but henceforth referred to herein as *bTG* (“bacterial transglutaminase” or, more specifically, *Bacillus subtilis* transglutaminase). Smaller and simpler than most other known transglutaminases, bTG

shows great potential as a biocatalyst: it is easily expressed solubly in *E. coli*[46] in its active form, and does not require the presence of Ca^{2+} for activity [47] as do the animal TGs.

Despite this potential, bTG is a reasonably little-known enzyme, and there have been few reports characterizing its catalytic activity. Transglutaminase activity was initially detected by assaying *B. subtilis* spore lysate, where they determined the presence of an enzyme capable of incorporating ^{14}C-labelled putrescine into dimethylcasein (as measured by radioactivity).[44] This assay was later used to assay purified bTG in a quantitative manner, revealing optimal activity conditions for the enzyme.[45] The authors determined that bTG has an optimal pH of ~8 and demonstrates the highest activity at 50 °C. Furthermore, bTG cross-linking activity is slightly inhibited in the presence of Ca^{2+} (contrary to mammalian transglutaminases), and enhanced in the presence of thiol reducing agents,[47] indicating the presence of a catalytic cysteine. Later crystallographic studies would confirm the presence of an active-site cysteine, and hypothesize the mechanism of a semi-redundant catalytic dyad between the cysteine and two proximal glutamate residues (See Figure 2.3). Later, purified bTG was used to crosslink bovine serum albumin (BSA), the extent to which was determined qualitatively by SDS-PAGE analysis,[45] indicating that BSA may act as both an acyl donor and acyl acceptor for bTG, and pointing towards its potential substrate promiscuity. Neither of these assays are convenient to determine activity: both are discontinuous and involve extensive manipulation, and the gel-based assay is not quantitative.

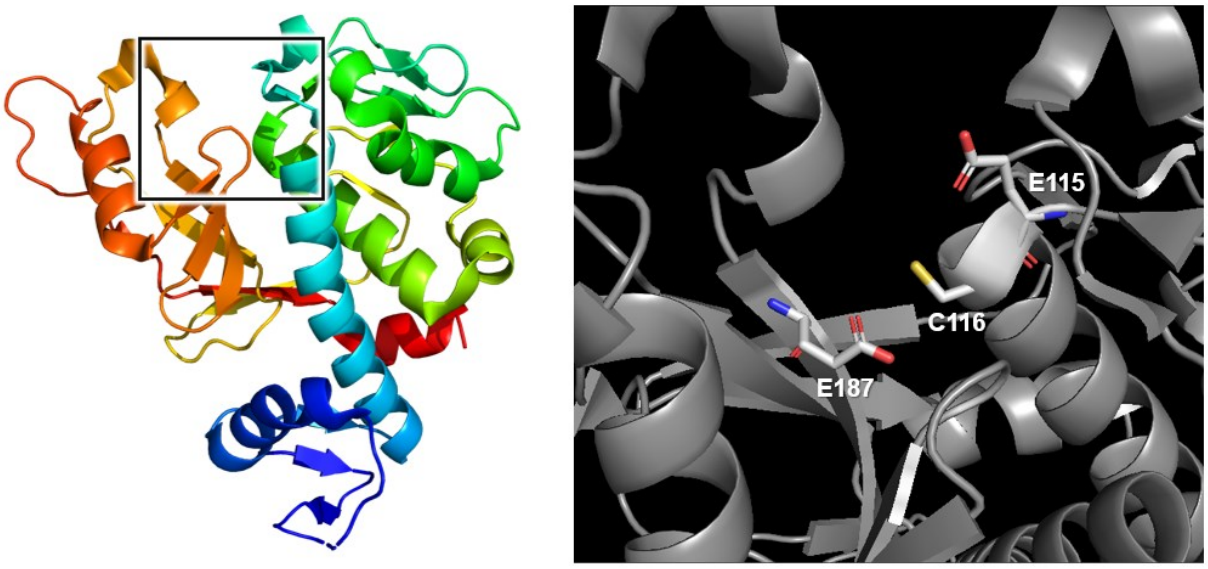

Figure 2.3. Crystal structure of bTG (PDB ID: 4P8I). Left: full structure, with active site indicated. Right: close-up of the active site of bTG, with the catalytic cysteine and proximal glutamine residues hypothesized to participate in catalysis.

More recently, a fluorescent version of the protein labelling assay was employed: the transglutaminase incorporates the fluorescent amine, dansylcadaverine, into an acceptor protein (casein or BSA). To observe labelling, aliquots are acquired over time, and the fluorescence of the substrate protein is evaluated following separation on SDS-PAGE.[48] While discontinuous and qualitative, this assay is the most convenient to perform of those reported, and has subsequently been used to identify certain residues involved in substrate binding for cross-linking activity.[49]

In this chapter, we will investigate the substrate scope and reactivity of bTG, probing its cross-linking and hydrolytic activities.

2.2. Results and Discussion

2.2.1. Evaluation of bTG *via* Standard Transglutaminase Assays

We began by confirming activity in our recombinant enzyme by repeating the previously described gel-based dansylcadaverine incorporation assay (Figure 2.4). We were pleased to observe reactivity by an increase in fluorescence intensity at the band corresponding to the molecular weight of BSA. These results are visually consistent with those reported:[48] we observed the appearance of a fluorescence signal after ~1 hour, whereas the reported assay shows fluorescence after 30 minutes, using twice the concentration of enzyme. With these results, we were confident that our recombinant bTG was active, but sought to quantify this activity.

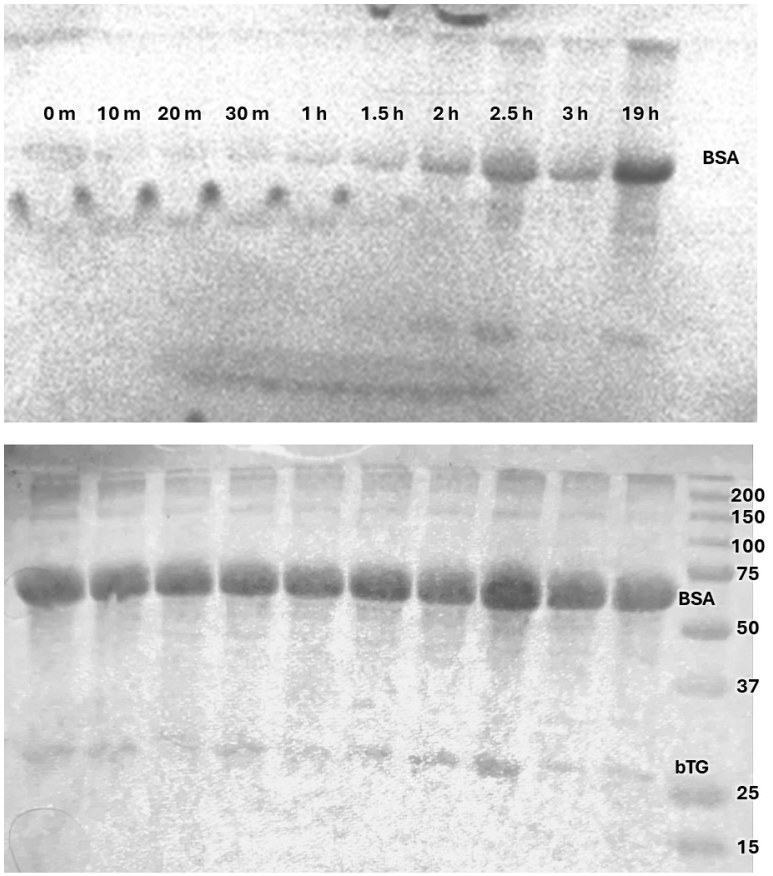

Figure 2.4. Above: SDS-PAGE (inverted image) of reaction mixture showing fluorescence when irradiated at 365 nm. BSA (66 kDa) is indicated. Below: the same gel, visualized by Coomassie staining, indicating consistent concentrations of BSA for each aliquot. Protein ladder molecular weights are indicated. Reaction mixtures contained MOPS buffer (100 mM, pH 8.0) bTG (8 μM), BSA (60 μM), and dansylcadaverine (500 μM).

A standard quantitative assay used to evaluate transglutaminase activity is the hydroxamate assay. Generally considered universal, it can detect transamidase activity with any glutamine substrate, using hydroxylamine as the acyl acceptor. The reaction is shown in Figure 2.5, below.

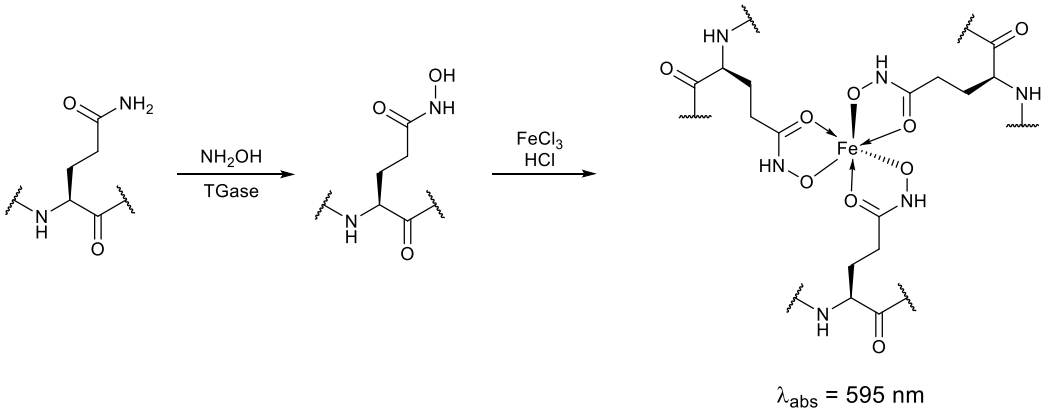

Figure 2.5. Transglutaminase incorporates hydroxylamine into an acyl donor, producing hydroxamic acid. In the presence of Fe^{3+}, a complex is formed that absorbs light at 595 nm.

This is a discontinuous, endpoint assay, which allows for quantification of the reaction products, but not reaction rates. After incubation of hydroxylamine and the acyl donor with the transglutaminase, the reaction is quenched with acid and $FeCl_3$, precipitating the protein and allowing for the formation of the iron-hydroxamate complex. This complex formation is accompanied by a

dramatic colour change of the assay solution, from yellow to deep purple, which can be quantified by spectrophotometry. We performed this reaction with bTG, adapting a previously reported method.[39] In our first attempt, we used the standard acyl-donor substrate for this reaction: the di-peptide, Cbz-glutaminyl glycine (ZQG). We saw a negligible difference in activity in the presence of enzyme compared to the no-enzyme blank (Table 2.1). To compare, under the same conditions, mTG demonstrated a difference in absorbance of 0.217 AU, converting 3.19 mM of substrate into product in the presence of 1.5 μM of enzyme (only 3% of the concentration of bTG used for this experiment).

Previous studies have identified glutamine-containing peptidic sequences that are preferentially recognized by bTG. In 2018, Oteng-Pabi *et al*. engineered a peptide tag, YAH**Q**AHY, which demonstrated high affinity for bTG when fused to a fluorescent protein.[50] In another study, isopeptidic linkages were observed in the spore coat of *B. subtilis* at a glutamine residue with the flanking sequence PAT**Q**RAY, which was attributed to cross-linking by bTG.[51] We synthesized *N*-acetylated heptameric peptides with these respective sequences and evaluated them by hydroxamate assay (Table 2.1). Unfortunately, these substrates also demonstrated negligible activity when compared to a no-enzyme blank, suggesting that the isolated peptides, in the absence of an accompanying protein, are not substrates for bTG.

Table 2.1. Absorbance values from the hydroxamate assay conducted with each substrate.

Substrate	**Absorbance -10 min (no enzyme blank)**	**Absorbance – 30 min (no enzyme blank)**	**Absorbance-60 min (no enzyme blank)**
ZQG	0.087 (0.090)	-	-
Ac-YAHQAHY-OH	-	0.076 (0.182)	0.133 (0.116)
Ac-PATQRAY-OH	-	0.077 (0.099)	0.098 (0.157)

One limitation of the hydroxamate assay is that it requires hydroxylamine as an acyl acceptor. If bTG recognizes the acyl acceptor (glutamine) substrates but not hydroxylamine, the assay would report a negative result. Therefore, we attempted a second assay (Figure 2.6.). The GDH-coupled assay quantifies activity via reaction with ammonia, which is produced as a byproduct of the trans-amidation reaction. This assay is, therefore, substrate-agnostic with respect to both the acyl donor and acyl acceptor. It is also a continuous assay: the rate of production of NH_3 can be correlated to the rate of consumption of NADH, as measured by absorbance at 340 nm, as GDH converts α-ketoglutarate into glutamic acid.

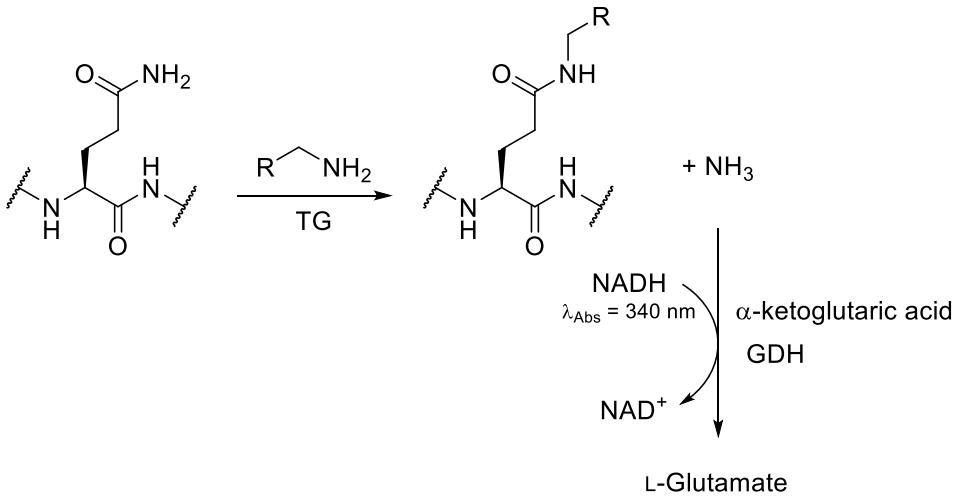

Figure 2.6. Reaction scheme for the GDH-coupled assay. One equivalent of ammonia, released due to TG-catalyzed transamidation, is converted to glutamate in the presence of glutamate dehydrogenase (GDH). This reaction consumes an equivalent of NADH, which absorbs at 340 nm.

The GDH-coupled assay was initially performed following the published protocol,[39] using ZQG as the acyl donor substrate and glycine methyl ester as the acyl acceptor. The reaction was

performed at a saturating acyl acceptor concentration (100 mM) and limiting acyl donor substrate concentrations of 0-10 mM). Results are shown in Figure 2.7. Here, we observe a slight increase in rate with increasing ZQG, but that rate increase is not dependent on the presence of enzyme, consistent with the results of the hydroxamate assay. These results taken together show that ZQG is not a substrate for bTG.

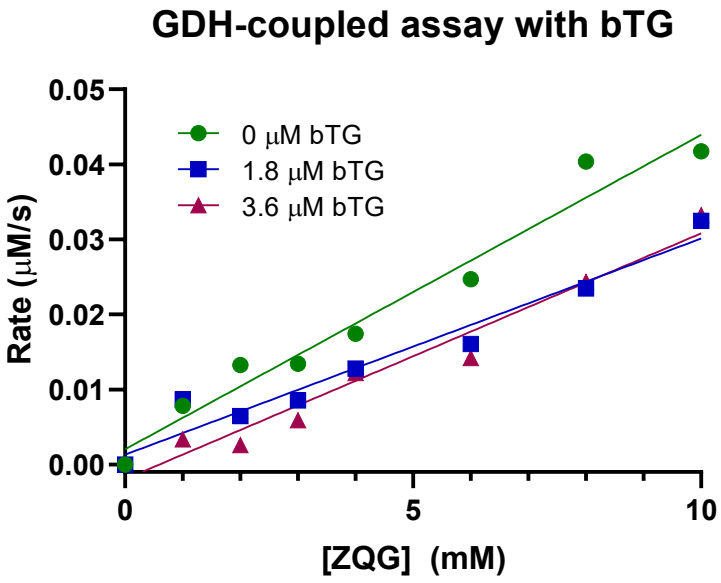

Figure 2.7. Observed rates are plotted vs. concentration of acyl donor substrate, at varying concentrations of bTG. Reaction conditions: MOPS buffer (200 μM, pH 7.2), EDTA (1 mM), NADH (500 μM), α-ketoglutarate (10 mM), glutamate dehydrogenase (10 U/mL) and glycine methyl ester (10 mM), ZQG (0-10 mm) and bTG (0, 1.8, or 3.6 μM). Initial slopes were converted to rates using an extinction coefficient of 6.22 L $mmol^{-1}$ cm^{-1}.[52]

We performed the same assay using the peptide substrate, YAHQAHY (Figure A2.1 in Appendix). Notably, this assay has previously been used to determine kinetic parameters for a *protein* substrate

tagged with this peptide.[50] In that study, a k_{cat}/K_M of 19 $\mu M^{-1}s^{-1}$ was determined for the tagged protein substrate. Here, we evaluated the tag alone. Unfortunately, due to limitations in availability, the substrate concentration range was reduced to 0-1000 μM, and under the conditions evaluated, we were not able to observe a clear enzyme- or substrate-concentration dependent increase in reaction rate.

Given this discrepancy, and inspired by its reactivity towards BSA (but inactivity towards small molecules), we hypothesized that bTG may be selective for protein (not simply peptidic) substrates.

2.2.2. A Continuous and Quantitative Transamidase Activity Assay

In seeking a continuous and quantitative assay, we investigated a report by Lorand *et al.* in 1971 describing a continuous assay for the human transglutaminase, Factor XIII. They observed that incorporation of dansylcadaverine into *N,N*-dimethylcasein (DMC) led to an increase in fluorescence intensity, due to increased hydrophobicity in the binding pockets of DMC. Since bTG was successful at covalently modifying BSA, we were optimistic that this assay would be capable of quantifying its activity.

To ensure that DMC was recognized by bTG, we first performed a discontinuous labelling assay, following the same protocol reported for BSA, as previously described (Figure 2.8).

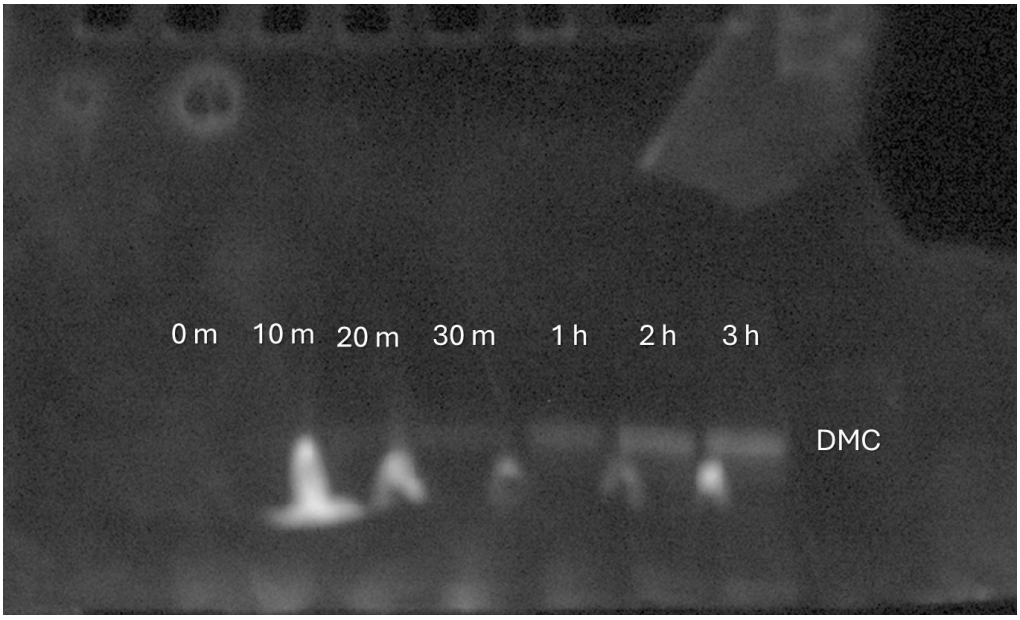

Figure 2.8. Covalent modification of dimethylcasein (DMC) by dansylcadaverine over time. Reaction conditions: Dansylcadaverine (500 μM), dimethylcasein (60 μM), bTG (8 μM), MOPS (200 mM, pH 8.0).

This discontinuous assay demonstrated that bTG was able to incorporate dansylcadaverine into dimethylcasein; thus, we sought to develop the continuous version of this assay for bTG. A preliminary experiment was performed at a constant concentration of dimethylcasein and dansylcadaverine and varying bTG concentration, in order to choose a concentration at which a continuous increase might be observed over a practical time period (Figure 2.9).

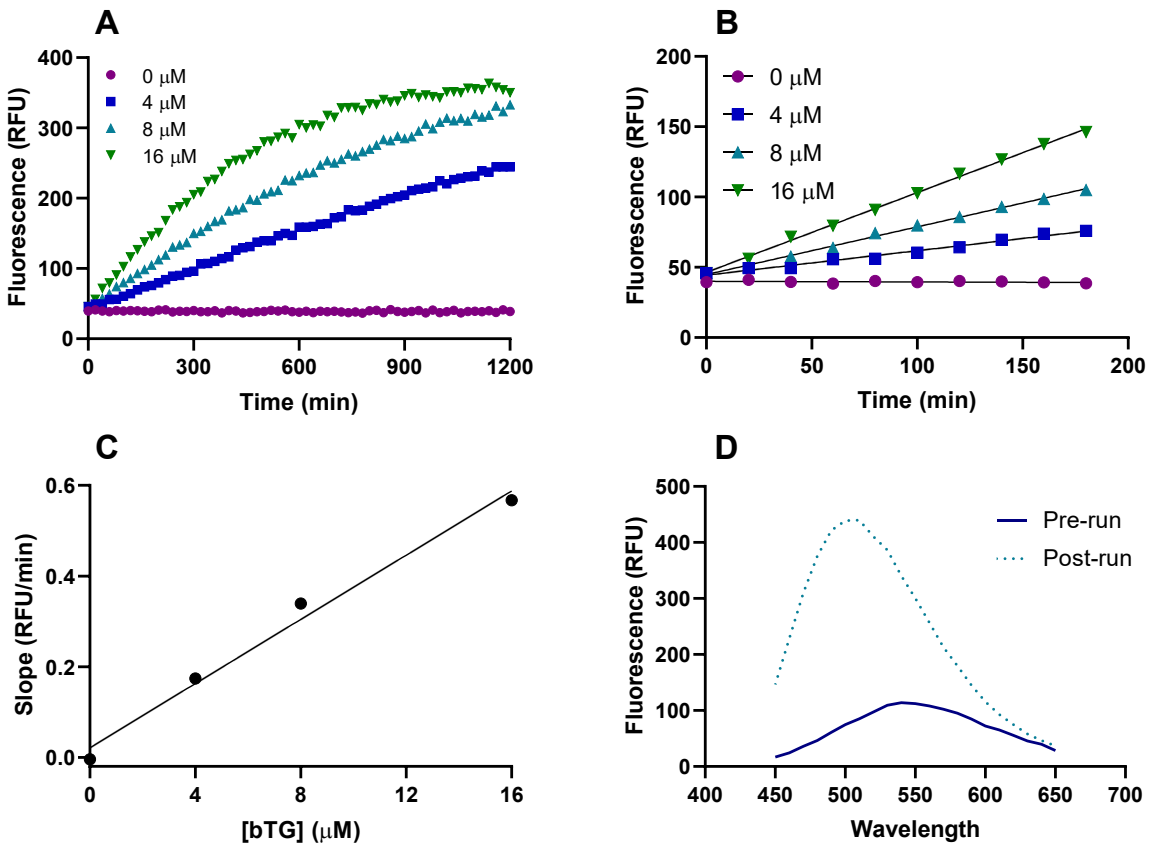

Figure 2.9. A) Covalent modification of DMC by dansylcadaverine, mediated by bTG at varying concentrations, leads to an increase in fluorescence (520 nm) over time. B) Initial slopes determined from the linear region of plot A. C) Slopes from plot B plotted against concentration of bTG reveals a linear relationship over this enzyme concentration range. D) Emission spectrum (λ_{ex}) of the reaction mixture before (solid line) or 20 hours after (dashed line) initiation of the reaction, in the presence of 8 μM bTG. Conditions: Dimethylcasein (80 μM), dansylcadaverine (60 μM), MOPS (100 mM, pH 8.0), bTG (0-16 μM).

We were pleased to observe a clear, enzyme-dependent increase in fluorescence as bTG mediated labelling of dimethylcasein by dansylcadaverine. These data allow us to quantify reaction rates, in

contrast to the qualitative activity we had previously observed in the discontinuous, gel-based assay.

We next performed Michaelis-Menten kinetics to quantify the efficiency of the reaction (Figure 2.10). As an exploratory assay, we chose to evaluate a range of 0-100 μM dimethylcasein. We further determined that 160 μM was an adequately high excess concentration of dansylcadaverine to minimally impact reaction kinetics while not saturating the detector due to intrinsic fluorescence, enabling for a clear increase in signal due to labelling of dimethylcasein.

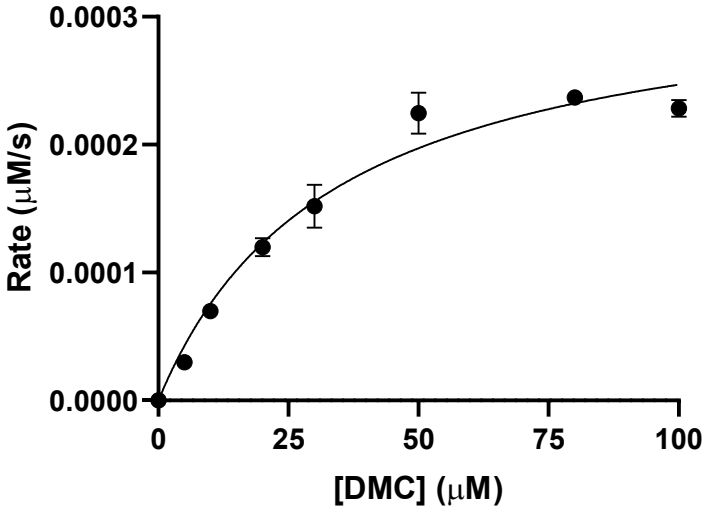

Figure 2.10. Michaelis-Menten plot for the covalent modification of dimethylcasein by dansylcadaverine, mediated by bTG. Reaction conditions: bTG (10 μM), dansylcadaverine (160 μM), dimethylcasein (0-100 μM), Tris (100 mM, pH 8.0). Datapoints are averages of 3 replicates, with error bars showing standard deviations. Rates in μM/s were determined by converting fluorescence signal (RFU) to concentration using a calibration curve established from endpoint measurements at varying concentrations of DMC (Figure A2.2 in Appendix).

The data were fit using the Michaelis-Menten equation (Equation 1) to determine kinetic parameters K_M and V_{max}. Then, the value of k_{cat} was determined from V_{max} using Equation 2.

$$v = \frac{V_{max}[S]}{K_M + [S]} \qquad (Equation\ 1)$$

$$V_{max} = k_{cat}[E]_{TOT} \qquad (Equation\ 2)$$

The Michaelis-Menten fit gave kinetic parameters of 34 μM (K_M) and 3.8×10^{-4} μM/s (V_{max}), the latter of which corresponds to a k_{cat} of 3.8×10^{-5} s^{-1} when the reaction is catalyzed by 10 μM of bTG. This corresponds to a k_{cat}/K_M of 1.1×10^{-7} μM^{-1} s^{-1} for the substrate, dimethylcasein.

Needless to say, this reaction is incredibly inefficient when catalyzed by bTG. As a comparison, we performed the same experiment using *Streptomyces mobarensis* transglutaminase (mTG), which gave the kinetic parameters 27 μM (K_M) and 8.98×10^{-3} μM/s (V_{max}), corresponding to a k_{cat} of 0.018 s^{-1} when catalyzed by 0.5 μM of enzyme (data shown in Figure A2.3 in Appendix). This enzyme gave an overall efficiency of 6.7×10^{-4} μM^{-1} s^{-1}, a greater than 600-fold increase over that of bTG.

Curious, we performed this assay using the human transglutaminase isozymes we had available, namely **TG1**, **TG2**, **TG3**, **TG6**, and **Factor XIII**. The results are summarized in Table 2.2.

It is perhaps unsurprising that the human transglutaminases perform this reaction with a significantly higher efficiency than the bacterial transglutaminases, and particularly, bTG. The role of bTG in *Bacillus* is to cross-link the spore coat during sporulation, a process that takes on the order of 7-8 hours.[53] In comparison, the role of FXIIIa in humans is to participate in blood clotting: a seconds-to minutes- long process that is essential to survival. Nevertheless, this is the first continuous, and truly quantitative assay to monitor bTG activity. These qualities are valuable in an assay

applied to future engineering strategies involving transglutaminases, to ensure that the catalytic function of the enzyme remains intact, and quantify any changes in activity.

Table 2.2. Kinetic parameters (apparent) for the covalent incorporation of dansylcadaverine (1.6 mM) into dimethylcasein (variable concentration, limiting) for a library of transglutaminases (variable for each TG). Data may be found in Figure A2.3 in the Appendix.

Enzyme	K_M^{app} (μM)	V_{max} ($\times 10^{-3}$ μM/s)	[Enzyme] (μM)	k_{cat}^{app} ($\times 10^{-3}$ s^{-1})	$(k_{cat}/K_M)^{app}$ (M^{-1} s^{-1})
bTG	34	0.38	10	0.038	1
mTG	27	8.98	0.5	17.95	670
TG1	27	25.21	0.1	252.1	9340
TG2	2	4.07	0.5	8.136	3272
TG3	33	3.59	0.1	35.85	1078
TG6	20	3.92	0.1	39.24	2012
FXIIIa	50	23.78	0.05	475.6	9459

2.2.3. Investigation of isopeptidase activity in bTG

Once we were able to quantify the transamidase activity of bTG, we sought to determine whether bTG could recognize and cleave an isopeptidic linkage. Since transglutaminases catalyze the formation and hydrolysis of amide bonds between glutamine and lysine residues, we considered that bTG was most likely to recognize an amide scaffold bearing these elements. We envisioned that installing a fluorophore on the α-amine of one residue and a corresponding fluorescence quencher on the opposite α-amine would result in a non-fluorescent probe, from which fluorescence would be restored upon hydrolysis of the isopeptide bond.

We chose *N,N*-dimethylaminonaphthalenesulfonyl (dansyl) as the fluorescent moiety, and *N,N*-dimethylaminoazobenzenesulfonic acid (dabsyl) as the quencher. These groups are reasonably compact, minimizing obfuscation of the target scissile bond, and are commercially available as the

corresponding sulfonyl chlorides, facilitating derivatization of amine groups. Dansyl has a high quantum yield and a large Stokes shift (λ_{ex} ~ 335 nm, λ_{em}~500 nm), and is effectively quenched by dabsyl (λ_{abs} ~475 nm), all of which are attractive characteristics for biochemical probes.

The substrate designs are shown in Figure 2.11. We initially designed two compounds, where the position of the fluorophore and quencher were switched to account for variability in substrate binding preferences of bTG. We also designed the corresponding "linear" substrates, where the glutamine and lysine were replaced by GABA and cadaverine, respectively, which more closely resembled the linear amide structure of nylon.

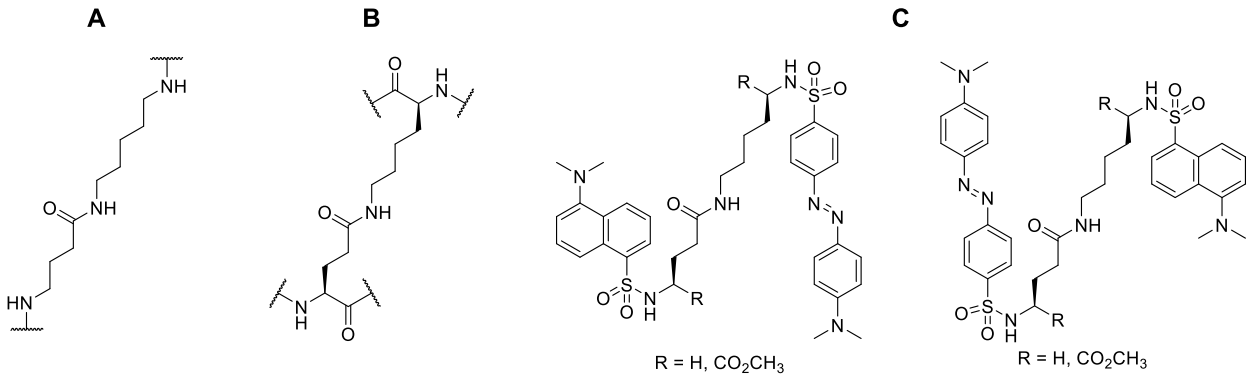

Figure 2.11. A) linear amide structural motif similar to Nylon-4,5. B) structural motif of an iso-peptidic linkage. C) general structure of fluorogenic substrates synthesized for this project.

The synthesis of compounds **3a-d** are shown in Figure 2.12. While these compounds could have been produced convergently and combinatorially, we observed that handling free carboxylic acids as synthetic intermediates was challenging, so we followed the longer but overall more efficient linear synthesis route. Deprotection of the Boc group by HCl/dioxane allowed for isolation of the free amine HCl salts by evaporation without any further purification, simplifying the synthesis and handling properties of the intermediates.

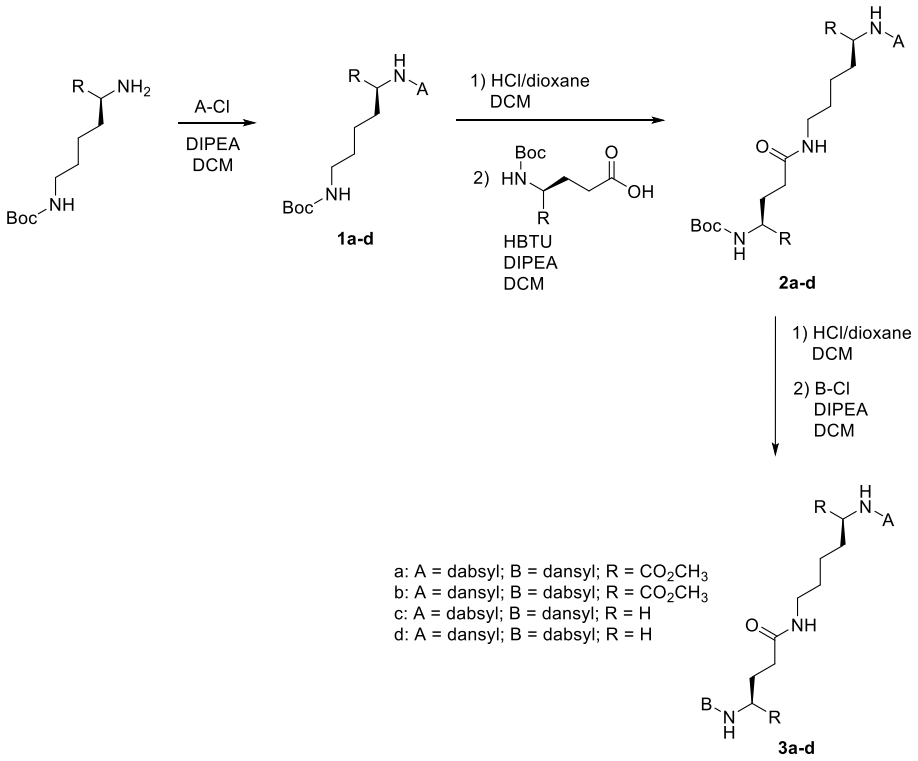

Figure 2.12. Synthesis of quenched fluorophore substrates **3a-d**.

We evaluated all four substrates for hydrolysis by bTG. However, we quickly realized that the exceptionally low solubility of the compounds was impeding reactivity. Consequently, the fluorescence signal we observed was not truly fluorescence but simply scattering of the substrate, as shown in Figure 2.13.

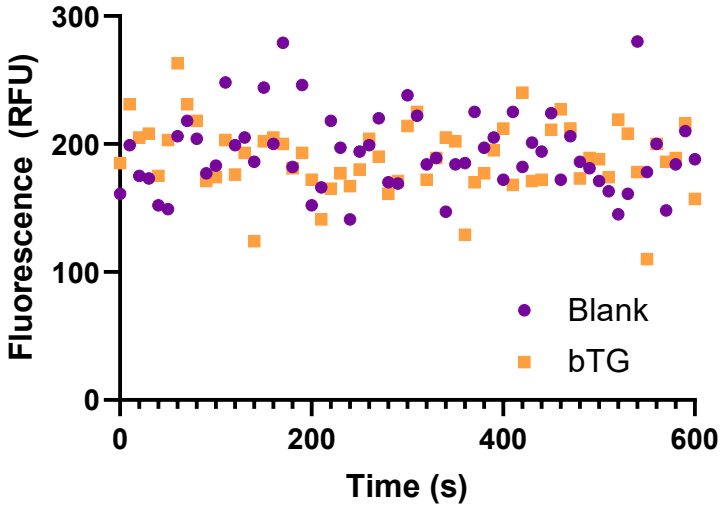

Figure 2.13. Observed fluorescence over time (518 nm) for compound **3a** in the absence (blank) or presence of bTG. Reaction conditions: Substrate **3a** (0.5 mM), MOPS buffer (100 mM, pH 8.0), bTG (0 μM (blank) or 8 μM), 30 °C.

The other substrates had similarly low solubility, and we observed no activity with any of them (see Figure A2.4a-c). We reasoned that low solubility combined with significant structural discrepancies compared to either the native peptidic substrates or the target, nylon-like substrates, precluded this series from further investigation.

2.2.4. Ester Hydrolysis by bTG

We wished to determine whether hydrolytic activity was possible for bTG at all. It is important to note that the hydrolysis mechanism is only enabled (once an acyl-enzyme complex is formed) if water can access the active site. Human transglutaminases have demonstrated the capacity for deamidation (hydrolysis of glutamine sidechain substrates), and by extension, hydrolysis of ester substrates, which follows the same mechanism after formation of the acyl enzyme intermediate.

This activity enables the use of rapid chromogenic or fluorogenic assays, which are commonly applied in medicinal chemistry campaigns to efficiently quantify enzyme inhibition. Two substrates that are commonly used to this end for hTG2 are the chromogenic substrate AL5,[33] and the fluorogenic substrate ZFBC[38] (Figure 2.14). We hypothesized that, if bTG were able to catalyze hydrolysis of these substrates, access of water would not be the limiting factor for the recognition and hydrolysis of polyamide substrates.

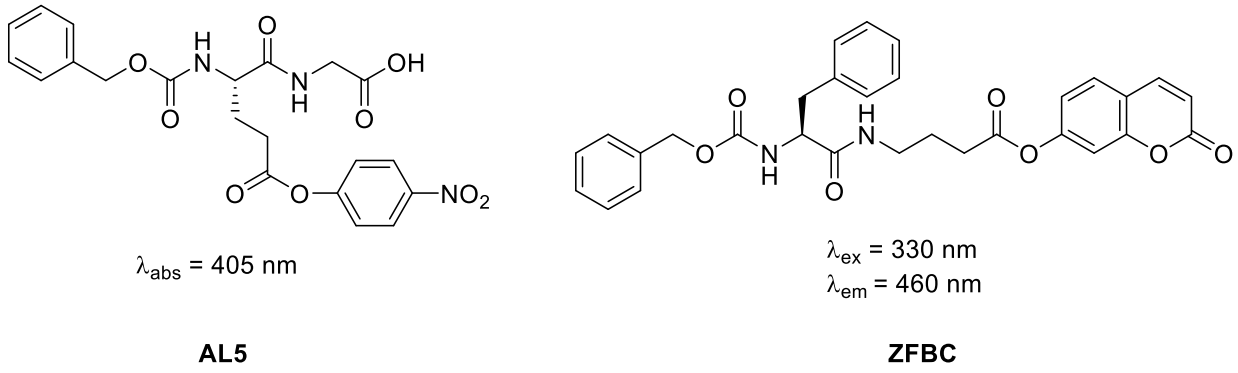

Figure 2.14. Left: chromogenic substrate, AL5, bearing a pNP ester chromophore. Right: fluorogenic substrate, ZFBC, bearing a coumarin ester fluorophore.

The chromogenic compound, AL5, was synthesized as previously described,[33] and evaluated as a substrate for bTG. This substrate is structurally similar to ZQG, but bears a 4-nitrophenyl glutamate ester. Since we observed no activity with ZQG as a substrate for transamidase reactions with bTG, we were skeptical that the enzyme would recognize AL5; nonetheless, the assay is fast and convenient, and it is possible that the ester is better recognized. We performed a preliminary evaluation at one relatively high substrate concentration: the results are shown in Figure 2.15.

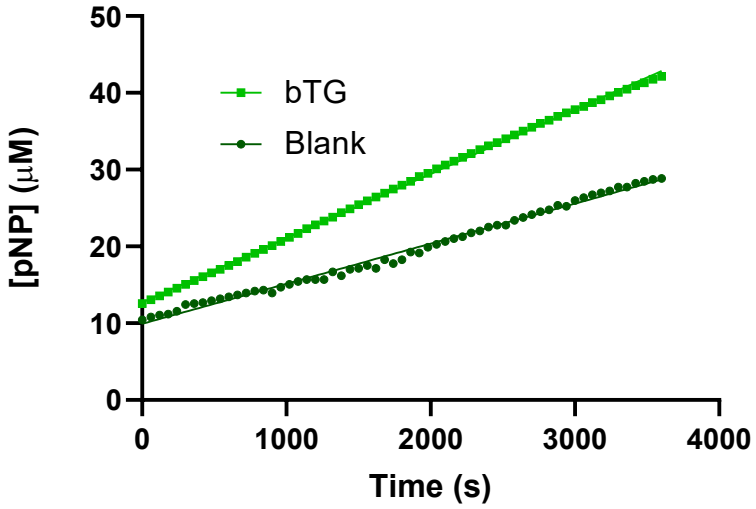

Figure 2.15. Hydrolysis of AL5 by bTG. Reaction conditions: AL5 (100 μM), bTG (8 μM), MOPS buffer (100 mM, pH 7.2). Absorbance values were pathlength-corrected and converted to units of product (4-nitrophenolate) concentration using the extinction coefficient, 8040 $M^{-1}cm^{-1}$. Error bars (2 replicates) are shown, but are smaller than the datapoint symbols.

The substrate AL5 is hydrolyzed by bTG at a rate of 0.19 μM/min, giving a specific activity of 8.4×10^{-4} U/mg of enzyme. While we were pleased to observe activity using this substrate, demonstrating the first instance of hydrolytic activity in bTG, the activity itself is low. The reaction rate in the presence of bTG is only approximately twice that of the blank condition containing no enzyme, representing buffer-mediated hydrolysis of the pNP ester. To further characterize its activity, we performed Michaelis-Menten kinetics with varying concentrations of AL5, as shown in Figure 2.16.

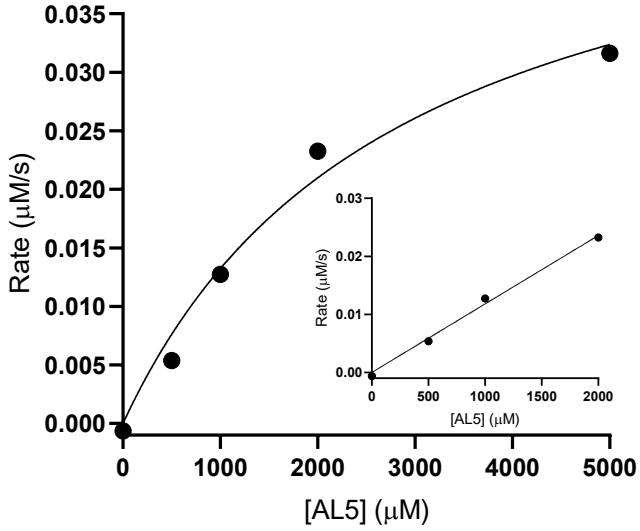

Figure 2.16. Michaelis-Menten plot of AL5 hydrolysis by bTG. Reaction conditions: AL5 (0 – 5000 μM), bTG (8 μM), MOPS buffer (100 mM, pH 7.2). Absorbance values were pathlength-corrected and converted to units of product (4-nitrophenolate) concentration using the extinction coefficient, 8040 $M^{-1}cm^{-1}$. Each rate was corrected by subtracting a blank reaction containing no enzyme at the corresponding concentration of AL5. Inset: linear region of the Michaelis-Menten plot.

Nonlinear regression was performed using the Michaelis-Menten equation as a model, to determine kinetic parameters K_M and k_{cat}. The nonlinear fit revealed a K_M value of 2837 μM, and a V_{max} of 0.051 μM/s, which corresponds to a k_{cat} of 6.4×10^{-3} s^{-1}. These values give an enzymatic efficiency (k_{cat}/K_M) of 2.25 M^{-1} s^{-1}. An estimate of k_{cat}/K_M was also determined *via* linear regression of the first 4 datapoints (See Figure 2.16, inset). This analysis gives an estimated value of 11.8 M^{-1} s^{-1}. To contrast, the kinetic parameters for TG2-mediated hydrolysis of AL5 have been reported as 0.28 s^{-1} (k_{cat}) and 20 μM (K_M), for an efficiency of 14 000 M^{-1} s^{-1}, greater than 6000-fold that of bTG.

As aforementioned, like its parent compound, ZQG, AL5 may not be the optimal substrate scaffold for this enzyme. We, therefore, proceeded to evaluate ZFBC as a substrate for bTG (Figure 2.17). While the reported synthetic route for ZFBC proceeds via the stepwise coupling of Cbz-Phenylalanine and GABA, followed by installation of the coumarin ester,[38] our synthetic route proceeded from the opposite terminus to facilitate later diversification at the amino acid position. Full synthetic details may be found in Figure A2.5 in the Appendix.

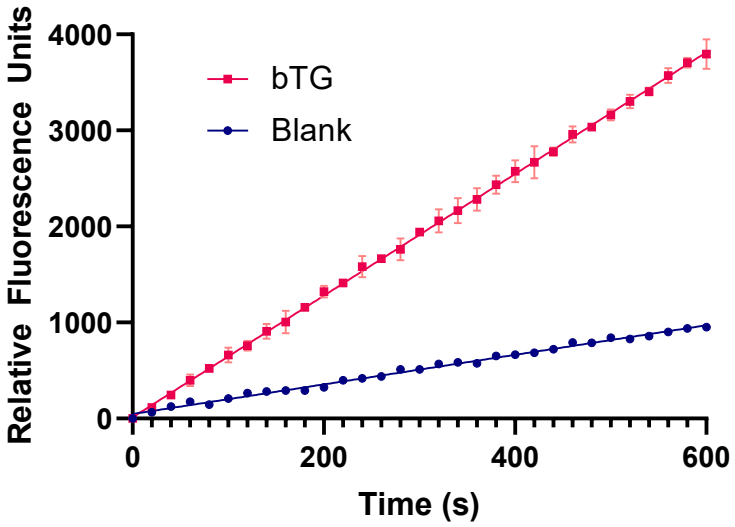

Figure 2.17. Hydrolysis of ZFBC by bTG. Reaction conditions: ZFBC (100 μM), bTG (12 μM), Tris buffer (200 mM, pH 8.4), 37 °C. Data points from the reaction with bTG are averaged from two replicates, with error bars indicating standard deviations. The blank reaction containing no enzyme was acquired as a single replicate. Each dataset was "zeroed" by subtracting the first datapoint from each other value, so as to better visualize slopes.

We were pleased to observe lower apparent background reactivity compared to reactions with AL5, due, in part, to the higher stability of coumarin esters compared to 4-nitrophenolate esters at higher

pH. (For reference, in the literature, reactions with AL5 are performed at pH 7.0[33] whereas those using ZFBC are performed at pH 8.0.[38]) Note that bTG was previously reported to demonstrate optimal activity at pH 8-9,[45,47] thus conducting the reaction at pH 8.4 may have increased the overall activity of the enzyme. However, the specific activity of ZFBC was determined to be 9.03 × 10^{-4} U/mg, similar to that initially observed for AL5. To better characterize its activity, we also performed Michaelis-Menten kinetics using ZFBC as a substrate (Figure 2.18).

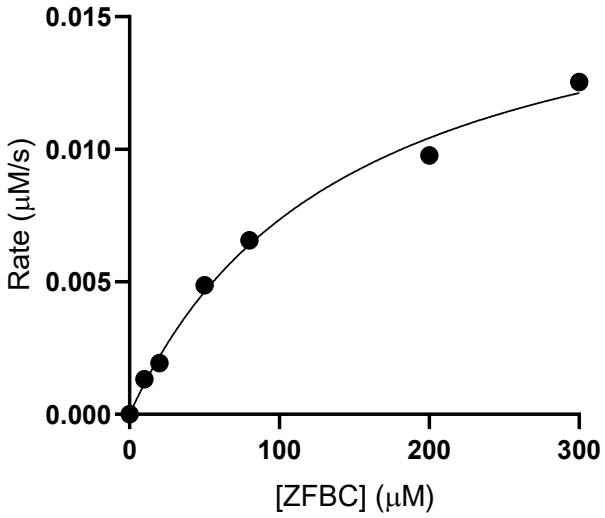

Figure 2.18. Michaelis-Menten plot for the hydrolysis of ZFBC by bTG. Reaction conditions: ZFBC (0-300 μM), bTG (12 μM), Tris buffer (200 mM, pH 8.4), 37 °C. Values were converted from fluorescence units (RFU) to concentration using the slope of a calibration curve of 7-hydroxycoumarin acquired under the same conditions (Figure A2.6 in the Appendix) which was determined to be 948.2 RFU/μM.

Kinetic parameters were determined by fitting Equation 1 to the data and gave values of 144 μM (K_M) and 0.018 μM s^{-1} (V_{max}), which corresponds to a k_{cat} value of 0.002 s^{-1}, and an overall

calculated efficiency of 13 M^{-1} s^{-1}. To compare, TG2 hydrolyzes ZFBC with an overall efficiency of 107 000 M^{-1} s^{-1},[38] over 8000 × higher than that of bTG. However, it was still notable that ZFBC is hydrolyzed more efficiently than AL5 by bTG.

It was also noted that TG2 hydrolyzes a glycine-containing analogue of ZFBC (named ZGBC) with a similar efficiency (139 000 M^{-1} s^{-1}) to that of ZFBC. We were curious about the substrate specificity of bTG for this structure, so we synthesized and evaluated ZGBC as a substrate (Figure 2.19).

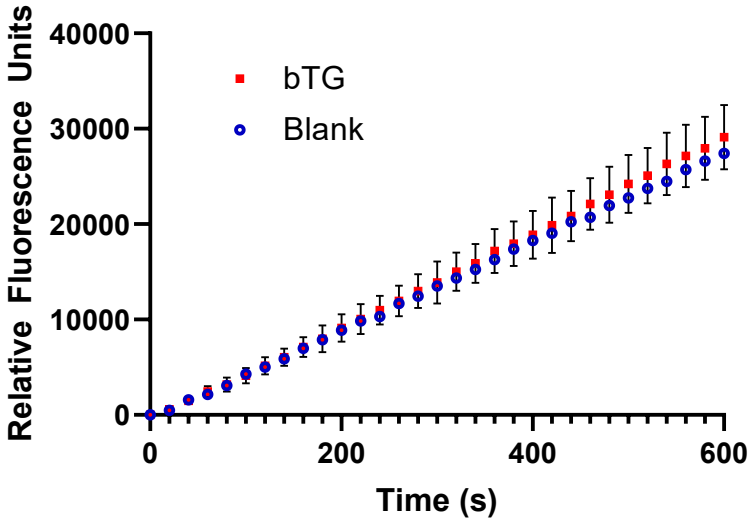

Figure 2.19. Reaction of ZGBC with bTG. Reaction conditions: ZGBC (100 μM), bTG (12 μM), Tris buffer (200 mM, pH 8.4), 37 °C. Data points from the reaction with bTG are averaged from two replicates, with error bars indicating standard deviations. The blank reaction containing no enzyme was acquired as a single replicate. Each dataset was "zeroed" by subtracting the first datapoint from each other value, so as to better visualize slopes.

We were surprised to observe a distinct lack of reactivity of bTG towards ZGBC, in that the reaction condition tracked closely with the blank. However, the absolute values of the fluorescence observed are significantly higher than those observed for ZFBC, perhaps suggesting that this substrate is more susceptible to spurious hydrolysis by the buffer. From these preliminary data, we concluded that bTG must demonstrate significant selectivity for the amino acid group present on this scaffold.

To further investigate this phenomenon, two additional analogues of ZFBC were synthesized: ZABC, containing an alanine group, and ZLBC, containing leucine. Reaction rates are shown in Figure 2.20. Full data may be found in Figure A2.7 in the Appendix.

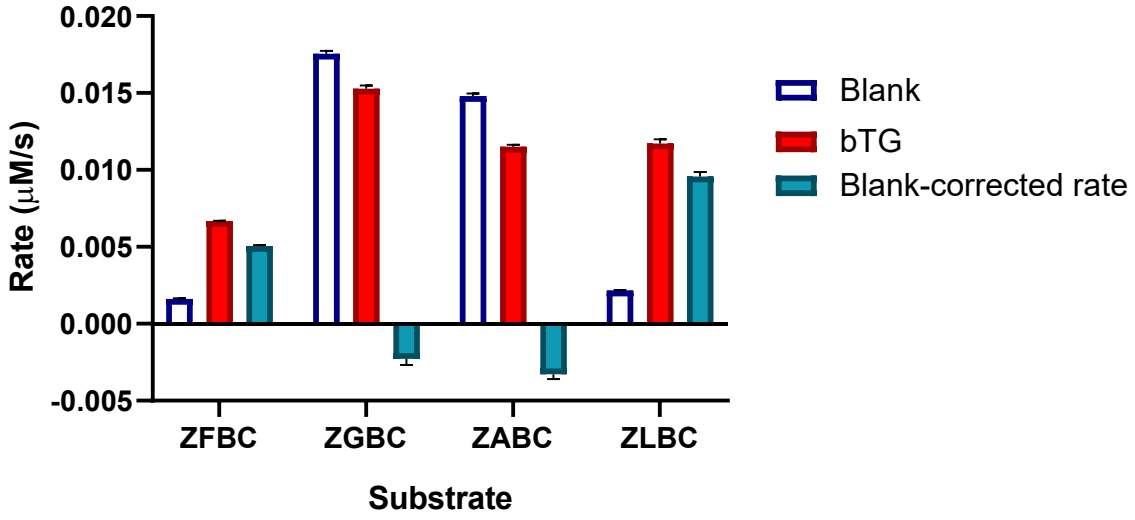

Figure 2.20. Hydrolysis of ZFBC analogues in the presence (red, solid) or absence (blue, outline) of enzyme, alongside blank-subtracted (turquoise, solid) rates. Reaction conditions: Substrate (50 μM), bTG (12 μM), Tris buffer (200 mM, pH 8.4), 37 °C.

While the leucine derivative, ZLBC, demonstrates higher activity than ZFBC, substrates ZGBC and ZABC demonstrated a lower apparent rate of hydrolysis than that of the blank, suggesting no recognition of these substrates. However, comparing the blank-corrected rates alone is somewhat misleading. Looking at the enzyme-mediated rates themselves (prior to blank correction), ZABC demonstrates a near-identical rate of hydrolysis to that of ZLBC, and the un-corrected rate of ZGBC hydrolysis is the highest among all the evaluated substrates. Conversely, greater variability is observed due to spontaneous, buffer-mediated hydrolysis (in the absence of enzyme) for each substrate, than in the presence of enzyme. This is surprising, given that these substrates are electronically similar, and the coumarin group should not be more or less activated due to the small variations in structure at the amino acid. Overall, this result led us to question whether hydrolysis of these substrates was in fact being catalyzed by bTG, or whether the mere presence of protein modulated nonspecific hydrolysis of these substrates.

To verify whether the observed hydrolysis was being mediated by the catalytic machinery of bTG, we prepared an inactive mutant by replacing the catalytic cysteine (C116) with an alanine residue, and evaluated its activity against ZFBC (Figure 2.21).

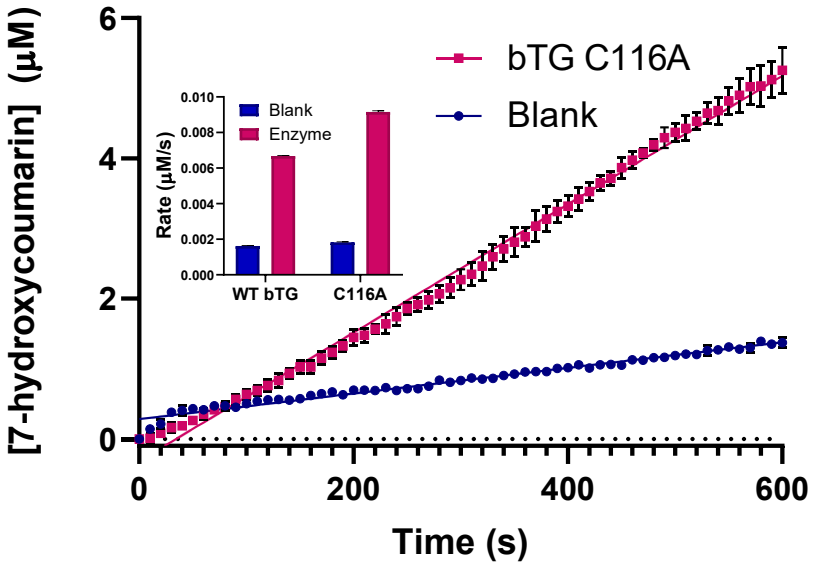

Figure 2.21. Hydrolysis of ZFBC in the presence (red squares) or absence (blue circles) of inactive mutant bTG C116A. Datapoints represent averages and error bars represent standard deviations of 3 replicates. Reaction conditions: Substrate (100 μM), bTG (12 μM), Tris buffer (200 mM, pH 8.4), 37 °C. Inset: comparison of hydrolysis rates in the presence of active (WT) and inactive (C116A) bTG.

To our immense amusement,[1] we observed the same activity in the presence of the inactive mutant as with the active enzyme, confirming that hydrolysis is not catalyzed by the active site cysteine. We hypothesized that a nucleophilic surface residue may be responsible for this activity, and that the mere presence of protein could be "catalyzing" the hydrolysis; thus, we evaluated the effect of varying concentrations on BSA on the rate of ZFBC hydrolysis (Figure 2.22).

[1] After two years of effort, one may as well laugh at a result like this.

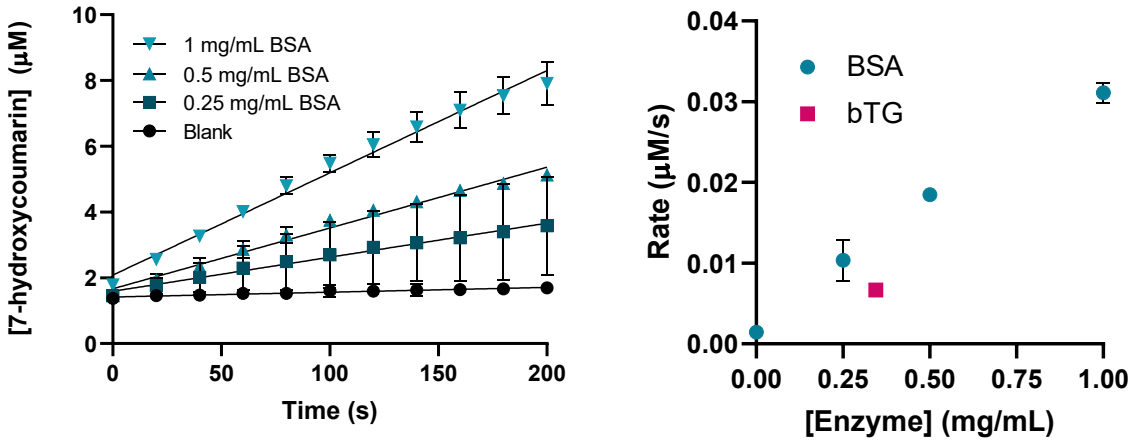

Figure 2.22. Left: hydrolysis of ZFBC in the presence of varying concentrations of BSA. Reaction conditions: Substrate (100 μM), BSA (0, 0.25, 0.5, 1 mg/mL), Tris buffer (200 mM, pH 8.4), 37 °C. Right: rates plotted against concentration of BSA, alongside the rate of ZFBC hydrolysis observed in the presence of 0.345 mg/mL (12 μM) bTG.

Not only is BSA capable of promoting hydrolysis of ZFBC in a concentration-dependent manner, but it also enhances the rate of hydrolysis *more efficiently* than does bTG. This lends credence to the hypothesis that a surface residue is promoting hydrolysis, and BSA, as a larger protein with a correspondingly larger surface area, is more likely to have one or more surface-exposed nucleophiles. It should be noted here that, while BSA leads to an observed increase in the hydrolysis rate of ZFBC that is comparable to that of bTG, this effect would be negligible when compared to an enzyme that recognizes ZFBC specifically. For instance, TG2, as aforementioned, has a ~8000-fold greater efficiency in hydrolyzing ZFBC than bTG, and so spurious hydrolysis by a nonspecific protein as BSA would constitute a negligible increase over background hydrolysis in this context.

2.3. Conclusion

We performed several standard transglutaminase assays to probe the substrate specificity of bTG, with the intent to investigate and quantify its cross-linking and hydrolysis activities. We observed no activity with any small molecule probe: the hydroxamate and GDH assays suggested no activity with small molecule or peptidic glutamine-containing substrates. The enzyme demonstrated no hydrolytic activity against isopeptidic mimic substrates: although convoluted by the low solubility of the substrates evaluated, no increase in fluorescence was observed whatsoever, suggesting that these substrates were not recognized, or else that bTG does not demonstrate isopeptidase activity. Furthermore, small molecule esters were not specifically recognized and hydrolyzed by bTG. This result could suggest that the active site has limited access to water, or that the small molecules, consistent with the trend of glutamine-containing substrates, are simply not recognized by bTG. Overall, the clearest (and, arguably, only) activity was observed when bTG performed cross-linking reactions with proteins. While this activity has previously been observed qualitatively *via* a discontinuous approach, we applied a direct, continuous, and quantitative variation of this assay to bTG. This allowed for the first time a direct comparison of the rates of bTG-mediated crosslinking with that of other well-characterized transglutaminases. Unfortunately, based on this activity assay, the rates of bTG-mediated crosslinking were substantially lower than any other transglutaminase. These results taken together suggest that bTG, despite its structural simplicity, is a highly specific and specialized enzyme. While its physical properties are attractive as a biocatalyst, we suggest that its applications may be limited to cross-linking of certain target protein substrates.

This first investigation into the activity of bTG was ultimately a learning experience, and the best lessons are learned the hard way. We originally sought an enzyme capable of degrading nylon, and took a rational, structure-based approach with bTG. However, going into this project, our

knowledge of the activity of bTG was too far removed, and our methods possibly too indirect, to serve that goal. In retrospect, we would take a different approach, and begin by identifying an enzyme already known to demonstrate the desired (linear amide hydrolysis) activity. As will be shown in later chapters of this thesis, an enzyme with improved biocatalytic characteristics (e.g. thermal stability, high activity, active expression) is easier to engineer than novel activity in an existing enzyme. Nevertheless, these results, while largely a treatise on "what not to do", will help inform subsequent studies: not only for those studying bTG, but all those in the field of biocatalysis.

2.4. Materials and Methods

2.4.1. General remarks

All reagents and solvents were purchased from commercial sources and used without further purification. ^{1}H- and ^{13}C-NMR spectra were recorded on Bruker 400 MHz or 600 MHz spectrometers, and chemical shifts were reported in ppm, referenced to the deuterated solvent peak. High resolution mass spectra were obtained with a quadrupole time-of-flight (QTOF) analyzer and electrospray ionization (ESI). Thin-layer chromatography (TLC) was performed using aluminium-backed silica plates and visualized using UV light, unless otherwise specified. SDS-PAGE was performed using Bio-Rad Mini-Protean TGX pre-cast, stain-free gels (4-20% polyacrylamide) and visualized using a Bio-Rad ChemiDoc MP imager. Agarose gels were prepared fresh prior to use, containing 1% agarose (w/v) and 1 μg/mL ethidium bromide. DNA was separated on agarose gel at 105 V in Tris-Acetate-EDTA (TAE) buffer and visualized using a Bio-Rad ChemiDoc MP imager. Assays were performed using either a plate reader (Biotek Synergy H1), a UV-vis spectrophotometer (Varian Cary 100 Bio, 1 cm path length), or a fluorescence spectrophotometer (Varian Cary Eclipse, 1 cm path length) as specified.

2.4.1. Molecular Biology Methods

Construction of the bTG expression plasmid

The gene for bTG was constructed by reverse-translation of the corresponding amino acid sequence,[48] with the addition of a GSS linker at the C-terminus. The sequence was codon-optimized for *E. coli*, modified to bear restriction sites for NdeI (N-terminal) and XhoI (C-terminal), and synthesized by GeneArt (Thermo-Fisher). The gene was cloned into a pET21a(+) expression vector, transformed into *E. coli* Top10 cells (selected on agar plates containing 100 μg/mL ampicillin), extracted using a plasmid miniprep kit (Omega Bio-tek) and sequenced to confirm the correct insertion.

Expression and purification of bTG

Expression was adapted from a reported protocol.[46] Briefly, the expression plasmid for bTG was transformed into *E. coli* BL21 DE3 cells and selected on agar plates containing 100 μg/mL ampicillin. Isolated colonies were picked and used to inoculate 5 mL precultures in LB medium containing 100 μg/mL ampicillin, which were grown overnight with shaking at 37 °C. These cultures were used to inoculate expression cultures (1% v/v), containing ZYM-5052 autoinducing medium.[54] Expression cultures were shaken for 20 hours at 37 °C. Cells were pelleted by centrifugation at 4000 × g for 20 minutes at 4 °C. The cell pellet was resuspended in Buffer A (20 mM CAPS (pH 10.0), 0.5 M NaCl, 10 mM imidazole) (2% culture volume), and lysed by homogenization (Avestin, 19000 lb in^{-2}). The cell lysate was clarified by centrifugation at 10 000 × g for 1 hour.

The resulting clarified lysate was incubated with Ni-IDA superflow resin (TaKaRa Biotek) (1/1000 culture volume, pre-equilibrated with Buffer A), for 1 hour at 4 °C. Nonspecific proteins were removed by successive washes of Buffer A containing 10% glycerol (3 × 10 column volumes), then Buffer A containing 40 mM imidazole (2 × 10 column volumes). Finally, bTG was eluted with buffer A containing 150 mM imidazole (2 × 10 column volumes). Fractions were evaluated by SDS-PAGE and fractions containing pure bTG were pooled, then concentrated by ultrafiltration using Amicon tubes with a 10-kDa molecular weight cutoff (Sigma-Aldrich). The concentrated protein was buffer-exchanged by three subsequent cycles of dilution and ultrafiltration using storage buffer (10 mM CAPS (pH 10.0), 0.1 M NaCl, 15% glycerol). The concentrated protein was quantified by Bradford assay (Bio-Rad), aliquoted, and frozen at -80 °C for later use.

Preparation of bTG C116A inactive mutant

The mutation C116A was created by site-directed mutagenesis using full-plasmid PCR. Custom primers were purchased from Integrated DNA technologies where the C116A mutation was encoded on the forward primer, and PCR was performed using Q5 High-Fidelity DNA polymerase (New England Biolabs) and the wild-type bTG/pET21a(+) construct as the template. Following amplification of the gene as confirmed by agarose gel electrophoresis, the DNA was purified (E.Z.N.A. Cycle Pure Kit, Omega BioTek) then a digest of the template was performed using DpnI (New England Biolabs). Following digestion, the amplicon was purified again using the Cycle Pure Kit, then phosphorylated (T4 PNK, New England Biolabs) and ligated (T4 DNA Ligase, New England Biolabs). The circularized amplicon was then transformed into chemically competent *E.*

coli Top10 cells in the presence of 100 μg/mL ampicillin. Five colonies containing mutant plasmid were picked, then DNA was extracted (E.Z.N.A Plasmid DNA mini kit, Omega BioTek) and sequenced (Génome Québec). Expression was performed as described for wild-type bTG.

2.4.2. Assay Methods

Hydroxamate assay

The hydroxamate assay was conducted as previously reported,[39] using bTG (92 μM) and either Cbz-Gln-Gly-OH or peptides Ac-YAHQAHY-OH or Ac-PATQRAY-OH as acyl donor substrates. Briefly, to a 200 μL solution containing acyl donor substrate (67 mM), hydroxylamine (222 mM), EDTA (2.2 mM) and Tris-Acetate buffer (444 mM, pH 6.5) was added bTG (50 μL) to a final concentration of 92 μM. The reaction was incubated for 10 minutes at 37 °C, after which it was quenched through addition of HCl (0.8 mM, 250 μL), $FeCl_3$ (2 M, 250 μL) and trichloroacetic acid (0.3 M, 250 μL). The resulting solution was centrifuged for 5 minutes at 14 000 RPM to remove any precipitated protein, then absorbance was determined at 525 nm using a UV-Vis spectrophotometer. Reactions evaluating peptidic substrates were performed under varying pH conditions (Tris buffer pH 7.2, 8.4, and 9.0).

The experiment was also performed with microbial transglutaminase using 1.5 μM of mTG, and Cbz-Gln-Gly-OH as a substrate.

GDH-coupled assay

The reaction was adapted from a published protocol.[39] Stock solutions of MOPS (2000 mM, pH 7.2), EDTA (10 mM), NADH (5 mM), alpha-ketoglutarate (100 mM), glutamate dehydrogenase (10 U/100 μL) and Gly-OMe (100 mM) were prepared in water or 200 mM MOPS buffer (for GDH). All were prepared and stored at 4°C for later use except for NADH and GDH stocks, which were prepared within an hour of use. Each stock solution (200 μL) was combined, and the resulting solution was diluted to 1.5 mL to produce Mixture 1.

A stock solution of acyl donor substrate ZQG (50 mM) was prepared in MOPS buffer (200 mM, pH 7.2), with the addition of one equivalent of NaOH to improve solubility. Dilutions of this solution (0, 5, 10, 15, 20, 30, 40, 50 mM) were prepared in water. Each of these dilutions (40 μL) were added to their respective wells in a 96 well plate.

To each well was added 150 μL of Mixture 1. The resulting solutions were allowed to incubate for 5 minutes. Then, the reaction was initiated through addition of 10 μL of bTG (71.4 or 35.7 μM) to each well (defrosted immediately before use), and absorbance of each well was monitored at 340 nm, at 37°C over 10 minutes using a 96-well plate reader.

The reaction was performed as described above using the acyl donor substrate YAHQAHY, at concentrations varying from 0-1000 μM.

Discontinuous dansylcadaverine incorporation assay

A 200-μL reaction solution was prepared containing protein (BSA or dimethylcasein, 60 μM), dansylcadaverine (500 μM) and MOPS buffer (200 mM, pH 8.0). The reaction was initiated through addition of bTG (8 μM). Aliquots (10 μL) were removed at varying time points from 0-18 hours. The aliquots were analyzed by SDS-PAGE and by irradiation at 365 nm to detect dansyl

incorporation. The gel was stained with Coomassie Brilliant Blue dye to visualize total protein content.

Continuous dansylcadaverine incorporation assay - Fluorimeter

Reaction mixtures (500 µL) were prepared containing dansylcadaverine (60 µM), dimethylcasein (80 µM), MOPS (100 mM, pH 8.0), and bTG (0, 4, 8, 16 µM). The reaction was monitored using a fluorescence spectrophotometer at 520 nm (slit width: 10 nm) with an excitation wavelength of 335 nm (slit width: 5 nm) and a PMT voltage of 600 V. An emission scan (λ_{ex} = 335 nm) was performed before and after kinetics on the reaction mixture containing 8 µM bTG.

General procedure (**GP1**) for the continuous dansylcadaverine incorporation assay on the plate reader

The following stock solutions were prepared freshly immediately before use:

- Dansylcadaverine: 1.6 mM in H_2O. Dissolution was aided through dropwise addition of 1 M HCl, then diluted with H_2O to a final concentration of 1.6 mM.
- Dimethylcasein: 2 mM in H_2O, mixed carefully by pipette to aid in dissolution with minimal formation of bubbles
    - From this stock, 6 or 8 dilutions were prepared at 10 × the final reaction concentration. Dilution ranges were optimized for each enzyme.
- Reaction buffer, either:

- Buffer 1: 250 mM Tris pH 7.5
- Buffer 2: 250 mM Tris pH 7.5, 37.5 mM $CaCl_2$

Reaction solutions were prepared as follows: to each well in a 96-well plate was added dimethylcasein at varying concentrations (20 µL of 10 × stock), buffer (40 µL), enzyme (concentration optimized for each isozyme) and water, up to 180 µL. Then, reactions were initiated through addition of dansylcadaverine stock (20 µL).

Reactions were monitored by fluorescence using a 96-well plate reader under the following conditions: λ_{Ex} = 335 nm, λ_{Em} = 518 nm, excitation slit width = 17.0 nm, emission slit width = 17.0 nm, detector gain = 80. Details for each enzyme experiment are described below. In all cases, initial slopes were determined from the linear region of each plot.

bTG: Enzyme was added to a final concentration of 10 µM; the reaction was performed in the presence of Buffer 1; dimethylcasein concentrations ranged from 0-100 µM; fluorescence measurements were acquired every 10 minutes for 16 hours.

mTG: Enzyme was added to a final concentration of 0.5 µM; the reaction was performed in the presence of Buffer 1; dimethylcasein concentrations ranged from 0-50 µM; fluorescence measurements were acquired every 5 minutes for 4 hours.

TG1: Enzyme was added to a final concentration of 0.1 µM; the reaction was performed in the presence of Buffer 2; dimethylcasein concentrations ranged from 0-100 µM; fluorescence measurements were acquired every 1 minute for 1 hour.

TG2: Enzyme was added to a final concentration of 0.5 μM; the reaction was performed in the presence of Buffer 2; dimethylcasein concentrations ranged from 0-10 μM; fluorescence measurements were acquired every 2 minutes for 20 minutes.

TG3: Enzyme was added to a final concentration of 0.1 μM; the reaction was performed in the presence of Buffer 2; dimethylcasein concentrations ranged from 0-100 μM; fluorescence measurements were acquired every 2 minutes for 10 hours.

TG6: Enzyme was added to a final concentration of 0.1 μM; the reaction was performed in the presence of Buffer 2; dimethylcasein concentrations ranged from 0-100 μM; fluorescence measurements were acquired every 30 seconds for 30 minutes.

FXIII: Enzyme was added to a final concentration of 0.05 μM; the reaction was performed in the presence of Buffer 2; dimethylcasein concentrations ranged from 0-50 μM; fluorescence measurements were acquired every 30 seconds for 10 minutes.

Hydrolysis of compounds **3a-d** by bTG

Stock solutions were prepared of compound **3** at 10 × the reaction concentration, in a solution of 1:1 DMSO: H_2O. Reaction mixtures were prepared by combining **3** (20 μL) MOPS buffer (10 μL of a 2000 mM stock, pH 8.0), and water up to 180 μL. Reactions were initiated through the addition of 20 μL of bTG (to a final concentration of 8 μM) or 20 μL of 200 mM MOPS buffer, in the case of the blank. The reaction was monitored by fluorescence on a 96-well plate reader, with an excitation wavelength of 325 nm (slit width 13 nm), an emission wavelength of 518 nm (slit width 13 nm), and a detector gain of 100. Reactions were performed for 1 hour at 30 °C.

Hydrolysis of AL5 by bTG

Stock solutions were prepared containing AL5 (20 mM in DMSO) and MOPS (2 M, pH 7.2). The solution of AL5 was further diluted to 20 × the assay concentration in DMSO. Into each well of a 96-well plate was added MOPS (10 μL), bTG (to a final concentration of 8 μM), and water up to 190 μL. The reaction was initiated through addition of 10 μL of AL5. The reaction was monitored at 405 nm for 1 hour at 25 ℃ using a 96-well plate reader.

General setup for hydrolysis of ZFBC and analogues by bTG

Tris buffer (200 mM, pH 8.4) was prepared in advance and stored at 4 °C until use. A stock solution of ZFBC (or analogue) substrate (4 mM) was prepared in DMSO immediately prior to use, then further diluted to 20 × the assay concentration in DMSO. Then, to each well in a 96-well plate was added water (150 μL), substrate (10 μL) and buffer (20 μL). The reaction was initiated through addition of bTG (20 μL, to a final concentration of 12 μM). The reaction was monitored using a 96-well plate reader at 460 nm (slit width: 13.5 nm) with an excitation wavelength of 330 nm (slit width: 13.5 nm) and a detector gain of 100, for 10 minutes at 37 ℃.

2.4.3. Synthetic Methods

Peptidic substrates Ac-YAHQAHY-OH and Ac-PATQRAY-OH were synthesized using a CEM Liberty Blue peptide synthesizer, and purified by preparative HPLC (Gilson).

Ac-PATQRAY-OH: HRMS (ESI) calc'd for $C_{37}H_{58}N_{11}O_{12}$ ($[MH]^+$): 848.4266, found: 848.4281.

Ac-YAHQAHY-OH: HRMS (ESI) calc'd for $C_{43}H_{55}N_{12}O_{12}$ ($[MH]^+$): 931.4062, found: 931.4070.

Synthesis of compounds **3a-d**

General procedure (**GP2**) for the synthesis of Compound **1**

To a stirred solution of amine (1 equiv.) and *N,N*-diisopropylethylamine (3 equiv.) in DCM (to an amine concentration of ~0.08 M) was added sulfonyl chloride (either dansyl or dabsyl chloride, 1.05 equiv.). The reaction was monitored by TLC analysis (1:1 hexanes: ethyl acetate, visualized by ninhydrin stain). Upon completion, the reaction mixture was diluted with DCM (10 mL) unless otherwise specified, and washed with water (2 × 15 mL). The aqueous washes were combined and extracted once with DCM (15 mL), then the organic phases were combined and washed with aqueous saturated $NaHCO_3$ (20 mL). The organic phase was collected, dried over $MgSO_4$ and evaporated. The residue was triturated with Et_2O (2 × 10 mL) and the ether layers decanted off to give the product.

Compound 1a. The reaction was performed following **GP2** on a 350 mg (1.176 mmol) scale of N-ϵ-Boc-lysine-OMe · HCl, with dabsyl chloride as the sulfonyl chloride. Following purification, the product was isolated as a flaky orange solid (636 mg, >95%). ^{1}H NMR (400 MHz, $CDCl_3$) δ 7.94 (m, 6H), 6.81 (d, J = 8.4 Hz, 2H), 5.26 (d, J = 8.9 Hz, 1H), 4.56 (s, 1H), 3.93 (m, 1H), 3.49 (s, 3H), 3.16 (s, 6H), 3.07 (m, 2H), 1.75 (m, 1H), 1.65 (m, 1H), 1.44 (m, 13H). ^{13}C NMR (101 MHz, $CDCl_3$) δ 171.99, 156.01, 138.90, 128.27, 122.27, 112.17, 77.20, 55.55, 52.62, 40.67, 40.02, 32.84, 29.34, 28.41, 22.06. HRMS (ESI) calc'd for $C_{26}H_{37}N_5O_6SNa$ ($[MNa]^+$): 570.2362, found: 570.2362.

Compound 1b. The reaction was performed following **GP2** on a 600 mg (2.022 mmol) scale of N-ϵ-Boc-lysine-OMe · HCl, with dansyl chloride as the sulfonyl chloride. Following completion of the reaction, the reaction mixture was evaporated in vacuo, and the residue redissolved in EtOAc purified by extraction as described in the general method. Following evaporation after washes, the product was isolated as a dark yellow, sticky foam (935 mg, 94%). ^{1}H NMR (400 MHz, $CDCl_3$) δ 8.53 (d, J = 8.5 Hz, 1H), 8.31 (d, J = 8.7 Hz, 1H), 8.22 (dd, J = 1.2, 7.3 Hz, 1H), 7.57 (dd, J = 7.6,

8.6 Hz, 1H), 7.49 (dd, *J* = 7.4, 8.5 Hz, 1H), 7.19 (d, *J* = 7.5 Hz, 1H), 5.69 (d, *J* = 8.5 Hz, 1H), 4.46 (s, 1H), 3.85 (m, *J* = 4.4 Hz, 1H), 3.27 (s, 1H), 2.86 (s, 1H), 2.08 (s, 1H), 1.56 (q, *J* = 7.0 Hz, 1H), 1.42 (s, 1H), 1.14 (q, *J* = 5.3 Hz, 1H).

Compound 1c. The reaction was performed following **GP2** on a 255 mg (1.261 mmol) scale of *N*-Boc cadaverine, with dabsyl chloride as the sulfonyl chloride. Following purification, the product was isolated as a red powder (481 mg, 78%). ^{1}H NMR (400 MHz, $CDCl_3$) δ 7.92 (m, 6H), 6.75 (d, 2H), 4.66 (br. t., 1H), 4.55 (br. s, 1H), 3.15 (m, 6H), 3.06 (q, 2H), 2.97 (q, 2H), 1.53 (m, 2H), 1.43 (m, 11H), 1.26 (m, 2H).

Compound 1d. The reaction was performed following **GP2** on a 412 mg scale of *N*-Boc cadaverine, with dansyl chloride as the sulfonyl chloride. Following purification, the product was isolated as a yellow foam (683 mg, 83%). ^{1}H NMR (400 MHz, $CDCl_3$) δ 8.55 (d, *J* = 8.5 Hz, 1H), 8.29 (d, *J* = 8.6 Hz, 1H), 8.25 (dd, *J* = 2.8 Hz, 1H), 7.55 (m, *J* = 4.7 Hz, 2H), 7.19 (d, *J* = 7.4 Hz, 1H), 4.66 (br. t, *J* = 6.1 Hz, 1H), 4.40 (br. s, 1H), 2.89 (m, 10H), 1.43 (s, 9H), 1.38 (m, 2H), 1.28 (m, 2H), 1.18 (m, 2H).

General procedure (**GP3**) for the synthesis of Compound **2**

Compound **1** (1 equiv.) was stirred in HCl (4 M in dioxane, ~16 equiv.). DCM (~4 volumes) was added to aid in precipitation of the product. The reaction was monitored by TLC analysis (1:1 hexanes: ethyl acetate). Following consumption of the starting material, the reaction mixture was evaporated in vacuo, then co-evaporated several times with DCM. To the resulting solid was added Et_2O, and the solid manipulated by stirring and/or sonication until a powder was acquired. The

supernatant was decanted off and the resulting solid was dried under vacuum to give the HCl salt intermediate.

Carboxylic acid (1.1 equiv.) was dissolved in DCM (~0.1 M), then HBTU (2 equiv.) and DIPEA (5 equiv.) was added. The reagents were stirred for 30 minutes, after which the HCl salt intermediate (1 equiv.) was added. The reaction was monitored by TLC (5% MeOH in DCM). Upon completion, the reaction mixture was diluted in DCM (15 mL), washed with an equal volume of saturated aqueous $NaHCO_3$, then the aqueous phase was extracted with 15 mL of DCM. The organic phases were combined, washed with 15 mL of brine, then dried over $MgSO_4$ and evaporated. The residue was purified by flash chromatography. Fractions containing product were evaporated, then triturated with Et_2O to give the purified product.

Compound **2a**. The reaction was performed following **GP3** using compound **1a** as the Boc-protected amine, and *N*-Boc-glutamic acid α-methyl ester as the carboxylic acid. The product was purified by chromatography using an elution gradient of 0-10% iPrOH in DCM. Product was isolated as an orange solid (190 mg, 95%). ^{1}H NMR (400 MHz, $CDCl_3$) δ 7.90 (m, 6H), 6.76 (m, 2H), 6.12 (s, 1H), 5.33 (t, J = 9.6 Hz, 2H), 4.28 (m, 1H), 3.93 (m, 1H), 3.74 (s, 3H), 3.47 (s, 3H), 3.23 (m, 2H), 3.12 (s, 6H), 2.27 (m, 2H), 2.19 (m, 1H), 1.93 (m, 1H), 1.78 (m, 1H), 1.67 (m, 1H), 1.44 (m, 13H). ^{13}C NMR (101 MHz, $CDCl_3$) δ 172.8, 171.9, 155.7, 153.2, 143.2, 138.9, 128.2, 125.8, 122.5, 111.5, 77.2, 55.4, 53.0, 52.6, 52.5, 40.3, 39.0, 32.6, 29.0, 28.3, 22.0.

Compound **2b**. The reaction was performed following **GP3** using compound **1b** as the Boc-protected amine, and *N*-Boc-glutamic acid α-methyl ester as the carboxylic acid. The product was purified by chromatography using an elution gradient of 0-2.5% MeOH in a 1:1 solution of DCM and hexanes. The product was isolated as a light green foam/oil (125 mg, 37%). NMR not available. HRMS (ESI) calc'd for $C_{30}H_{44}N_4O_9S$ ($[MNa]^+$): 659.2727, found: 659.2709.

Compound **2c**. The reaction was performed following **GP3** using compound **1c** as the Boc-protected amine, and N-Boc-GABA as the carboxylic acid. The product was purified by chromatography using an elution gradient of 0-3% MeOH in 1:1 DCM: hexanes. The product was isolated as an orange film (131 mg, 53%). NMR data not available. HRMS (ESI) calc'd for $C_{28}H_{42}N_6O_5S$ ($[MNa]^+$): 597.2835, found: 597.2846.

Compound **2d**. The reaction was performed following **GP3** using compound **1d** as the Boc-protected amine, and N-Boc-GABA as the carboxylic acid. The product was purified by chromatography using an elution gradient of 0-2% MeOH in 1:1 DCM: hexanes. The product was isolated as a yellow-green foam (168 mg, 53%). NMR data not available. HRMS (ESI) calc'd for $C_{26}H_{40}N_4O_5S$ ($[MNa]^+$): 543.2617, found: 543.2630.

General procedure (**GP4**) for the synthesis of Compound **3**

Compound **2** (1 equiv.) was dissolved in 1:1 DCM: Et_2O (~0.02 M), then HCl (4 M in dioxane, 0.2 volumes) was added. The reaction was monitored by TLC (5% MeOH in DCM), and the product precipitated out of the reaction mixture. Upon completion of the reaction by TLC, the supernatant was decanted off, and the precipitate was resuspended in 10 mL Et_2O, stirred briefly, then decanted to remove the supernatant. The resulting solid was dried under high vacuum to give the intermediate product.

The amine HCl salt (1 equiv.) was dissolved in DCM (to a concentration of ~0.03 M of 2) and DIPEA (4 equiv.), then sulfonyl chloride (1.1 equiv.) was added. The reaction was monitored by TLC (5% MeOH in DCM, unless otherwise specified). Upon completion by TLC analysis, the reaction mixture was diluted in DCM (10 mL), and washed with aqueous AcOH (10%, 2 × 15 mL),

then brine (10 mL). The organic phase was dried over $MgSO_4$ and evaporated to give an orange solid, which was washed with Et_2O, then dried under vacuum.

Compound **3a**. The reaction was performed following **GP4** using compound **2a** as the Boc protected amine, and dansyl chloride as the sulfonyl chloride. The product was isolated as a flaky orange solid (107 mg, 86%). ^{1}H NMR (400 MHz, $CDCl_3$) δ 8.53 (d, *J* = 8.5 Hz, 1H), 8.30 (d, *J* = 8.7 Hz, 1H), 8.20 (dd, *J* = 1.2, 7.3 Hz, 1H), 7.90 (m, 6H), 7.59 (dd, *J* = 7.6, 8.6 Hz, 1H), 7.50 (q, *J* = 7.6, 8.6 Hz, 1H), 7.19 (d, *J* = 7.4 Hz, 1H), 6.76 (m, 2H), 5.78 (d, *J* = 8.9 Hz, 1H), 5.61 (t, *J* = 5.1 Hz, 1H), 5.42 (d, *J* = 9.1 Hz, 1H), 3.96 (m, 1H), 3.87 (m, 1H), 3.47 (s, 3H), 3.18 (m, 5H), 3.12 (s, 6H), 2.88 (s, 6H), 2.24 (m, 2H), 2.06 (m, 1H), 1.87 (m, 1H), 1.77 (m, 1H), 1.68 (m, 1H), 1.46 (m, 4H). ^{13}C NMR (101 MHz, $CDCl_3$) δ 172.0, 171.8, 171.3, 155.7, 153.2, 143.6, 139.0, 134.3, 130.8, 129.8, 129.7, 129.6, 128.5, 128.2, 125.8, 123.2, 122.5, 118.9, 115.3, 111.5, 55.6, 55.4, 52.6, 52.2, 45.4, 40.3, 38.9, 32.5, 31.9, 28.5, 28.5, 21.9. HRMS (ESI-QTOF) m/z $[M+Na]^+$ calc'd for $C_{39}H_{49}N_7O_9S_2Na$ 846.2931; found 846.2931.

Compound **3b**. The reaction was performed following **GP4** using compound **2b** as the Boc-protected amine, and dabsyl chloride as the sulfonyl chloride. The reaction was monitored by TLC using 1:1 hexanes: ethyl acetate as an eluent. Following extraction, the organic material was purified by flash chromatography: impurities were removed by washing with 1:1 hexanes: ethyl acetate, then the product was eluted with 5% MeOH in DCM. The product was collected as a light orange powder (42 mg, 44%). ^{1}H NMR (400 MHz, $CDCl_3$) δ 8.56 (d, *J* = 8.2 Hz, 1H), 8.34 (d, *J* = 8.4 Hz, 1H), 8.23 (dd, *J* = 1.1, 7.3 Hz, 1H), 7.90 (m, 6H), 7.58 (dd, *J* = 7.6, 8.5 Hz, 1H), 7.52 (t, *J* = 7.9 Hz, 1H), 7.21 (d, *J* = 7.5 Hz, 1H), 6.76 (m, 2H), 5.72 (m, 1H), 5.62 (d, *J* = 9.0 Hz, 1H), 3.91 (m, 2H), 3.47 (s, 3H), 3.24 (s, 3H), 3.12 (s, 6H), 3.06 (m, 2H), 2.89 (s, 6H), 2.37 (m, 2H), 2.30 (m, 1H), 2.17 (m, 1H) 1.90 (m, 1H), 1.62 (m, 2H, overlaps with HOD), 1.32 (m, 3H, overlaps

with hexane). ^{13}C NMR (101 MHz, $CDCl_3$) δ 171.8, 171.7, 171.7, 155.7, 153.2, 143.6, 138.8, 134.7, 130.6, 129.8, 129.7, 128.4, 128.2, 125.8, 123.3, 122.6, 115.4, 111.5, 55.6, 55.4, 52.7, 52.2, 49.4, 45.5, 40.3, 38.9, 32.2, 31.9, 30.7, 28.6, 28.3, 21.9, 17.7. HRMS (ESI) calc'd for $C_{39}H_{49}N_7O_9S_2$ ($[MNa]^+$): 846.2931, found: 846.2957.

Compound **3c**. The reaction was performed following **GP4** using compound **2c** as the Boc-protected amine, and dansyl chloride as the sulfonyl chloride. Following extraction and ether washes, the product was isolated as a microcrystalline red-orange solid (24 mg, 37%). ^{1}H NMR (400 MHz, DMSO) δ 8.51 (d, *J* = 6.9 Hz, 1H), 8.38 (d, *J* = 5.8 Hz, 1H), 8.10 (d, *J* = 4.4 Hz, 1H), 7.89 (m, 7H), 7.66 (m, 4H), 7.39 (s, 1H), 6.84 (d, *J* = 7.0 Hz, 2H), 3.08 (s, 6H), 2.90 (m, 8H), 2.74 (m, 4H), 1.98 (s, 2H), 1.55 (m, 2H), 1.35 (m, 2H), 1.22 (m, 4H (confirmed by COSY and HSQC)). ^{13}C NMR (101 MHz, DMSO) δ 171.7, 154.8, 153.6, 143.1, 140.8, 136.6, 129.5, 129.4, 129.0, 128.8, 128.2, 128.2, 125.9, 124.5, 122.6, 116.4, 112.1, 55.3, 46.6, 45.8, 42.9, 42.6, 38.7, 32.8, 29.2, 29.0, 26.0, 23.9. HRMS (ESI) calc'd for $C_{35}H_{45}N_7O_5S_2$ ($[MNa]^+$): 730.2821, found: 730.2834.

Compound **3d**. The reaction was performed following **GP4** using compound **2d** as the Boc-protected amine, and dabsyl chloride as the sulfonyl chloride. The reaction was monitored by TLC using 2:1 ethyl acetate : hexanes. Following extraction and ether washes, the product was isolated as a dark purple-red microcrystalline solid (57 mg, 56%). ^{1}H NMR (400 MHz, DMSO) δ 8.43 (d, *J* = 8.5 Hz, 1H), 8.28 (d, *J* = 8.8 Hz, 1H), 8.07 (dd, *J* = 1.2, 7.2 Hz, 1H), 7.86 (m, 5H), 7.81 (d, *J* = 9.2 Hz, 2H), 7.61 (m, 4H), 7.24 (d, *J* = 7.3 Hz, 1H), 6.84 (m, 2H), 3.08 (s, 6H), 2.80 (m, 8H), 2.72 (q, *J* = 6.6 Hz, 4H), 2.00 (t, *J* = 7.3 Hz, 2H), 1.57 (qu., *J* = 7.3 Hz, 2H), 1.24 (m, 2H (confirmed by COSY and HSQC analysis)), 1.12 (m, 2H), 1.04 (m, 2H). ^{13}C NMR (101 MHz, DMSO) δ 171.7, 154.9, 153.6, 151.2, 143.0, 140.6, 136.6, 129.6, 129.5, 129.3, 128.7, 128.2, 125.9, 124.2, 122.7,

121.7, 120.0, 115.8 112.1, 45.6, 42.7, 42.7, 38.6, 32.8, 29.2, 28.9, 25.7, 23.7, 18.5. HRMS (ESI) calc'd for $C_{35}H_{45}N_7O_5S_2$ ($[MNa]^+$): 730.2821, found: 730.2810.

Synthesis of compounds **4-6**

Boc-GABA

The compound was synthesized as previously described.[55] Characterization data are consistent with literature.[55]

Boc-GABA coumarin ester (**4**)

A solution of Boc-GABA (1000 mg, 4.92 mmol), HBTU (2799 mg, 7.38 mmol) and DIPEA (1714 μL, 9.84 mmol) in DCM (20 mL) was stirred at R.T. for 1 hour, after which 7-hydroxycoumarin (877 mg, 5.41 mmol) was added. The reaction was complete 30 minutes following addition of the 7-hydroxycoumarin, according to TLC analysis (5% MeOH, 47.5% DCM, 47.5% hexanes). Upon completion, the reaction mixture was evaporated in vacuo, and redissolved in EtOAc (50 mL). The organic phase was washed with 5% AcOH (2 × 20 mL), brine (20 mL), saturated $NaHCO_3$ (3 × 20 mL), and a final wash with brine (20 mL). The organic phase was dried over $MgSO_4$, then evaporated. The resultant residue was dissolved in a minimal amount of DCM and precipitated by addition of hexane to give the product as a white powder (1742 mg, >95%.). ^{1}H NMR (400 MHz, $CDCl_3$) δ 7.69 (d, J = 9.6 Hz, 1H), 7.49 (d, J = 8.4 Hz, 1H), 7.12 (d, J = 2.1 Hz, 1H), 7.06 (dd, J = 2.2, 8.4 Hz, 1H), 6.40 (d, J = 9.6 Hz, 1H), 4.66 (s, 1H), 3.26 (q, J = 6.4 Hz, 2H), 2.65 (t, J = 7.3 Hz, 2H), 1.94 (t, J = 7.0 Hz, 2H), 1.45 (s, 9H).

GABA coumarin ester HCl salt (**5**)

To a stirred solution of **4** (600 mg, 1.727 mmol) in DCM (7 mL) was added HCl (4 M in dioxane, 7 mL). The reaction was monitored by TLC (5% MeOH, 47.5% DCM, 47.5% hexanes). Upon completion, the solvent was removed in vacuo, then the residue resuspended in DCM. The solid was collected by filtration (360 mg, 74%). ^{1}H NMR (400 MHz, DMSO) δ 8.09 (d, *J* = 9.6 Hz, 1H), 7.99 (br. s, 3H), 7.79 (d, *J* = 8.5 Hz, 1H), 7.32 (d, *J* = 2.1 Hz, 1H), 7.19 (dd, *J* = 2.2, 8.4 Hz, 1H), 6.50 (d, *J* = 9.6 Hz, 1H), 2.90 (sextet, *J* = 6.9 Hz, 2H), 2.78 (t, *J* = 7.3 Hz, 2H), 1.93 (t, *J* = 7.5 Hz, 2H).

General procedure (**GP5**) for the coupling of Cbz-protected amino acids with GABA-coumarin ester HCl

A solution of Cbz-amino acid (1.1 equiv.), HBTU (1.6 equiv.) and DIPEA (3 equiv.) in DCM (0.05 M of limiting reagent) was stirred at R.T. for 1 hour, after which GABA coumarin ester (1 equiv.) was added. The reaction was stirred overnight; upon completion by TLC analysis, the reaction mixture was evaporated. The residue was redissolved in EtOAc (10 mL) and washed with saturated $NaHCO_3$ (3 × 10 mL), brine (10 mL), 10% AcOH (10 mL) and a second wash with brine (10 mL). The organic phase was collected, dried over $MgSO_4$, and evaporated to give a pale yellow oil. The oil was triturated with Et_2O and cooled to -20 ℃ to promote precipitation. Then the supernatant was decanted off and the solid washed with cold Et_2O, then dried under vacuum. The product was recovered as a white solid.

ZFBC (**6a**). The reaction was performed following **GP5** on an 80 mg (0.282 mmol) scale of **5** using Cbz-phenylalanine as the amino acid. Following isolation, 77 mg (52%) of product was recovered. Characterization data are consistent with literature.[38]

ZGBC (**6b**). The reaction was performed following **GP5** on a 40 mg (0.141 mmol) scale of **5** using Cbz-glycine as the amino acid. Following isolation, 34 mg (55%) of product was recovered. Characterization data are consistent with literature.[38]

ZABC (**6c**). The reaction was performed following **GP5** on a 60 mg (0.213 mmol) scale of **5** using Cbz-alanine as the amino acid. Following isolation, 45 mg (47%) of product was recovered. ^{1}H NMR (400 MHz, $CDCl_3$) δ 7.68 (d, *J* = 9.6 Hz, 1H), 7.48 (d, *J* = 8.4 Hz, 1H), 7.34 (m, 5H), 7.12 (d, *J* = 2.1 Hz, 1H), 7.06 (dd, *J* = 2.2, 8.5 Hz, 1H), 6.40 (d, *J* = 9.6 Hz, 1H), 6.27 (s, 1H), 5.22 (s, 1H), 5.10 (m, 2H), 4.19 (qu, *J* = 7.3 Hz, 1H), 3.39 (q, *J* = 6.3 Hz, 2H), 2.64 (t, *J* = 6.9 Hz, 2H), 1.96 (qu, *J* = 7.2 Hz, 2H), 1.39 (d, *J* = 7.0 Hz, 3H). ^{13}C NMR (101 MHz, $CDCl_3$) δ 172.4, 160.3, 154.7, 153.1, 142.8, 128.6, 128.3, 128.1, 118.4, 116.7, 116.1, 110.4, 67.2, 50.8, 38.6, 31.5, 24.5, 18.3.

ZLBC (**6d**). The reaction was performed following **GP5** on a 60 mg (0.213 mmol) scale of **5** using Cbz-leucine as the amino acid. Following isolation, 46 mg (44%) of product was recovered. ^{1}H NMR (400 MHz, $CDCl_3$) δ 7.67 (d, *J* = 9.5 Hz, 1H), 7.46 (d, *J* = 8.5 Hz, 1H), 7.31 (m, 5H), 7.11 (d, *J* = 2.0 Hz, 1H), 7.04 (dd, *J* = 2.1, 8.4 Hz, 1H), 6.50 (s, 1H), 6.38 (d, *J* = 9.6 Hz, 1H), 5.31 (d, *J* = 7.8 Hz, 1H), 5.08 (m, 2H), 4.16 (m, 1H), 3.36 (m, 2H), 2.62 (t, *J* = 7.1 Hz, 2H), 1.93 (m, 2H), 1.65 (m, 2H), 1.52 (m, 1H), 0.92 (d, *J* = 6.0 Hz, 6H). ^{13}C NMR (101 MHz, $CDCl_3$) δ 172.6, 171.1, 160.40, 154.6, 153.1, 142.9, 136.1, 128.6, 128.6, 128.3, 128.1, 118.4, 116.7, 116.1, 110.4, 67.1, 53.7, 41.3, 38.6, 31.5, 24.7, 24.5, 22.9, 22.0.

Chapter 3. Small Molecule Substrates for the Rapid Quantification of Acyl Transfer Activity of Nylon Hydrolase Enzymes

Preamble

Much of the work presented in this chapter has been published in: Alana M. M. Rangaswamy, Francis M. Roy, Jeffrey W. Keillor. Small molecule substrates for the rapid quantification of acyl transfer activity of nylon hydrolase NylCA. *Analytical Biochemistry*, **2024**, *693*, 115598. Here I also provide additional contextualization, data, and perspectives on this work.

3.1. Introduction

3.1.1. Discovery of the Aminohexanoate Oligomer Hydrolases (NylCs)

In the early 1960's, bacteria were discovered growing in a water line of a nylon manufacturing plant.[56] This seminal discovery launched a decades-long investigation into the identification and characterization of enzymes employed by these bacteria to convert nylon into food. Evolution by environmental pressure is the most robust strategy that both nature and science have in order to develop biochemical tools, from natural products to biocatalysts. In this section, we will explore a family of nylon-degrading enzymes arising from selective pressure, and how they may be engineered for bioremediation efforts.

Bacteria from the nylon plant water line (sometimes somewhat ambiguously referred to as "sludge")[57] were isolated by selection on agar plates supplemented with water-insoluble aminohexanoic acid (AHX) cyclic oligomer (n>2 units) as the sole source of nitrogen. The first bacterial strain isolated in this way, originally referred to as *Achromobacter*,[57] then *Flavobacterium*[58] and most recently, *Arthrobacter*[59] sp. KI72 was studied extensively to determine the enzymatic

pathway responsible for converting AHX oligomers into nutrients. It was determined that a single plasmid, pOAD2, contained enzymes capable of degrading oligomers,[58] and linear and cyclic dimers[60] of AHX. *Arthrobacter* was also found to express proteins capable of converting AHX into adipate, by co-opting and adapting enzymes homologous to those responsible for converting GABA into succinate.[61] Among these, the enzyme of interest for its potential application to bioremediation is the oligomer-degrading enzyme named NylC. This enzyme hydrolyzes linear and cyclic oligomers ($n \geq 3$) of AHX specifically, and produces the linear dimer, $H_2N\text{-}(AHX)_2\text{-}OH$, as its primary hydrolysis product.[58] This first NylC enzyme would later be called $NylC_{p2}$ after its localization on the plasmid, pOAD2 in *Arthrobacter* (a plasmid that also encodes other AHX oligomer degrading enzymes, NylA and NylB).[62]

A later study identified homologous NylC enzymes from the bacteria *Agromyces* and *Kocuria*, which were isolated from nylon factory waste and sewage, respectively.[59] These enzymes, named $NylC_A$ and $NylC_K$ for their respective bacterial strains, showed a greater alkaline pH tolerance and higher activity (13- and 15-fold greater efficiency, respectively) towards hydrolysis of nylon oligomer mixture, while retaining >96% sequence identity between all 3 variants.[59] This increase in activity accompanies the observation that the NylC-coding gene in *Agromyces* was determined to be incorporated into its genome, rather than found on a plasmid.[63]

3.1.2. NylCs as Biocatalysts

While intrinsically interesting as a study in evolution and horizontal gene transfer, researchers are primarily interested in the NylC enzymes from a biocatalysis perspective – which is to say, their capacity to degrade bulk nylon. It has been discovered in the development of highly efficient PETases (the most represented in the literature among engineered plastic-degrading enzymes) that high thermostability is advantageous for this application.[10,64] Performing reactions at elevated

temperatures increase flexibility of the polymer, allowing improved access of the enzyme to the individual strands of the polymer.[65] Furthermore, thermally stable enzymes tend to have higher overall stability,[66] allowing for reactivity over longer periods of time[67] which is advantageous for enzymatic reactions at solid surfaces, where the limited availability of substrate necessarily decreases the reaction rate.

With the intent to develop a more thermostable variant of NylC, Negoro *et al.* noted that $NylC_A$ and $NylC_K$ natively had higher melting temperatures (60 °C and 67 °C respectively) than that of $NylC_{p2}$ (52 °C).[68] Logically, the different residues (5 between $NylC_A$ and $NylC_{p2}$, and 10 between $NylC_K$ and $NylC_A$) effected this difference in melting temperature. Negoro's team systematically and rationally introduced mutations into $NylC_{p2}$, borrowed from the other homologues' sequences, to develop a thermostable variant (referred to by them as NylC-TS, or henceforth here as $NylC_{p2}TS$). This variant had 4 mutations (G122, Y130, A36, Q263) that increased the melting temperature of the enzyme from 52 °C to 88 °C.[68] This same strategy was used more recently by Bell *et al.*, adapting Negoro's findings, to develop thermostable versions of $NylC_A$ and $NylC_K$, each with a reported melting temperature of 87 °C.[69]

With a thermostable enzyme in hand, Negoro *et al.* reported the successful degradation of nylon powder by $NylC_{p2}TS$ at 60 °C, as determined by mass spectroscopic analysis of the polymer, and detection of oligomer fragments in the reaction supernatant.[68] In a follow-up study, it was determined that $NylC_{p2}TS$ degraded both powdered Nylon-6 and Nylon-66, although the reaction was slower with the latter polymer, at approximately 60% the rate of Nylon-6 degradation.[70] Interestingly, hydrolysis was accelerated when degrading Nylon-(66-co-46) copolymers with an increasing proportion of succinyl units, compared to that of Nylon-66 alone. This was also observed in the hydrolysis of nylon film, where bulk Nylon-6 and Nylon-(66-co-46) were degraded at

approximately the same rate, and faster than Nylon-66, when assayed at 30 °C. A later study evaluated hydrolysis of Nylon-6 film by the three wild-type NylCs and their engineered thermostable variants, at a variety of temperatures.[69] From this study, the most efficient hydrolysis was observed by NylC_KTS at 60 °C; while faster initial rates were observed at 80 °C, the reaction rate plateaued after 3 days, whereas activity was retained over 10 days at 60 °C.

In all studies of Nylon-6 degradation by NylCs, the primary hydrolysis product is aminohexanoic acid dimer (Figure 3.1),[69,70] consistent with their activity against nylon oligomer mixtures.[58] The proposed mechanism of nylon hydrolysis involves initial, slow hydrolysis of the amorphous, surface-exposed polymer strands to release oligomers, followed by rapid consumption of the oligomers into dimers,[68,70] leading to the classification of these enzymes as endohydrolases.

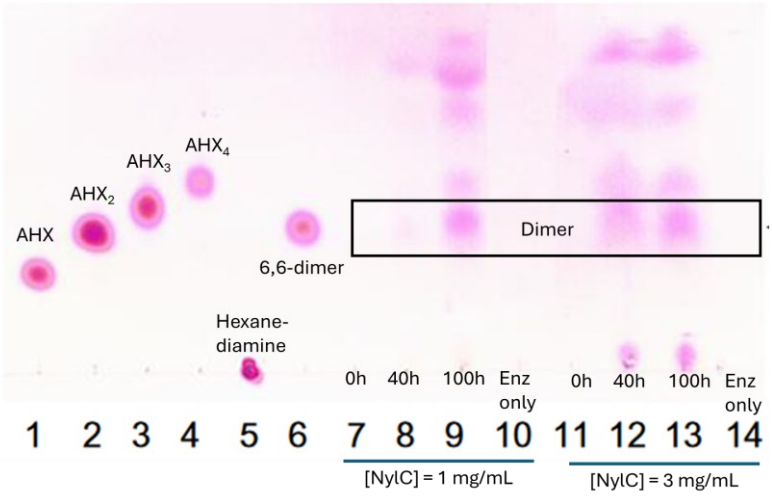

Figure 3.1. Hydrolysis of Nylon-(66-co-46) by NylC_{p2}TS, monitored by TLC. The major product of nylon-66 hydrolysis is the linear heterodimer of hexanediamine and adipic acid "6,6-dimer". Lanes 1-6: genuine samples of aminohexanoic acid monomer, dimer, trimer, tetramer, hexanediamine, and adipoylhexanediamine respectively. Lanes 7-9 and 11-13: reaction products at varying

time points (indicated) in the presence of 1 or 3 mg/mL NylC, respectively. Lanes 10 and 14: no substrate blanks. This figure was adapted from Nagai *et al.*[70]

3.1.3. Structure and Enzymology of NylC

NylC bears certain structural features that complicate its use as a biocatalyst. The NylCs belong to the *N*-terminal nucleophile hydrolase class of enzymes,[68] meaning that its active site catalytic nucleophile (Thr267, in the case of NylC) is at the *N*-terminus of a peptide chain, i.e. bearing an α-NH_2. The enzyme achieves this by first expressing as a single, inactive peptide; then, upon folding, Thr267 catalyzes the hydrolysis at its own *N*-terminal peptide bond to produce two subunits that form the active enzymatic unit as a heterodimer. The α-NH_2 is thought to act as a general base, activating the threonine hydroxyl group to enable it to attack the amide substrate, making this "autoprocessing" step necessary for activity.[71] However, the rate of autoprocessing can be affected by mutations both proximal and distal to the active site.[71] This is an important consideration for downstream engineering efforts, where observed activity during a screen may be artificially lower due to a variable fraction of inactive enzyme.

Another important feature of NylC is the enzyme's quaternary structure (Figure 3.2). Through size-exclusion chromatography, analytical centrifugation, and crystallographic analyses, it was determined that $NylC_A$ and $NylC_K$ assembled as a doughnut-shaped tetramer of activated heterodimers.[68,72] Conversely, the other wild-type enzyme, $NylC_{p2}$, is believed to adopt a mixture of dimer and trimer states in equilibrium.[72–74] Notably, it was observed that mutations that affected thermal stability, which tended to reside at the interfaces between subunits,[68] also impacted the oligomerization state of the enzyme: thus, prevalence of the tetrameric conformation is correlated to thermal

stability.[72] As an illustration of this, the engineered NylC$_{p2}$TS was found to exhibit a tetrameric structure, but the destabilizing mutation, NylC$_{p2}^{L137A}$ resulted in an enzyme dimer, while decreasing the melting temperature by 11 °C compared to NylC$_{p2}$.[72]

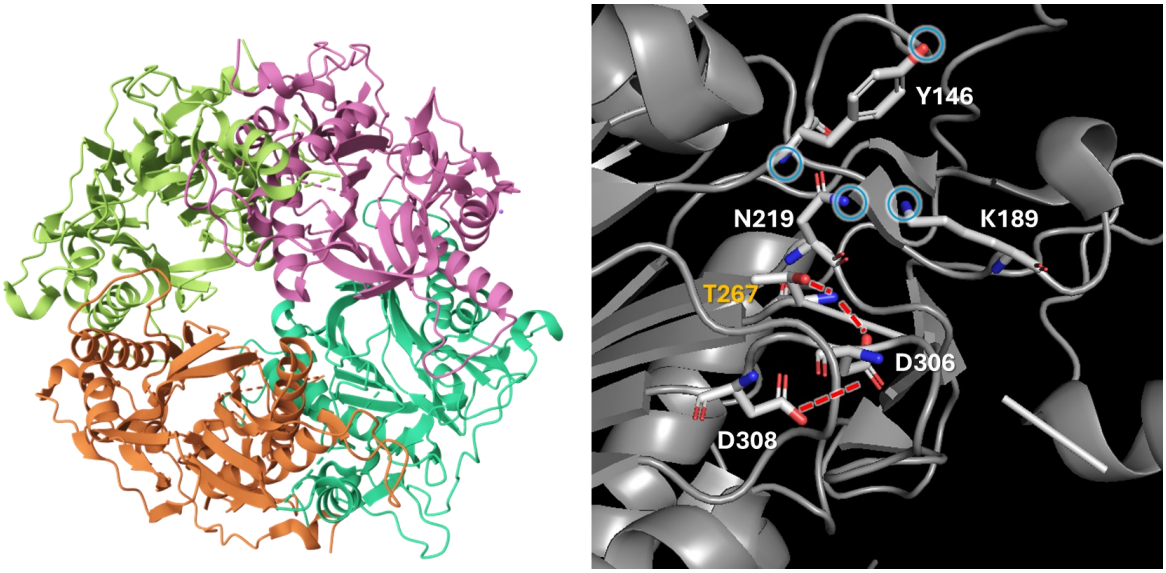

Figure 3.2. Crystal structure of NylC$_A$ (PDB ID: 3AXG).[68] Left: tetrameric quaternary structure, where each subunit represents one active heterodimer. Right: Active site threonine (labelled, yellow) and associated residues believed to participate in substrate hydrolysis by either proton shuttling to activate the Thr (red dashes) or stabilization of the oxyanion reaction intermediate (blue circles).

3.1.4. Engineering of NylC

As summarized above, a variety of studies have probed the structural and functional characteristics of the NylC family of enzymes; however, to date only one study has sought to engineer a NylC variant with improved nylon-degrading activity. Using random mutagenesis and screening, Puetz *et al*. reported a double mutant of NylC$_{p2}$TS$^{P27Q/F301L}$ with 2-fold increased activity over the

original enzyme against Nylon-6 film.[75] Given that NylC was characterized as early as the 1990's, it is perhaps surprising that no other engineering campaigns have been reported.

In protein engineering, variants can be evaluated either through selection, where the desired activity is tied to the viability of the organism, or by screen, where activity is identified through some kind of detectable change. In the absence of a selection, to which not all enzymes are amenable, the efficiency of an engineering campaign is dictated by the throughput of the screen. In the case of engineering nylon-hydrolyzing enzymes, there are two major barriers to a high throughput screen: first, aliphatic amides are chemically stable, and hydrolysis thereof, especially on a solid surface, is slow. Second, hydrolysis of nylon does not produce any easily-detectable output, unlike, for instance, PET hydrolysis, which produces UV-active soluble products. Therefore, quantifying nylon hydrolysis has relied on long reaction times and discontinuous detection methods. Previous studies determine the extent of nylon hydrolysis by chromatographic analysis by TLC[70] or LCMS[69], or else detection of the free amines produced in hydrolysis by reaction with a chromogenic agent.[59,75] The former strategy, while providing the most information, is exceptionally slow, requiring at minimum minutes of analysis for a single kinetic datapoint, and is unsuitable to most engineering campaigns. The latter strategy, while more high-throughput, requires several manipulations and reaction steps, which, in the absence of advanced automation, is slow and can increase error. In addition to the analysis time, reactions with nylon are often conducted over hours to days in order to generate enough detectable product to quantify. Most engineering campaigns require the screening of thousands of variants in order to identify a variant with increased activity. Taken together, few labs would have the resources to conduct this type of study, and it is ultimately unsurprising that there are not more reports of NylCs engineered for enhanced activity.

In the remaining chapters of this thesis, we will describe the development and application of activity assays for NylC using surrogate substrates, with the intent to accelerate the identification and quantification of enzymatic activity. In this chapter, we investigate water-soluble, chromogenic substrates optimized *via* a structure-activity relationship study, as a rapid activity assay for NylC.

3.2. Results and Discussion

3.2.1. Probing Esterase Activity

While investigating $NylC_A$, we simultaneously investigated commercially available lipases for nylon-degrading capability. As such, we wished first to assay the lipase using a known activity assay. The recommended substrate for activity determination was 4-nitrophenyl octanoate, which we synthesized for that purpose. While we did not continue with the lipase enzyme, this substrate became the basis for a preliminary investigation of NylC hydrolysis activity.

While not an amide, hydrolysis of an ester substrate is expected to follow a similar mechanism as for amide hydrolysis: namely, through formation of an acyl-enzyme intermediate *via* nucleophilic attack by the catalytic threonine. The application of ester substrate surrogates has been used extensively to determine activity of transglutaminases (see section 2.2.4. Ester Hydrolysis by bTG). Similarly, chromogenic or fluorogenic amides have been used as standard activity substrates for proteases.[76] We were interested to observe whether $NylC_A$ could recognize and cleave the chromogenic substrate, 4-nitrophenyl octanoate, so we evaluated a range of substrate concentrations in the presence of $NylC_A$ (Figure 3.3). Learning from our experiences of nonspecific ester hydrolysis due to the presence of protein, (see Figure 2.22) we evaluated an equivalent concentration of BSA,

and observed negligible hydrolysis compared to the reactions in the presence of $NylC_A$, confirming that the reaction was specifically mediated by NylC.

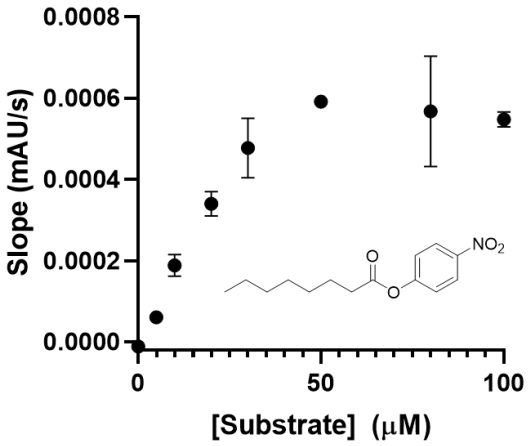

Figure 3.3. Michaelis-Menten plot for the hydrolysis of 4-nitrophenyl octanoate. Reaction conditions: $NylC_A$ (0.2 mg/mL, or 5.4 μM), 4-nitrophenyloctanoate (0-100 μM), Tris buffer (100 μM, pH 6.9). Blanks were performed at each substrate concentration containing 0.2 mg/mL BSA instead of $NylC_A$.

3.2.2. Substrate scope and Structure-Activity Relationship

Given that NylC is known to hydrolyze aminohexanoate oligomers, we expected that 4-nitrophenyl octanoate would not be the optimal substrate analogue for NylC. Therefore, we prepared a series of substrates with varying alkyl chain, with the expectation that the 6-carbon chain (present in aminohexanoate) may be best-recognized. We also hypothesized that a second amide bond may

help with recognition of the substrates, so we prepared 4-nitrophenyl ester derivatives of *N*-acetylated linear amino acids. This series was intended to evaluate the optimal inter-amide distance that would be recognized by NylC, and provide some insight into binding preferences and substrate specificity of this enzyme. The full series of substrates is shown in Figure 3.4. Full synthetic details for their preparation may be found in Section 3.4.4.

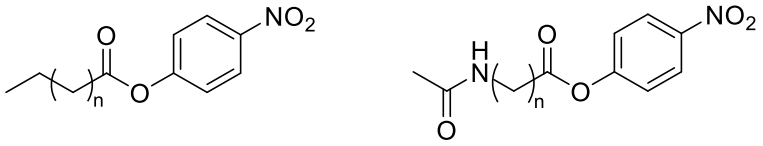

Figure 3.4. All 4-nitrophenyl derivative substrates evalutated for hydrolysis by $NylC_A$.

We performed Michaelis-Menten kinetics for each substrate, with substrate concentrations ranging from 0-50 μM. Several substrates did not reach saturation within this range, so in order to determine preliminary kinetic parameters, linear regression was performed to predict a k_{cat}/K_M value for each substrate. All k_{cat}/K_M values from this screen may be found in Table A3.1 in the Appendix. A summary of these data may be found in Figure 3.5.

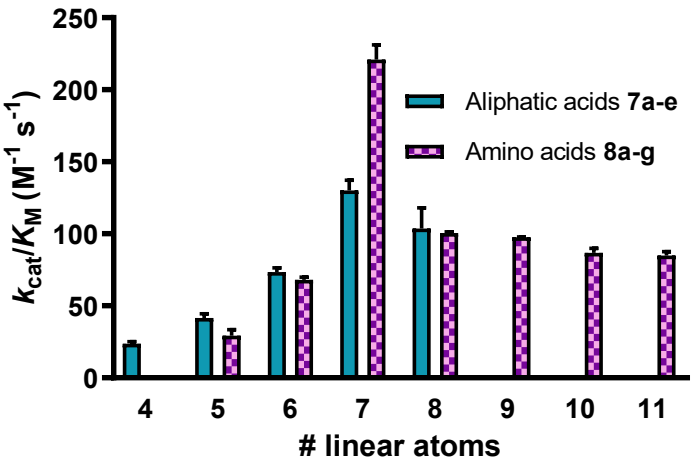

Figure 3.5. Catalytic efficiency of all substrates, plotted against the number of heavy atoms in the linear chain, counting from the electrophilic carbonyl of the pNP ester. Reaction conditions: $NylC_A$ (0.1 mg/mL, or 2.7 μM), substrate (0-50 μM), Tris buffer (100 μM, pH 6.9), 10% DMSO.

The two series in Figure 3.5 are arranged by number of linear heavy (non-hydrogen) atoms, counting from the electrophilic carbonyl, and displayed a clear trend: in both series, substrates containing seven linear atoms were preferred by $NylC_A$. By far the substrate with the highest catalytic efficiency was *N*-acetyl GABA pNP ester (compound **8c**). This was interesting to us, given that we expected the substrate containing an aminohexanoyl unit (compound **8e**) to have the highest catalytic efficiency, as the closest Nylon-6 analogue in the series. We hesitate to draw conclusions based on this result to predict affinity for solid nylon architectures, since the small, water-soluble substrate is both structurally and morphologically distinct from nylon plastic. However, it could point to microscopic changes in binding interactions of the substrates within the active site of NylC, from an enzymology perspective. To investigate this, we modelled the binding

interactions of compounds **8c** and **7d** in the active site of $NylC_A$ using the predictive protein structure and ligand interaction tool, Chai-1[77] (Figure 3.6).

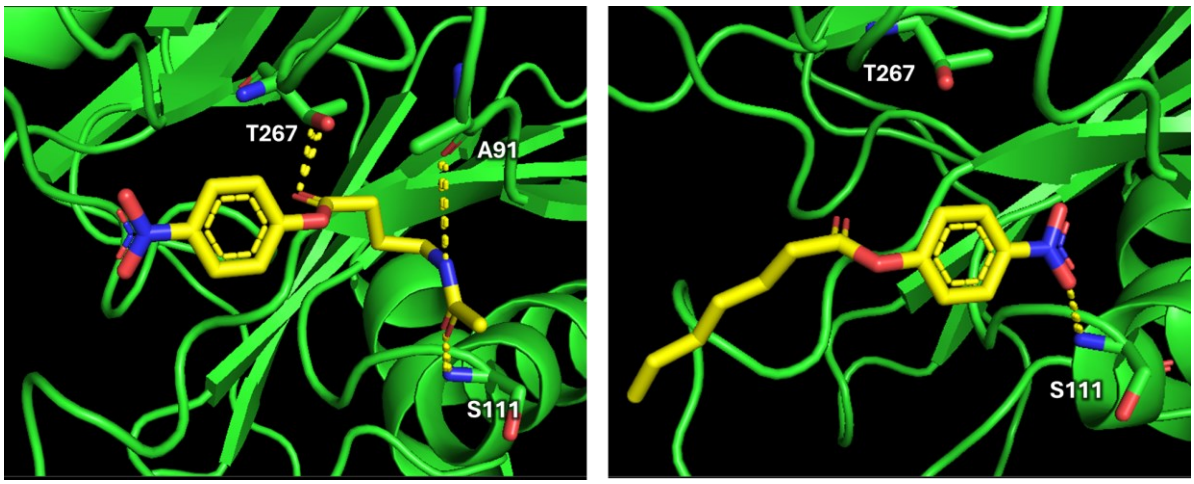

Figure 3.6. Chai-1 model predicting potential interactions of substrate **8c** (left) and substrate **7d** (right) with $NylC_A$. Potential H-bonding interactions are shown as dashed yellow lines.

Based on the predicted interactions, compound **8c** is oriented with the scissile ester carbonyl within H-bonding distance of the catalytic threonine hydroxyl, with an interatomic distance of 2.7 Å between the carbonyl carbon and the threonine oxygen. Additional stabilizing interactions are predicted between the distal acetyl amide and the backbone amide groups of residues A91 and S111. Conversely, in the absence of the amide bond (as in **7d**), the ligand is predicted to sit in the opposite orientation, with a potential H-bonding interaction between the pNP nitro group and the backbone S111 amide. This prediction places the scissile ester further from the catalytic threonine, with an interatomic distance of 6.2 Å. Overall, this prediction suggests that the second acyl group of substrate **8c** aids in positioning the scissile bond near the catalytic threonine in the active site.

3.2.3. Characterization of NylC by Compound **8a**

We performed saturation kinetics on lead compound **8c** to isolate kinetic parameters, k_{cat} and K_M (Figure 3.7). Nonlinear regression of these data provided a k_{cat} of 0.370 ± 0.017 s^{-1}, and a K_M of 256 ± 47 μM, for a calculated efficiency of 1460 ± 273 M^{-1} s^{-1}. We also analyzed the linear region, up to the same concentration as the initial screen (0-50 μM of substrate), which provided an estimated k_{cat}/K_M value of 1066 ± 8 M^{-1} s^{-1}. Both the calculated and estimated values for k_{cat}/K_M from this experiment were higher than that of the initial screen, which gave an estimated value of 221 ± 10 M^{-1} s^{-1} (see Table A3.1b in the Appendix). This second experiment evaluating **8c** over a larger range of enzyme concentrations was performed using a different batch of enzyme, which could account for the discrepancy. Although the same enzyme concentration was (nominally) used for each experiment, differences in enzyme purity, incomplete autoprocessing, or variance in assembly (i.e. oligomerization) of the enzyme could account for differences in activity.

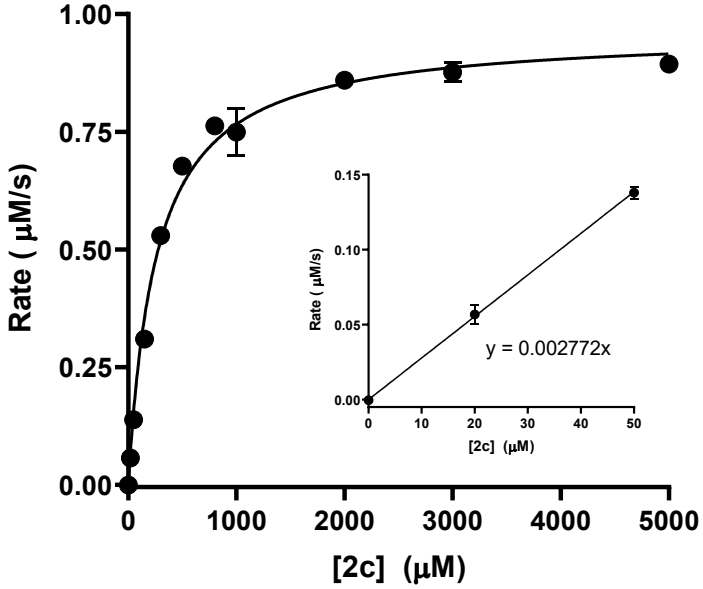

Figure 3.7. Michaelis-Menten plot for the hydrolysis of compound **8c** by $NylC_A$. Reaction conditions: $NylC_A$ (0.1 mg/mL); Tris buffer (100 mM, pH 6.9); **8c** (0-5000 μM); DMSO (10% v/v). Datapoints represent averages of two replicates, and error bars show standard deviations. Inset: low-concentration datapoints of the Michaelis-Menten plot, to which a linear regression, constrained through the origin, is applied. The slope of the fitted line is indicated.

We used compound **8c** to determine the specific activity of the batch of $NylC_A$ used to acquire saturation kinetics. The reaction was performed using 2000 μM of substrate, or approximately 8-fold that of the calculated K_M, within the saturating region of the Michaelis-Menten plot. For that batch of enzyme, we determined a specific activity of 0.516 U/mg, where U is defined as the amount of enzyme required to hydrolyze 1 μmol of **8c** in one minute. This metric allows us to normalize the activity between batches of enzyme expressed, mitigating any differences in enzyme purity or other factors.

Given our previous experiences in our study of bTG, where the presence of protein promoted nonspecific hydrolysis of activated esters (see section 2.2.4), we wished to confirm that hydrolysis of **8c** was occurring *via* the active-site catalytic threonine. We prepared an inactivated mutant, $NylC_A^{T267A}$. Following expression and purification of the enzyme, we performed SDS-PAGE to confirm that the mutant was autoproteolytically inactive, as confirmed by a single band on the SDS-PAGE at 37 kDa (see Figure A3.1 in the Appendix). Hydrolysis of **8c** was performed by $NylC_A^{T267A}$, and results are shown in Figure 3.8.

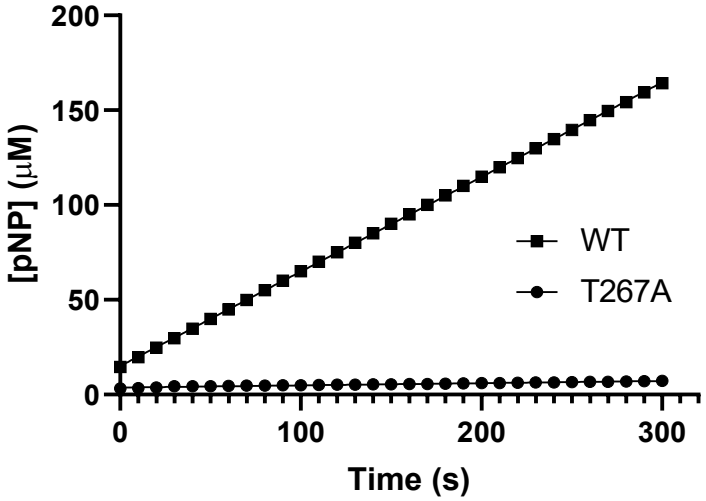

Figure 3.8. Hydrolysis of **8c** by mutant enzyme $NylC_A^{T267A}$ compared to the wild-type enzyme, $NylC_A$ (WT). Reaction conditions: Enzyme (0.1 mg/mL), Tris buffer (100 mM, pH 6.9), substrate **8c** (2000 μM), and DMSO (10% v/v). Reactions were performed in duplicate and blank-corrected by subtraction of the signal from a reaction mixture containing no enzyme, to account for background hydrolysis. Average values are shown, with error bars representing the standard deviations being smaller than the data point symbols.

Compared to the wild-type with a specific activity of 0.516 U/mg, we determined a specific activity of 0.007 U/mg for $NylC_A^{T267A}$ under the same conditions, corresponding to 1.3% of the wild-type activity. This experiment confirmed that the active site threonine was responsible for the observed hydrolysis of **8c**, rather than a surface-exposed residue. This experiment provides further evidence that **8c** is probing activity only of the autoprocessed, correctly assembled enzyme.

As a means to determine the selectivity of **8c** for NylC over other potential ester-hydrolyzing enzymes in complex biological media, we evaluated the hydrolysis of **8c** by *E. coli* cell lysate. We prepared two cultures, inoculated by *E. coli* transformed with either pET21c containing the $NylC_A$

gene, or pET21c alone. Following cell lysis and clarification, the soluble fraction of each sample was applied to reaction mixtures containing **8c** (Figure 3.9). The lysate containing $NylC_A$ demonstrated notably enhanced hydrolysis of **8c**: in the presence of enzyme, a rate of hydrolysis of 1.8 μM/s was measured. Comparatively, the reaction containing empty vector lysate demonstrated a rate of hydrolysis of 0.14 μM/s, or approximately 8% of the former reaction. Since protein concentration is not easily determined in cell lysate, relative protein concentration must be considered as a convoluting factor; however, these results suggest that **8c** is selective for NylC over other endogenous *E. coli* esterases.

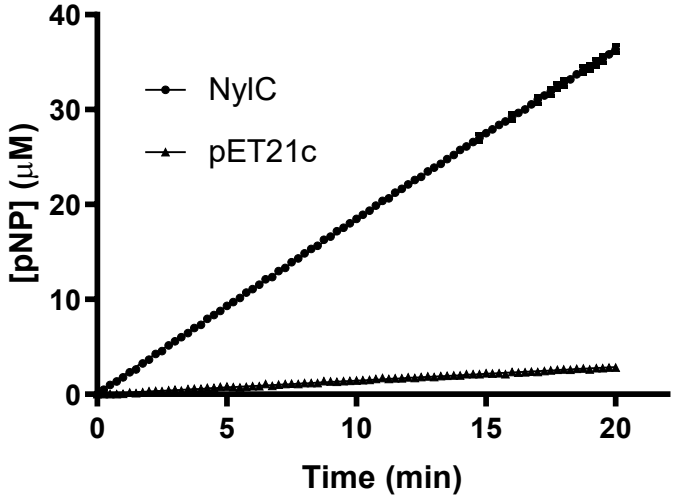

Figure 3.9. Hydrolysis of **8c** in cell lysate containing either $NylC_A$ or empty pET21c vector (no protein overexpressed). Reaction conditions: cell lysate (4% v/v), Tris buffer (100 mM, pH 6.9), **8c** (500 μM), DMSO (10% v/v). The reaction mixture containing $NylC_A$ lysate was run in duplicate. Data points represent average of two values and standard deviations are shown as error bars, although these are smaller than most of the data point symbols. Traces have been blank-corrected to account for background hydrolysis.

3.2.4. Chromogenic Amide Substrates

For this project, we chose to develop an activated ester substrate to probe the acyl transfer activity of NylC. Synthesis of 4-nitrophenyl esters is simple, which expedited the generation of an expanded substrate scope. Furthermore, activated esters are labile and tend to be hydrolyzed quickly, providing a convenient activity assay for hydrolases. However, the biocatalytically-relevant activity of NylC is its amide hydrolysis activity. Therefore, we prepared compound **9**, a 4-nitroaniline derivative of compound **8c**, and evaluated its hydrolysis by $NylC_A$ (Figure 3.10).

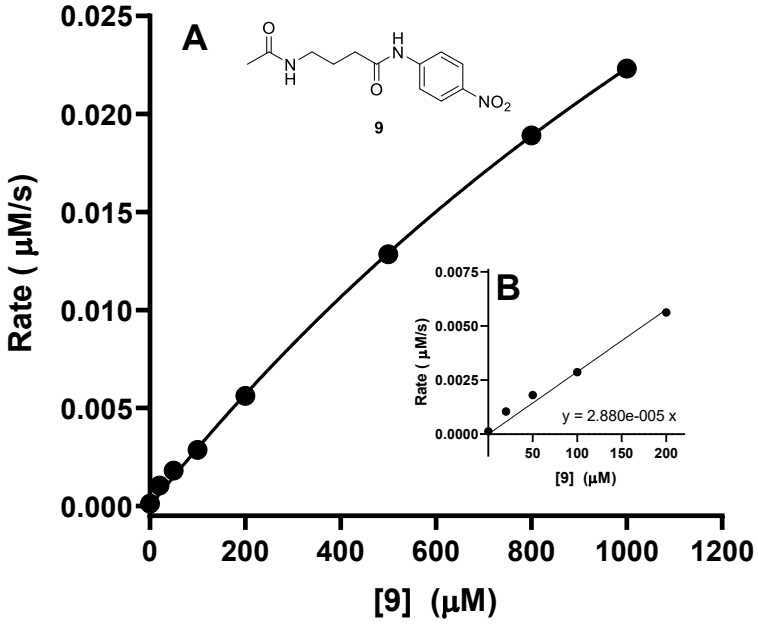

Figure 3.10. Kinetic characterization of **9**. Reaction conditions: $NylC_A$ (0.1 mg/mL); Tris buffer (100 mM, pH 6.9); **9** (0-1000 µM); DMSO (10% v/v). A) Michaelis-Menten plot for the hydrolysis of **9** by $NylC_A$. B) Low substrate concentration region of the Michaelis-Menten plot, from which a linear fit, constrained through the origin, was determined. The slope of the fitted line is indicated.

Unfortunately, we were not able to reach saturation within the concentration range evaluated, which was limited as we observed non-linearity in signal with respect to product concentration above 1000 μM (see Figure A3.2 in the Appendix). However, we saw some curvature in the data and thus we attempted a nonlinear fit. We also estimated k_{cat}/K_M using a linear regression of the initial datapoints. These values for compound **9** are presented in Table 3.1, alongside the corresponding values for the analogous ester compound, **8c**.

Table 3.1. Estimated kinetic parameters for the hydrolysis of **8c** and **9** by $NylC_A$. Values represent best fits and standard errors.

Parameter	Value (Compound 8c)	Value (Compound 9)
k_{cat} (s^{-1})	0.370 ± 0.017	0.032 ± 0.009
K_M (μM)	256 ± 47	2710 ± 954
k_{cat}/K_M (calculated) ($M^{-1}s^{-1}$)	1460 ± 273	11.8 ± 5.1
k_{cat}/K_M (from linear regression) ($M^{-1}s^{-1}$)	1066 ± 8	11.1 ± 0.5

Based on these values, both the affinity (as represented by K_M) and reactivity (k_{cat}) are decreased by a factor of ~10 between compounds **8c** and **9**. This result is unsurprising, given that an amide bond is intrinsically less readily hydrolyzed than an ester, and amide hydrolysis reactions typically require protonation of the leaving group (i.e. the chromophore is the neutral aniline, whereas ester hydrolysis produces the phenolate anion as the chromophore). To ensure that ester hydrolysis probes the same reaction mechanism as amide hydrolysis, we evaluated several expression batches of $NylC_A$ with varying activity using both compounds **8c** and **9** (Figure 3.11). We observed a drastic difference in specific activities despite using the same nominal concentration of enzyme, highlighting the importance of this method for normalization of activity. This variability could be

due to differences in purity of the enzyme, since only total protein concentration (*via* Bradford assay) is quantified, or else differences in the extent of autoprocessing. It should be noted here that the expression conditions employed for this experiment were optimized for the $NylC_A$ plasmid we constructed. We have since switched to a (recently made available) commercial plasmid for this enzyme, which expresses more reliably. We have also incorporated an incubation step to ensure full autoprocessing of the enzyme (see Methods, section 3.4.1), which could mitigate this variabilty.

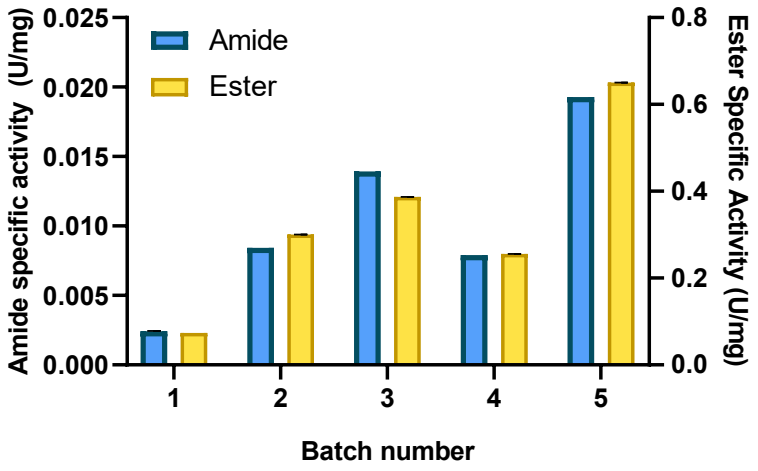

Figure 3.11. Activity determination of various batches of $NylC_A$ by hydrolysis of amide substrate **9** or ester substrate **8c**. Reaction conditions: $NylC_A$ (0.1 mg/mL); Tris buffer (100 mM, pH 6.9); substrate (ester **8c**: 2 mM, amide **9**: 1 mM); DMSO (10% v/v). Values are averages of duplicates, and error bars indicate standard deviation.

Qualitatively, the two assays demonstrate highly correlated rates, indicating that hydrolysis of **8c** likely probes the same catalytic machinery as **9** does. To quantify this correlation, we plotted amidase activity against esterase activity (Figure A3.3 in the Appendix), and observed a slope of

32.29 (R^2 = 0.98), indicating that on average the esterase activity of $NylC_A$ is 32-fold higher than its amidase activity, within this scaffold.

While we were carrying out this project, an article was published that utilized 4-nitrophenylbutyramide (pNBA) as a generic substrate to screen potential nylon-degrading enzymes, including the NylCs, for amidase activity.[69] We wished to determine whether our optimized scaffold of **9** bearing the *N*-acetyl GABA moiety conferred improved affinity for NylC compared to pNBA (Figure 3.12). From this experiment, we immediately observed a drastically increased reaction rate when $NylC_A$ hydrolyzed **9** compared to pNBA. Evaluating the initial rates, compound **9** is hydrolyzed at a rate of 1.19 μM/min, compared to 0.18 μM/min for pNBA, representing an overall 6.6-fold increase in activity for the more specific substrate. This result provides further evidence that the more polyamide-like structure of compounds **8c** and **9** are better recognized by NylCs. As a preliminary screen, compounds like **9** may be preferentially used over pNBA in the future when seeking new polyamide-degrading enzymes; however, this screen would have obvious limitations when seeking out enzymes to hydrolyze solid, aliphatic polyamide substrates.

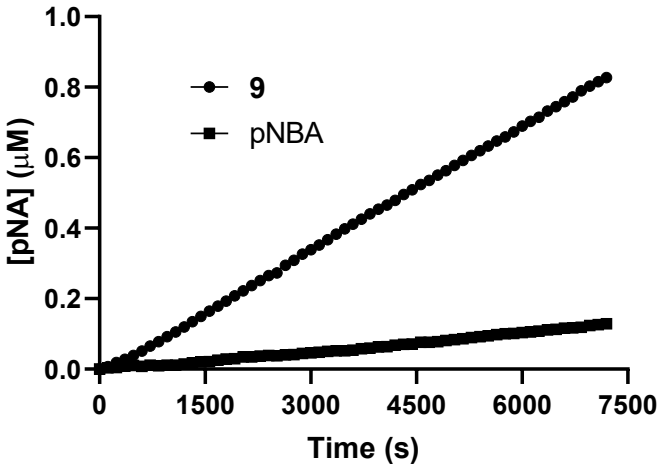

Figure 3.12. Hydrolysis of 4-nitroanilide substrates **9** and pNBA by $NylC_A$. Reaction conditions: $NylC_A$ (0.1 mg/mL), Tris buffer (100 mM, pH 6.9), substrate (1000 μM), DMSO (10% v/v). Reactions were run in duplicate, and data points represent average values. Standard deviations are shown as error bars, although these are smaller than most of the data point symbols. Traces have been blank-corrected to account for background hydrolysis with reactions performed in the absence of enzyme.

3.2.5. Applications of **8c**-Based Activity Assay

While not an ideal substrate for screening engineered or discovered libraries of enzymes, we have found a variety of uses for the rapid activity assay using **8c**. Following completion of this initial study, we were able to acquire the plasmids encoding, and subsequently express, all six reported NylC variants.[69] Despite the >96% homology between the enzymes, Yasuhira *et al*. observed variability in reactivity between the three wild-type NylCs towards aminohexanoic acid cyclic oligomer[59], with $NylC_A$ and $NylC_K$ demonstrating higher activity under their assay conditions compared to $NylC_{p2}$. We evaluated each of the six enzymes for hydrolysis of compound **8c** (Figure 3.13).

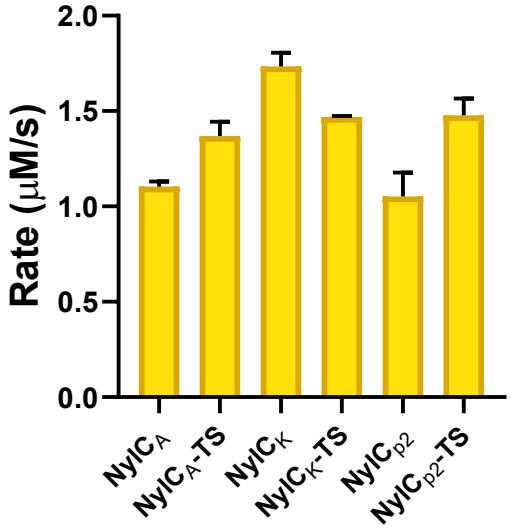

Figure 3.13. Hydrolysis of **8c** by all six NylC variants. Reaction conditions: Enzyme (0.1 mg/mL), Tris buffer (100 mM, pH 6.9), substrate **8c** (2000 μM), and DMSO (10% v/v).

With our substrate, we see some variability in activity between NylC enzymes. Like Yasuhira *et al*. observed when assaying the hydrolysis of AHX cyclic oligomers,[59] NylC$_{p2}$ demonstrates the lowest activity here, and NylC$_K$, the highest; however, NylC$_A$ has a similar initial rate in hydrolyzing **8c** compared to NylC$_{p2}$. This perhaps suggests that NylC$_A$ is more specific for the linear amide, or perhaps that the assay pH of 6.9 falls more comfortably within the range for NylC$_{p2}$ (with an optimal pH of 6.5-7.5) than for NylC$_A$ (pH 7-8.5).[59] Regardless, we were pleased to see that **8c** was recognized well by all homologues.

As previously discussed in section 3.1.3, NylC is an *N*-terminal nucleophile hydrolase, meaning that it undergoes autocatalytic cleavage (autoprocessing) at the active site threonine to produce the active protein as a heterodimer. In our hands, the six NylC homologues autoprocess nearly to completion during the induction stage, and we have incorporated an incubation step into our expression

protocol to ensure full autoprocessing (see Figure A3.4 in the Appendix) such that our measured enzyme activity is not convoluted by the rate of cleavage. However, another *N*-terminal nucleophile hydrolase with nylon-degrading activity has since been discovered and characterized.[78] This enzyme, TvgC, is derived from a thermophilic organism, and is correspondingly intrinsically "hyperthermostable" (with a melting temperature of 93 °C), requiring elevated temperatures to perform both its autoprocessing and amidase activities. We expressed and purified TvgC, then incubated the purified enzyme at 50 °C to induce autoprocessing. We discovered that we were able to correlate the extent of autoprocessing to activity *via* assay with **8c**, which demonstrates improved sensitivity over qualitative evaluation by SDS-PAGE (Figure 3.14). Notably, while the incubation to induce autoprocessing was performed at 50 °C, the activity assay itself is performed at 25 °C. This temperature is adequate for rapid hydrolysis of **8c** by the NylC enzymes, causing saturation of the instrument detector in minutes, but is below the optimal reaction temperature of TvgC (~60 °C). This could explain the low relative activity that TvgC demonstrates towards **8c** compared to the NylC enzymes (with a highest observed rate of ~0.04 μM/s, or ~25-fold slower than $NylC_{p2}$ and $NylC_A$). Despite this, the assay remains adequately sensitive to detect minute changes in activity due to incomplete autoprocessing.

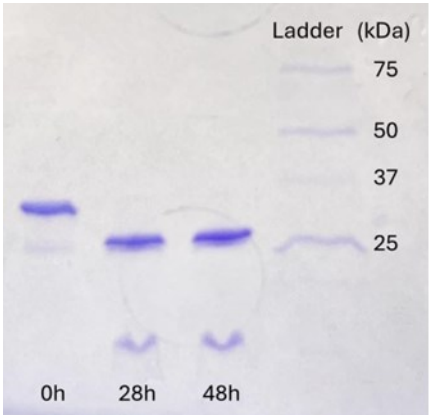

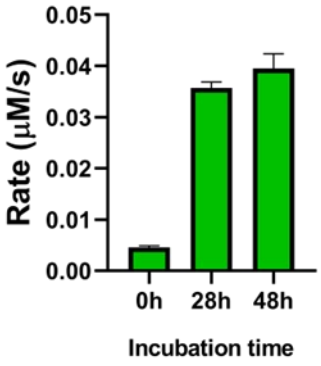

Figure 3.14. Left: SDS-PAGE analysis of TvgC analyzed at varying timepoints (0 h, 28 h, 48 h) during incubation at 50 °C. The unprocessed enzyme has a molecular weight of ~34 kDa; upon autocleavage it produces two fragments of approximately 24 and 10 kDa. Right: rates of hydrolysis of **8c** by TvgC at the same timepoints (0-48 h) Reaction conditions: TvgC (0.1 mg/mL), Tris buffer (100 mM, pH 6.9), substrate **8c** (2000 μM), and DMSO (10% v/v).

Among the NylCs, while long-term nylon hydrolysis experiments have been performed,[69,70,75] it is difficult to determine whether a "plateau" in the rate of nylon hydrolysis is due to denaturation/inactivation of the enzyme over time, or inaccessibility of the substrate. There has been speculation to the latter: that the availability of surface-exposed amorphous nylon is the defining factor of observed NylC activity.[69] To deconvolute this, we used the substrate **8c** to assess the tolerance of the NylC enzymes towards long term heating. Each enzyme was diluted to reaction concentration (0.1 mg/mL), and incubated at 50 °C for 8 days. Throughout this time, aliquots were acquired and activity was assessed. Figure 3.15 shows the residual activity for each enzyme after each incubation period.

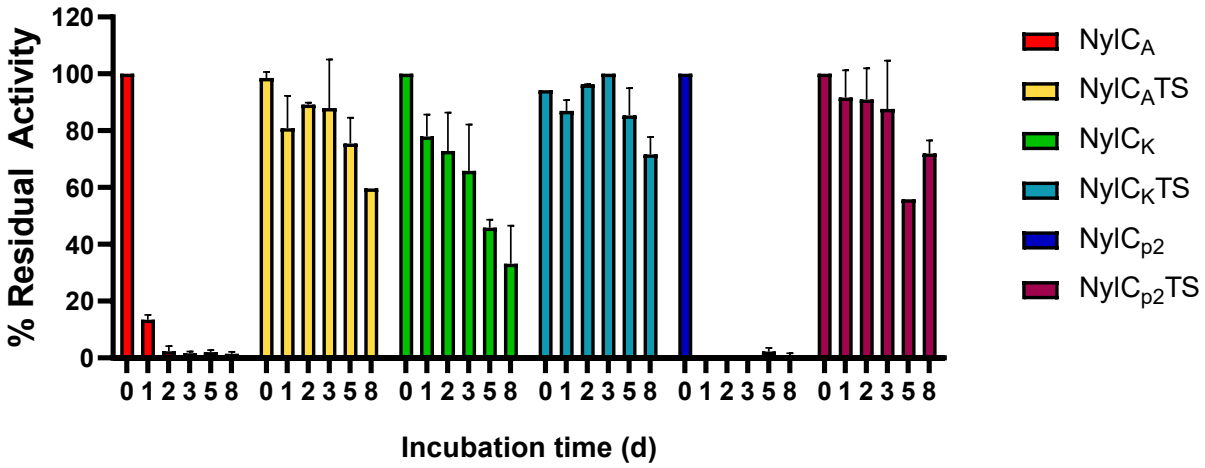

Figure 3.15. Residual activity of NylCs after heating at 50 ℃ for 0-8 days, as assessed by hydrolysis rate of **8c**. Data are represented as percentage of the maximum activity for each enzyme. Incubation conditions: enzyme (0.1 mg/mL), potassium phosphate buffer (20 mM, pH 7.3), 50 ℃. Ester hydrolysis conditions: enzyme (0.005 mg/mL), Tris buffer (100 mM, pH 6.9), **8c** (2 mM), DMSO (10%). Data are averages of two replicates with error bars indicating standard deviations.

Unsurprisingly, $NylC_A$ and $NylC_{p2}$, with relatively low melting temperatures of 60 ℃ and 52 ℃ respectively, lost activity after shorter periods incubating at 50 ℃. However, $NylC_K$, with a melting temp of only 67 ℃, was much more tolerant of an extended incubation, retaining ~30% of its activity after 8 days at 50 ℃. All of the thermostable enzymes retained a good deal of activity (~60-80%) throughout the duration of the experiment, only beginning to lose activity between 3-5 days of incubation. This study gives us a framework for the range of time over which we may conduct nylon degradation studies with these enzymes, in order to assess initial rates with accuracy.

3.3. Conclusion

We developed a rapid, sensitive, continuous and quantitative assay to report acyltransferase activity in NylC and related enzymes based on a 4-nitrophenyl ester chromogenic substrate. Among two small libraries of substrate analogues, we identified a scaffold, **8c**, with a relatively high affinity (K_M ~256 μM) for $NylC_A$, allowing for the quantification of activity in minutes. We demonstrated that this activity assay can be used to identify active NylC in cell lysate and shows notable activity with a variety of NylC enzymes. Furthermore, we determined that NylC-mediated

hydrolysis of the ester substrate **8c** correlates strongly with hydrolysis of an analogous amide substrate, **9**, indicating that this substrate probes the same catalytic machinery responsible for amide hydrolysis. We propose that this activity assay is best applied to determine the relative activity during the maturation and degradation of a single enzyme species, as different enzymes demonstrate variable activity towards hydrolysis of **8c**. To this end, we demonstrated that rates of **8c** hydrolysis track with rates of autoprocessing, reporting only on the activity of the cleaved enzyme. Finally, we use this activity assay to quantify long-term tolerance of NylCs towards elevated temperatures, which is necessary for nylon hydrolysis.

3.4. Materials and Methods

General Remarks

All reagents and solvents were purchased from commercial sources and used without further purification. ^{1}H- and ^{13}C-NMR spectra were recorded on Bruker 400 MHz or 600 MHz spectrometers, and chemical shifts were reported in ppm, referenced to the deuterated solvent peak. High resolution mass spectra were obtained with a quadrupole time-of-flight (QTOF) analyzer and electrospray ionization (ESI). Thin-layer chromatography (TLC) was performed using aluminium-backed silica plates and visualized using UV light, unless otherwise specified. SDS-PAGE was performed using Bio-Rad Mini-Protean TGX pre-cast, stain-free gels (4-20% polyacrylamide) and visualized using a Bio-Rad ChemiDoc MP imager. Agarose gels were prepared fresh prior to use, containing 1% agarose (w/v) and 1 μg/mL ethidium bromide. DNA was separated on agarose gel at 105 V in Tris-Acetate-EDTA (TAE) buffer and visualized using a Bio-Rad ChemiDoc MP imager. Ester and amide hydrolysis assays were performed using either a plate reader (Biotek Synergy H1) for experiments run in 96-well plates or a UV-vis spectrophotometer (Varian Cary 100 Bio) for experiments run in cuvettes, as specified.

3.4.1. Molecular Biology Methods

Plasmid Preparation

The amino acid sequence of $NylC_A$ obtained from the Protein Data Bank (PDB ID 3AXG)[68] was reverse-translated with codon-optimization for *E. coli*, and modified with an *N*-terminal NdeI recognition sequence and a *C*-terminal XhoI recognition sequence. The modified gene was commercially synthesized by GeneArt (Thermo Fisher). The gene was cloned into the expression vector pET21c, then transformed into chemically competent *E. coli* XL1-Blue cells in the presence of 100 μg/mL ampicillin. The recombinant plasmid, pAR2-1, was then extracted and the sequence was confirmed by Génome Québec.

Site-Directed Mutagenesis

The mutation T267A was created by site-directed mutagenesis using full-plasmid PCR. Custom primers were purchased from Integrated DNA Technologies (See Table A3.2 in the Appendix) where the T267A mutation was encoded on the forward primer, and PCR was performed using Q5 High-Fidelity DNA polymerase (New England Biolabs) and pAR2-1 as the template. Following amplification of the gene as confirmed by agarose gel electrophoresis, the DNA was purified (E.Z.N.A. Cycle Pure Kit, Omega BioTek) then a digest of the template was performed using DpnI (New England Biolabs). Following digestion, the amplicon was purified again using the Cycle Pure Kit, then phosphorylated (T4 PNK, New England Biolabs) and ligated (T4 DNA Ligase, New England Biolabs). The circularized amplicon was then transformed into chemically competent *E. coli* XL1-Blue cells in the presence of 100 μg/mL ampicillin. Five colonies containing mutant plasmid were picked and sequenced (Génome Québec).

General Procedure for the Expression of $NylC_A$

The recombinant plasmid pAR2-1 was transformed into BL21 (DE3) cells that were then inoculated on LB agar plates supplemented with 100 μg/mL of ampicillin. Single colonies were picked and incubated at 37 °C for 18 h in LB medium supplemented with ampicillin (100 μg/mL). These cultures were used to inoculate a large culture (1% bacterial culture/broth) of ZYM-5052 autoinduction medium[54] supplemented with 100 μg/mL ampicillin and 1 mM IPTG. These cultures were incubated at 16 °C for 60 h. Bacteria were pelleted through centrifugation at 3400 × g then resuspended (1:50 v/v) in lysis buffer (20 mM potassium phosphate (pH 7.3) containing 10% glycerol) and lysed with a homogenizer (AVESTIN). The lysate was clarified via centrifugation at 11 600 × g. The soluble fraction was incubated with His 60 Ni Superflow resin (Takara) (1:1000 v/v resin: culture volume) at 4 °C for 1 hour on a rotary shaker. The immobilized protein was then washed with lysis buffer (10 column volumes) and eluted with an imidazole gradient of 10-150 mM (10 column volumes per fraction). The fractions were analyzed by SDS-PAGE, and fractions containing pure protein were concentrated using a 10-kDa Amicon tube (Sigma Aldrich) and the buffer was exchanged with 3 × 10 volumes of storage buffer (potassium phosphate 20 mM pH 7.3 containing 10% glycerol). Protein concentration was determined according to a Bradford assay. Protein aliquots were flash-frozen and stored at -80°C until use.

General procedure for the expression of NylCs from commercially available plasmids

Overexpression of NylC enzymes was performed following the protocol published by Bell et al.[69] with certain modifications. In summary, the corresponding NylC gene, inserted into pET28a

vectors, were obtained from AddGene (Table A3.3 in the Appendix), transformed into BL21-DE3 *E. coli* cells, and selected on LB agar plates supplemented with 30 μg/mL kanamycin. Single colonies were picked to prepare liquid small cultures, which served to inoculate 2×YT medium expression cultures supplemented with 30 μg/mL of kanamycin. Those cultures were incubated at 37 °C to an OD of 1, then 0.1 mM IPTG was added and expression was induced by shaking for 20 hours at 20 °C. To purify the enzymes, cells were collected by centrifugation at 3400 × g for 20 minutes at 4 °C. The cells were then resuspended (1:50 v/v) in lysis buffer (Tris 50 mM pH 7.5, 10 mM imidazole, 300 mM NaCl and 1 mg/mL of lysozyme) and lysed by sonication (Hielscher Ultrasonic Processor UP50H) at 70% amplitude using a 3:2 seconds on and off cycle for a minute followed by a minute on ice, 3 times. The soluble and insoluble fractions were separated by centrifugation at 19 300 × g for 15 minutes at 4 °C. The soluble fraction was incubated with His 60 Ni Superflow resin (1:1000 v/v resin: culture) at 4 °C for 60 minutes on a rotary shaker. Bound proteins were then washed with 4 × 10 column volumes of lysis buffer containing no lysozyme and eluted using 3 ×10 column volumes of elution buffer (Tris 50 mM pH 7.5, 300 mM imidazole and 300 mM NaCl). Collected fractions were analyzed by SDS-PAGE and fractions containing pure protein were concentrated using 10-kDa MWCO Amicon tubes (Sigma Aldrich) then buffer-exchanged with 3 × 15 mL storage buffer (20 mM potassium phosphate pH 7.3 and 10% glycerol). Purified protein was incubated at 37 ℃ for 16 hours to promote autoprocessing. Samples were then centrifuged briefly to remove any precipitated protein, then protein concentration was quantified via Bradford assay. The enzymes were aliquoted, then flash-frozen and stored at -80 °C until use.

Expression and purification of TvgC

The plasmid encoding TvgC (in pET28a) was a generous gift from the lab of Prof. Graeme Howe (Queen's University). Protein expression proceeded as reported,[78] except using ZYM-5052[54] as the autoinducing medium. Following buffer exchange, a 50 μL aliquot was taken and stored at 4 ℃. The remaining protein was incubated at 50 ℃ for 48 h, during which a second aliquot was removed at 28 h. After 48 hours, the sample was removed from heat, centrifuged to remove precipitated protein, and quantified by Bradford assay. The aliquots and a sample from the final protein stock were evaluated by SDS-PAGE and ester hydrolysis assay.

Preparation of cell lysate for crude lysate assays

Chemically-competent BL21-DE3 cells were transformed with either pAR2-1 or pET21c plasmids. Single colonies from each transformation were picked and incubated at 37 °C for 18 h in 5 mL LB medium supplemented with ampicillin (100 μg/mL). Following the general procedure for expression of $NylC_A$, a 25-mL culture was prepared from each small culture and incubated with shaking at 16 °C for 60 hours. The cells were then pelleted by centrifugation at 3400 × g for 20 minutes, then resuspended in lysis buffer. The resuspended cells were then subjected to 8 freeze-thaw cycles at alternating -78 °C and 37 °C. The lysates were clarified by centrifugation at 15 300 × g for 10 minutes, then the soluble fraction was aliquoted and flash-frozen at -78 °C until use.

3.4.2. Assay Methods

Ester Hydrolysis Assay

All ester hydrolysis assays with purified enzyme were performed in a 96-well microtiter plate in 200-μL reaction volumes at 25 °C. Each reaction mixture contained 100 mM of Tris buffer

(pH 6.9), and reactions were initiated through addition of a 10 × stock solution of substrate in dimethylsulfoxide (DMSO), such that the final concentration of DMSO was 10% (v/v). The absorbance of the hydrolysis product, 4-nitrophenolate, was monitored at 399 nm with readings acquired every 10 seconds over 20 minutes using a plate reader. A calibration curve (Figure A3.5 in the Appendix) was produced using standard concentrations of pNP at pH 6.9 (in the presence of 100 mM Tris buffer) in order to convert absorbance values into product concentrations.

The initial, exploratory reaction with the substrate, 4-nitrophenyl octanoate (**7e**), was performed using 0.2 mg/mL of $NylC_A$ and substrate concentrations ranging from 0-100 μM. Each reaction was performed in duplicate.

Initial screening of substrates was performed using 0.1 mg/mL of $NylC_A$ at substrate concentrations ranging from 0 to 50 μM. Each reaction was performed in duplicate alongside a blank containing no enzyme for each substrate concentration. The initial rates of the duplicate reactions were averaged and blank-corrected for background hydrolysis, then used to evaluate the catalytic efficiency of the enzyme towards each substrate in the form of k_{cat}/K_M.

The Michaelis-Menten characterization of substrate **8c** was performed with substrate concentrations ranging from 0 to 5000 μM, in the presence of 2.4 U/mL of enzyme. Initial rates were measured as above and fitted by nonlinear regression to the following Michaelis-Menten equation (Equation 1, Equation 2), providing the parameters k_{cat} and K_M. In this equation, $[E]_{TOT}$ was calculated using 38 kDa as the molecular weight of the heterodimer,[59] constituting one of four active units in the fully assembled enzyme. Thus, the concentration of enzyme in each reaction mixture was 2.6 μM.

The activity of point mutant NylC$_A$-T267A was evaluated by monitoring the absorbance at 399 nm for 20 minutes of a reaction mixture containing 100 mM Tris, 2 mM of substrate **8c**, and 0.1 mg/mL of NylC$_A$-T276A at pH 6.9. The reaction was run in duplicate alongside one blank reaction containing no enzyme.

The NylC stability assay was performed as follows: solutions of enzyme (0.1 mg/mL, 150 μL, in duplicate for each enzyme) were prepared in 20 mM phosphate buffer, and incubated at 50 ℃. Aliquots (20 μL) were removed at 0, 1, 2, 3, 5, and 8 days, and stored at -20 ℃ until evaluation by hydrolysis of **8c**. Ester hydrolysis reactions were performed using 10 μL of enzyme aliquot (final concentration of 0.005 mg/mL) under standard assay conditions (100 mM Tris, pH 6.9; 2 mM **8c**, 10% DMSO). Reactions were performed alongside blank reactions containing no enzyme.

Amide Hydrolysis Assay

Assays monitoring hydrolysis of amide substrates **9** and *p*NBA were performed in a 96-well microtiter plate in 200-μL reaction volumes at 25 °C. Each reaction mixture contained 100 mM of Tris buffer (pH 6.9), and 10% v/v DMSO. The absorbance of the hydrolysis product, 4-nitroaniline (pNA), was monitored at 383 nm over 180 minutes using a plate reader. A calibration curve (Figure A3.6 in the Appendix) was produced using standard concentrations of pNA at pH 6.9 (in the presence of 100 mM Tris buffer) in order to convert absorbance values into product concentrations.

Characterization of compound **9** by Michaelis-Menten kinetics was performed with substrate concentrations ranging from 0-1000 μM in the presence of 0.1 mg/mL (2.6 μM) enzyme. Initial rates were determined and plotted against substrate concentration. The data were fitted by nonlinear regression with the Michaelis-Menten equation (see above). The linear region of the Michaelis-

Menten plot, spanning substrate concentrations of 0-200 μM, were fitted by linear regression to estimate k_{cat}/K_M values.

Specific activity of $NylC_A$ with compound **9** was performed using 1000 μM of substrate in the presence of 0.1 mg/mL enzyme. Specific activity determination was otherwise identical to that of compound **8c**.

Evaluation of the relative activity of **9** and ***p*NBA** was performed using 1000 μM of the corresponding substrate, and 0.1 mg/mL $NylC_A$.

Hydrolysis of **8c** by cell lysate

Hydrolysis reactions were performed in 1 mL reaction volumes in cuvettes at 25 °C in the presence of buffer (100 mM Tris, pH 6.9) and 500 μM of substrate **8c**. Reaction mixtures contained either no protein (blank), lysate from pET21c–transformed cells (40 μL), or lysate from pAR2-1–transformed cells (40 μL, in duplicate). The formation of the hydrolysis product, 4-nitrophenolate, was monitored over 20 minutes at 399 nm.

3.4.3. Methods for Predictive Modelling using Chai-1

The Chai-1 structure prediction tool was accessed using the web interface, currently available at https://lab.chaidiscovery.com/. The sequence for $NylC_A$ was taken from the UniProt database (entry Q1EPR5). To simulate the active enzyme with an accessible active site, the following modifications were made to the sequence:

- The N-terminal methionine was removed

- The sequence was split into two peptide chains, where T267 was at the N-terminus of the second chain, simulating autoprocessing
- The C-terminal sequence VTGEAN from the first chain (i.e. residues immediately prior to T267) were removed to circumvent the possibility that this disordered loop, which is not present in the crystal structure, would obfuscate the active site in the model.

The resultant protein sequences inputted into Chai-1were as follows:

Chain 1: NTTPVHALTDIDGGIAVDPAPRLAGPPVFGGPGNDAFDLAPVRSTGREM-
LRFDFPGVSIGAAHYEEGPTGATVIHIPAGARTAVDARGGAVGLSGGYDFNHAICLAGGA
SYGLEAGAGVSGALLERLEYRTGFAEAQLVSSAVIYDFSARSTAVYPDKALGRAALEFAV-
PGEFPQGRAGAGMSASAGKVDWDRTEITGQGAAFRRLGDVRILAVVVPNPVGVIMDRA
GTVVRGNYDAQTGVRRHPVFDYQEAFAEQVPP

Chain 2: TTISAIVTNVRMSPVELNQFAKQVHSSMHRGIQPFHTDMDGDTLFAVTTDEID-
LPTTPGSSRGRLSVNATALGAIASEVMWDAVLEAGK

The SMILES codes inputted for each ligand were as follows:

- Compound **8c**: O=C(OC1=CC=C([N+]([O-])=O)C=C1)CCCNC(C)=O
- Compound **7d**: O=C(OC1=CC=C([N+]([O-])=O)C=C1)CCCCCC

For the structure prediction, Multiple Sequence Alignments (MSAs) and Templates were used, to allow Chai-1 to use the known structures of NylC to guide the structure prediction. However, no restraints were used to guide ligand placement, meaning the substrates were placed in the active site in an unbiased manner.

The outputted structure predictions were visualized using PyMol.

3.4.4. Synthetic Methods

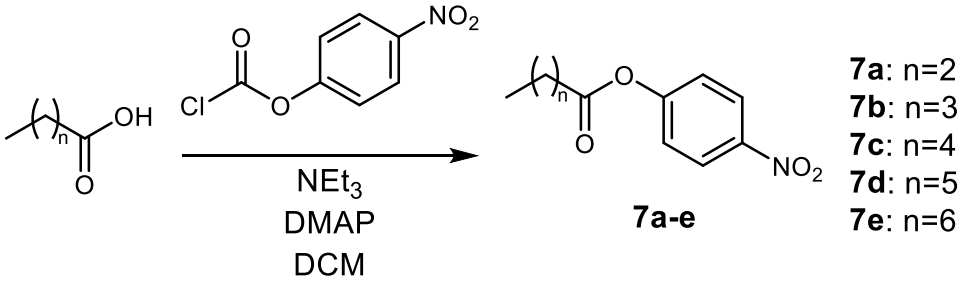

General procedure for the synthesis of compounds **7a-e** (**GP6**):

Preparation of *p*-nitrophenyl esters proceeded as adapted from a literature protocol.[79] The corresponding aliphatic carboxylic acid (100 mg, 1 eq.) was dissolved in DCM (5 mL) in a round bottom flask in the presence of NEt_3 (2 eq.) and DMAP (0.1 eq.) with gentle stirring. To the flask was then added 4-nitrophenyl chloroformate (1.1 eq.) and the mixture was stirred until reaction completion as determined by TLC (15% EtOAc in hexane). The DCM was evaporated under vacuum and the resulting residue was redissolved in EtOAc (10 mL). The EtOAc solution was then washed with water (1 × 10 mL), saturated $NaHCO_3$ (2 × 10 mL) and brine (1 × 10 mL). The organic phase was dried over $MgSO_4$. The filtrate was concentrated *in vacuo* leaving the product as a yellow oil.

4-Nitrophenyl butyrate (7a). Following GP6, isolated yield: 142 mg, 60%. ^{1}H NMR (400 MHz, $CDCl_3$) δ 8.27 (m, 2H), 7.28 (m, 2H), 2.59 (t, J = 7.4 Hz, 2H), 1.80 (sextet, J = 7.4 Hz, 2H), 1.05 (t, J = 7.4 Hz, 3H). Characterization data are consistent with literature.[80] No molecular ion was observable by mass spectrometry.

4-Nitrophenyl valerate (7b). Following GP6, isolated yield: 175 mg, 80%. ^{1}H NMR (400 MHz, CDCl3) δ 8.27 (m, 2H), 7.27 (m, 2H), 2.61 (t, *J* = 7.5 Hz, 2H), 1.75 (qu, *J* = 7.5 Hz, 2H), 1.45 (q, *J* = 7.5 Hz, 2H), 0.98 (t, *J* = 7.4 Hz, 3H). ^{13}C NMR (151 MHz, $CDCl_3$) δ 171.5, 155.7, 145.4, 125.3, 122.6, 34.2, 26.9, 22.3, 13.8. No molecular ion was observable by mass spectrometry.

4-Nitrophenyl hexanoate (7c). Following GP6, isolated yield: 157 mg, 77%. ^{1}H NMR (400 MHz, $CDCl_3$) δ 8.27 (m, 2H), 7.27 (m, 2H), 2.60 (t, *J* = 7.5 Hz, 2H), 1.76 (qu, *J* = 4.4 Hz, 2H), 1.40 (m, 4H), 0.93 (t, *J* = 3.5 Hz, 3H). Characterization data are consistent with literature.[80] No molecular ion was observable by mass spectrometry.

4-Nitrophenyl heptanoate (7d). Following GP6, isolated yield: 130 mg, 68%. ^{1}H NMR (400 MHz, $CDCl_3$) δ 8.27 (m, 2H), 7.27 (m, 2H, overlaps with $CHCl_3$ residual), 2.60 (t, *J* = 7.5 Hz, 2H), 1.76 (qu, *J* = 7.5 Hz, 2H), 1.38 (m, 6H), 0.91 (t, *J* = 4.7 Hz, 3H). ^{13}C NMR (151 MHz, $CDCl_3$) δ 171.5, 155.7, 145.4, 125.3, 122.6, 34.5, 31.5, 28.8, 24.8, 22.6, 14.2. No molecular ion was observable by mass spectrometry.

4-Nitrophenyl octanoate (7e). Following GP6, isolated yield: 162 mg, 88%. ^{1}H NMR (400 MHz, $CDCl_3$) δ 8.27 (m, 2H), 7.27 (m, 2H), 2.60 (t, *J* = 7.5 Hz, 2H), 1.76 (qu, *J* = 7.4 Hz, 1H), 1.35 (m, 8H), 0.89 (t, *J* = 6.8 Hz, 3H). Characterization data are consistent with the literature.[80] No molecular ion was observable by mass spectrometry.

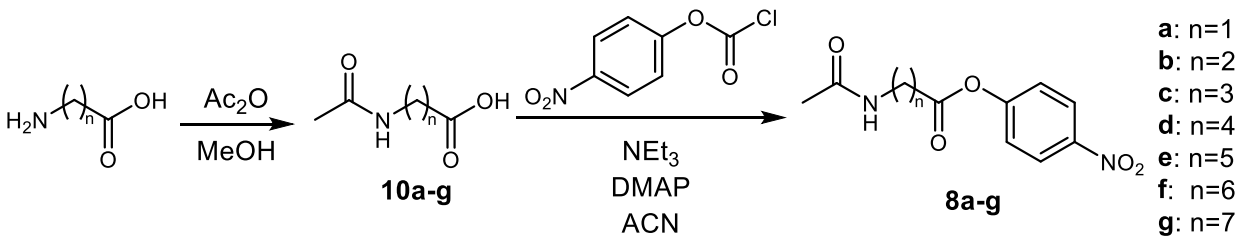

General procedure for the synthesis of compounds **10a-g** (**GP7**):

The corresponding ω-amino carboxylic acid (200 mg, 1 eq.) was dissolved in MeOH (3 mL) in a round bottom flask with stirring. Then acetic anhydride (2 eq.) was added dropwise, unless specified otherwise. The solution was left stirring until the reaction completion as determined by TLC (10% MeOH in DCM) followed by ninhydrin staining. The solvent was then evaporated *in vacuo*, and the product was isolated as described below.

***N*-Acetylglycine (10a)**. The reaction was set up following GP7, except as follows: solubility of the glycine reagent was aided through dropwise addition of water until the reaction mixture became homogeneous. An additional 2 equivalents of acetic anhydride were added. After completion, the reaction mixture was concentrated to remove the MeOH, and the resulting solution was left at -20 °C until a white precipitate formed. The supernatant was filtered, and the white solid was suspended in Et_2O which was then evaporated under vacuum into a white solid. That solid was suspended in acetone and dried *in vacuo* to leave the product as a fine white powder. The compound was used without further purification.^{1}H NMR (400 MHz, DMSO) δ 8.18 (br. t, J = 5.6 Hz, 1H), 3.71 (d, J = 5.9 Hz, 2H), 1.84 (s, 3H). Characterization data are consistent with literature.[81,82]

***N*-Acetyl-β-alanine (10b)**. The reaction was performed following GP7. Following the evaporation of methanol, the resulting oil was co-evaporated with Et_2O, then triturated from Et_2O and left at -20 °C overnight, during which a white precipitate formed. The supernatant was then filtered, the resulting solid was suspended in Et_2O and then dried in vacuo, leaving the product as a white powder. Isolated yield: 279 mg, 94.7%. ^{1}H NMR (400 MHz, DMSO) δ 7.92 (br. s, 1H), 3.20 (q, J

= 6.5 Hz, 2H), 2.35 (t, *J* = 6.9 Hz, 2H), 1.77 (s, 3H). ^{13}C NMR (151 MHz, DMSO) δ 172.9, 169.3, 34.8, 33.9, 22.5. HRMS (ESI) calc'd for $C_5H_9NO_3Na$ ($[MNa]^+$): 154.0480, found: 154.0449.

***N*-Acetyl-4-aminobutyric acid (10c)**. The reaction was performed following GP7. Evaporation of the MeOH produced a homogeneous sticky white solid. Et_2O was added to the flask, the mixture was sonicated, then solvent was removed in vacuo leaving the product as a white powder. Isolated yield: 283 mg, > 95%. ^{1}H NMR (400 MHz, DMSO) δ 7.85 (br. s, 1H), 3.01 (q, *J* = 6.5 Hz, 2H), 2.20 (t, *J* = 7.4 Hz, 2H), 1.78 (s, 3H), 1.60 (qu., *J* = 7.2 Hz, 2H). ^{13}C NMR (151 MHz, DMSO) δ 174.3, 169.2, 37.9, 31.1, 24.6, 22.6. HRMS (ESI) calc'd for $C_6H_{11}NO_3Na$ ($[MNa]^+$): 168.0637, found: 168.0627.

N-Acetyl-5-aminovaleric acid (10d). The reaction was performed following GP7. Following the evaporation of methanol, the resulting viscous residue was co-evaporated once with diethyl ether, then redissolved in a minimal amount of DCM (~0.5 mL). Et_2O (3 mL) was then added to give a fine, cloudy suspension which was then cooled to -20 °C overnight to give a white crystalline solid. The supernatant was decanted off and the solid dried under vacuum to give the product (205 mg, 78%). ^{1}H NMR (400 MHz, $CDCl_3$) δ 5.78 (s, 1H), 3.26 (q, *J* = 6.5 Hz, 2H), 2.38 (t, *J* = 7.1 Hz, 2H), 1.99 (s, 3H), 1.66 (m, 2H), 1.57 (m, 2H). ^{13}C NMR (151 MHz, DMSO) δ 173.8, 168.3, 37.5, 32.7, 28.0, 22.0, 21.4. HRMS (ESI) calc'd for $C_7H_{13}NO_3Na$ ($[MNa]^+$): 182.0793, found: 182.0781.

***N*-Acetyl-6-aminohexanoic acid (10e)**. This reaction was performed on a 500 mg (3.81 mmol) scale of 6-aminohexanoic acid, following GP7. The MeOH was evaporated, then Et_2O was added which resulted in a small amount of solid precipitating out of solution. The mixture was left at -20 °C to promote precipitation, then the supernatant was filtrated and the solid dried under vacuum, resulting in a white solid. Isolated yield: 344 mg, 52%. ^{1}H NMR (400 MHz, DMSO) δ 12.00 (s, 1H), 7.79 (s, 1H), 2.99 (q, *J* = 6.5 Hz, 2H), 2.18 (t, *J* = 7.4 Hz, 2H), 1.77 (s, 3H), 1.48 (qu., *J* =

7.5 Hz, 2H), 1.36 (qu., *J* = 7.2 Hz, 2H), 1.24 (m, 2H). Characterization data are consistent with literature.[82,83]

***N*-Acetyl-7-aminoheptanoic acid (10f)**. The reaction was performed according to GP7. Following evaporation of the methanol, the resulting oil was triturated with Et_2O, then left at -20°C until a white precipitate formed. The solid was then collected by filtration and dried in vacuo, leaving the product as a white powder. Isolated yield: 173 mg, 67%. ^{1}H NMR (600 MHz, $CDCl_3$) δ 5.81 (br. s, 1H), 3.22 (q, *J* = 6.7 Hz, 2H), 2.33 (t, *J* = 7.4 Hz, 2H), 1.98 (s, 3H), 1.62 (m, 2H), 1.49 (m, 2H), 1.34 (m, 4H). ^{13}C NMR (151 MHz, $CDCl_3$) δ 178.4, 170.8, 39.7, 34.1, 29.4, 28.7, 26.6, 24.7, 23.3. HRMS (ESI) calc'd for $C_{19}H_{17}NO_3Na$ ($[MNa]^+$): 210.1106, found: 210.1108.

***N*-Acetyl-8-aminooctanoic acid (10g)**. This reaction was performed in the absence of methanol, by heating a solution of 8-aminooctanoic acid in neat acetic anhydride (3 mL) to 95 °C. Upon completion, the reaction mixture was cooled to room temperature, then concentrated in vacuo. The resulting residue was diluted with Et_2O and cooled to -20 °C until a white precipitate formed. The precipitate was collected by filtration and dried under vacuum to give the product as a white powder. Isolated yield: 186 mg, 74%. ^{1}H NMR (400 MHz, DMSO) δ 7.80 (s, 1H), 2.99 (q, *J* = 6.6 Hz, 2H), 1.77 (s, 3H), 1.53 (m, 2H), 1.30 (m, 10H). ^{13}C NMR (151 MHz, MeOD) δ 177.7, 173.2, 171.2, 40.4, 40.4, 35.8, 34.9, 34.7, 30.3, 30.2, 30.1, 30.1, 30.0, 29.9, 29.8, 27.8, 27.7, 26.4, 26.0, 25.9, 25.2, 22.5. Conformational isomers observed in ^{13}C spectrum; all peaks reported. HRMS (ESI) calc'd for $C_{10}H_{19}NO_3Na$ ($[MNa]^+$): 224.1263, found: 224.1281.

General procedure for the synthesis of compounds **8a-g** (**GP8**):

The corresponding *N*-acetylcarboxylic acid (50 mg, 1 eq.) was stirred in acetonitrile with NEt_3 (2 eq.) and DMAP (0.1 eq.). Then 4-nitrophenyl chloroformate (1.1 eq.) was added and the reaction

mixture was stirred until reaction completion as determined by TLC (50% EtOAc in hexane). The solvent was evaporated *in vacuo* and left a yellow residue that was then redissolved in 10 mL EtOAc. That solution was washed with water (1 × 10 mL), saturated aqueous $NaHCO_3$ (2 ×10 mL) and brine (1 × 10 mL). The organic phase was then dried with magnesium sulfate, filtered, and evaporated under vacuum, leaving the product as a white powder unless specified otherwise.

***N*-Acetylglycine 4-nitrophenyl ester (8a)**. Following GP8, isolated yield: 34 mg, 33%. ^{1}H NMR (400 MHz, $CDCl_3$) δ 8.29 (d, J = 9.2 Hz, 2H), 7.32 (d, J = 9.2 Hz, 2H), 6.01 (br. s, 1H), 4.34 (d, J = 5.5 Hz, 2H), 2.11 (s, 3H). ^{13}C NMR (151 MHz, $CDCl_3$) δ 171.0, 168.0, 154.9, 145.7, 125.5, 122.4, 41.7, 23.0. HRMS (ESI) calc'd for $C_{10}H_{10}N_2O_5Na$ ($[MNa]^+$): 261.0487, found: 261.0479.

***N*-Acetyl-β-alanine 4-nitrophenyl ester (8b).** Following GP8, isolated yield: 52 mg, 54%. ^{1}H NMR (400 MHz, $CDCl_3$) δ 8.29 (d, J = 9.1 Hz, 2H), 7.30 (d, J = 9.1 Hz, 2H), 6.00 (br. s, 1H), 3.63 (q, J = 6.0 Hz, 2H), 2.87 (t, J = 5.9 Hz, 2H), 2.00 (s, 3H). ^{13}C NMR (151 MHz, $CDCl_3$) δ 170.5, 170.4, 155.2, 145.6, 125.4, 122.5, 35.0, 34.5, 23.4. HRMS (ESI) calc'd for $C_{11}H_{12}N_2O_5Na$ ($[MNa]^+$): 275.0644, found: 275.0625.

***N*-Acetyl-4-aminobutyric acid 4-nitrophenyl ester (8c).** Following GP8, isolated yield: 65 mg, 71%. ^{1}H NMR (400 MHz, $CDCl_3$) δ 8.28 (d, J = 9.1 Hz, 2H), 7.30 (d, J = 9.1 Hz, 2H), 5.62 (br. s, 1H), 3.39 (q, J = 6.6 Hz, 2H), 2.67 (t, J = 7.2 Hz, 2H), 2.00 (s, 3H), 1.96 (qu., J = 7.0 Hz, 2H). ^{13}C NMR (151 MHz, $CDCl_3$) δ 171.0, 170.6, 155.5, 145.5, 125.4, 122.6, 38.8, 31.7, 24.7, 23.4. HRMS (ESI) calc'd for $C_{12}H_{14}N_2O_5Na$ ($[MNa]^+$): 289.0800, found: 289.0775.

***N*-Acetyl-5-aminovaleric acid 4-nitrophenyl ester (8d).** Following GP8, isolated yield: 49 mg, 76%. ^{1}H NMR (400 MHz, $CDCl_3$) δ 8.27 (d, J = 8.9 Hz, 2H), 7.29 (d, 2H), 5.71 (br. s, 1H), 3.32

(d, J = 4.8 Hz, 2H), 2.66 (t, J = 7.0 Hz, 2H), 2.02 (s, 3H), 1.80 (qu., J = 7.0 Hz, 2H), 1.66 (qu., J = 6.2 Hz, 2H). ^{13}C NMR (151 MHz, $CDCl_3$) δ 171.2, 170.4, 155.6, 145.6, 125.4, 122.6, 39.24, 33.9, 29.2, 23.6, 22.0. HRMS (ESI) calc'd for $C_{12}H_{16}N_2O_5Na$ ($[MNa]^+$): 303.0957, found: 303.0956.

***N*-Acetyl-6-aminohexanoic acid 4-nitrophenyl ester (8e)**. Following GP8, isolated yield: 60 mg, 71%. ^{1}H NMR (400 MHz, $CDCl_3$) δ 8.20 (dt, J = 2.1, 9.1 Hz, 2H), 7.22 (dt, J = 2.1, 9.1 Hz, 2H), 6.02 (br. s, 1H), 3.22 (q, J = 6.7 Hz, 2H), 2.56 (t, J = 7.4 Hz, 2H), 1.94 (s, 3H), 1.72 (qu., J = 7.5 Hz, 2H), 1.53 (qu., J = 7.3 Hz, 2H), 1.41 (m, 2H). ^{13}C NMR (151 MHz, $CDCl_3$) δ 171.2, 170.2, 155.5, 145.4, 125.3, 122.5, 39.4, 34.2, 29.5, 26.4, 24.4, 23.5. HRMS (ESI) calc'd for $C_{14}H_{18}N_2O_5Na$ ($[MNa]^+$): 317.1113, found: 317.1096.

***N*-Acetyl-7-aminoheptanoic acid 4-nitrophenyl ester (8f)** Following GP8, the product was isolated as a pale-yellow powder. Isolated yield: 69 mg, 83% ^{1}H NMR (400 MHz, $CDCl_3$) δ 8.27 (m, 2H), 7.28 (d, J = 3.5 Hz, 2H), 5.45 (br. s, J = 10.6 Hz, 1H), 3.26 (q, J = 6.8 Hz, 2H), 2.60 (t, J = 7.4 Hz, 2H), 1.98 (s, 3H), 1.76 (m, 3H), 1.54 (qu., J = 7.2 Hz, 2H), 1.41 (m, 4H). ^{13}C NMR (151 MHz, $CDCl_3$) δ 171.3, 170.3, 155.6, 145.4, 125.3, 122.5, 39.6, 34.3, 29.6, 28.7, 26.6, 24.6, 23.5. HRMS (ESI) calc'd for $C_{15}H_{20}N_2O_5Na$ ($[MNa]^+$): 331.1270, found: 331.1290.

***N*-Acetyl-8-aminooctanoic acid 4-nitrophenyl ester (8g)**. Following GP8, the product was isolated as a yellow powder. Isolated yield: 25.1 mg, 31%. ^{1}H NMR (600 MHz, $CDCl_3$) δ 8.26 (d, J = 3.0 Hz, 2H), 7.27 (d, J = 4.6 Hz, 2H), 5.56 (br. s, 1H), 3.24 (q, J = 6.8 Hz, 2H), 2.59 (t, J = 7.4 Hz, 2H), 1.98 (s, 3H), 1.75 (qu., J = 7.4 Hz, 2H), 1.51 (qu., J = 7.2 Hz, 2H), 1.38 (m, 6H). ^{13}C NMR (151 MHz, $CDCl_3$) δ 171.4, 170.5, 155.6, 145.4, 125.3, 122.6, 39.8, 34.4, 29.7, 29.0, 29.0, 26.8, 24.7, 23.5. HRMS (ESI) calc'd for $C_{16}H_{22}N_2O_5Na$ ($[MNa]^+$): 345.1426, found: 345.1432.

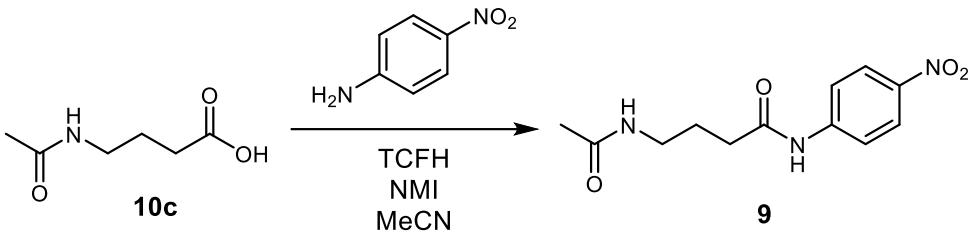

***N*-Acetyl-4-aminobutyric acid 4-nitroanilide (9).** To a stirred solution of p-nitroaniline (100 mg, 0.724 mmol), **10c** (115 mg, 0.796 mmol) and N-methylimidazole (202 µL, 2.53 mmol) in MeCN (3 mL) was added *N*,*N*,*N*′,*N*′-tetramethylchloroformamidinium hexafluorophosphate (TCFH) (250 mg, 0.890 mmol). The reaction was stirred at R.T. and found to be complete after 40 h by TLC analysis (7:3 EtOAc : Hexanes). Upon completion, the solvent was removed in vacuo, then the residue was resuspended in 10 mL H_2O. The suspension was sonicated to break up particulate, then the solid was collected by vacuum filtration. The solid was washed with an additional 20 mL H_2O, then collected and dried under gentle heating to give the product as a powdery, tan solid (105 mg, 55%). ^{1}H NMR (400 MHz, DMSO) δ 10.54 (s, 1H), 8.21 (dt, *J* = 2.0, 7.2 Hz, 2H), 7.89 (t, *J* = 5.0 Hz, 1H), 7.83 (dt, *J* = 2.0, 7.2 Hz, 2H), 3.07 (q, *J* = 6.5 Hz, 2H), 2.38 (t, *J* = 7.5 Hz, 2H), 1.79 (s, 3H), 1.72 (qu, *J* = 7.2 Hz, 2H). ^{13}C NMR (101 MHz, DMSO) δ 171.9, 169.2, 145.5, 142.0, 125.0, 118.6, 38.0, 34.0, 24.9, 22.6. HRMS (ESI) calc'd for $C_{12}H_{15}N_3O_4Na$ ($[MNa]^+$): 288.0960, found: 288.0949.

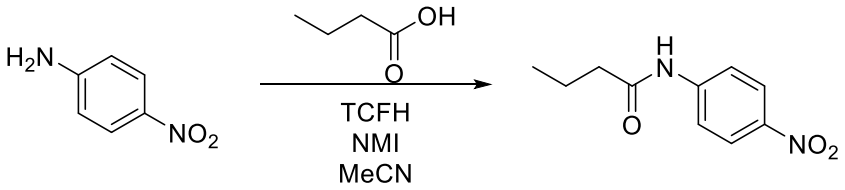

***p*-Nitrophenylbutyramide (pNBA)**. To a stirred solution of *p*-nitroaniline (100 mg, 0.724 mmol), butyric acid (73 µL, 0.796 mmol) and *N*-methylimidazole (202 µL, 2.53 mmol) in MeCN (3 mL) was added *N*,*N*,*N*′,*N*′-tetramethylchloroformamidinium hexafluorophosphate (TCFH) (250 mg,

0.890 mmol). The reaction was stirred for 60 h at R.T. until no further conversion was observed by TLC analysis (eluted with 100% DCM). The reaction mixture was evaporated in vacuo and co-evaporated with DCM, then the residue was triturated through addition of 15 mL H_2O. The resulting suspension was sonicated, then the solid collected by filtration and washed several times with water. The solid was dried under ambient conditions for 72 hours to give the product as shiny, yellow-brown crystals (66 mg, 44%). ^{1}H NMR (400 MHz, DMSO) δ 10.51 (s, 1H), 8.20 (d, J = 9.3 Hz, 2H), 7.83 (d, J = 9.3 Hz, 2H), 2.35 (t, J = 7.3 Hz, 2H), 1.62 (sextet, J = 7.4 Hz, 2H), 0.91 (t, J = 7.4 Hz, 3H). Characterization data are consistent with literature.[84]

Chapter 4. Nylon Analogue Substrates for Continuous Quantification of Polyamidase Activity in Nylon-Degrading Enzymes

Preamble

This chapter contains selections that were reproduced from: A. M. M. Rangaswamy, F. M. Roy, J. W. Keillor, *ChemRxiv* preprint **2024**, DOI: 10.26434/chemrxiv-2024-2t7jc.

4.1. Introduction

In her 2018 Nobel Prize lecture,[85] Professor Frances Arnold stated what has become one of the central tenets of protein engineering: "*you get what you screen for*". Thus, in protein engineering campaigns, a researcher must balance efficiency of a screen with accuracy of criteria. As discussed in Section 3.1.4. Engineering of NylC, development of a high-throughput screen for plastic degradation is difficult, since the reactions are intrinsically slow, detection of products can be challenging, and even standardization of the plastic substrate (surface area, crystallinity) can pose complications. Conversely, extremely high-throughput approaches using, for example, substrates like pNP palmitate[86,87] or tributyrin[88] to screen for PET degrading enzymes by identifying esterases, can lack specificity, inadvertently causing researchers to pursue the wrong activity. For this reason, we excluded the possibility of using compound **8c** (Chapter 3) as a screen for nylon-degrading activity, as it is structurally and electronically remote from the target (aliphatic amide polymers).

Instead, we sought to develop a substrate analogue that could, as closely as possible, mimic the activity of nylon degradation upon reaction with NylC. We initially envisioned the synthesis and evaluation of a quenched-fluorophore substrate (Figure 4.1), taking an approach similar to that of the isopeptidic substrates we designed for bTG (see Section 2.2.3). However, synthesis proved challenging due to the handling properties of the intermediates: in particular, their intrinsically low

solubility. We recalled that the similarly low solubility of the isopeptidic substrates led to scattering in the sample and interfered with the fluorescence measurement, effectively nullifying this strategy at the conceptual level.

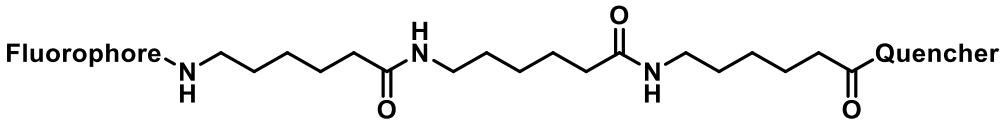

Figure 4.1. Initial design for a polyamide-like substrate to screen for nylonase activity.

Instead, we took inspiration from analogue substrates such as 2PET[89] and 3-PET,[90] substrate analogues of polyethylene terephthalate, which are used to characterize PETase activity in more microscopic detail. This chapter explores the design and evaluation of nylon analogue substrates for the determination of NylC activity, and a serendipitous discovery towards a high-throughput screen for nylon-degrading activity.

4.2. Results and Discussion

4.2.1. Design and synthesis of nylon oligomer analogues

NylCs are reported to be endo-type hydrolases, which do not hydrolyze aminohexanoate dimers.[58] To determine the minimum scaffold recognized by NylC, we synthesized compounds **11**, **12**, and **13**, bearing 1, 2, or 3 internal amide bonds (Figure 4.2). We chose to synthesize these substrates instead of true aminohexanoate oligomers for ease of synthesis, and to determine if the alkyl-capped substrates would still be recognized by the enzyme. These substrates are, in theory, easily prepared using simple amide coupling chemistry with Boc-protected aminohexanoic acid (in the

case of compounds **12** and **13**). However, the higher oligomers quickly became difficult to handle with increasing chain length, decreasing in both aqueous and organic solubility while holding onto impurities. Compounds **12** and **13** were eventually isolated by extracting into 2-methyltetrahydrofuran, an unusual but highly effective (and in this case, necessary) extraction solvent, as no other water-immiscible solvent we evaluated was capable of dissolving the material.

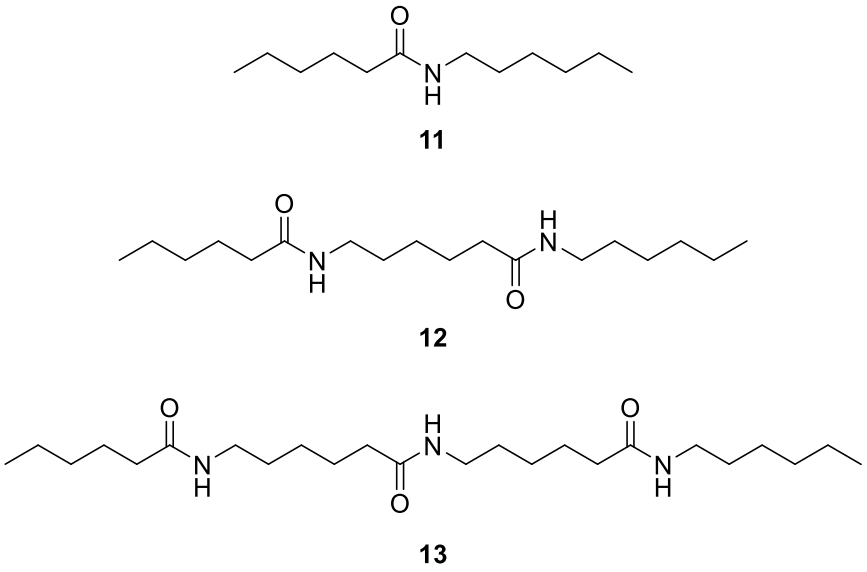

Figure 4.2. Substrate analogues of Nylon-6.

4.2.2. Evaluation of hydrolysis by NylC

We performed preliminary reactions with $NylC_A$, the only NylC homologue available to us when we started this project. These substrates bear no obvious chromophore, and were thus not amenable to a continuous assay; therefore, we intended to incubate each substrate with enzyme, and monitor hydrolysis by LCMS. We prepared reaction mixtures containing enzyme (0.1 mg/mL), reaction buffer (20 mM potassium phosphate, pH 7.3, 15% glycerol), and substrate (1 mM), which was prepared as a 20 × stock in MeOH and added to initiate the reaction. However, while compound

11 was an oil and solubilized in the reaction mixture with 5% cosolvent, compounds **12** and **13** immediately formed fine, cloudy precipitates upon addition to their respective reaction mixtures. We observed, over ~2 hours, that the reaction mixture containing **12** had clarified, whereas the reaction with **13** remained cloudy for the duration of the experiment.

We analyzed the reaction products of all three reactions by LCMS after an overnight incubation (Figure 4.3, and Figures A4.1 and A4.2). We observed disappearance of the peaks corresponding to **11** and **12**, but only partial consumption of **13**. The hydrolysis of **11** by NylC, which does not recognize the aminohexanoate linear dimer, suggests that NylC preferentially recognizes nonpolar substrates, and perhaps the aminohexanoate dimer, which is zwitterionic at physiological pH, is excluded on that basis.

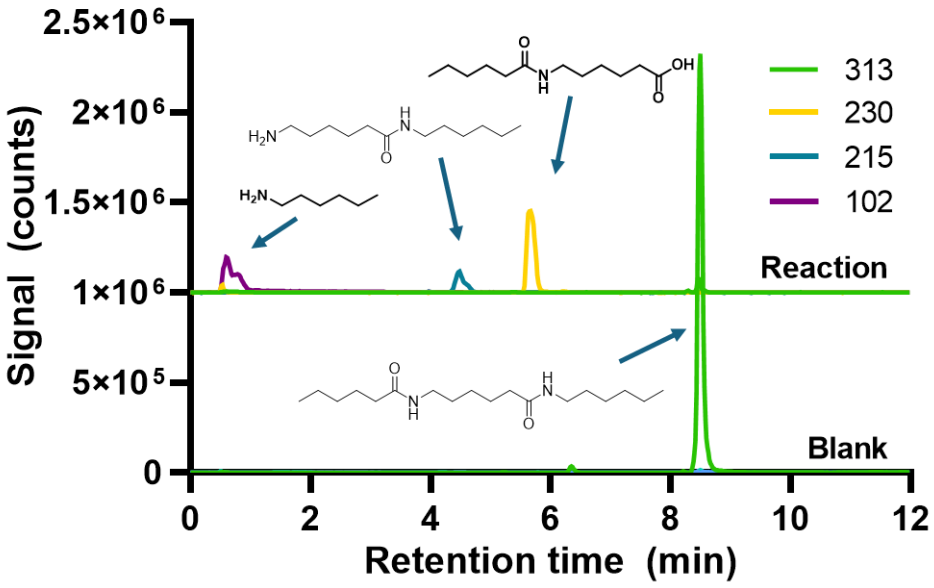

Figure 4.3. LCMS analysis of compound **12** after a 16-hour incubation in the presence (upper trace) or absence (lower trace) of $NylC_A$. Traces represent extracted ion chromatograms for the

indicated *m/z* values (M+H of the corresponding molecular ions for the compounds indicated in parentheses). Putative structures are shown, with major hydrolysis products bolded.

Analyzing the reaction products of compound **12** hydrolysis, we observed an unprecedented selectivity for hydrolysis at the "C-terminal" amide bond (the right-most bond, as shown in Figure 4.2). Indeed, quantification of product peak areas (Figures A4.4-4.6 in the Appendix) revealed >99% hydrolysis at the C-terminal amide. Based on this observation, and on the increased affinity granted to the pNP ester substrates we designed bearing *N*-acyl groups (see Section 3.2.2), we propose that the enzyme contains a binding region for the second amide bond that helps position the scissile amide bond. We observe a similar pattern in the hydrolysis of compound **13**, where hydrolysis occurs at the central and C-terminal amide bonds but not at the *N*-terminal amide (see Figure A4.2 in the Appendix). This provides further evidence that the *N*-terminal amide of a given polyamide substrate primarily aids in recognition and substrate binding within NylC.

We were intrigued by the conversion of **12** from an insoluble precipitate to soluble products, and we envisioned that this conversion could be monitored continuously by measuring light scattering *via* optical density at 600 nm (OD_{600}). Figure 4.4 shows the results of preliminary experiments to optimize this assay. A major issue we encountered was the instability of the suspension in the absence of protein, which would aggregate and lead to an apparent decrease in OD_{600} in the blank measurement. We discovered that the addition of 0.1 mg/mL BSA to the reaction mixture helped maintain a consistent suspension, providing a more stable OD_{600} signal over time.

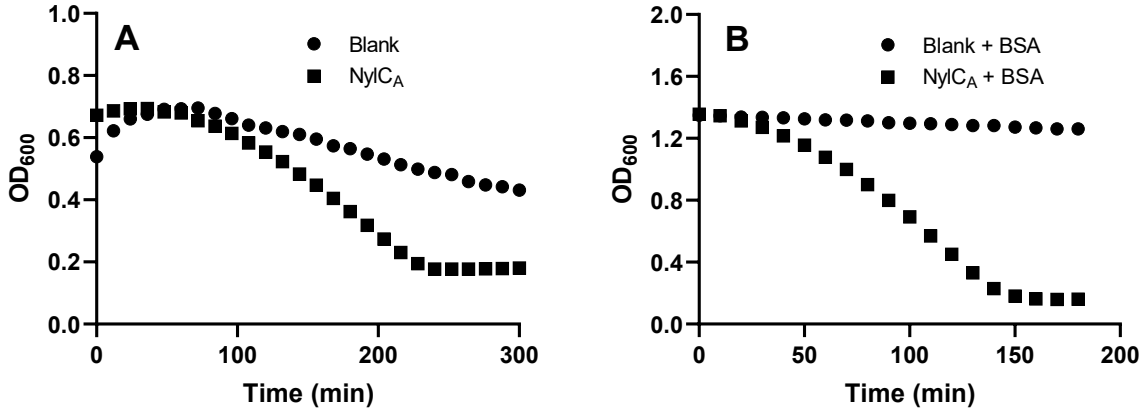

Figure 4.4. Hydrolysis of compound **12** by $NylC_A$, monitored by OD_{600} over time. Reaction mixtures contained potassium phosphate buffer (20 mM, pH 7.3), glycerol (15%), **2** (1 mM), MeOH (5%), and $NylC_A$ (0.1 mg/mL). A) Reactions performed in the absence of BSA demonstrate inconsistent scattering in the blank due to aggregation of the substrate. B) Reactions contain 0.1 mg/mL BSA, preventing aggregation and stabilizing the OD_{600} values over time.

We observe a higher initial OD_{600} measurement in the presence of BSA, and the reaction is completed more quickly, with a plateau observed around 150 minutes, compared to 230 minutes in the absence of BSA. Since NylC is acting on a finely precipitated substrate, reaction rates are highly dependent on the accessibility of the substrate, which is to say, the surface area of the particulate. BSA enhances the homogeneity of the substrate suspension over time, which could correspond to smaller average particle size (i.e. less aggregation), leading to overall more particulate in the line of the measurement (higher OD_{600} values) while promoting a faster reaction.

We prepared calibration curves of **12** to correlate concentration to observed OD_{600} signal (Figure A4.7 in the Appendix), and observed that under these conditions, $NylC_A$ hydrolyzed **12** at a rate

of 0.166 μM/s (one replicate). However, full kinetic characterization of the reaction (i.e. *via* Michaelis-Menten kinetics) could not be performed since, for solid substrates, only surface-exposed substrate molecules are available to the enzyme, making the concentration values inaccurate for the purposes of the model.

4.2.3. Expanded Substrate Scope

Compounds **12** and **13** are analogues of the Nylon-6 polymer; however, we were interested to know if NylC would recognize other nylon architectures. We synthesized compounds **14-17** (Figure 4.5), diamides that, like **12**, should be converted to water-soluble products upon hydrolysis. Unlike **12**, these compounds are all symmetric, and represent scaffolds of Nylon-66, Nylon-64, or Nylon-46, so named by the number of carbons in the dicarbonyl and diamine moieties respectively. It should be noted here that **14** has previously been reported as a nylon surrogate substrate,[90] but never used as a substrate for NylC, nor in a clarification-based assay.

Compounds **14** and **15** were synthesized in one step from the corresponding commercially available dicarboxylic acid chloride and two equivalents of hexylamine. Compounds **16** and **17** were prepared by pre-stirring hexanoic acid in thionyl chloride to produce hexanoyl chloride, followed by addition to a solution of the corresponding diamine. In all cases, the product immediately precipitated out of solution, and could be collected by filtration followed by several washing steps, to obtain the pure product.

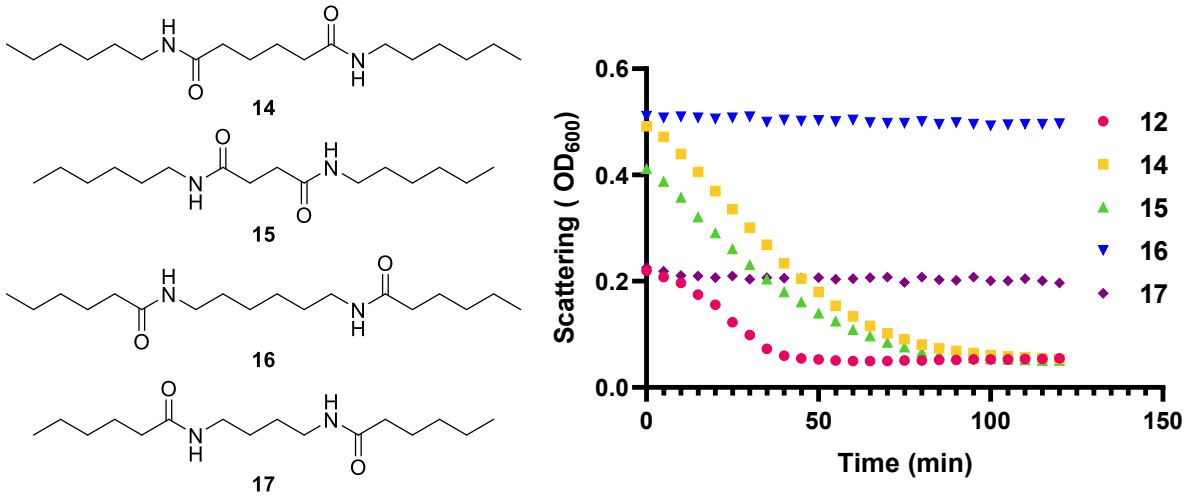

Figure 4.5. Left: structures of symmetric diamides **14-17**. Right: evaluation of each diamide as a substrate for $NylC_A$ by OD_{600} measurement. Reaction conditions: $NylC_A$ (0.1 mg/mL), substrate (1 mM), potassium phosphate buffer (20 mM, pH 7.3), glycerol (15%), and BSA (0.1 mg/mL). Reactions shown here were performed in a single replicate.

We evaluated each substrate by OD_{600} assay with $NylC_A$ (Figure 4.5). We were surprised to observe hydrolysis only of compounds **14** and **15** in addition to **12**. We noted that among the symmetrical diamides, those bearing a central dicarbonyl moiety were readily hydrolyzed, whereas those with a central diamine were not. This observation, along with the discovery that **12** is hydrolyzed selectively at the "C-terminal" amide, suggests to us that the scissile amide bond must be oriented with the leaving group amine on the "outside", i.e. opposite to the second amide.

Anticipating that these compounds could be used for downstream applications, we developed a shorthand nomenclature: the hydrolysable analogues were named "Trylons", for their resemblance to nylon "trimers" (i.e. bearing two internal amide bonds). Correspondingly, compound **12** is

Trylon-6; **14** is Trylon-66; and **15** is Trylon-46, named after their respective representative nylon architectures. These compounds will henceforth be referred to as such.

4.2.4. A High-Throughput Assay using Trylon

Following the preliminary synthesis and characterization of the Trylon substrates, we were able to express all six of the reported NylC homologues (three wild-type enzymes and three engineered thermostable variants). We were interested to quantify the hydrolysis of all substrates by all enzymes. Conducting these measurements in triplicate with the inclusion of blank reactions for each substrate corresponds to 63 simultaneous individual kinetic traces; thus, we adapted our assay to a 96-well plate setup.

Due to the nature of working with a suspended substrate, we encountered a few complications when optimizing this assay. Whereas in a cuvette, the optical density measurement is performed side-on, a plate-reader is read top-down through an air-water interface. We noted that the suspension may float non-homogeneously on the surface, leading to discrepancies in initial scattering values within replicates. To mitigate this, we prepared a master mixture of substrate, buffer (containing glycerol and BSA) and water, and thoroughly mixed the solution before aliquoting to the reaction plate. We also observed an initial decrease in the blank OD_{600} measurement (containing no enzyme) followed by a plateau, so we incorporated a pre-incubation period prior to addition of the enzyme to allow the suspension to equilibrate. This ensured that any decrease in OD_{600} that we observed was due to substrate hydrolysis, not aggregation.

We conducted the Trylon hydrolysis assays at both room temperature and 50 °C. The latter temperature was chosen because nylon hydrolysis reactions are usually performed at elevated temperatures, as discussed in Section 3.1.2. Thus, if applied to screening of mutant libraries, we would

need to ensure that an assay could be conducted at elevated temperatures to assess enzymes under the relevant conditions. Figure 4.6 shows the rates of hydrolysis of each substrate, by each enzyme, for each temperature condition. Calibration curves of each substrate were acquired at each temperature to account for the expected increased solubility at elevated temperatures (Figures A4.8 and A4.9 in the Appendix).

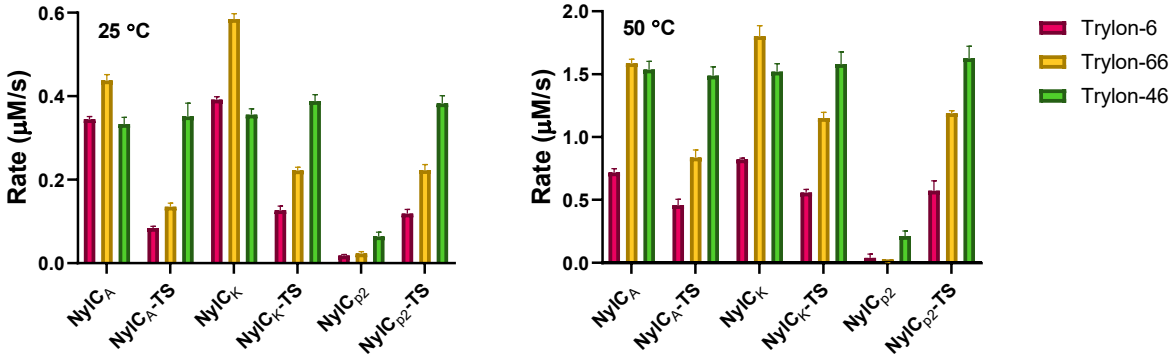

Figure 4.6. Rates of hydrolysis of Trylon-6, Trylon-66 and Trylon-46 at 25 °C (left) and 50 °C (right) by wild-type and thermostable (TS) NylC enzymes. Reaction conditions: Enzyme (0.1 mg/mL), substrate (1 mM), potassium phosphate buffer (20 mM, pH 7.3), glycerol (15%), BSA (0.1 mg/mL), MeOH (5%). Rates were determined from the maximum slopes of OD_{600} plotted over time (see Figures A4.9 and A4.10 in the Appendix). Values represent averages of three replicates, blank-corrected with reactions with the corresponding substrates in the absence of enzyme, with error bars indicating standard deviation.

There are three bases on which to compare these results, as there are three independent variables evaluated: substrate, enzyme, and temperature. First, among the substrates, Trylon-46 (green columns) demonstrates consistent, high rates of reactivity, whereas the reaction rates of Trylon-6 (red)

and Trylon-66 (yellow) are more variable. Trylon-66, meanwhile, demonstrates consistently higher reactivity across all enzymes than Trylon-6. There are two possible explanations for these observations, considering either chemical structure or morphology of the suspension. In the first consideration, we could propose that NylCs preferentially recognize the succinyl or adipoyl unit (present in Trylon-46 and -66), as opposed to the aminohexanoyl unit (Trylon-6). Based on our observations in this chapter (Section 4.2.2) and in Chapter 3 (Section 3.2.2), NylC recognizes a second amide, and the relative affinity for the position and orientation of that amide may correspondingly affect the rate of hydrolysis. Conversely, considering their morphology, these substrates demonstrate variable aqueous solubilities, and consequently, variable particle size. As previously discussed, when reacting at a solid substrate, surface area is an essential consideration, since only the surface-exposed substrate is accessible to the enzyme. While both considerations are possible contributors to the observed differences in the rates of hydrolysis between substrates, we are inclined to believe that the latter prevails. We have observed, in our experience handling these substrates, vastly different reaction rates for a single substrate depending on the way the suspension was prepared, reaction volumes and vessels, and composition of the reaction mixture. This suggests that the quality of the suspension itself dictates reactivity, which is variable between substrates.

The second basis of comparison is between the NylC homologues. $NylC_K$ and $NylC_A$ consistently demonstrate the highest hydrolysis rates for Trylon-6 and Trylon-66 hydrolysis, whereas the rate of hydrolysis by $NylC_{p2}$ severely lags in comparison. This is consistent with the observations of Yasuhira *et al*, who observed faster hydrolysis of aminohexanoate cyclic oligomer by $NylC_K$ and $NylC_A$.[59] The rates of hydrolysis by the thermostable enzymes are similar to each other, and lower than the corresponding mesophilic enzymes (with the exception of $NylC_{p2}$). This is an established phenomenon among thermostable enzymes at low temperatures[66] which are generally less flexible

and mobile than their mesophilic counterparts. Therefore we would expect to see higher activity from $NylC_A$ and $NylC_K$ than their respective thermostable derivatives at 50 °C, which is sufficiently below their respective melting temperatures.

The third basis compares the rates at lower and higher temperatures. Unsurprisingly, for all enzymes save for $NylC_{p2}$, reaction rates are elevated at higher temperatures (as is reflected by the difference in y-axis ranges in Figure 4.6. Furthermore, the difference in activity between the wild-type and thermostable enzymes (e.g. between $NylC_A$ and $NylC_A$TS) is smaller at 50 °C than at 25 °C, supporting the idea that these more thermostable enzymes are "activated" at elevated temperatures.

4.2.5. Hydrolysis of Nylon Film by NylCs

Hydrolysis of Trylon is fast, convenient, and adaptable to high-throughput applications. However, we thought it necessary to compare the activity of NylCs against Trylon to the hydrolysis of nylon plastic, which is the more relevant activity from a bioremediation perspective. That is to say, if we seek to use Trylon as a surrogate screen for nylon degradation activity, it is essential to demonstrate that Trylon hydrolysis can faithfully represent nylon hydrolysis.

We evaluated the hydrolysis of Nylon-6 and Nylon-66 film by the six NylC enzymes at 50 °C. To acquire kinetic curves, aliquots were removed at varying timepoints over the course of 24 hours. The extent of hydrolysis at each timepoint was determined by secondary reaction of the aliquot with TNBS, which produces a chromophore at 335 nm upon reaction with free amines. Rates were determined from the linear region of the resulting kinetic curves. Results are summarized in Figure 4.7, and data may be found in Figure A4.12 and Table A4.1 in the Appendix.

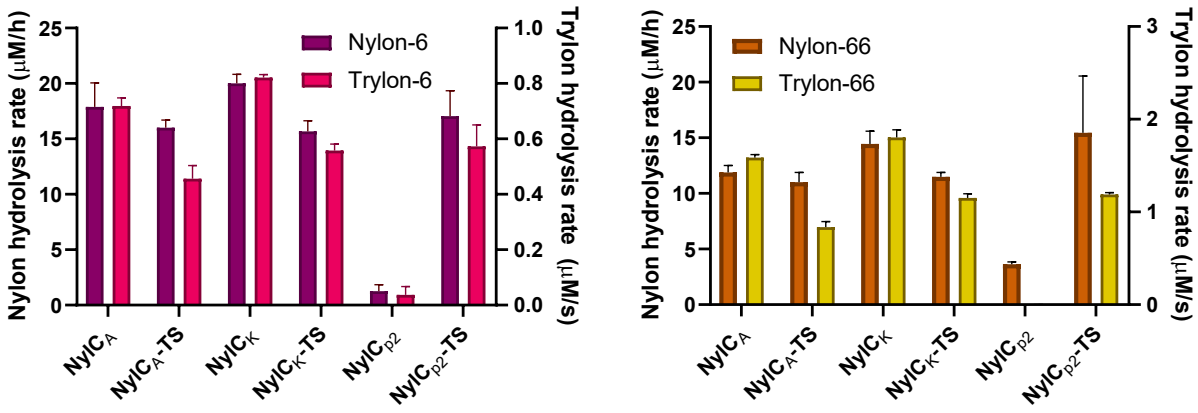

Figure 4.7. Comparison of the relative rates of hydrolysis nylon film (left y-axes) and their corresponding diamide substrates (right y-axes) for the polymers, Nylon-6 (left graph) and Nylon-66 (right graph). Reaction conditions for nylon hydrolysis: NylC (0.1 mg/mL), potassium phosphate buffer (20 mM, pH 7.3), nylon film (Nylon-6: 8.2 mg, Nylon-66: 18.1 mg). Values for nylon hydrolysis are averages of two replicates, with error bars showing standard deviations.

In all cases, the rate of Trylon hydrolysis is much (~150-fold) higher than the rate of nylon hydrolysis. Furthermore, the relative rates of hydrolysis by each enzyme show a clear trend, where rate of nylon hydrolysis and the rate of Trylon hydrolysis are strongly correlated. This correlation is strongest for the wild-type enzymes, but weaker for the thermostable enzymes, where the relative rates of nylon hydrolysis are slightly higher than those of the corresponding Trylon substrate. This may be explained by considering that, while both reactions are conducted at elevated temperature (50 °C), the reactions with Trylon take place over a much shorter period of time. For reactions with Trylon, the enzymes need only retain activity for 30 minutes at 50 °C, compared to the corresponding reactions with Nylon, where the enzymes must remain active for 24 hours. The thermostable enzymes demonstrate continued activity for longer at elevated temperatures relative to their non-

thermostable counterparts, thus, the relative activities observed for nylon hydrolysis by the thermostable enzymes are higher than Trylon would predict.

Additionally, it should be noted that the rates of Nylon-6 and Nylon-66 hydrolysis are relatively comparable (see Table A4.1 in the Appendix). Depending on the enzyme, NylC demonstrated 66-91% activity towards Nylon-66 compared to Nylon-6, with the exception of $NylC_{p2}$, which demonstrates higher activity towards Nylon-66 in our hands, but markedly lower overall activity due to its low melting temperature. Conversely, the article reporting hydrolysis of nylon thin films did not compare the rates of *film* hydrolysis between the two polymers, but observed that $NylC_{p2}TS$ (the only enzyme evaluated in that study) degraded Nylon-66 *powder* at an efficiency of ~60% that of Nylon-6.[70]

4.2.6. Hydrolysis of Trylon-6 by Cell Lysate

In order to be a useful tool for protein engineering, we wished to demonstrate that this assay is amenable to high-throughput screening of crude enzyme in cell lysate. We prepared cell lysate from *E. coli* BL21 DE3 cells containing either empty pET28a vector, or plasmids encoding each of the NylC variants. Reactions were performed in 200-µL volumes on a 96-well plate and contained 10% v/v lysate. We were pleased to observe rapid hydrolysis of **12** by all enzymes even in crude form (Figure A4.13 in the Appendix). In order to demonstrate that the activity by cell lysate was reflective of the activity of purified enzyme, we compared the relative rates of hydrolysis by each enzyme (Figure 4.8).

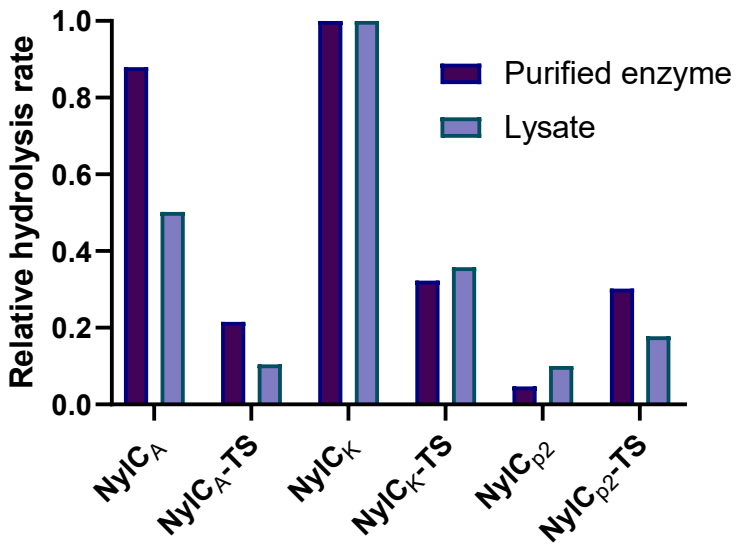

Figure 4.8. Relative rates of hydrolysis of **12** by all NylC variants as either purified enzyme or crude cell lysate. Rates were determined by slopes of OD_{600} vs time plots (see Figure A4.13 in the Appendix) and are normalized to the highest activity ($NylC_K$ in both cases) for comparison.

Qualitatively, we observe a consistent trend between rates of hydrolysis by crude lysate and purified enzyme. Potential differences in levels of expression and degree of autoprocessing are to be expected between the homologues, which convolutes this correlation, but which will always be uncontrolled factors when working with cell lysates. Overall, this result suggests that hydrolysis of Trylon-6 by cell lysate could provide a preliminary, quantitative report on active variants of NylC, supporting its use as a screen in an engineering context.

4.3. Conclusion

In this chapter, we report the design, synthesis, and evaluation of aliphatic amides which act as substrates for NylC enzymes. Using these substrates, we determined that NylC demonstrates selective hydrolysis at amide bonds where the leaving group amide is positioned externally to the second amide (e.g. at the "C-terminus" of aminohexanoate oligomer analogues). Furthermore, we observe that hydrolysis of the diamide substrates, Trylon-6, Trylon-66 and Trylon-46, corresponds to a decrease in turbidity as the insoluble substrates are converted to water-soluble products. Taking advantage of this phenomenon, we used these substrates to develop a continuous, quantitative assay for NylC by monitoring changes in scattering *via* OD_{600} measurement. This assay can be performed at room temperature or elevated temperature, and reaction rates can be determined in minutes, compared to reactions with Nylon which are performed over days, plus the time required for analysis (two hours plus manipulation steps). We demonstrate that hydrolysis of Trylon-6 and Trylon-66 correlates to hydrolysis of their corresponding Nylon architectures (Nylon-6 and Nylon-66), and that reaction rates are well-represented in hydrolysis of Trylon-6 by cell lysate. Taken together, these results suggest that Trylon substrates would enable a rapid and continuous screen for NylC variants in a protein engineering campaign.

4.4. Materials and Methods

4.4.1. Molecular Biology Methods

Expression of NylC enzymes

Protocols for expression of NylC homologues can be found in Section 3.4.1.

Preparation of crude cell lysate containing NylC homologues

Expression plasmids encoding NylC homologues and pET28 (empty vector) were transformed into chemically competent BL21-DE3 *E. coli* cells and selected on LB agar supplemented with 50 μg/mL of kanamycin. Single colonies were used to inoculate 5 mL of LB supplemented with 50 μg/mL of kanamycin and were incubated 18 hours at 37 °C. Those cultures were used to inoculate 25 mL cultures of 2×YT media (1:50 bacterial culture: broth ratio) supplemented with 50 μg/mL of kanamycin that were then incubated at 37 °C for 4 hours. Protein expression was then induced by the addition of IPTG to a concentration of 0.1 mM and the cultures were incubated at 20 °C for 20 hours. Cells were then pelleted by centrifugation at 11 600 × g for 10 minutes at 4°C and resuspended (1:50 v/v) in lysis buffer (50mM tris pH 7.5, 300 mM NaCl, 10 mM imidazole and 1 mg/mL lysozyme) and lysed via 8 freeze-thaw cycles at -78 °C and 40 °C. Lysates were clarified via centrifugation at 19 300 × g for 15 minutes at 4°C , and soluble lysates were used immediately.

4.4.2. Assay Methods

Hydrolysis of compounds **11**, **12** and **13** by $NylC_A$ for LCMS analysis

Reactions were performed in 1 mL reaction volumes containing potassium phosphate (20 mM, pH 7.3), methanol (MeOH, 5%), substrate (1 mM), $NylC_A$ (0.1 mg/mL) and 15% glycerol. Substrate suspensions were prepared by adding 50 μL of a 20 mM solution of substrate in methanol to reaction solutions containing all components except enzyme. The reaction was initiated through addition of enzyme, then incubated for 16 hours at room temperature. Following the incubation period, 60-μL aliquots were taken from each reaction mixture and processed for analysis by LCMS (see

below). Reactions were performed in duplicate, alongside blank reactions containing no enzyme for each corresponding substrate.

Sample preparation and data analysis by LCMS

Samples were prepared for LCMS analysis by diluting 1:1 in MeOH, then filtering if necessary to remove insoluble protein (note that substrate **12** is fully soluble in 1:1 MeOH: H_2O). Samples were analyzed by LCMS (Shimadzu Prominence UFLC system, LCMS-2020 single quadrupole MS). Separation was achieved at a flow rate of 1 mL/min over 12 minutes using a Phenomenex Luna Omega C18 column with a mobile phase consisting of a gradient of 5-50% MeCN in water, supplemented with 0.05% formic acid. Mass data were collected in ESI+ mode between 75 to 650 mass units, and quantitation of reaction components was determined from integration of extracted ion chromatograms for each species.

General procedure for Trylon hydrolysis assay and measurement *via* spectrophotometer (**GP9**)

Reaction mixtures were performed in 1.5 mL cuvettes in 1 mL reaction volumes. Reaction mixtures contained $NylC_A$ (0.1 mg/mL), substrate (1 mM), methanol (5%), potassium phosphate buffer (20 mM, pH 7.3), glycerol (15%), and BSA (0.1 mg/mL) unless otherwise specified. Suspensions were prepared by adding 50 μL of a 20 mM solution of substrate in MeOH to a reaction mixture containing all components except enzyme, and mixing thoroughly. Reactions were initiated through addition of $NylC_A$, and monitored at 600 nm at time intervals indicated, using a Varian Cary 100 Bio UV-Vis spectrophotometer. Reactions were conducted at room temperature.

Comparison of reaction progress in the presence and absence of BSA

Reactions were performed according to **GP9** using Trylon-6 as the substrate. Reactions contained either 0 or 0.1 mg/mL BSA. Scattering (OD_{600}) was measured every 10 minutes. Reactions were performed as single replicates, alongside blank reactions containing no enzyme.

Exploratory evaluation of diamide analogues **12** and **14-17** via UV-Vis spectrophotometry

Reactions were performed according to **GP9** using compounds **12** or **14-17** as substrates, in the presence of 0.1 mg/mL BSA. Reactions were performed as single replicates.

Trylon hydrolysis assay on plate reader

The following stock solutions were prepared prior to preparation of reaction mixtures:

- Potassium phosphate buffer (200 mM, pH 7.3)
- Glycerol (50% w/w in H_2O)
- BSA (1 mg/mL)
- Substrate (20 mM in MeOH)
- Enzyme: 1 mg/mL

A master mix was prepared containing all components except enzyme, to a final volume such that each well of a reaction plate contained 180 µL of master mix. Thus, each 180-µL portion of master mix would contain:

- 70 µL of H_2O

- 20 μL of buffer stock
- 60 μL of glycerol stock
- 20 μL of BSA stock
- 10 μL of substrate stock

For example, if 10 reactions were being performed, 1.8 mL of master mix would theoretically be required, containing 700 μL of H_2O, 200 μL of buffer stock, 600 μL of glycerol stock, 20 μL of BSA stock, and 100 μL of substrate stock. A minimum of 1.1 × the theoretical master mix volume was prepared in each instance.

The master mix was vortexed thoroughly to homogenize the suspension of substrate, then aliquoted (180 μL) into a 96-well reaction plate. The absorbance was monitored for ~10 minutes at 600 nm to ensure minimal change in OD_{600} value, then reactions were initiated through addition of 20 μL of 1 mg/mL enzyme stock. Absorbance was monitored at 600 nm for either 3 hours (at 50 ℃) or 16 hours (at 25 ℃).

Nylon Hydrolysis assay

Nylon-6 (0.2 mm thickness) and Nylon-66 (0.5 mm thickness) film was purchased from Goodfellow. Standard-size disks were created using a 6.5-mm diameter hole puncher, to produce samples of 8.2 mg or 18.1 mg for Nylon-6 and Nylon-66 respectively. Reactions were performed in 1 mL reaction volumes and contained potassium phosphate buffer (20 mM, pH 7.3), enzyme (0.1 mg/mL) and nylon film (Nylon-6: 8.2 mg, Nylon-66: 18.1 mg). Reaction mixtures containing all components except enzyme were heated to 50 ℃ for 5 minutes, followed by initiation of the reaction through addition of enzyme. Reactions were incubated at 50 ℃ for 24 hours, and 80-μL

aliquots were acquired at various time points, and stored at -20 ℃ until quantification by trinitrobenzenesulfonate (TNBS). Blank reactions were performed containing all components except enzyme, and rates were corrected by subtracting the rate of un-catalyzed nylon degradation.

Quantification of liberated amines by TNBS

TNBS was purchased from Sigma Aldrich as a 5% solution in H_2O. The TNBS stock was diluted 360 × in sodium bicarbonate buffer (0.5 M, pH 8.5). In a 96-well plate, the TNBS solution (160 μL) was added to 40 μL of sample. Calibration curves were prepared on each 96-well plate alongside the samples, by diluting 40 μL of aminohexanoic acid dimer (0-500 μM in 20 mM potassium phosphate buffer, pH 7.3) with TNBS solution (160 μL). The plate was incubated at 37 ℃ for 2 hours, then carefully sonicated to liberate any bubbles produced. Absorbance was measured at 335 nm, and converted to concentration using the slope of the calibration curve.

Lysate-mediated hydrolysis of Trylon-6

The hydrolysis of Trylon-6 by cellular lysate was evaluated in 20 mM potassium phosphate buffer (pH 7.3), 15% glycerol, 5% MeOH, 1 mM of **2** and 10% v/v of lysate (either from cells containing empty pET28 vector, acting as a negative control for non-specific hydrolysis, or plasmids encoding NylC enzymes). Reactions were performed in duplicate and contained either NylC variants, the empty pET28a lysate, or no lysate, to account for background hydrolysis. The reactions were initiated by addition of the cell lysates following a 90-minute incubation of all other components. Hydrolysis of the starting material was evaluated by monitoring the OD_{600} over time and rates of

hydrolysis were determined by averaging the rates observed in both duplicate and then subtracting the average rate measured in the blank reactions.

Synthesis

General procedure (**GP10**) for amide coupling reactions

A solution of acid (1.1 equiv.), HBTU (1.6 equiv.), and DIPEA (3 equiv.) in DCM (0.16 M with respect to the limiting reagent) was stirred at R.T. for 30 minutes, following which amine (1 equiv.) was added. The reaction was monitored by TLC (10% MeOH, 45% DCM, 45% hexanes) and visualized with ninhydrin stain. Following completion of the reaction, the reaction mixture was evaporated *in vacuo*, then the residue was purified as specified.

General procedure (**GP11**) for Boc deprotection

To a solution of amine in dioxane (0.2 M) was added an equal volume of HCl (4 M in dioxane). The reaction was monitored by TLC (10% MeOH, 45% DCM, 45% hexanes) and visualized with ninhydrin stain. Upon completion, the reaction was evaporated *in vacuo*, then the residue was further purified as specified.

***N*-hexylhexanamide (11)**

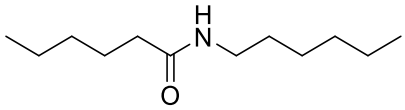

A solution of hexanoic acid (68 µL, 0.543 mmol), HBTU (300 mg, 0.790 mmol), and DIPEA (172 µL, 0.988 mmol) in DCM (3 mL) was stirred at R.T. for 30 minutes, following which hexylamine (65 µL, 0.494 mmol) was added. The reaction was monitored by TLC (10% MeOH, 45% DCM, 45% hexanes) and visualized with ninhydrin stain. The reaction was complete after 4 hours, whereupon the reaction solvent was removed *in vacuo* and the residue redissolved in ethyl acetate. The organic phase was washed sequentially with 10% AcOH (2 × 10 mL), brine (10 mL), saturated sodium bicarbonate (3 × 10 mL) and brine (10 mL). The organic phase was dried over $MgSO_4$ and evaporated *in vacuo* to give a colourless oil (82 mg, 84%). ^{1}H NMR (300 MHz, $CDCl_3$) δ 5.52 (br. s, 1H), 3.22 (m, 2H), 2.14 (t, J = 7.6 Hz, 2H), 1.61 (qu, J = 7.5 Hz, 2H), 1.47 (m, 2H), 1.29 (m, 10H), 0.87 (m, 6H). Characterization data are consistent with literature.[91]

***N*-hexyl-6-(*N*-Boc)aminohexanamide (18)**

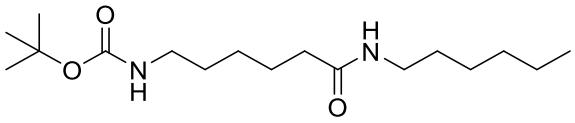

Compound **18** was synthesized following **GP10** with 200 mg (1.965 mmol) of hexylamine. Following evaporation of the reaction mixture, the residue was redissolved in EtOAc (~20 mL), then washed with equal volumes of 10% AcOH, brine, saturated $NaHCO_3$ (3 ×) and a final wash with brine. The organic phase was dried over $MgSO_4$, then evaporated to give a viscous oil, which

turned into to a white solid after drying overnight. The solid was then resuspended in hexanes, sonicated to give a fine suspension, then collected the solid by filtration. The product was dried to give a flaky white solid (587 mg, 95%). ^{1}H NMR (400 MHz, $CDCl_3$) δ 5.48 (s, 1H), 4.55 (s, 1H), 3.22 (q, *J* = 6.7 Hz, 2H), 3.10 (q, *J* = 6.4 Hz, 2H), 2.15 (t, *J* = 7.5 Hz, 2H), 1.64 (qu., *J* = 7.6 Hz, 2H), 1.48 (m, 4H), 1.43 (s, 9H), 1.31 (m, 8H), 0.87 (t, *J* = 6.7 Hz, 3H). ^{13}C NMR (101 MHz, $CDCl_3$) δ 172.9, 156.2, 79.2, 40.5, 39.7, 36.8, 31.6, 29.9, 29.8, 28.5, 26.7, 26.5, 25.5, 22.7, 14.1. HRMS (ESI) calc'd for $C_{17}H_{34}N_2O_3Na$ ($[MNa]^+$): 337.2467, found: 337.2468.

_N_-hexyl-6-aminohexanamide hydrochloride (12b)

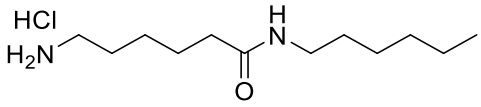

This reaction was performed following **GP11** on a 500 mg (1.590 mmol) scale of boc protected amine **18**. Following evaporation of the reaction mixture, the residue was suspended in hexane and triturated with sonication. The hexane was decanted off and the product dried under high vacuum. The product was isolated in quantitative yield (400 mg). ^{1}H NMR (400 MHz, DMSO) δ 7.83 (m, 4H), 2.99 (q, *J* = 6.5 Hz, 2H), 2.73 (s, 2H), 2.04 (t, *J* = 7.4 Hz, 2H), 1.49 (m, 4H), 1.35 (m, 2H), 1.22 (m, 8H), 0.84 (t, *J* = 6.8 Hz, 3H). ^{13}C NMR (101 MHz, DMSO) δ 172.2, 38.9, 38.6, 35.3, 31.1, 29.2, 26.9, 26.2, 25.6, 25.0, 22.2, 14.1. HRMS (ESI) calc'd for $C_{12}H_{27}N_2O$ ($[MH]^+$): 215.2123, found: 215.2123.

***N*-hexyl-6-(*N*-hexanoyl)aminohexanamide (12)**

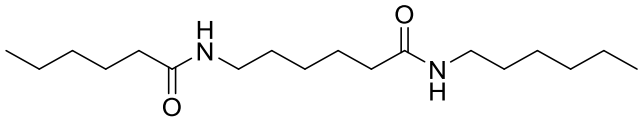

The reaction proceeded following **GP10** with 70 mg (0.279 mmol) of amine **12b**. Following evaporation of the reaction mixture, the residue was redissolved in 2-methyl-THF (10 mL), then washed with an equal volume of 10 % AcOH, then brine, then 3 × 10 mL saturated $NaHCO_3$, then brine. The organic phase was dried over $MgSO_4$ and evaporated to give a white solid, which was triturated with a solution of 1:1 hexanes: ethyl acetate, then filtered to give a white powder (58 mg, 67%). ^{1}H NMR (400 MHz, MeOD) δ 3.15 (dt, *J* = 2.3, 7.1 Hz, 4H), 2.17 (q, *J* = 7.0 Hz, 4H), 1.61 (q, *J* = 7.5 Hz, 4H), 1.50 (q, *J* = 7.5 Hz, 4H), 1.32 (m, 12H), 0.91 (m, 6H).^{13}C NMR (101 MHz, MeOD) δ 176.3, 176.0, 40.4, 40.2, 37.1, 37.0, 32.7, 32.5, 30.4, 30.1, 27.7, 27.5, 26.8, 26.7, 23.6, 23.4, 14.4, 14.3. HRMS (ESI) calc'd for $C_{18}H_{36}N_2O_2Na$ ($[MNa]^+$): 335.2674, found: 335.2649.

***N*-hexyl-6-((N-Boc)-6-aminohexanoyl)aminohexanamide (19)**

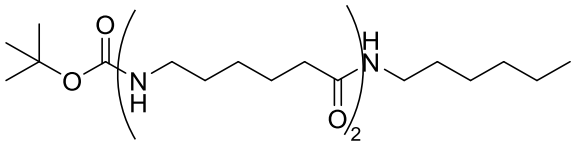

The reaction proceeded following **GP10** with 250 mg (0.997 mmol) of amine **12b**. Following evaporation of the reaction mixture, the residue was redissolved in 2-methyl-THF (20 mL), then washed with an equal volume of 10 % AcOH, then brine, then 3 × 10 mL saturated $NaHCO_3$, then brine. The organic phase was dried over $MgSO_4$ and evaporated to give a white solid (233 mg, 54%). ^{1}H NMR (400 MHz, $CDCl_3$) δ 5.75 (s, 1H), 5.67 (s, 1H), 4.61 (s, 1H), 3.23 (m, 4H), 3.09

(q, J = 6.5 Hz, 2H), 2.16 (m, 4H), 1.64 (m, 4H), 1.49 (m, 6H), 1.43 (s, 9H), 1.31 (m, 10H), 0.87 (t, J = 6.6 Hz, 3H). ^{13}C NMR (101 MHz, $CDCl_3$) δ 172.9, 172.8, 156.2, 79.1, 40.4, 39.6, 39.1, 36.6, 36.5, 31.5, 29.8, 29.6, 29.2, 28.4, 26.6, 26.4, 26.3, 25.4, 25.1, 22.6, 14.10 HRMS (ESI) calc'd for $C_{23}H_{45}N_3O_4Na$ ($[MNa]^+$): 450.3308, found: 450.3292.

_N_-hexyl-6-(6-aminohexanoyl)aminohexanamide (13b)

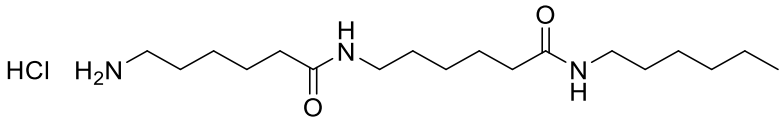

The title compound was synthesized following **GP11** with 90 mg (0.212 mmol) of **19**. Following evaporation of the solvent, the residue was resuspended in 1:1 DCM : hexanes and triturated with sonication. The supernatant was decanted off and the solid dried under high vacuum, then used without further purification.

_N_-hexyl-6-((_N_-hexanoyl)-6-aminohexanoyl)aminohexanamide (13)

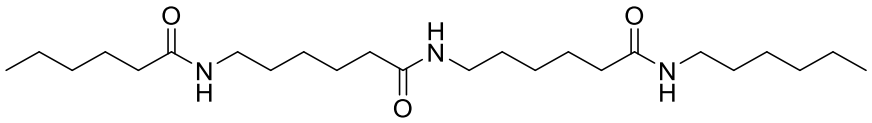

The title compound was prepared following **GP11** using 40 mg (0.110 mmol) of compound **13b**. Following evaporation of the reaction mixture, the residue was redissolved in 2-MeTHF (10 mL) and washed with 10% AcOH (3 × 10 mL), brine (10 mL), sat. $NaHCO_3$ (3 × 10 mL) and brine (10 mL). The organic phase was collected, dried over $MgSO_4$ and evaporated. The resultant solid was washed with a solution of 1:1 hexanes : ethyl acetate, then the supernatant decanted off and

the solid dried under vacuum to give the product as a white powder (33 mg, 58%). ^{1}H NMR (400 MHz, MeOD) δ 3.15 (dt, *J* = 2.4, 7.0 Hz, 6H), 2.17 (m, 6H), 1.61 (sextet, *J* = 7.6 Hz, 6H), 1.51 (m, 6H), 1.33 (m, 14H), 0.91 (dt, *J* = 2.0, 7.13 Hz, 6H). ^{13}C NMR (101 MHz, MeOD) δ 176.2, 176.00, 175.98, 40.4, 40.2, 37.1, 3.70, 32.7, 32.5, 30.4, 30.1, 27.7, 27.5, 26.8, 26.7, 26.7, 23.7, 23.4, 14.4, 14.3. HRMS (ESI) calc'd for $C_{24}H_{47}N_3O_3Na$ ([MNa]$^{+}$): 448.3515, found: 448.3517.

Hexanedioic acid bis-hexylamide (14)

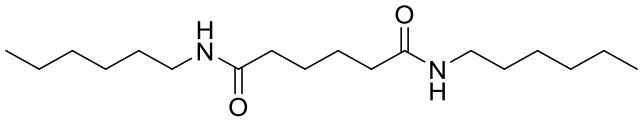

To a stirred solution of hexylamine (261 µL, 1.976 mmol) and DIPEA (494 µL, 2.823 mmol) in Et_2O (4 mL) was added adipoyl chloride (137 µL, 0.941 mmol) dropwise over ~1 minute. Immediately following addition of the diacyl chloride, a large amount of white precipitate formed. The suspension was diluted with 15 mL of Et_2O, then the precipitate collected by vacuum filtration. The solid was resuspended in H_2O (aided by sonication), then collected by vacuum filtration. The resulting solid was washed with acetone and dried to give the product as a white powder (133 mg, 45%). ^{1}H NMR (400 MHz, $CDCl_3$) δ 5.78 (br. s, 2H), 3.22 (q, *J* = 7.0 Hz, 4H), 2.18 (m, 4H), 1.65 (m, 4H), 1.49 (m, 4H), 1.29 (m, 12H), 0.87 (t, *J* = 6.8 Hz, 6H). Characterization data are consistent with literature.[92]

Butanedioic acid bis-hexylamide (15)

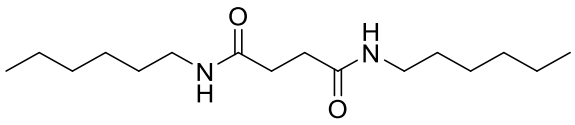

This compound was prepared following the same protocol as described for **14**, except using succinyl chloride (104 µL, 0.941 mmol) as the diacyl chloride. The product was collected as a white powder (63 mg, 23%). ^{1}H NMR (400 MHz, MeOD) δ 3.12 (t, *J* = 7.1 Hz, 4H), 2.42 (s, 4H), 1.45 (q, *J* = 6.9 Hz, 4H), 1.29 (m, 12H), 0.88 (t, *J* = 6.8 Hz, 6H). ^{13}C NMR (101 MHz, MeOD) δ 174.5, 40.5, 32.7, 32.4, 30.4, 27.7, 23.6, 14.3. HRMS (ESI) calc'd for $C_{16}H_{32}N_2O_2Na$ ($[MNa]^+$): 307.2361, found: 307.2354.

(*N*,*N*′-bis-hexanoyl)-1,6-hexanediamine (16)

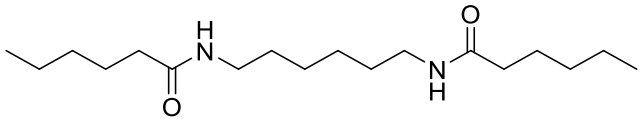

To a stirred solution of hexanoic acid (237 µL, 1.893 mmol) and DMF (2 drops) in DCM (2 mL) was added oxalyl chloride (175 µL 2.066 mmol) under a stream of nitrogen. The consumption of oxalyl chloride was indicated by the evolution of gas, and the reaction was stirred until no more bubbles were formed (~5 minutes). In a separate vessel was stirred 1,6-hexanediamine (120 µL, 0.861 mmol) and DIPEA (450 µL, 2.583 mmol) in DCM (2 mL). To the solution of diamine was added the solution of hexanoyl chloride dropwise over ~2 minutes. Immediately following addition of the acyl chloride, a large amount of white precipitate formed. The suspension was diluted with 15 mL of Et_2O, and the solid collected by vacuum filtration. The solid was washed with water

(20 mL) and acetone (20 mL), and dried on vacuum to give the product as a fluffy white solid (143 mg, 55%). ^{1}H NMR (400 MHz, $CDCl_3$) δ 5.58 (br. s, 2H), 3.24 (q, J = 6.6 Hz, 4H), 2.16 (t, J = 7.6 Hz, 4H), 1.64 (m, 4H), 1.49 (m, 4H), 1.31 (m, 12H), 0.89 (t, J = 6.8 Hz, 6H). Characterization data are consistent with literature.[93]

(*N*,*N*′-bis-hexanoyl)-1,6-butanediamine (17)

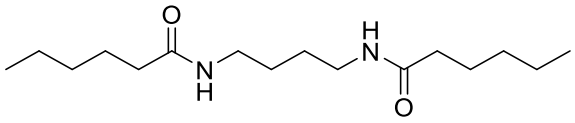

This compound was prepared following the same protocol as described for **16**, except using 1,4-butanediamine as the diamine. The product was isolated as a white powder (147 mg, 60%). ^{1}H NMR (400 MHz, MeOD) δ 3.17 (t, J = 5.0 Hz, 4H), 2.16 (t, J = 7.5 Hz, 4H), 1.60 (qu, J = 7.5 Hz, 4H), 1.51 (m, 4H), 1.33 (m, 8H), 0.91 (t, J = 7.0 Hz, 6H). ^{13}C NMR (101 MHz, MeOD) δ 176.3, 39.9, 37.1, 32.5, 27.8, 26.8, 23.4, 14.3. HRMS (ESI) calc'd for $C_{16}H_{32}N_2O_2Na$ ($[MNa]^+$): 307.2361, found: 307.2324.

Methyl (*N*-hexanoyl)-6-aminohexanoate (20)

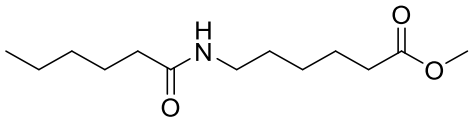

The reaction proceeded following **GP10** with 200 mg (1.100 mmol) of methyl-6-aminohexanoate hydrocholoride. The reaction was complete after 18 hours. Following evaporation of the reaction mixture, the residue was redissolved in ethyl acetate (20 mL), then washed with 3 × 10 mL of 10 %

AcOH, then brine, then 3 × 10 mL saturated $NaHCO_3$, then brine. The organic phase was dried over $MgSO_4$ and concentrated to give a colourless residue. The crude product was adsorbed onto silica, washed with 1:1 hexanes : DCM, then eluted with 9:1 DCM : MeOH. The fraction containing the product was evaporated in vacuo and dried under high vacuum to give the product as a colourless oil (158 mg, 59%). ^{1}H NMR (400 MHz, $CDCl_3$) δ 5.53 (br. s, 1H), 3.66 (s, 3H), 3.24 (q, J = 5.0 Hz, 2H), 2.31 (t, J = 7.4 Hz, 2H), 2.14 (t, J = 7.6 Hz, 2H), 1.63 (m, 4H), 1.50 (qu, J = 7.4 Hz, 2H), 1.32 (m, 6H), 0.88 (t, J = 6.9 Hz, 3H). ^{13}C NMR (101 MHz, $CDCl_3$) δ 174.2, 173.4, 51.6, 39.3, 37.0, 34.0, 31.6, 29.4, 26.5, 25.6, 24.6, 22.5, 14.1. HRMS (ESI) calc'd for $C_{13}H_{25}NO_3Na$ ($[MNa]^+$): 266.1732, found: 266.1759.

_N_-hexanoyl-6-aminohexanoic acid (12a)

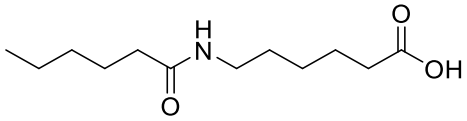

Compound **20** was dissolved in MeOH (3 mL) and aqueous NaOH (2 M, 3 mL) and the reaction was stirred for 48 hours at R.T. The reaction mixture was concentrated *in vacuo* to remove the methanol, then diluted in H_2O (10 mL) and washed with Et_2O (10 mL). The aqueous phase was acidified through dropwise addition of 12 M HCl to a pH of ~1, then extracted with 3 × 10 mL EtOAc, The EtOAc extracts were combined and washed with 10 mL of brine, then dried over $MgSO_4$ and evaporated to give a clear residue, which was dried under vacuum to produce flaky white crystals (125 mg, 89%). ^{1}H NMR (400 MHz, DMSO) δ 7.75 (t, J = 5.4 Hz, 1H), 2.99 (q, J = 6.5 Hz, 2H), 2.17 (t, J = 7.4 Hz, 2H), 2.01 (t, J = 7.4 Hz, 2H), 1.46 (m, 4H), 1.36 (qu, J = 7.2 Hz, 2H), 1.23 (m, 6H), 0.84 (t, J = 7.1 Hz, 3H). ^{13}C NMR (101 MHz, DMSO) δ 174.4, 172.0, 38.1,

35.3, 33.5, 30.8, 28.7, 25.8, 24.9, 24.1, 21.7, 13.8. HRMS (ESI) calc'd for $C_{12}H_{23}NO_3Na$ ($[MNa]^+$): 252.1576, found: 252.1594.

Chapter 5. Application of Trylon-6 as a High-Throughput Screen to Evaluate Amide Hydrolysis Activity in NylC Variants

5.1. Introduction

Several studies have been performed where mutants of NylC enzymes were prepared to identify residues necessary for thermal stability, autoprocessing, oligomerization state, and amide hydrolysis activity.[68,71,72] For example, position 122 was identified as being highly relevant for thermal stability and oligomerization, due to its location at the interface between two subunits in the NylC tetramer.[72] Similarly, inactivation mutants at residues near the catalytic site (e.g. Y146A, K189A, and N266A) affected rates of autoprocessing and enzyme activity.[72] While most of these studies involved fully rational mutagenesis, i.e. *via* site-directed mutagenesis, one study in 2018 reported the use of random mutagenesis to generate a library of variants.[72] However, these variants were not screened for activity: instead, they were sequenced, and selected variants were expressed and investigated for (in this case) subunit assembly and protein aggregation.[72] While these studies have been extensive and informative, they have not focused on the generation of enzymes with improved catalytic activity.

In Chapter 4, we discussed the development of a rapid, continuous, and quantitative assay for linear amide hydrolysis, using the substrates we have dubbed *Trylons*. Since Trylon can identify amide hydrolysis activity in minutes at 50 °C, we were eager to use this new method in screen of NylC mutants, towards a protein engineering application. Generally, if an enzyme of interest already demonstrates a desired activity, which we seek to enhance through engineering, directed evolution (through random mutagenesis and selection or screening) is an incredibly powerful strategy.[94] As discussed in Section 3.1.4, this method has been used to identify a double mutant of $NylC_{p2}TS$

with a 2-fold increase in enzymatic activity against Nylon-6.[75] (Note here that that study employed a discontinuous assay by chromogenic amide detection to screen variants.) However, while nearing the end of this project, we did not have the time and resources to pursue a directed evolution campaign. Therefore, in order to demonstrate the power of our screening technique, we chose to narrow our scope to a few small libraries of variants, through semi-rational design.

In this chapter, we will discuss the use of the Trylon assay to screen libraries generated through site-saturation mutagenesis. This strategy allows us to evaluate the capacity of the Trylon assay to rapidly identify active mutants, while also giving insight into specific positions relevant for amide hydrolysis activity, and trends in residues that favour or disfavour this activity.

5.2. Results and Discussion

5.2.1. Library Design

We are fortunate to have crystal structures of several NylC variants,[68,71] and extensive knowledge of the residues responsible for NylC catalysis, both of which allow us to focus our mutational studies on specific regions. For this study, we chose residues at the surface of the active site surrounding the catalytic threonine. We hypothesized that these residues would be implicated in substrate binding, and thus hydrolysis activity would be sensitive to mutations at these positions. Figure 5.1 shows a single heterodimer (one of four subunits in the NylC structure) at the active site (nylon-binding) groove, and the location of the residues chosen for this study.

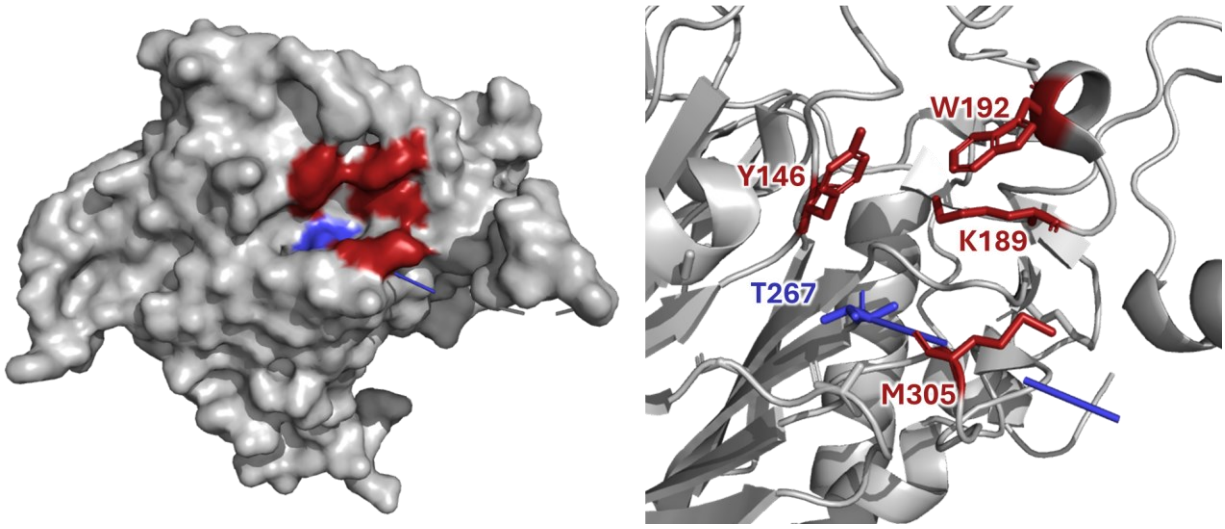

Figure 5.1. Crystal structure of a single active subunit (heterodimer) of $NylC_A$ (PDB ID: 3AXG). Left: surface view, where threonine 267 is highlighted in blue, and surface-exposed residues near the active site are highlighted in red. Right: close-up of the active site, with residues of interest to be mutated for this study, indicated.

We selected positions Y146, K189, W192, and M305 as potential locations where substrate binding could be modulated through mutagenesis. Note that while the crystal structure of $NylC_A$ was used to select these positions, all of these amino acids are conserved among wild-type and thermostable variants of NylC. Qualitatively, all of the selected residues are bulky and hydrophobic, which would natively enhance binding interactions with an equally hydrophobic substrate.

As mentioned in Section 5.1, positions 146 and 189 have previously been investigated for their participation in amide hydrolysis, via preparation of alanine mutants at each of those positions.[71] In that study, where these mutations were performed starting from $NylC_{p2}TS$, reduced autoprocessing (6-10% for K189A, 37% for Y146A), and reduced activity (0.6% for K189A and 3.6% for Y146A) were observed, compared to $NylC_{p2}TS$. From these results, molecular dynamics

simulations and crystallographic analyses, it was hypothesized that both of these residues participate in both activities, with Y146-OH contributing to oxyanion stabilization in the tetrahedral intermediate formed during amide hydrolysis. Therefore, we expect that mutation at these positions may lead to zero activity in all but the wild-type enzyme.

We chose to use NylC$_K$TS, derived from the most active NylC enzyme (NylC$_K$, see Section 4.2.5), as the basis for site-saturation mutagenesis. As previously discussed in Section 3.1.2, thermostable enzymes are inherently advantageous in polymer degrading applications, and beginning with a thermostable enzyme for this study decreases the likelihood that any one mutation will lower the melting temperature below a useful temperature for nylon hydrolysis.

For each library, where each position to be mutated represents one library, we designed primers for full-plasmid PCR (see Table A5.1 in the Appendix). The forward primers annealed at the position to be mutated, and began with the degenerate codon, NNK, where N represents any amino acid, and K represents either T or G. With this degenerate codon, 32 possible codons are generated, representing all 20 amino acids. However, following transformation, we will be unsure of which mutation is present in which colony. Therefore, we must oversample to be confident that all possible mutations are being represented. Mathematically, if we select 90 colonies, we are 94% confident that all possible mutations at a given position have been picked. These calculations were performed using the CASTER tool for degenerate codon design.[95] This number of colonies to be picked fits conveniently in a 96-well plate, leaving 6 wells behind for controls. For these, we performed three conditions in duplicate: either wild-type enzyme (positive control), or empty vector (negative control), or no-cells control (to ensure sterility).

5.2.2. Library screen using Trylon-6

Libraries were prepared by PCR using the site-directed mutagenesis protocol (see Section 5.4.1), however, while all amplifications were successful, the mutation of K189R gave a low yield of DNA (see Figure A5.1 in the Appendix). Nonetheless, transformation of all mutant libraries gave enough colonies such that we could select 90 from each plate for screening.

Protein expression was performed in 1 mL volumes, in deep well, 96-well plates. First, each colony served to inoculate a 1 mL pre-culture, then each of those pre-cultures in turn was used to inoculate 1 mL expression cultures. The plate containing the pre-cultures was kept as a reference plate, where each culture was mixed with glycerol and stored at -80 ℃. Following screening of the lysates, the reference plates were used as records, allowing us to extract and sequence the DNA from that culture to determine which mutations are related to the observed activity.

Following cell lysis *via* repeated freeze-thaw cycles, and centrifugation to remove insoluble debris, the resultant cell lysate was evaluated via the Trylon assay (see section 4.4.2 for method), using the substrate, Trylon-6. We performed the reaction at 50 ℃ as we had previously observed that we could obtain full consumption of the substrate by NylC_KTS in 20 minutes at this elevated temperature, significantly expediting the screen. Figure 5.2 shows an example of the data collected for a screen of NylC_KTS^{Y146X} mutants.

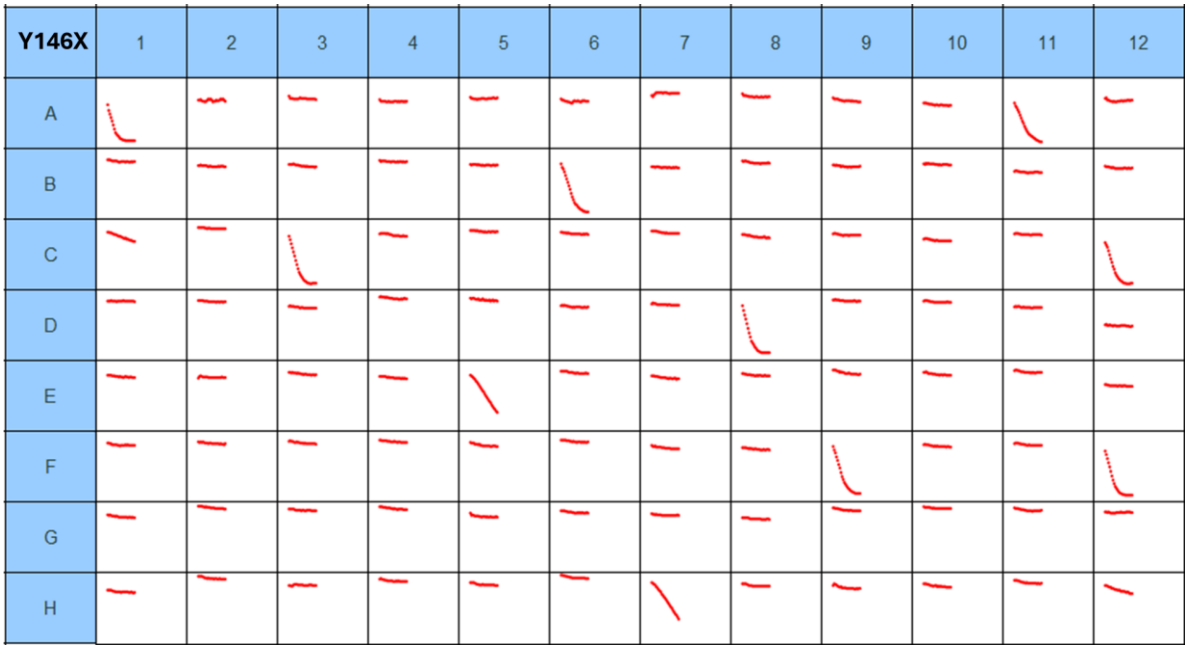

Figure 5.2. Hydrolysis of Trylon-6 by cell lysate containing NylC$_K$TS^{Y146X} mutants as measured by OD_{600} over time. Reaction mixtures contain: Trylon-6 (1 mM), potassium phosphate buffer (20 mM, pH 7.3), glycerol (15%), BSA (0.1 mg/mL), MeOH (5%), cell lysate (20 µL). All wells were inoculated with cell lysate containing unknown Y146X mutants except for control wells: wild-type (NylC$_K$TS) – A1 and F12; Empty pET28 vector (B1 and G12); no cell blank (C1, H12).

Immediately, we could observe hydrolysis at active wells, indicated by an immediate decrease in OD_{600}. We chose to sequence 15 mutants from each plate, and included both active and inactive mutants to ensure that the differences in activity we were observing were indeed due to the corresponding mutation, and not simply varying levels of expression. The sequencing results for all 4 libraries can be found in Figures A5.3a-d (in the Appendix), superimposed over the corresponding well indicating activity. A summary of active mutants can be found in Table 5.1.

Table 5.1. Amino acid residues giving rise to activity at each position investigated.

Position	Wild-Type Residue	Active Mutants
146	Y	F
189	K	-
192	W	F, L, M
305	M	L, H, V, C

We observe some trends in the mutations that give rise to activity. First, at position 146, only the phenylalanine mutant was active was besides the wild-type bearing tyrosine. This indicates that an aromatic residue is likely necessary at this position. However, phenylalanine does not bear the H-bond donor group of tyrosine, which was hypothesized by Negoro *et al.* to contribute to oxyanion stabilization during substrate hydrolysis,[71] suggesting that this function by residue 146 is not necessary for catalysis. Conversely, the lysine at position 189 *does* appear to be necessary for activity based on our screen, consistent with the observations reported,[71] as no mutants at that position were active. We observe a greater diversity of active mutations at positions 192 and 305; particularly intriguing is position 305 where polar, nonpolar, charged, and aromatic residues are all permitted for activity, but a variety of mutants are notably inactive, including glycine and threonine (Figure A5.2d in the Appendix).

5.2.3. Evaluation of active mutants

While the Trylon assay is quantifiable, and can give us some indication of relative activity of the variants, this activity is affected by rates of expression and degree of autoprocessing; thus, in order

to study the effects of these mutations more closely, we expressed the active mutants indicated in Table 5.1 on a preparative scale for further characterization.

Following purification of the enzymes, an aliquot was taken prior to incubation of the enzymes overnight at 37 ℃ to induce autoprocessing. The aliquots were analyzed by SDS-PAGE alongside aliquots taken after the incubation, to determine the extent of autoprocessing at each point (Figure 5.3).

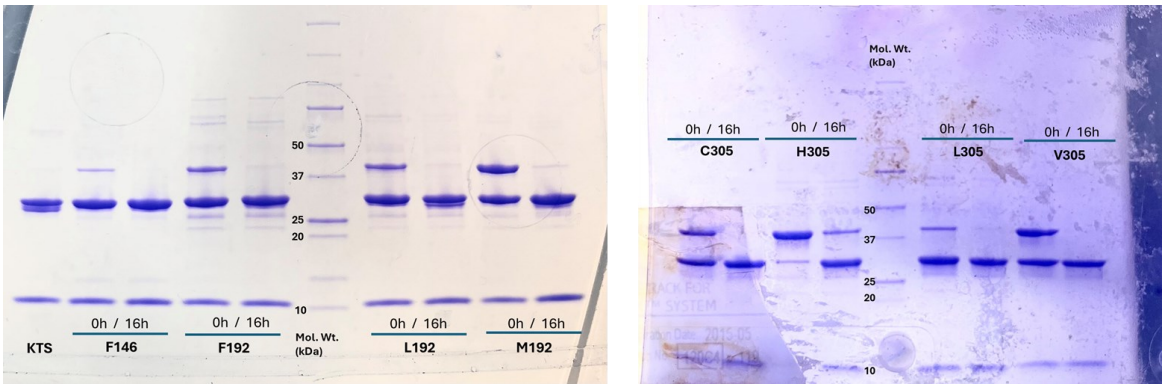

Figure 5.3. Analysis of each active variant by SDS-PAGE after 0 h or 16 h of incubation at 37 ℃. The inactive precursor appears as a band at ~37 kDa, whereas the active protein appears as two bands at 27 and 10 kDa.

None of the enzymes we expressed are fully autoprocessed prior to incubation, but all were fully autoprocessed after an overnight incubation at 37 ℃ except for the M305H mutant, which was allowed to incubate for an additional day to promote full autoprocessing. This phenomenon likely contributes to the variability in activity we observed from the screen, where the M305H mutant showed decreased apparent activity against Trylon-6 relative to the other mutations at that position (see Figure A5.2d in the Appendix). With this result, we were curious about position 189, for which

the screen revealed no activity for non-wild-type enzymes. K189 is believed to be necessary for autoprocessing activity, as previously discussed,[71] though the mechanism of its role is not known. In the screen, we observed that the K189R mutant demonstrated no activity (Figure A5.2c in the Appendix), despite being the most structurally and electronically similar to lysine of the amino acids. Out of interest, we also expressed $NylC_KTS^{K189R}$ on preparative scale. We analyzed the purified protein by SDS-PAGE before and after incubation at 37 °C, and were surprised to see partial autoprocessing even prior to incubation (see Figure A5.3 in the Appendix). Lysine 189 in the wild-type enzymes is thought to be involved in H-bonding with water molecules in the enzyme active site, participating in the proton shuttle that eventually deprotonates the nucleophilic threonine leading to autocleavage.[71] While autoprocessing was not observed in the reported K189A mutant,[71] we hypothesize that arginine at that position could equally form H-bonding interactions similarly to lysine, allowing autoprocessing to occur.

We evaluated the purified and fully autoprocessed enzymes for hydrolysis activity against Nylon-6 film (Figure 5.4). It should be noted here that the TNBS assay used to quantify nylon hydrolysis is prone to error due to extensive manipulation steps, and each batch of assays was performed alongside $NylC_KTS$ as a positive control to account for this. The batch of assays evaluating $NylC_KTS^{M305H}$ and $NylC_KTS^{K189R}$ demonstrated overall much lower activity than the batch evaluating the other mutants shown, and this was reflected in the lower rates for the wild-type, $NylC_KTS$. Thus, for analysis purposes, the rate values for the M305H and K189R mutants were adjusted by the ratio of rates of the $NylC_KTS$ controls.

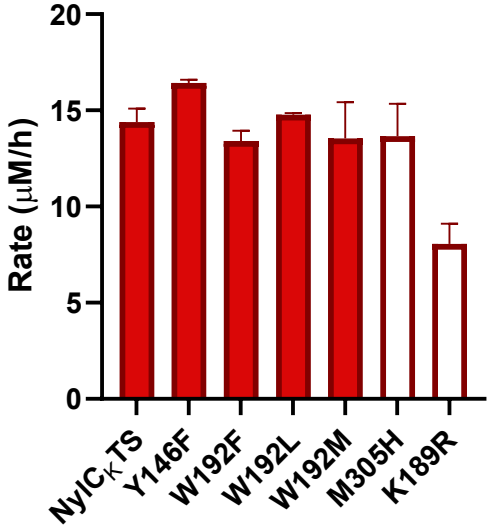

Figure 5.4. Rates of Nylon-6 hydrolysis by NylC$_K$TS and active mutants. The white bars indicate rates from reactions that were performed separately and normalized to a NylC$_K$TS control run concurrently (see Section 5.4.2). Values are averages of three replicates, with error bars indicating standard deviations. Data may be found in Figure A5.4 in the Appendix.

All of the enzymes were active against nylon, with the active mutants from the screen demonstrating approximate equivalent activity to the wild-type, NylC$_K$TS, and NylC$_K$TS^{Y146F} demonstrating slightly higher activity than the wild-type. This result lends further credence to the notion that perhaps the OH group of Y146 in the wild-type enzyme does not contribute to oxyanion stabilization as previously believed,[71] or at least, if it does, this stabilization does not affect the rate-limiting step. Interestingly, NylC$_K$TS^{K189R} also demonstrated activity, though it was notably lower than the other mutants tested. In the proposed mechanism of amide hydrolysis, K189 is thought to participate in stabilization of the oxyanion hole through H-bonding.[71] Arginine could also participate in

this manner, but the proximity of a bulky, charged residue at the surface of the active site could disfavour binding of the nonpolar nylon substrate.

Finally, we evaluated the melting temperature of the active mutants by differential scanning fluorimetry. A summary of the melting temperatures can be found in Figure 5.5. Overall, the effect of these mutations on melting temperature was minimal: the largest difference was observed in the NylC$_K$TS^{Y146F} mutant, where melting temperature decreased from 87 °C in the wild-type enzyme to 82.5 °C, a difference of -4.5 degrees. This result could also explain the slightly increased activity observed by NylC$_K$TS^{Y146F} compared to NylC$_K$TS: since higher melting temperature is correlated to lower activity at a temperature where both enzymes are stable, as discussed in Section 4.2.4.

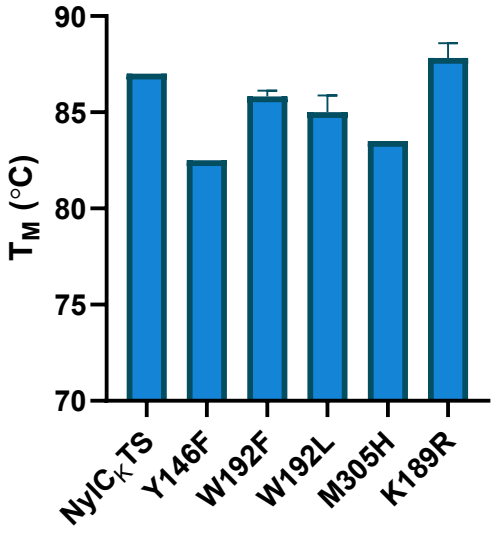

Figure 5.5. Melting temperatures of NylC$_K$TS mutants, as determined by differential scanning fluorimetry (see Figure A5.5 in the Appendix). Data values are averages of triplicates, and error bars show standard deviations. All data values may be found in Table A5.2 in the Appendix.

5.3. Conclusion

In order to demonstrate the utility of the Trylon assay as a screen for amidase activity, we constructed site-saturation mutant libraries based on the enzyme, NylC_KTS, and screened them for activity using Trylon-6. This screen was able to identify active variants in 20 minutes at 50 ℃, such that all four libraries (360 total variants) could be screened in less than two hours. From the screen, we identified and sequenced active variants, revealing certain trends pertaining to the mutations that permitted activity at each of these locations. We expressed active variants and evaluated them for autoprocessing and nylon hydrolysis activities, as well as melting temperature. The Trylon-based pre-screen rapidly eliminated mutants with low or no activity, reducing our library size from 370 to 8 enzymes. This allowed us to dedicate the greater time and resources required for more in-depth study to a handful of mutants with known amide hydrolysis activity. In the future, we hope to use the Trylon assay in a directed evolution campaign, to identify enzymes with improved activity towards Nylon hydrolysis.

5.4. Materials and Methods

5.4.1. Molecular Biology Methods

General protocol for site-saturation mutagenesis

The gene encoding NylC_KTS was used as the template for mutagenesis. For each position in the gene to be mutated (corresponding to a single amino acid), forward and reverse primers were designed, where the forward primer contained the degenerate codon NNK at the 5′-end. PCR was performed using Q5 High-Fidelity DNA polymerase (New England Biolabs) and NylCK-TS_pET28a as the template. Following amplification of the gene as confirmed by agarose gel electrophoresis, the DNA was purified (E.Z.N.A. Cycle Pure Kit, Omega BioTek) then a digest of

the template was performed using DpnI (New England Biolabs). Following digestion, the amplicon was purified again using the Cycle Pure Kit, then phosphorylated (T4 PNK, New England Biolabs) and ligated (T4 DNA Ligase, New England Biolabs). The circularized amplicon was then transformed into chemically competent *E. coli* BL21-DE3 cells and selected on LB agar plates supplemented with 50 µg/mL kanamycin.

Expression of mutant enzymes and preparation of cell lysate for screening

Colonies (90 per plate) were selected from *E. coli* BL21-DE3 cells transformed with each NylC$_K$TS site-saturation library (1 library = 1 mutant position) and used to inoculate 1 mL cultures containing LB-kan in a deep-well 96-well plate (Axygen®) (referred to as the *reference plate*). Plates also contained duplicate control wells, either inoculated with colonies transformed with the wild-type plasmid (NylCK-TS_pET28a) or empty vector (pET28a), or nothing (no bacteria control). Plates were sealed and shaken overnight at 37 °C. Then, 200 µL of each pre-culture was used to inoculate 1 mL expression cultures containing 2×YT media supplemented with kanamycin (50 µg/mL), in a deep-well 96-well plate (*expression plate*). To each well of the reference plate was added 1 mL of sterile LB media containing glycerol (60% w/w). The cultures were mixed by pipetting, then the reference plates were stored at -80 °C.

The expression plates were shaken at 37 °C for 4 hours, then induced through addition of IPTG to each 1 mL culture, to a final concentration of 0.1 mM. The plates were then shaken at room temperature for 18 hours. Cells were pelleted by centrifugation of the plates at 2700 × g for 20 minutes at 4 °C. The pellets were resuspended in 40 µL lysis buffer (50 mM Tris pH 7.5, 10 mM imidazole, 100 mM NaCl, containing 0.1 mg/mL lysozyme and 10 µg/mL DNase). The cells were lysed by 8

freeze-thaw cycles (alternating between -78 ℃ and 40 ℃ baths). The lysates were then clarified by centrifugation at 2700 × g for 1 hour, and used immediately.

Preparative expression of NylC mutants

Expressions were performed on 200 mL scale of expression culture, following the method described in Section 3.4.1.

5.4.2. Assay Methods

Activity screen via Trylon assay

Reaction mixtures were prepared in 96-well plates as described in Section 4.4.2 for the 50 ℃ condition, except reactions were initiated through addition of 20 μL of clarified lysate. Reactions were monitored at 600 nm for 1 hour, though the assay was sometimes manually terminated if the reactions were complete prior to that time. All reactions with wild-type enzyme were complete after 20 minutes.

Nylon hydrolysis

Nylon hydrolysis experiments were performed as described in Section 4.4.2. Reactions with mutants of NylC$_K$TS were run alongside wild-type NylC$_K$TS as a positive control to account for any differences in observed activity due to handling of samples. Rate values from the second batch were normalized through multiplication by the ratio of activities between each NylC$_K$TS dataset. For the first dataset, NylC$_K$TS gave a rate of 14.4 ± 0.7 μM/h; for the second dataset, the same

enzyme gave a rate of 8.1 ± 1.7 μM/h. Therefore, the rates from the second dataset were multiplied by a factor of 1.77, the ratio between these two values.

Melting temperature determination by differential scanning fluorimetry

Samples were prepared in PCR 8-strips in 25 mL volumes, and contained enzyme (2 mg/mL), phosphate buffer (20 mM, pH 7.3) and SYPRO® Orange dye (5 ×, diluted from a 5000 × stock). Samples were prepared in triplicate, alongside blanks in triplicate, containing no enzyme. DSF was performed using a Bio-Rad CFX Connect qPCR thermocycler using the FRET settings for excitation and emission wavelengths. The temperature was increased from 10 ℃ to 95 ℃ with an increment of 0.5 ℃ every 10 seconds. Melting points were determined from the minimum value of the negative first derivative of the output data, RFU/temperature.

Chapter 6. Conclusions and Future Directions

6.1. Conclusions

Enzymatic degradation is a promising avenue for the remediation of plastic waste, with the potential of literally turning a massive global problem into a feedstock for new materials. However, this technology is still in its infancy, and there is a need to develop more efficient biocatalysts for this application. Over the last 5 years, since the beginning of my PhD, the amount of research output on nylon-degrading enzymes has exploded globally, and we are fortunate to be participating in this rapidly accelerating progress in real time.

In Chapter 2, representing the first project discussed herein, we investigated *Bacillus subtilis* transglutaminase (bTG) for isopeptidase activity, with the intent to develop this activity towards the hydrolysis of nylon. While conducting this work, we developed a continuous, quantitative activity assay for bTG, enabling for the first time quantitation of its transglutaminase activity. However, unfortunately, we were unable to detect any hydrolysis activity from this enzyme, either towards isopeptide-like substrates or even simple chromogenic ester substrates. We hypothesize that bTG is highly specific towards protein substrates, and, demonstrating no observable hydrolytic activity, is potentially incapable of permitting water into its active site. However, demonstrating certain ideal qualities for a biocatalyst (high stability, pH tolerance, ease of expression), bTG may find a home in other applications more amenable to its eponymous cross-linking activity.

In Chapters 3-5, we turned towards a family of enzymes with known polyamide-degrading activity, NylC. While these enzymes have been extensively studied for their enzymatic properties, little work had been done to improve their hydrolysis activity towards nylon, due in part to lack of accessible assays to quantify their activity. In Chapter 3, we investigated the substrate specificity

of NylC using a series of chromogenic ester and amide substrates. We identified a high-affinity substrate that can enable quantification of acyltransfer activity of NylC in minutes, and showed that NylC preferentially recognizes substrates with a distal (non-scissile) amide group, hinting at its specificity as an oligomer (not dimer) hydrolase.

In Chapter 4, we applied NylC to the hydrolysis of a series of nylon trimer analogue substrates, which are insoluble until hydrolyzed by the enzyme. These substrates, known as "Trylons", allow for the first time direct quantification of aliphatic amide hydrolysis, which is the relevant activity for nylon hydrolysis. We demonstrate that the hydrolysis of these "Trylon" substrates correlates strongly to hydrolysis of nylon, suggesting that the substrate surrogate can be used in a protein engineering context to screen enzymes for nylon-degrading activity. In Chapter 5, we put that hypothesis to the test, and demonstrated that the Trylon assay allows for the screening of hundreds of NylC variants in less than an hour, rapidly eliminating enzymes that show no linear amide hydrolysis activity. Using this screen, we were able to identify residues near the active site of NylC that are relevant to autoprocessing and substrate hydrolysis.

6.2. Future Directions

There are several potential directions in which to take this project. Since demonstrating the applicability of the Trylon assay for the rapid screening of mutants, we could envision a directed evolution campaign through the development and screening of a random mutant library. For this, we could begin with either the template enzyme NylC$_K$TS, or perhaps a modified NylC$_K$TS with the incorporation of known activity-improving mutations, P27Q and F301L. Our group is concurrently developing a circularly-permutated version of NylC, which seeks to decouple the autoprocessing and catalytic activities of NylC; thus, we could instead begin with this ("cpNylC") as a template for random mutagenesis. This circularly-permutated NylC places the nucleophilic

threonine at the natural *N*-terminus of the peptide sequence, removing the need for the autoprocessing step. This method would thus mitigate the presence of false negatives in a screen due to slow autoprocessing, as we have observed in some of the mutants evaluated in Chapter 5.

If we were to begin a directed evolution campaign, we envision that we could screen, for instance, 10 plates (900 mutants) in less than four hours by continuous monitoring of Trylon hydrolysis. Conversely, this could be even further accelerated by incubating each of 10 assay plates simultaneously at 50 °C for 20 minutes (or less, for a more stringent screen!), then performing endpoint assays, via a single read at 600 nm. This would enable us to identify active enzymes almost instantaneously, though this endpoint-type assay would not provide preliminary rate data (as does the currently employed method, with a *continuous* read at 600 nm). With this strategy, however, we would be able to screen nearly a thousand variants in approximately an hour, even when accounting for manipulation time. From there, we could choose up to 10 active mutants per plate and evaluate those in one single plate for Nylon hydrolysis activity. In addition to saving time, this would save 90% of the resources required for Nylon activity screening (including the expensive nylon substrate and TNBS reagent). Furthermore, we would already be starting with variants with known activity, meaning that every datapoint in the second, more focused screen with nylon has value.

We have previously considered developing an even more direct preliminary screen by embedding the Trylon-6 substrate into agar plates. Using this strategy, active variants could be identified by a "zone of clearance" around the colony if active protein is expressed. Our initial attempts produced inconsistent precipitates (as opposed to a cloudy suspension) in the agar, so this method would need to be further optimized prior to application, but could further accelerate engineering efforts.

Overall, we believe that this screen can drastically increase the pace of nylon hydrolase discovery and engineering, and I am excited to see where this project goes next.

References

(1) Environment and Climate Change Canada. *Economic Study of the Canadian Plastic Industry, Markets and Waste : Summary Report to Environment and Climate Change Canada*; Government of Canada, 2019.

(2) Kabir, M. S.; Wang, H.; Luster-Teasley, S.; Zhang, L.; Zhao, R. Microplastics in Landfill Leachate: Sources, Detection, Occurrence, and Removal. *Environ. Sci. Ecotechnology* **2023**, *16*, 100256. https://doi.org/10.1016/j.ese.2023.100256.

(3) US EPA, O. *Plastics: Material-Specific Data*. https://www.epa.gov/facts-and-figures-about-materials-waste-and-recycling/plastics-material-specific-data (accessed 2025-07-12).

(4) Golkaram, M.; Mehta, R.; Taveau, M.; Schwarz, A.; Gankema, H.; Urbanus, J. H.; De Simon, L.; Cakir-Benthem, S.; van Harmelen, T. Quality Model for Recycled Plastics (QMRP): An Indicator for Holistic and Consistent Quality Assessment of Recycled Plastics Using Product Functionality and Material Properties. *J. Clean. Prod.* **2022**, *362*, 132311. https://doi.org/10.1016/j.jclepro.2022.132311.

(5) de Lorenzo, V. Systems Biology Approaches to Bioremediation. *Curr. Opin. Biotechnol.* **2008**, *19* (6), 579–589. https://doi.org/10.1016/j.copbio.2008.10.004.

(6) Dharmasiddhi, I. P. W.; Chen, J.; Arab, B.; Lan, C.; Euler, C.; Chou, C. P.; Liu, Y. Engineering a Cross-Feeding Synthetic Bacterial Consortium for Degrading Mixed PET and Nylon Monomers. *Processes* **2025**, *13* (2), 375. https://doi.org/10.3390/pr13020375.

(7) Tournier, V.; Topham, C. M.; Gilles, A.; David, B.; Folgoas, C.; Moya-Leclair, E.; Kamionka, E.; Desrousseaux, M.-L.; Texier, H.; Gavalda, S.; Cot, M.; Guémard, E.; Dalibey, M.; Nomme, J.; Cioci, G.; Barbe, S.; Chateau, M.; André, I.; Duquesne, S.; Marty, A. An Engineered PET Depolymerase to Break down and Recycle Plastic Bottles. *Nature* **2020**, *580* (7802), 216–219. https://doi.org/10.1038/s41586-020-2149-4.

(8) Clark, R. A.; Shaver, M. P. Depolymerization within a Circular Plastics System. *Chem. Rev.* **2024**, *124* (5), 2617–2650. https://doi.org/10.1021/acs.chemrev.3c00739.

(9) Kumar, A.; von Wolff, N.; Rauch, M.; Zou, Y.-Q.; Shmul, G.; Ben-David, Y.; Leitus, G.; Avram, L.; Milstein, D. Hydrogenative Depolymerization of Nylons. *J. Am. Chem. Soc.* **2020**, *142* (33), 14267–14275. https://doi.org/10.1021/jacs.0c05675.

(10) Bell, E. L.; Smithson, R.; Kilbride, S.; Foster, J.; Hardy, F. J.; Ramachandran, S.; Tedstone, A. A.; Haigh, S. J.; Garforth, A. A.; Day, P. J. R.; Levy, C.; Shaver, M. P.; Green, A. P. Directed Evolution of an Efficient and Thermostable PET Depolymerase. *Nat. Catal.* **2022**, *5* (8), 673–681. https://doi.org/10.1038/s41929-022-00821-3.

(11) *Enzymatic recycling*. Carbios. https://www.carbios.com/fr/enzymatic-recycling/ (accessed 2025-03-09).

(12) Pérez-Venegas, M.; Friščić, T.; Auclair, K. Efficient Mechano-Enzymatic Hydrolysis of Polylactic Acid under Moist-Solid Conditions. *ACS Sustain. Chem. Eng.* **2023**, *11* (27), 9924–9931. https://doi.org/10.1021/acssuschemeng.2c06847.

(13) Thomas, G. M.; Quirk, S.; Huard, D. J. E.; Lieberman, R. L. Bioplastic Degradation by a Polyhydroxybutyrate Depolymerase from a Thermophilic Soil Bacterium. *Protein Sci.* **2022**, *31* (11), e4470. https://doi.org/10.1002/pro.4470.

(14) Schmidt, J.; Wei, R.; Oeser, T.; Dedavid e Silva, L. A.; Breite, D.; Schulze, A.; Zimmermann, W. Degradation of Polyester Polyurethane by Bacterial Polyester Hydrolases. *Polymers* **2017**, *9* (2), 65. https://doi.org/10.3390/polym9020065.

(15) *Nylon 6: Definition, properties and common uses*. EuroPlas. https://europlas.com.vn/en-US/blog-1/nylon-6-definition-properties-and-common-uses (accessed 2025-07-07).
(16) Kim, S.; Kim, Y. T.; Oh, L. S.; Kim, H. J.; Lee, J. Marine Waste Upcycling—Recovery of Nylon Monomers from Fishing Net Waste Using Seashell Waste-Derived Catalysts in a CO2-Mediated Thermocatalytic Process. *J. Mater. Chem. A* **2022**, *10* (37), 20024–20034. https://doi.org/10.1039/D2TA02060B.
(17) Tian, J.-J.; Liu, X.; Ye, L.; Zhang, Z.; Quinn, E. C.; Shi, C.; Broadbelt, L. J.; Marks, T. J.; Chen, E. Y.-X. Redesigned Nylon 6 Variants with Enhanced Recyclability, Ductility, and Transparency. *Angew. Chem. Int. Ed.* **2024**, *63* (17), e202320214. https://doi.org/10.1002/anie.202320214.
(18) Singh, A. *6 Alarming Ways Plastic Waste is Destroying Marine Life (And What You Can Do)*. Marine Biodiversity Science Center. https://www.marinebiodiversity.ca/6-alarming-ways-plastic-waste-is-destroying-marine-life-and-what-you-can-do/ (accessed 2025-07-07).
(19) de Witt, J.; Luthe, T.; Wiechert, J.; Jensen, K.; Polen, T.; Wirtz, A.; Thies, S.; Frunzke, J.; Wynands, B.; Wierckx, N. Upcycling of Polyamides through Chemical Hydrolysis and Engineered Pseudomonas Putida. *Nat. Microbiol.* **2025**, *10* (3), 667–680. https://doi.org/10.1038/s41564-025-01929-5.
(20) Castanha, N.; Dantas, F. B. H.; Marangoni Júnior, L. Mechanical Recycling of Polyamides: A Review. *Trends Food Sci. Technol.* **2025**, *162*, 105107. https://doi.org/10.1016/j.tifs.2025.105107.
(21) Mondragon, G.; Kortaberria, G.; Mendiburu, E.; González, N.; Arbelaiz, A.; Peña-Rodriguez, C. Thermomechanical Recycling of Polyamide 6 from Fishing Nets Waste. *J. Appl. Polym. Sci.* **2020**, *137* (10), 48442. https://doi.org/10.1002/app.48442.
(22) Tonsi Giulia; Maesani Cristiano; Alini Stefano; Ortenzi Marco Aldo; Pirola Carlo. Nylon Recycling Processes: A Brief Overview. *Chem. Eng. Trans.* **2023**, *100*, 727–732. https://doi.org/10.3303/CET23100122.
(23) Minor, A.-J.; Goldhahn, R.; Rihko-Struckmann, L.; Sundmacher, K. Chemical Recycling Processes of Nylon 6 to Caprolactam: Review and Techno-Economic Assessment. *Chem. Eng. J.* **2023**, *474*, 145333. https://doi.org/10.1016/j.cej.2023.145333.
(24) Wursthorn, L.; Beckett, K.; Rothbaum, J. O.; Cywar, R. M.; Lincoln, C.; Kratish, Y.; Marks, T. J. Selective Lanthanide-Organic Catalyzed Depolymerization of Nylon-6 to ϵ-Caprolactam. *Angew. Chem. Int. Ed.* **2023**, *62* (4), e202212543. https://doi.org/10.1002/anie.202212543.
(25) *Our Facilities - Nylene Specialty Nylon*. https://nylene.com/manufacturing-capabilities/our-facilities/ (accessed 2025-09-03).
(26) Coates, G. W.; Getzler, Y. D. Y. L. Chemical Recycling to Monomer for an Ideal, Circular Polymer Economy. *Nat. Rev. Mater.* **2020**, *5* (7), 501–516. https://doi.org/10.1038/s41578-020-0190-4.
(27) Sun, S. Enzymatic Depolymerization of Polyamides (Nylons): Current Challenges and Future Directions. *Polym. Degrad. Stab.* **2025**, *238*, 111341. https://doi.org/10.1016/j.polymdegradstab.2025.111341.
(28) Deguchi, T.; Kitaoka, Y.; Kakezawa, M.; Nishida, T. Purification and Characterization of a Nylon-Degrading Enzyme. *Appl. Environ. Microbiol.* **1998**, *64* (4), 1366–1371. https://doi.org/10.1128/aem.64.4.1366-1371.1998.

(29) Fujisawa, M.; Hirai, H.; Nishida, T. Degradation of Polyethylene and Nylon-66 by the Laccase-Mediator System. *J. Polym. Environ.* **2001**, *9* (3), 103–108. https://doi.org/10.1023/A:1020472426516.
(30) Komáromi, I.; Bagoly, Z.; Muszbek, L. Factor XIII: Novel Structural and Functional Aspects. *J. Thromb. Haemost.* **2011**, *9* (1), 9–20. https://doi.org/10.1111/j.1538-7836.2010.04070.x.
(31) Griffin, M.; Casadio, R.; Bergamini, C. M. Transglutaminases: Nature's Biological Glues. *Biochem. J.* **2002**, *368* (2), 377–396. https://doi.org/10.1042/bj20021234.
(32) Keillor, J. W.; Clouthier, C. M.; Apperley, K. Y. P.; Akbar, A.; Mulani, A. Acyl Transfer Mechanisms of Tissue Transglutaminase. *Bioorganic Chem.* **2014**, *57*, 186–197. https://doi.org/10.1016/j.bioorg.2014.06.003.
(33) Leblanc, A.; Gravel, C.; Labelle, J.; Keillor, J. W. Kinetic Studies of Guinea Pig Liver Transglutaminase Reveal a General-Base-Catalyzed Deacylation Mechanism. *Biochemistry* **2001**, *40* (28), 8335–8342. https://doi.org/10.1021/bi0024097.
(34) Ichinose, A.; Aoki, N. Reversible Cross-Linking of α2-Plasmin Inhibitor to Fibrinogen by Fibrin-Stabilizing Factor. *Biochim. Biophys. Acta BBA - Protein Struct. Mol. Enzymol.* **1982**, *706* (2), 158–164. https://doi.org/10.1016/0167-4838(82)90482-4.
(35) Király, R.; Thangaraju, K.; Nagy, Z.; Collighan, R.; Nemes, Z.; Griffin, M.; Fésüs, L. Isopeptidase Activity of Human Transglutaminase 2: Disconnection from Transamidation and Characterization by Kinetic Parameters. *Amino Acids* **2016**, *48* (1), 31–40. https://doi.org/10.1007/s00726-015-2063-5.
(36) Nayak, A.; Müller, S. SUMO-Specific Proteases/Isopeptidases: SENPs and Beyond. *Genome Biol.* **2014**, *15* (7), 422. https://doi.org/10.1186/s13059-014-0422-2.
(37) Chekan, J. R.; Koos, J. D.; Zong, C.; Maksimov, M. O.; Link, A. J.; Nair, S. K. Structure of the Lasso Peptide Isopeptidase Identifies a Topology for Processing Threaded Substrates. *J. Am. Chem. Soc.* **2016**, *138* (50), 16452–16458. https://doi.org/10.1021/jacs.6b10389.
(38) Gillet, S. M. F. G.; Pelletier, J. N.; Keillor, J. W. A Direct Fluorometric Assay for Tissue Transglutaminase. *Anal. Biochem.* **2005**, *347* (2), 221–226. https://doi.org/10.1016/j.ab.2005.09.035.
(39) Oteng-Pabi, S. K.; Keillor, J. W. Continuous Enzyme-Coupled Assay for Microbial Transglutaminase Activity. *Anal. Biochem.* **2013**, *441* (2), 169–173. https://doi.org/10.1016/j.ab.2013.07.014.
(40) Csosz, E.; Bagossi, P.; Nagy, Z.; Dosztanyi, Z.; Simon, I.; Fesus, L. Substrate Preference of Transglutaminase 2 Revealed by Logistic Regression Analysis and Intrinsic Disorder Examination. *J. Mol. Biol.* **2008**, *383* (2), 390–402. https://doi.org/10.1016/j.jmb.2008.08.026.
(41) Motoki, M.; Seguro, K. Transglutaminase and Its Use for Food Processing. *Trends Food Sci. Technol.* **1998**, *9* (5), 204–210. https://doi.org/10.1016/S0924-2244(98)00038-7.
(42) Oteng-Pabi, S. K.; Pardin, C.; Stoica, M.; Keillor, J. W. Site-Specific Protein Labelling and Immobilization Mediated by Microbial Transglutaminase. *Chem. Commun.* **2014**, *50* (50), 6604–6606. https://doi.org/10.1039/C4CC00994K.
(43) Rachel, N. M.; Quaglia, D.; Lévesque, É.; Charette, A. B.; Pelletier, J. N. Engineered, Highly Reactive Substrates of Microbial Transglutaminase Enable Protein Labeling within Various Secondary Structure Elements. *Protein Sci.* **2017**, *26* (11), 2268–2279. https://doi.org/10.1002/pro.3286.

(44) Kobayashi, K.; Kumazawa, Y.; Miwa, K.; Yamanaka, S. Ɛ-(γ-Glutamyl)Lysine Cross-Links of Spore Coat Proteins and Transglutaminase Activity in *Bacillus Subtilis*. *FEMS Microbiol. Lett.* **1996**, *144* (2–3), 157–160. https://doi.org/10.1111/j.1574-6968.1996.tb08523.x.
(45) Kobayashi, K.; Suzuki, S.-I.; Izawa, Y.; Miwa, K.; Yamanaka, S. Transglutaminase in Sporulating Cells of Bacillus Subtilis. *J. Gen. Appl. Microbiol.* **1998**, *44* (1), 85–91. https://doi.org/10.2323/jgam.44.85.
(46) Plácido, D.; Fernandes, C. G.; Isidro, A.; Carrondo, M. A.; Henriques, A. O.; Archer, M. Auto-Induction and Purification of a *Bacillus Subtilis* Transglutaminase (Tgl) and Its Preliminary Crystallographic Characterization. *Protein Expr. Purif.* **2008**, *59* (1), 1–8. https://doi.org/10.1016/j.pep.2007.12.004.
(47) SUZUKI, S.; IZAWA, Y.; KOBAYASHI, K.; ETO, Y.; YAMANAKA, S.; KUBOTA, K.; YOKOZEKI, K. Purification and Characterization of Novel Transglutaminase from Bacillus Subtilis Spores. *Biosci. Biotechnol. Biochem.* **2000**, *64* (11), 2344–2351. https://doi.org/10.1271/bbb.64.2344.
(48) Fernandes, C. G.; Plácido, D.; Lousa, D.; Brito, J. A.; Isidro, A.; Soares, C. M.; Pohl, J.; Carrondo, M. A.; Archer, M.; Henriques, A. O. Structural and Functional Characterization of an Ancient Bacterial Transglutaminase Sheds Light on the Minimal Requirements for Protein Cross-Linking. *Biochemistry* **2015**, *54* (37), 5723–5734. https://doi.org/10.1021/acs.biochem.5b00661.
(49) Fernandes, C. G.; Martins, D.; Hernandez, G.; Sousa, A. L.; Freitas, C.; Tranfield, E. M.; Cordeiro, T. N.; Serrano, M.; Jr, C. P. M.; Henriques, A. O. Temporal and Spatial Regulation of Protein Cross-Linking by the Pre-Assembled Substrates of a Bacillus Subtilis Spore Coat Transglutaminase. *PLOS Genet.* **2019**, *15* (4), e1007912. https://doi.org/10.1371/journal.pgen.1007912.
(50) Oteng-Pabi, S. K.; Clouthier, C. M.; Keillor, J. W. Design of a Glutamine Substrate Tag Enabling Protein Labelling Mediated by Bacillus Subtilis Transglutaminase. *PLOS ONE* **2018**, *13* (5), e0197956. https://doi.org/10.1371/journal.pone.0197956.
(51) Ursem, R.; Swarge, B.; Abhyankar, W. R.; Buncherd, H.; de Koning, L. J.; Setlow, P.; Brul, S.; Kramer, G. Identification of Native Cross-Links in Bacillus Subtilis Spore Coat Proteins. *J. Proteome Res.* **2021**, *20* (3), 1809–1816. https://doi.org/10.1021/acs.jproteome.1c00025.
(52) Veskoukis, A. S.; Margaritelis ,Nikos V.; Kyparos ,Antonios; Paschalis ,Vassilis; and Nikolaidis, M. G. Spectrophotometric Assays for Measuring Redox Biomarkers in Blood and Tissues: The NADPH Network. *Redox Rep.* **2018**, *23* (1), 47–56. https://doi.org/10.1080/13510002.2017.1392695.
(53) Piggot, P. J.; Coote, J. G. Genetic Aspects of Bacterial Endospore Formation. *Bacteriol. Rev.* **1976**, *40* (4), 908–962. https://doi.org/10.1128/br.40.4.908-962.1976.
(54) Studier, F. W. Protein Production by Auto-Induction in High-Density Shaking Cultures. *Protein Expr. Purif.* **2005**, *41* (1), 207–234. https://doi.org/10.1016/j.pep.2005.01.016.
(55) Rangaswamy, A. M. M.; Navals, P.; Gates, E. W. J.; Shad, S.; Watt, S. K. I.; Keillor, J. W. Structure–Activity Relationships of Hydrophobic Alkyl Acrylamides as Tissue Transglutaminase Inhibitors. *RSC Med. Chem.* **2022**, *13* (4), 413–428. https://doi.org/10.1039/D1MD00382H.
(56) FUKUMURA, T. BACTERIAL BREAKDOWN OF ε-CAPROLACTAM AND ITS CYCLIC OLIGOMERS. *Plant Cell Physiol.* **1966**, *7* (1), 93–104. https://doi.org/10.1093/oxfordjournals.pcp.a079172.

(57) Kinoshita, S.; Kageyama ,Sadao; Iba ,Kazuhiko; Yamada ,Yasuhiro; and Okada, H. Utilization of a Cyclic Dimer and Linear Oligomers of ε-Aminocaproic Acid by Achrornobacter Guttatus KI 72. *Agric. Biol. Chem.* **1975**, *39* (6), 1219–1223. https://doi.org/10.1080/00021369.1975.10861757.
(58) Kakudo, S.; Negoro, S.; Urabe, I.; Okada, H. Nylon Oligomer Degradation Gene, nylC, on Plasmid pOAD2 from a Flavobacterium Strain Encodes Endo-Type 6-Aminohexanoate Oligomer Hydrolase: Purification and Characterization of the nylC Gene Product. *Appl. Environ. Microbiol.* **1993**, *59* (11), 3978–3980. https://doi.org/10.1128/aem.59.11.3978-3980.1993.
(59) Yasuhira, K.; Tanaka, Y.; Shibata, H.; Kawashima, Y.; Ohara, A.; Kato, D.; Takeo, M.; Negoro, S. 6-Aminohexanoate Oligomer Hydrolases from the Alkalophilic Bacteria *Agromyces* Sp. Strain KY5R and *Kocuria* Sp. Strain KY2. *Appl. Environ. Microbiol.* **2007**, *73* (21), 7099–7102. https://doi.org/10.1128/AEM.00777-07.
(60) Negoro, S.; Shinagawa, H.; Nakata, A.; Kinoshita, S.; Hatozaki, T.; Okada, H. Plasmid Control of 6-Aminohexanoic Acid Cyclic Dimer Degradation Enzymes of Flavobacterium Sp. K172. *J. Bacteriol.* **1980**, *143* (1), 238–245. https://doi.org/10.1128/jb.143.1.238-245.1980.
(61) Takehara, I.; Fujii, T.; Tanimoto, Y.; Kato, D.-I.; Takeo, M.; Negoro, S. Metabolic Pathway of 6-Aminohexanoate in the Nylon Oligomer-Degrading Bacterium Arthrobacter Sp. KI72: Identification of the Enzymes Responsible for the Conversion of 6-Aminohexanoate to Adipate. *Appl. Microbiol. Biotechnol.* **2018**, *102* (2), 801–814. https://doi.org/10.1007/s00253-017-8657-y.
(62) Kato, K.; Ohtsuki, K.; Koda, Y.; Maekawa, T.; Yomo, T.; Negoro, S.; Urabe, I. A Plasmid Encoding Enzymes for Nylon Oligomer Degradation: Nucleotide Sequence and Analysis of pOAD2. *Microbiology* **1995**, *141* (10), 2585–2590. https://doi.org/10.1099/13500872-141-10-2585.
(63) Yasuhira, K.; Uedo, Y.; Takeo, M.; Kato, D.-I.; Negoro, S. Genetic Organization of Nylon-Oligomer-Degrading Enzymes from Alkalophilic Bacterium, *Agromyces* Sp. KY5R. *J. Biosci. Bioeng.* **2007**, *104* (6), 521–524. https://doi.org/10.1263/jbb.104.521.
(64) Sun, J.; Pang, Y.; Lei, Z.; OuYang, B.; Lai, W.; Wang, Y.; Lan, D. Enzymatic Depolymerization of Plastic Materials by a Highly Efficient Two-Enzyme System. *Biochem. Eng. J.* **2024**, *204*, 109222. https://doi.org/10.1016/j.bej.2024.109222.
(65) Zhang, J.; Wang, H.; Luo, Z.; Yang, Z.; Zhang, Z.; Wang, P.; Li, M.; Zhang, Y.; Feng, Y.; Lu, D.; Zhu, Y. Computational Design of Highly Efficient Thermostable MHET Hydrolases and Dual Enzyme System for PET Recycling. *Commun. Biol.* **2023**, *6* (1), 1135. https://doi.org/10.1038/s42003-023-05523-5.
(66) Roca, M.; Liu, H.; Messer, B.; Warshel, A. On the Relationship between Thermal Stability and Catalytic Power of Enzymes. *Biochemistry* **2007**, *46* (51), 15076–15088. https://doi.org/10.1021/bi701732a.
(67) Poor, C. B.; Andorfer, M. C.; Lewis, J. C. Improving the Stability and Catalyst Lifetime of the Halogenase RebH Using Directed Evolution. *Chembiochem Eur. J. Chem. Biol.* **2014**, *15* (9), 1286–1289. https://doi.org/10.1002/cbic.201300780.
(68) Negoro, S.; Shibata, N.; Tanaka, Y.; Yasuhira, K.; Shibata, H.; Hashimoto, H.; Lee, Y.-H.; Oshima, S.; Santa, R.; Oshima, S.; Mochiji, K.; Goto, Y.; Ikegami, T.; Nagai, K.; Kato, D.; Takeo, M.; Higuchi, Y. Three-Dimensional Structure of Nylon Hydrolase and Mechanism of

Nylon-6 Hydrolysis. *J. Biol. Chem.* **2012**, *287* (7), 5079–5090. https://doi.org/10.1074/jbc.M111.321992.
(69) Bell, E. L.; Rosetto, G.; Ingraham, M. A.; Ramirez, K. J.; Lincoln, C.; Clarke, R. W.; Gado, J. E.; Lilly, J. L.; Kucharzyk, K. H.; Erickson, E.; Beckham, G. T. Natural Diversity Screening, Assay Development, and Characterization of Nylon-6 Enzymatic Depolymerization. *Nat. Commun.* **2024**, *15* (1), 1217. https://doi.org/10.1038/s41467-024-45523-5.
(70) Nagai, K.; Iida, K.; Shimizu, K.; Kinugasa, R.; Izumi, M.; Kato, D.; Takeo, M.; Mochiji, K.; Negoro, S. Enzymatic Hydrolysis of Nylons: Quantification of the Reaction Rate of Nylon Hydrolase for Thin-Layered Nylons. *Appl. Microbiol. Biotechnol.* **2014**, *98* (20), 8751–8761. https://doi.org/10.1007/s00253-014-5885-2.
(71) Negoro, S.; Shibata, N.; Kato, D.; Tanaka, Y.; Yasuhira, K.; Nagai, K.; Oshima, S.; Furuno, Y.; Yokoyama, R.; Miyazaki, K.; Takeo, M.; Hengphasatporn, K.; Shigeta, Y.; Lee, Y.-H.; Higuchi, Y. X-Ray Crystallographic and Mutational Analysis of the NylC Precursor: Catalytic Mechanism of Autocleavage and Substrate Hydrolysis of Nylon Hydrolase. *FEBS J.* **2023**, *290* (13), 3400–3421. https://doi.org/10.1111/febs.16755.
(72) Negoro, S.; Shibata, N.; Lee, Y.-H.; Takehara, I.; Kinugasa, R.; Nagai, K.; Tanaka, Y.; Kato, D.; Takeo, M.; Goto, Y.; Higuchi, Y. Structural Basis of the Correct Subunit Assembly, Aggregation, and Intracellular Degradation of Nylon Hydrolase. *Sci. Rep.* **2018**, *8* (1), 9725. https://doi.org/10.1038/s41598-018-27860-w.
(73) Kakudo, S.; Negoro, S.; Urabe, I.; Okada, H. Characterization of Endo-Type 6-Aminohexanoate-Oligomer Hydrolase from Flavobacterium Sp. *J. Ferment. Bioeng.* **1995**, *80* (1), 12–17. https://doi.org/10.1016/0922-338X(95)98169-L.
(74) Nagai, K.; Yasuhira, K.; Tanaka, Y.; Kato, D.; Takeo, M.; Higuchi, Y.; Negoro, S.; Shibata, N. Crystallization and X-Ray Diffraction Analysis of Nylon Hydrolase (NylC) from Arthrobacter Sp. KI72. *Acta Crystallograph. Sect. F Struct. Biol. Cryst. Commun.* **2013**, *69* (Pt 10), 1151–1154. https://doi.org/10.1107/S1744309113024263.
(75) Puetz, H.; Janknecht, C.; Contreras, F.; Vorobii, M.; Kurkina, T.; Schwaneberg, U. Validated High-Throughput Screening System for Directed Evolution of Nylon-Depolymerizing Enzymes. *ACS Sustain. Chem. Eng.* **2023**, *11* (43), 15513–15522. https://doi.org/10.1021/acssuschemeng.3c01575.
(76) Lentz, C. S.; Ordonez, A. A.; Kasperkiewicz, P.; La Greca, F.; O'Donoghue, A. J.; Schulze, C. J.; Powers, J. C.; Craik, C. S.; Drag, M.; Jain, S. K.; Bogyo, M. Design of Selective Substrates and Activity-Based Probes for Hydrolase Important for Pathogenesis 1 (HIP1) from Mycobacterium Tuberculosis. *ACS Infect. Dis.* **2016**, *2* (11), 807–815. https://doi.org/10.1021/acsinfecdis.6b00092.
(77) Chai Discovery; Boitreaud, J.; Dent, J.; McPartlon, M.; Meier, J.; Reis, V.; Rogozhnikov, A.; Wu, K. Chai-1: Decoding the Molecular Interactions of Life. *bioRxiv* **2024**, 2024.10.10.615955. https://doi.org/10.1101/2024.10.10.615955.
(78) Hoffman, E. R.; Rangaswamy, A. M. M.; Cleveland, M. E.; Keillor, J. W.; Howe, G. W. Targeted Genome Mining Facilitates the Discovery of a Promiscuous, Hyperthermostable Amidase from Thermovenabulum Gondwanense with Notable Nylon-Degrading Capacity. *Angew. Chem. Int. Ed.* **2025**, *64* (2), e202414842. https://doi.org/10.1002/anie.202414842.
(79) Gagnon, P.; Huang, X.; Therrien, E.; Keillor, J. W. Peptide Coupling of Unprotected Amino Acids through in Situ P-Nitrophenyl Ester Formation. *Tetrahedron Lett.* **2002**, *43* (43), 7717–7719. https://doi.org/10.1016/S0040-4039(02)01840-3.

(80) Arifuzzaman, M.; Zhao, Y. Artificial Zinc Enzymes with Fine-Tuned Active Sites for Highly Selective Hydrolysis of Activated Esters. *ACS Catal.* **2018**, *8* (9), 8154–8161. https://doi.org/10.1021/acscatal.8b02292.
(81) Williams, T. J.; Reay, A. J.; Whitwood, A. C.; Fairlamb, I. J. S. A Mild and Selective Pd-Mediated Methodology for the Synthesis of Highly Fluorescent 2-Arylated Tryptophans and Tryptophan-Containing Peptides: A Catalytic Role for Pd0 Nanoparticles? *Chem. Commun.* **2014**, *50* (23), 3052–3054. https://doi.org/10.1039/C3CC48481E.
(82) Mesaik, M. A.; Rahat, S.; Khan, K. M.; Zia-Ullah; Choudhary, M. I.; Murad, S.; Ismail, Z.; Atta-ur-Rahman; Ahmad, A. Synthesis and Immunomodulatory Properties of Selected Oxazolone Derivatives. *Bioorg. Med. Chem.* **2004**, *12* (9), 2049–2057. https://doi.org/10.1016/j.bmc.2004.02.034.
(83) National Institute of Advanced Industrial Science and Technology. *mass spectrum; SDBS No.:23681; RN 57-08-9*. Spectral Database for Organic Compounds (SDBS). https://sdbs.db.aist.go.jp/sdbs/cgi-bin/direct_frame_top.cgi (accessed 2023-11-29).
(84) Colombo, M.; Bossolo, S.; Aramini, A. Phosphorus Trichloride-Mediated and Microwave-Assisted Synthesis of a Small Collection of Amides Bearing Strong Electron-Withdrawing Group Substituted Anilines. *J. Comb. Chem.* **2009**, *11* (3), 335–337. https://doi.org/10.1021/cc900011z.
(85) *Frances H. Arnold – Nobel Lecture*. NobelPrize.org. https://www.nobelprize.org/prizes/chemistry/2018/arnold/lecture/ (accessed 2025-07-11).
(86) Wang, N.; Guan, F.; Lv, X.; Han, D.; Zhang, Y.; Wu, N.; Xia, X.; Tian, J. Enhancing Secretion of Polyethylene Terephthalate Hydrolase PETase in Bacillus Subtilis WB600 Mediated by the SPamy Signal Peptide. *Lett. Appl. Microbiol.* **2020**, *71* (3), 235–241. https://doi.org/10.1111/lam.13312.
(87) Helleckes, L. M.; Müller, C.; Griesbach, T.; Waffenschmidt, V.; Moch, M.; Osthege, M.; Wiechert, W.; Oldiges, M. Explore or Exploit? A Model-Based Screening Strategy for PETase Secretion by Corynebacterium Glutamicum. *Biotechnol. Bioeng.* **2023**, *120* (1), 139–153. https://doi.org/10.1002/bit.28261.
(88) Sulaiman, S.; Yamato, S.; Kanaya, E.; Kim, J.-J.; Koga, Y.; Takano, K.; Kanaya, S. Isolation of a Novel Cutinase Homolog with Polyethylene Terephthalate-Degrading Activity from Leaf-Branch Compost by Using a Metagenomic Approach. *Appl. Environ. Microbiol.* **2012**, *78* (5), 1556–1562. https://doi.org/10.1128/AEM.06725-11.
(89) Belisário-Ferrari, M. R.; Wei, R.; Schneider, T.; Honak, A.; Zimmermann, W. Fast Turbidimetric Assay for Analyzing the Enzymatic Hydrolysis of Polyethylene Terephthalate Model Substrates. *Biotechnol. J.* **2019**, *14* (4), 1800272. https://doi.org/10.1002/biot.201800272.
(90) New Model Substrates for Enzymes Hydrolysing Polyethyleneterephthalate and Polyamide Fibres. *J. Biochem. Biophys. Methods* **2006**, *69* (1–2), 89–99. https://doi.org/10.1016/j.jbbm.2006.02.005.
(91) Dong, K.; Fang, X.; Jackstell, R.; Laurenczy, G.; Li, Y.; Beller, M. Rh(I)-Catalyzed Hydroamidation of Olefins via Selective Activation of N–H Bonds in Aliphatic Amines. *J. Am. Chem. Soc.* **2015**, *137* (18), 6053–6058. https://doi.org/10.1021/jacs.5b02218.
(92) Reynolds, M. M.; Zhou, Z.; Oh, B. K.; Meyerhoff, M. E. Bis-Diazeniumdiolates of Dialkyldiamines: Enhanced Nitric Oxide Loading of Parent Diamines. *Org. Lett.* **2005**, *7* (14), 2813–2816. https://doi.org/10.1021/ol050541z.

(93) Gunanathan, C.; Ben-David, Y.; Milstein, D. Direct Synthesis of Amides from Alcohols and Amines with Liberation of H2. *Science* **2007**, *317* (5839), 790–792. https://doi.org/10.1126/science.1145295.
(94) Vidal, L. S.; Isalan, M.; Heap, J. T.; Ledesma-Amaro, R. A Primer to Directed Evolution: Current Methodologies and Future Directions. *RSC Chem. Biol.* **2023**, *4* (4), 271–291. https://doi.org/10.1039/D2CB00231K.
(95) Reetz, M. T.; Carballeira, J. D. Iterative Saturation Mutagenesis (ISM) for Rapid Directed Evolution of Functional Enzymes. *Nat. Protoc.* **2007**, *2* (4), 891–903. https://doi.org/10.1038/nprot.2007.72.

Appendix to Chapter 2

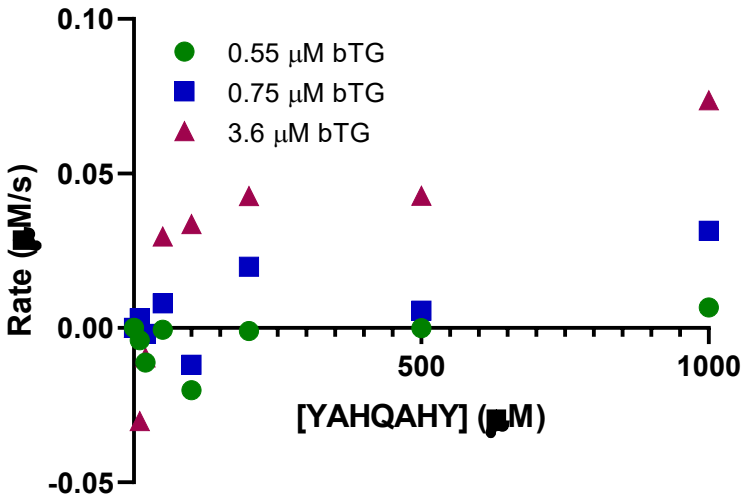

Figure A2.1. Observed rates are plotted vs. concentration of acyl donor substrate, at varying concentrations of bTG. Reaction conditions: MOPS buffer (200 μM, pH 7.2), EDTA (1 mM), NADH (500 μM), α-ketoglutarate (10 mM), glutamate dehydrogenase (10 U/mL) and glycine methyl ester (10 mM), YAHQAHY (0-1000 μM) and bTG (0.55, 0.75, or 3.6 μM). Initial slopes were converted to rates using an extinction coefficient of 6.22 L $mmol^{-1}$ cm^{-1}.[52]

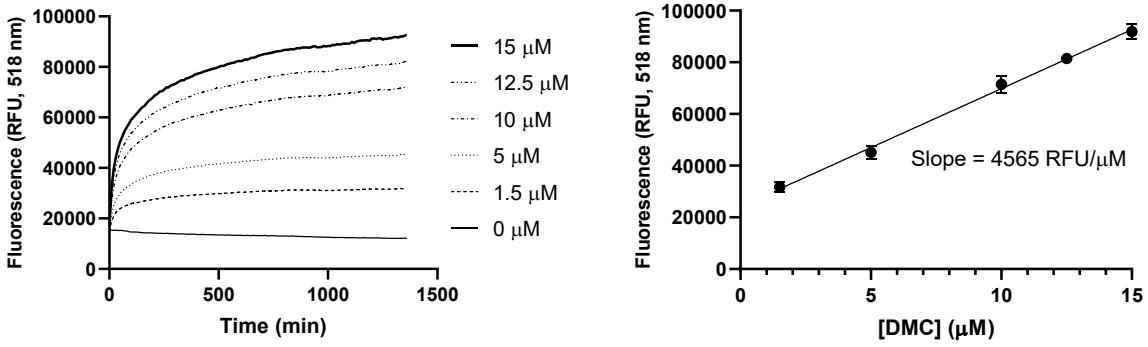

Figure A2.2. Relationship between dimethylcasein concentration and fluorescence signal in the continuous dansylcadaverine incorporation assay. Left: reactions were run to completion (plateau)

in the presence of 0.5 μM mTG. Right: final fluorescence values are plotted against enzyme concentration. The slope of this curve is used to convert all dansylcadaverine incorporation data into rates (μM of product over time).

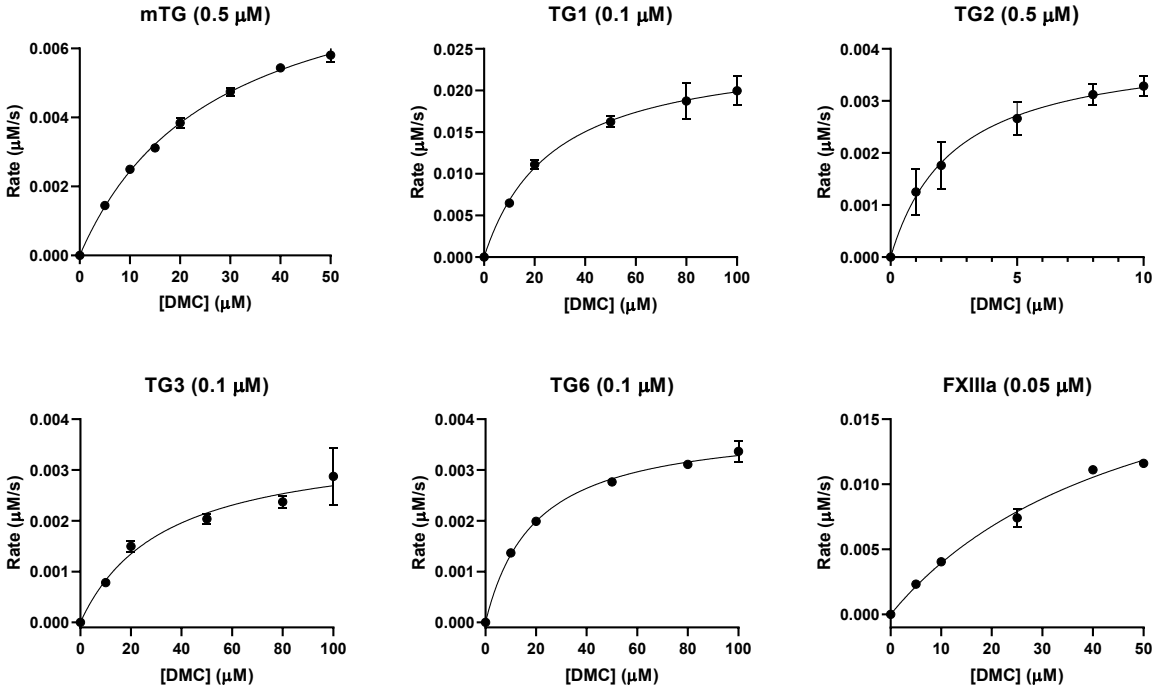

Figure A2.3. Michaelis-Menten plots for dansylcadaverine incorporation into dimethylcasein by transglutaminases. Reaction conditions: TG (concentration as indicated), dansylcadaverine (160 μM), dimethylcasein (variable concentrations), Tris (100 mM, pH 8.0). Datapoints are averages of two or three (mTG) replicates, with error bars indicating standard deviations.

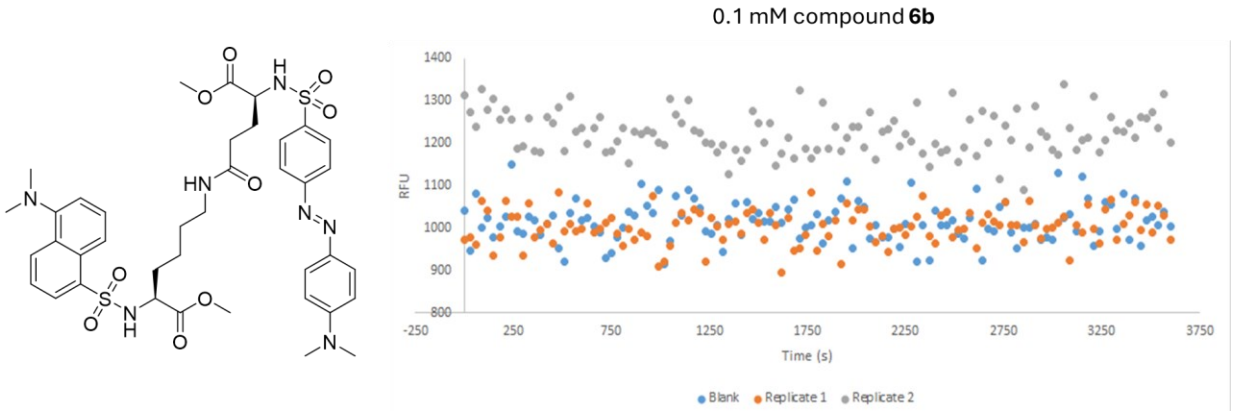

Figure A2.4a. Reaction of bTG (8 µM) with compound **6b**. Reaction was performed at the limit of solubility (0.1 mM) of substrate.

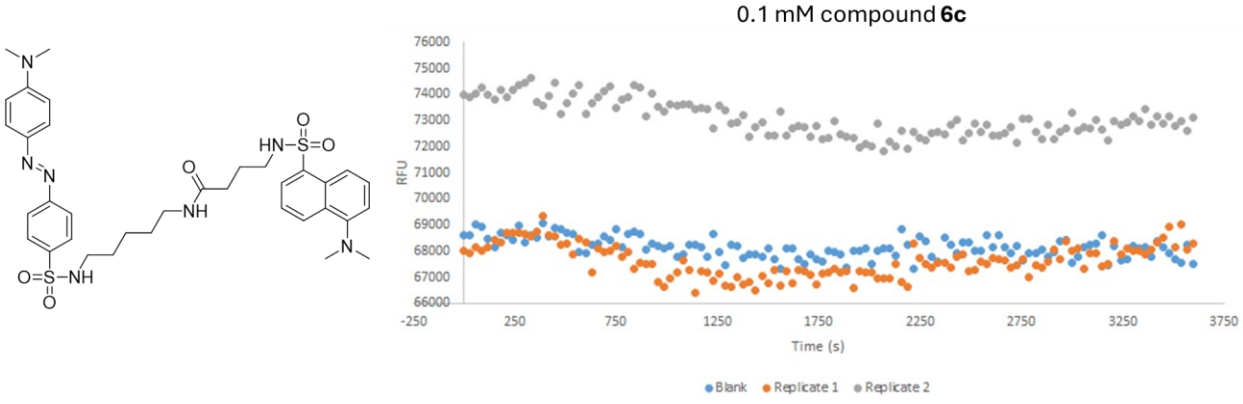

Figure A2.4b. Reaction of bTG (8 µM) with compound **6c**. Reaction was performed at the limit of solubility (0.1 mM) of substrate.

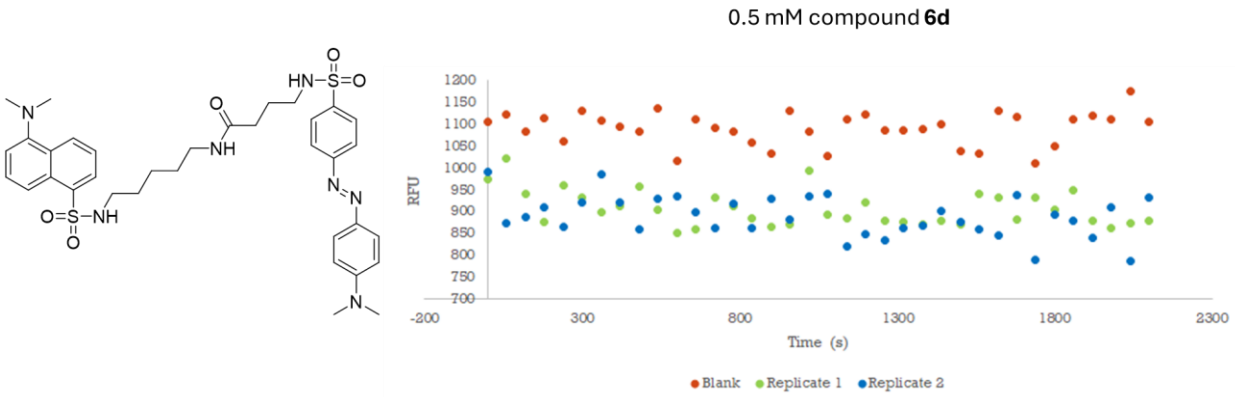

Figure A2.4c. Reaction of bTG (8 μM) with compound **6d**. Reaction was performed at the limit of solubility (0.5 mM) of substrate.

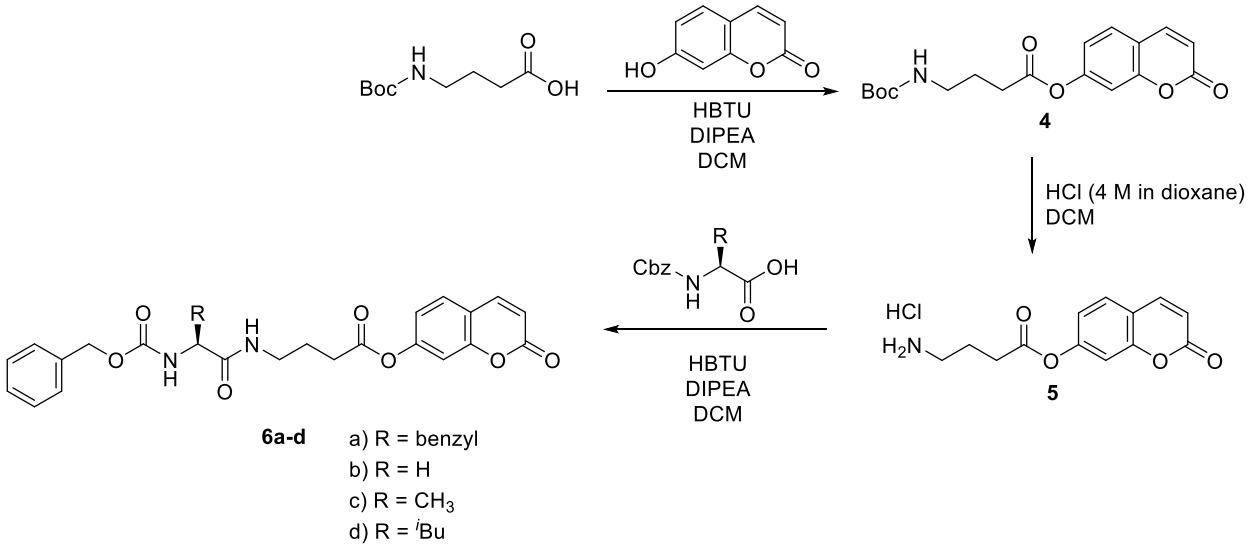

Figure A2.5. General synthetic route for ZFBC and its analogues.

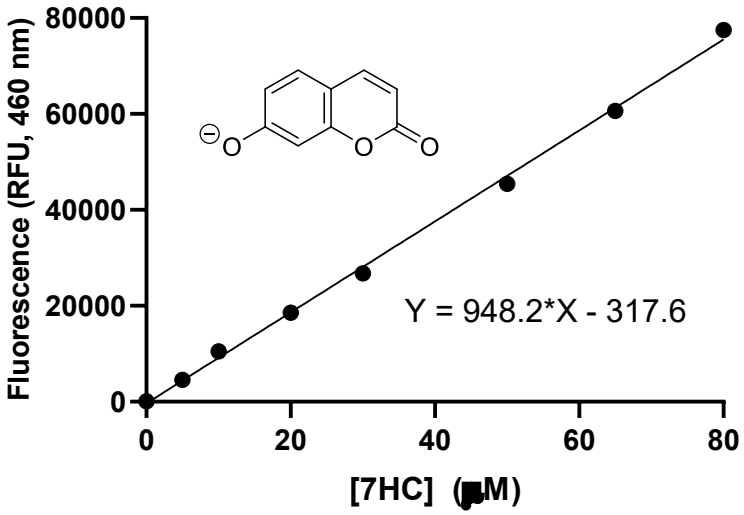

Figure A2.6. Relationship between product (7-hydroxycoumarin) concentration and fluorescence signal due to hydrolysis of ZFBC and its analogues.

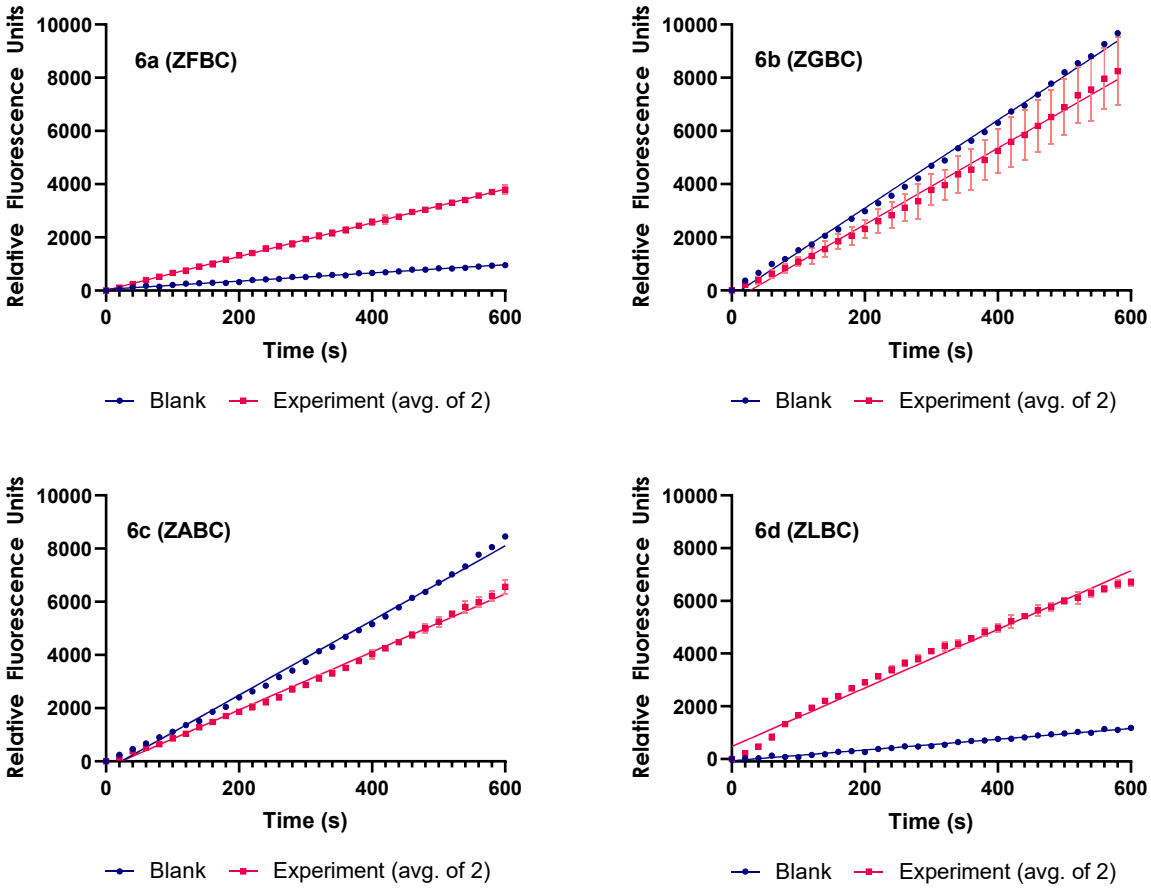

Figure A2.7. Raw data (fluorescence over time) for all four ZFBC analogues.

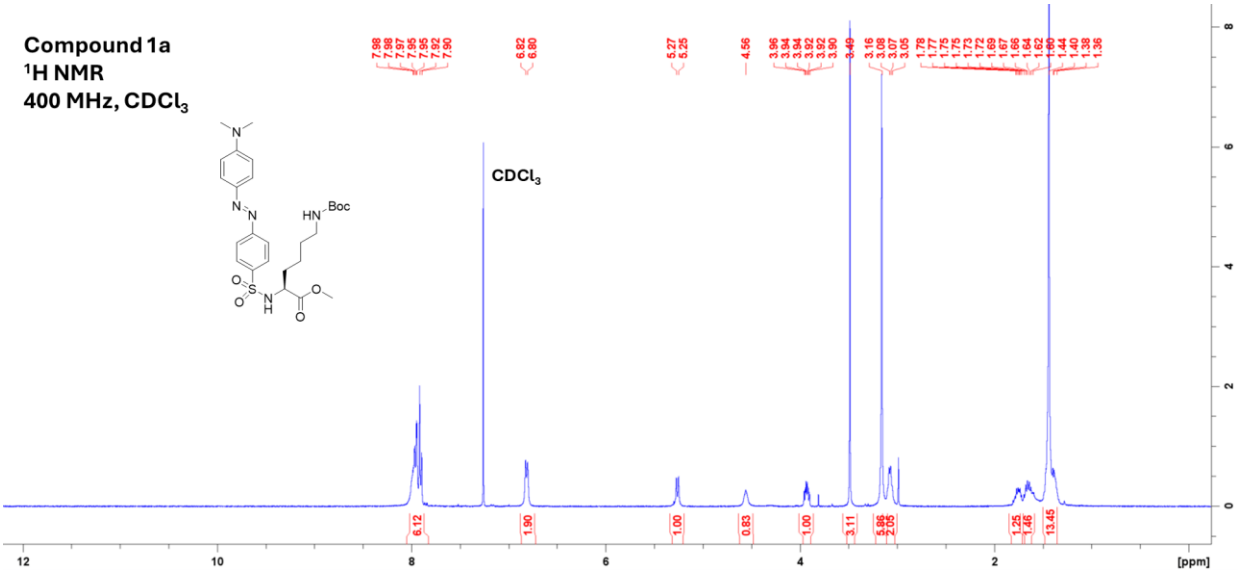

Figure A2.8. Compound **1a** – ^{1}H NMR, 400 MHz, $CDCl_3$

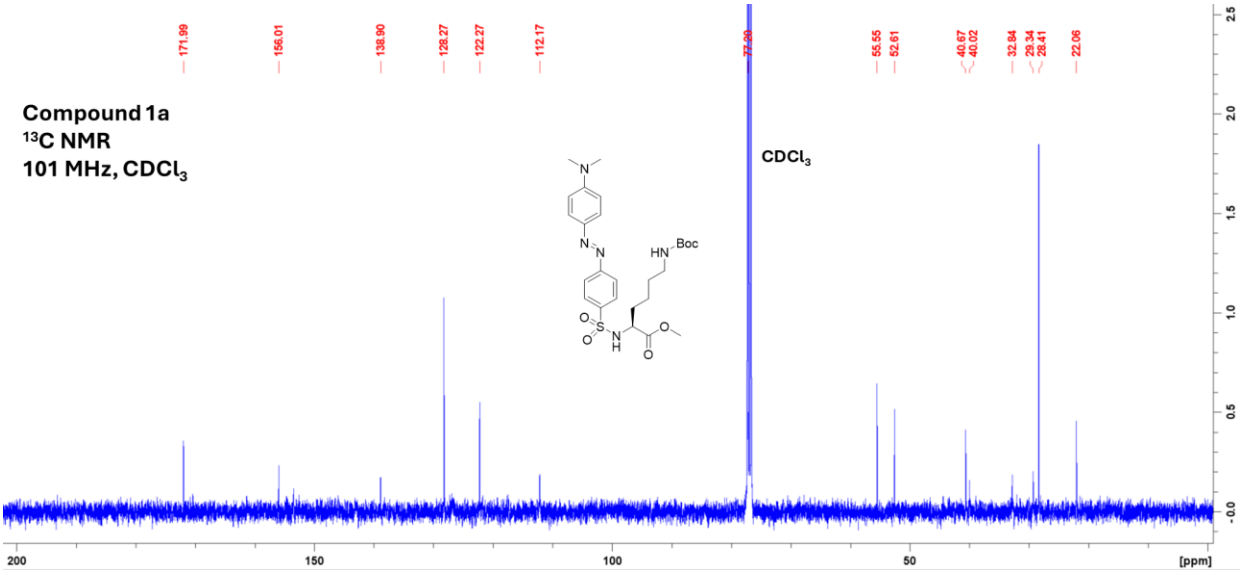

Figure A2.9. Compound **1a** – ^{13}C NMR, 101 MHz, $CDCl_3$

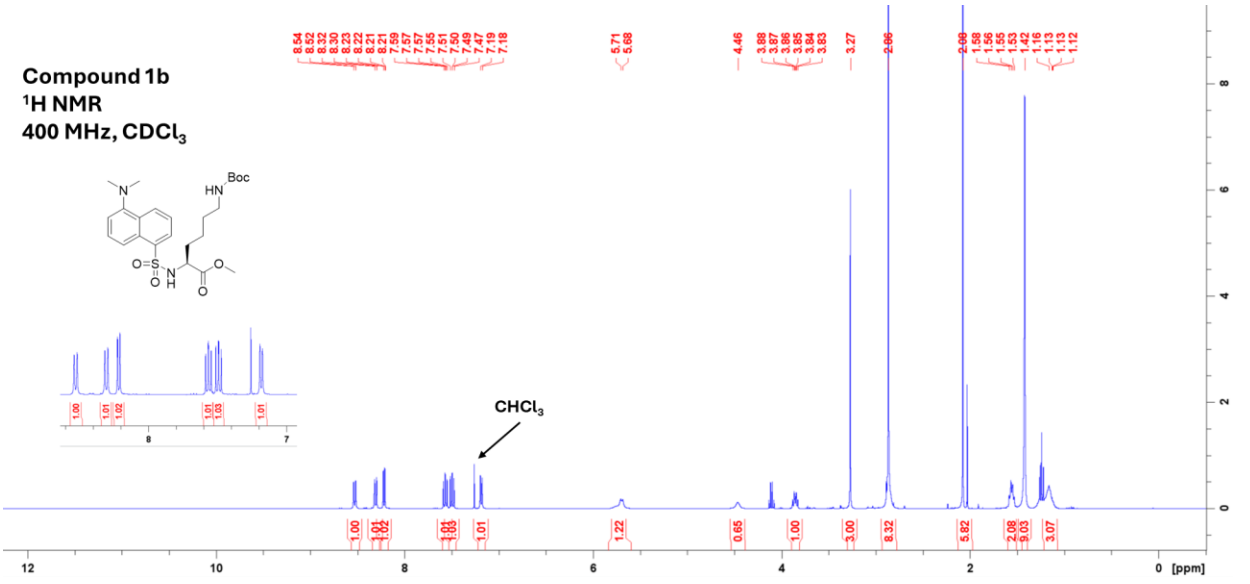

Figure A2.10. Compound **1b** – ^{1}H NMR, 400 MHz, $CDCl_3$

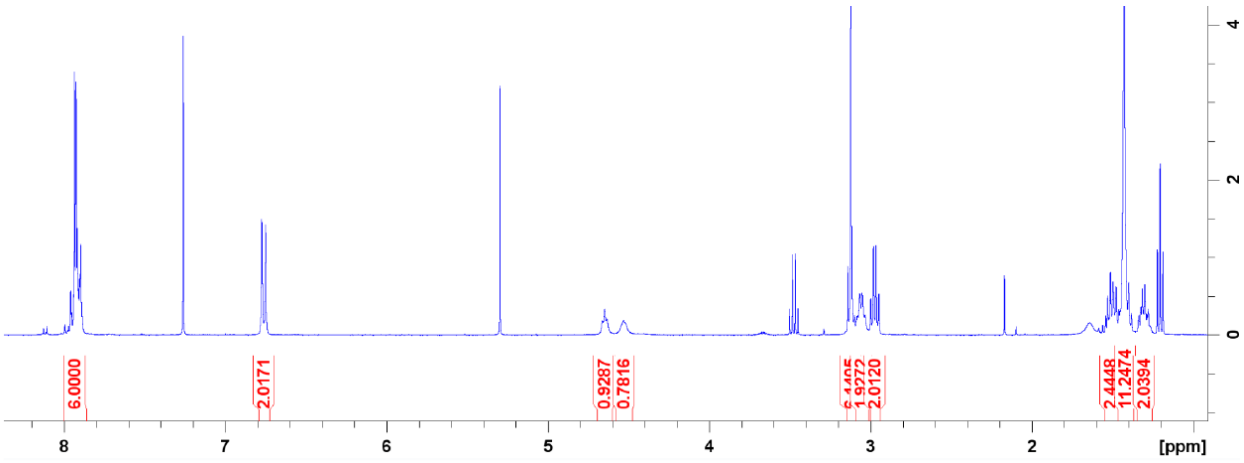

Figure A2.11. Compound **1c** – ^{1}H NMR, 400 MHz, $CDCl_3$

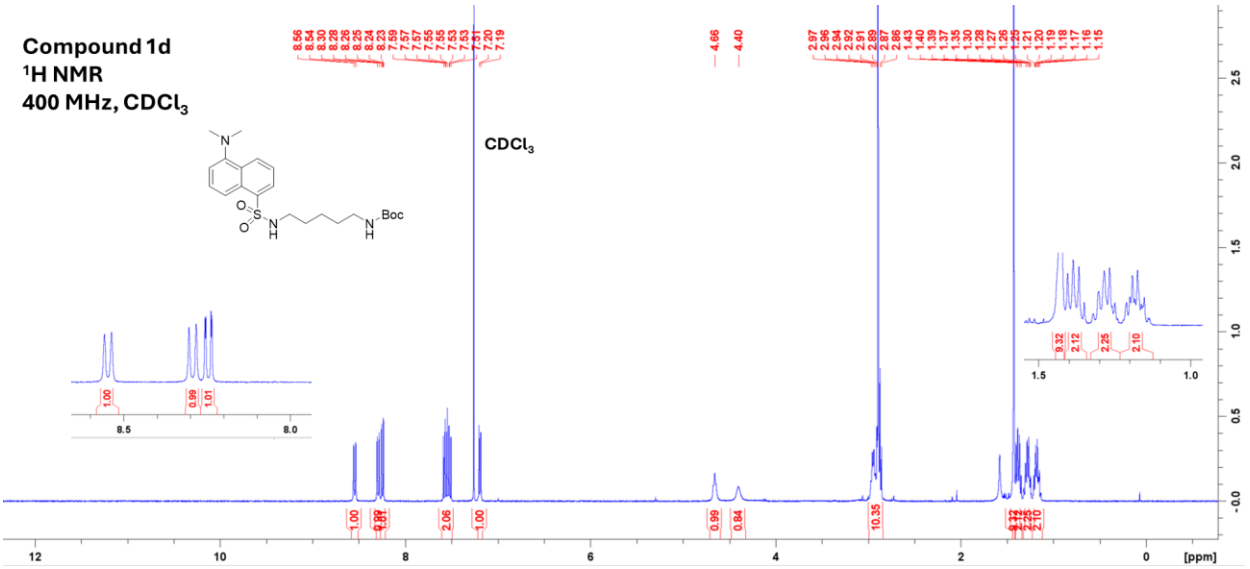

Figure A2.12. Compound **1d** – ^{1}H NMR, 400 MHz, $CDCl_3$

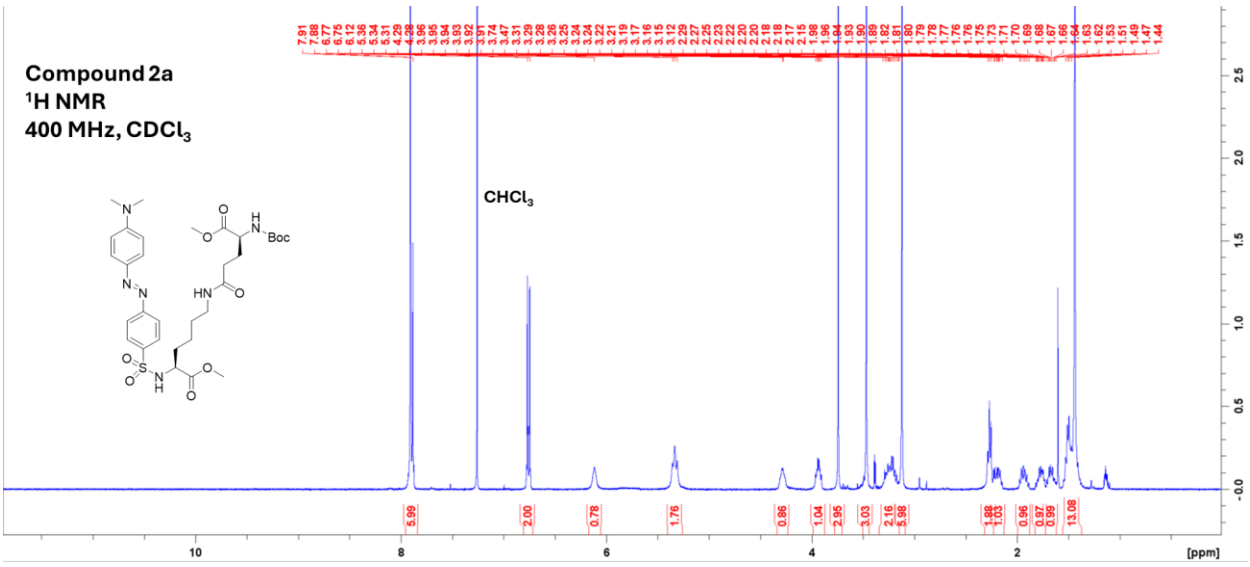

Figure A2.13. Compound **2a** – ^{1}H NMR, 400 MHz, $CDCl_3$

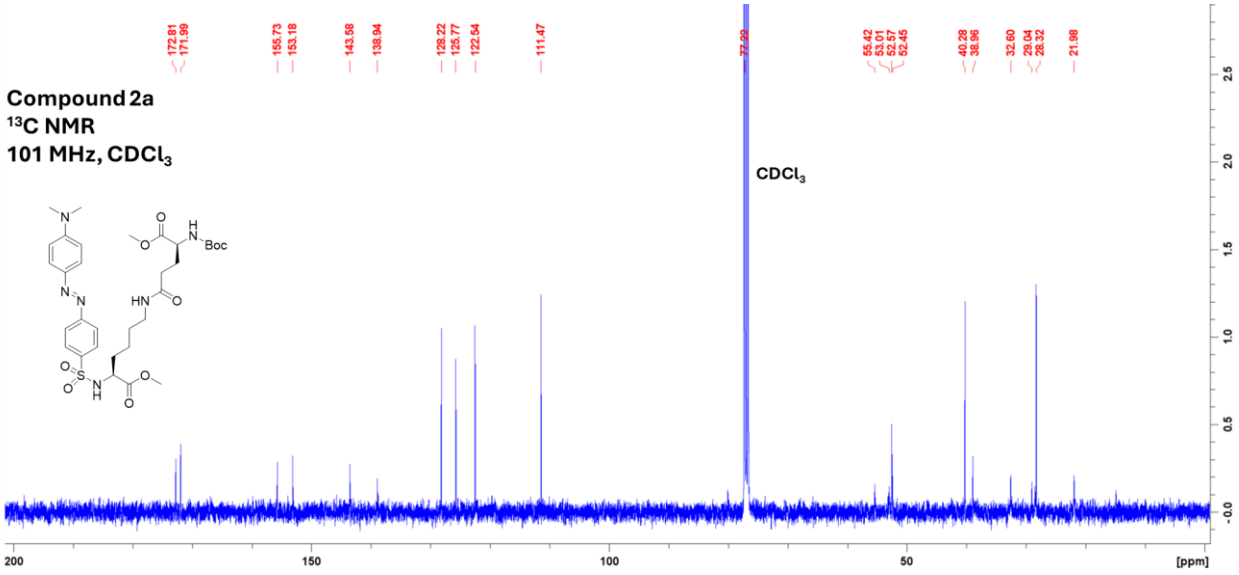

Figure A2.14. Compound **2a** – ^{13}C NMR, 101 MHz, $CDCl_3$

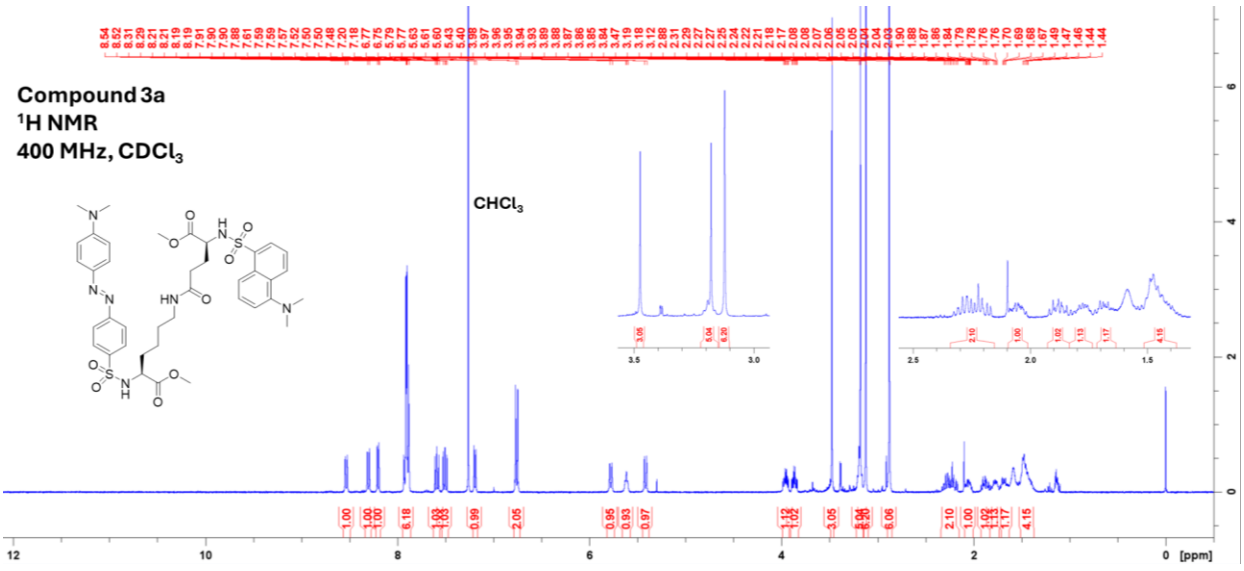

Figure A2.15. Compound **3a** – ^{1}H NMR, 400 MHz, $CDCl_3$

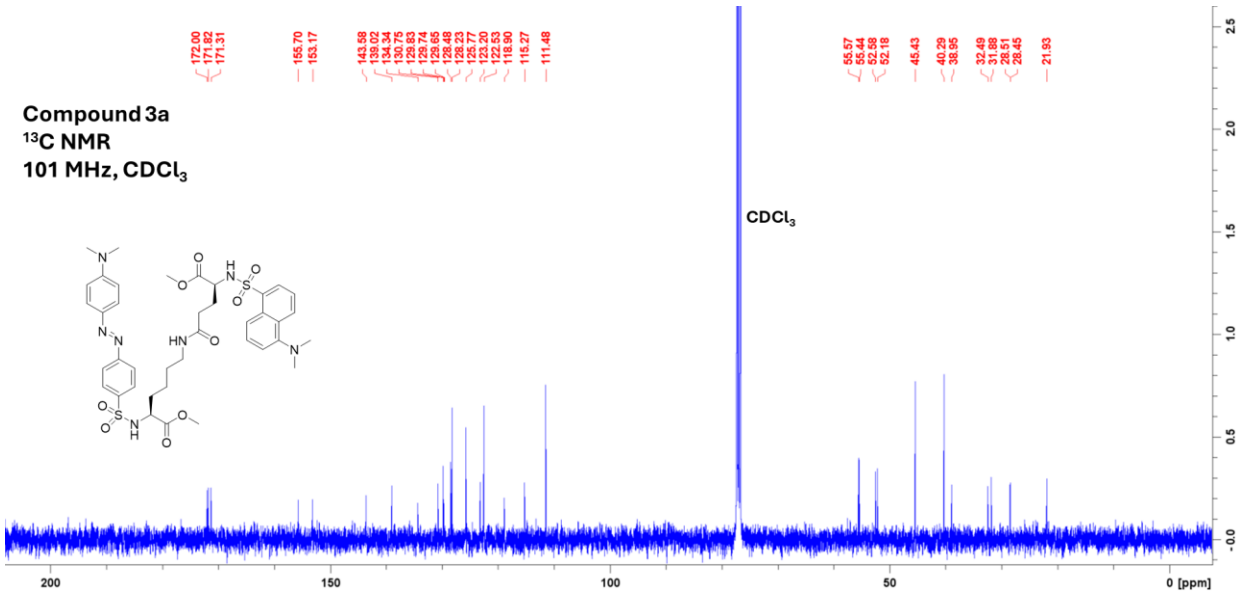

Figure A2.16. Compound **3a** – ^{13}C NMR, 101 MHz, $CDCl_3$

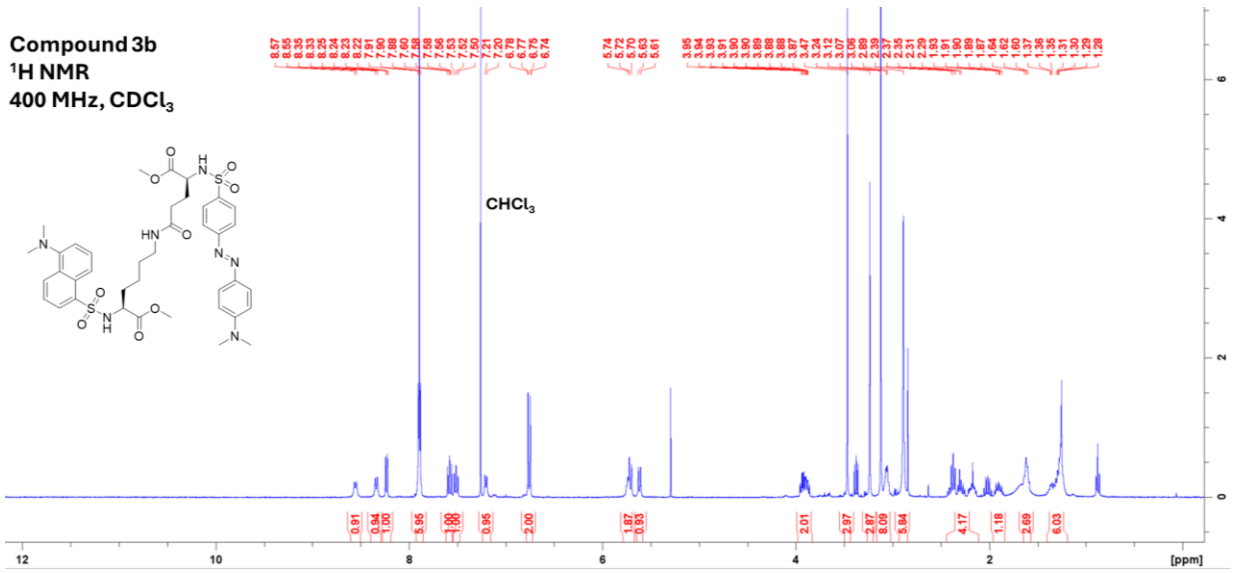

Figure A2.17. Compound **3b** – ^{1}H NMR, 400 MHz, $CDCl_3$

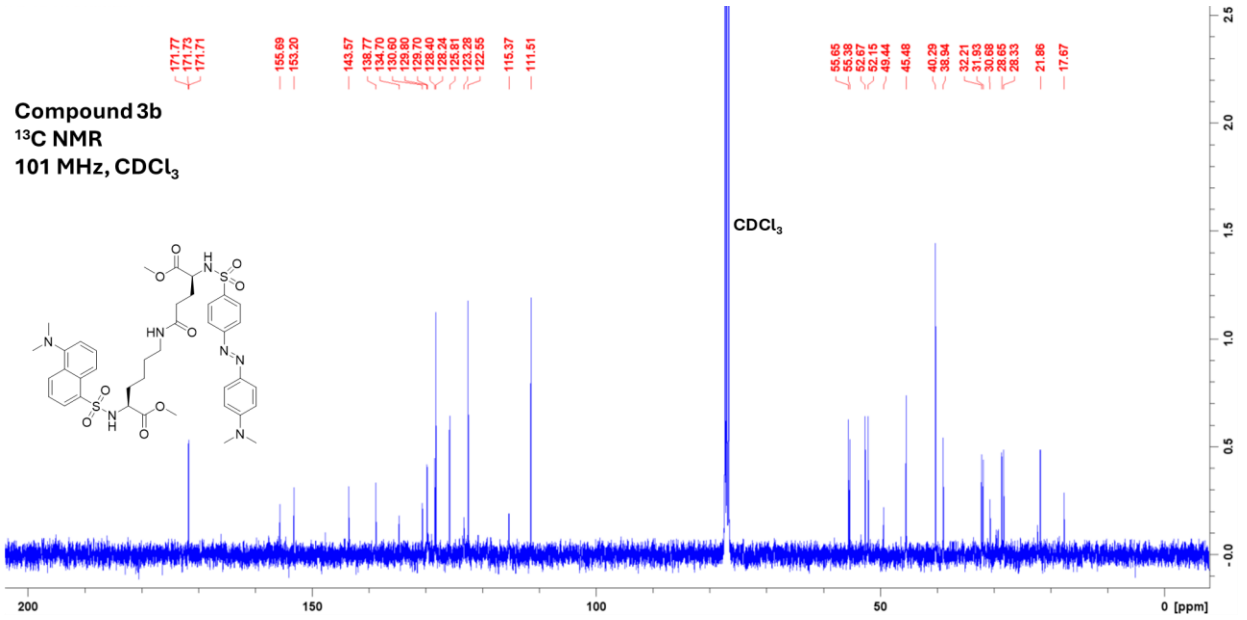

Figure A2.18. Compound **3b** – ^{13}C NMR, 101 MHz, $CDCl_3$

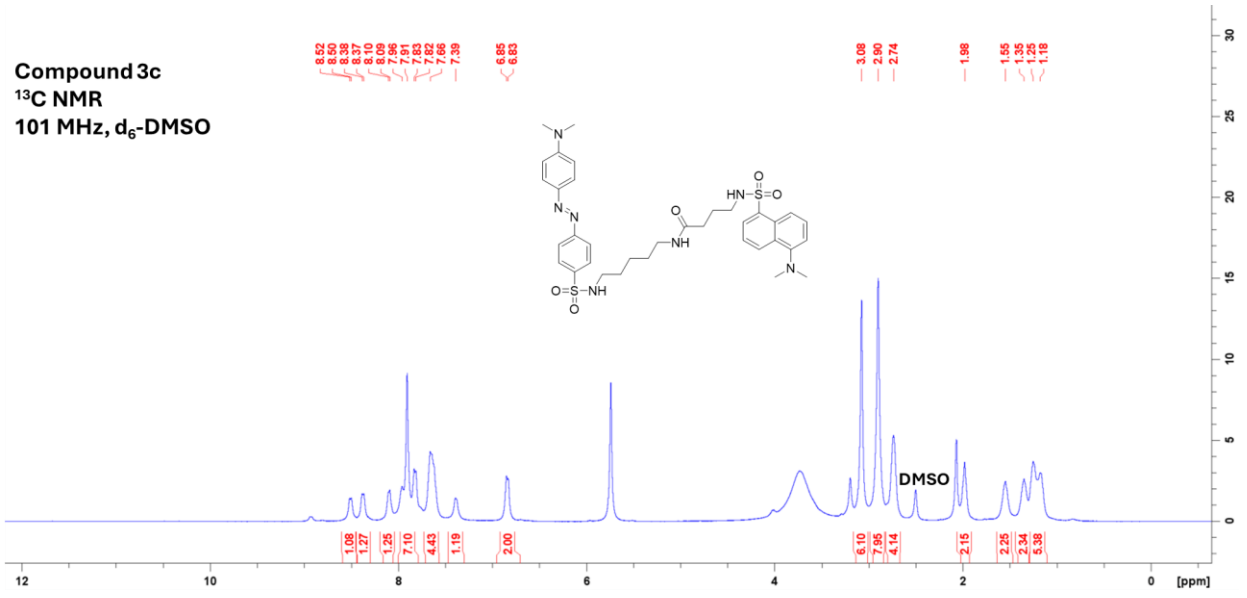

Figure A2.19. Compound **3c** – ^{1}H NMR, 400 MHz, $CDCl_3$

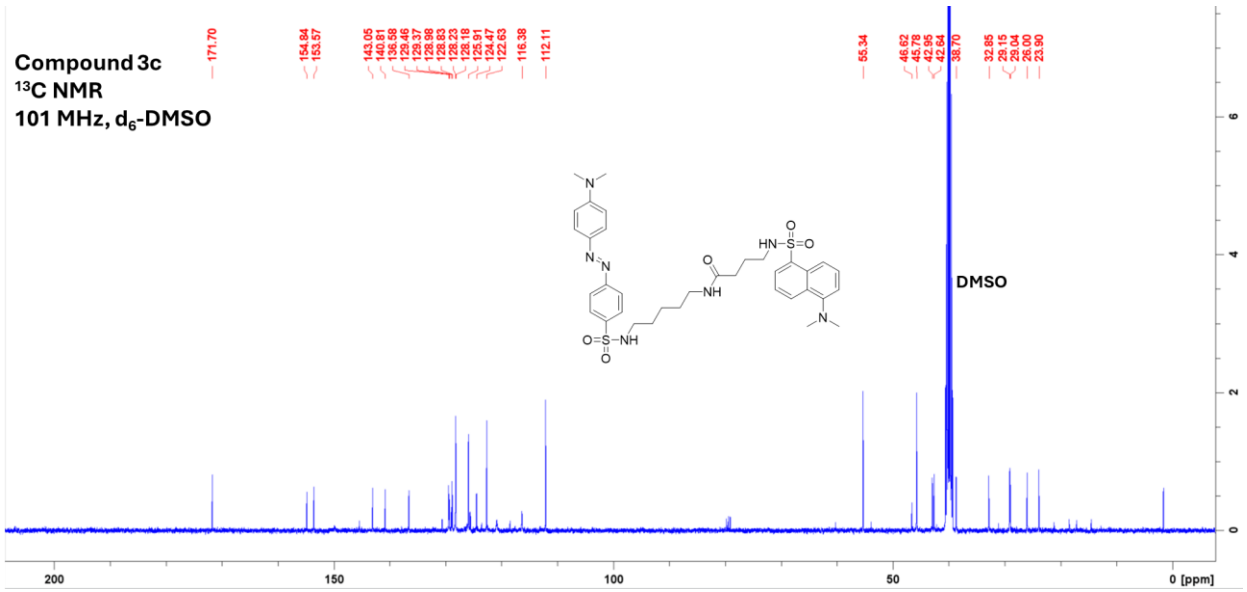

Figure A2.20. Compound **3c** – ^{13}C NMR, 101 MHz, $CDCl_3$

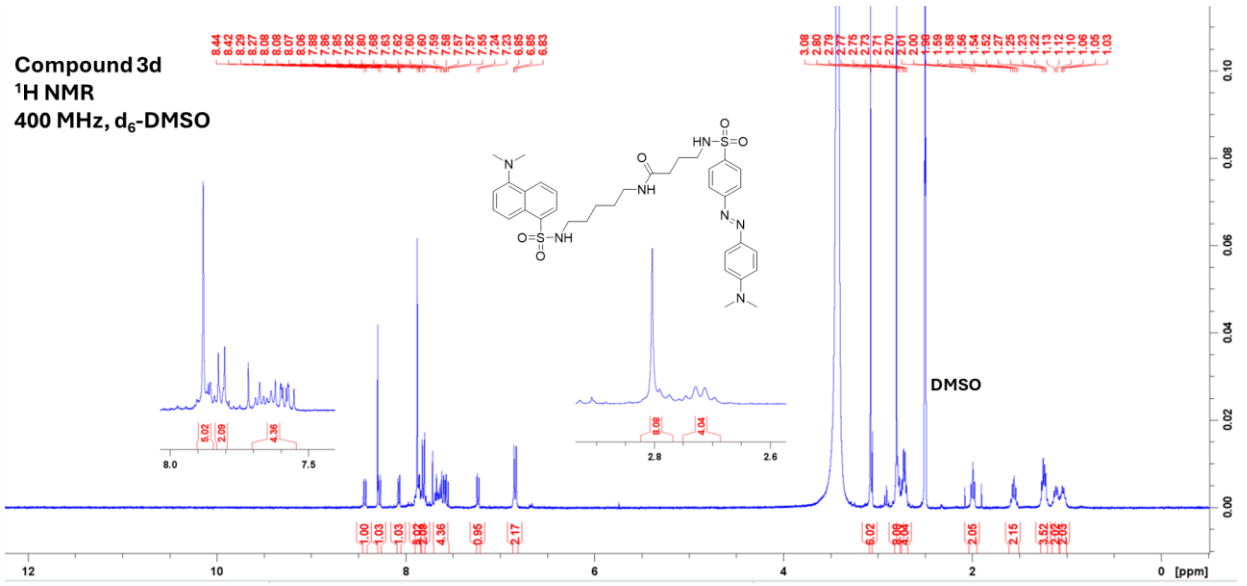

Figure A2.21. Compound **3d** – ^{1}H NMR, 400 MHz, $CDCl_3$

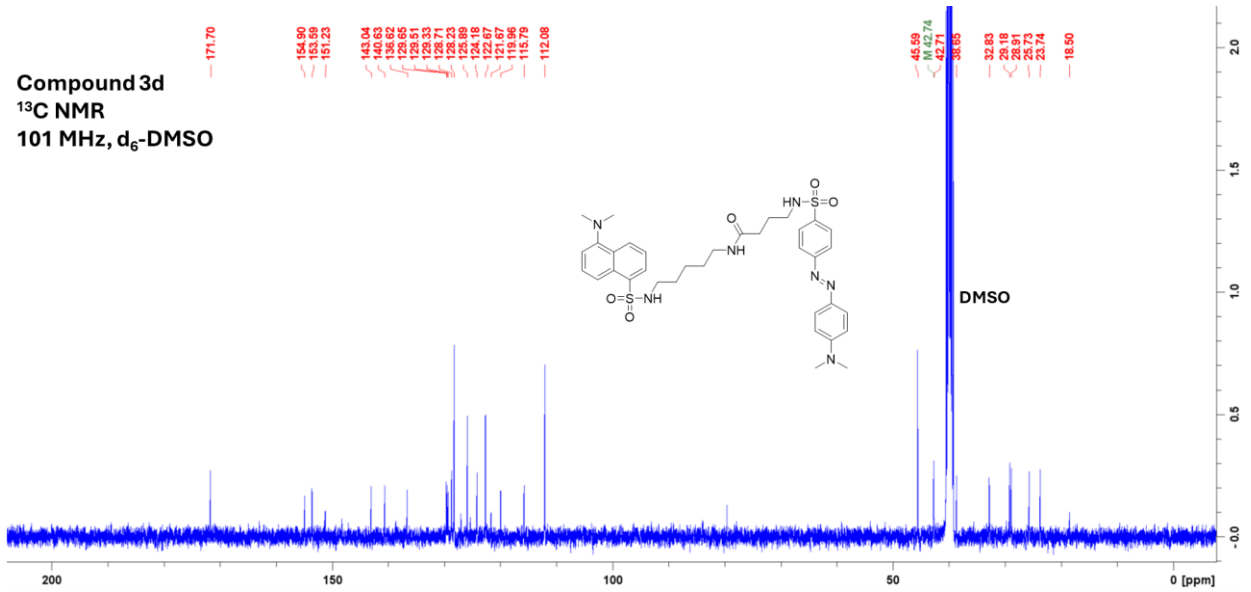

Figure A2.22. Compound **3d** – ^{13}C NMR, 101 MHz, $CDCl_3$

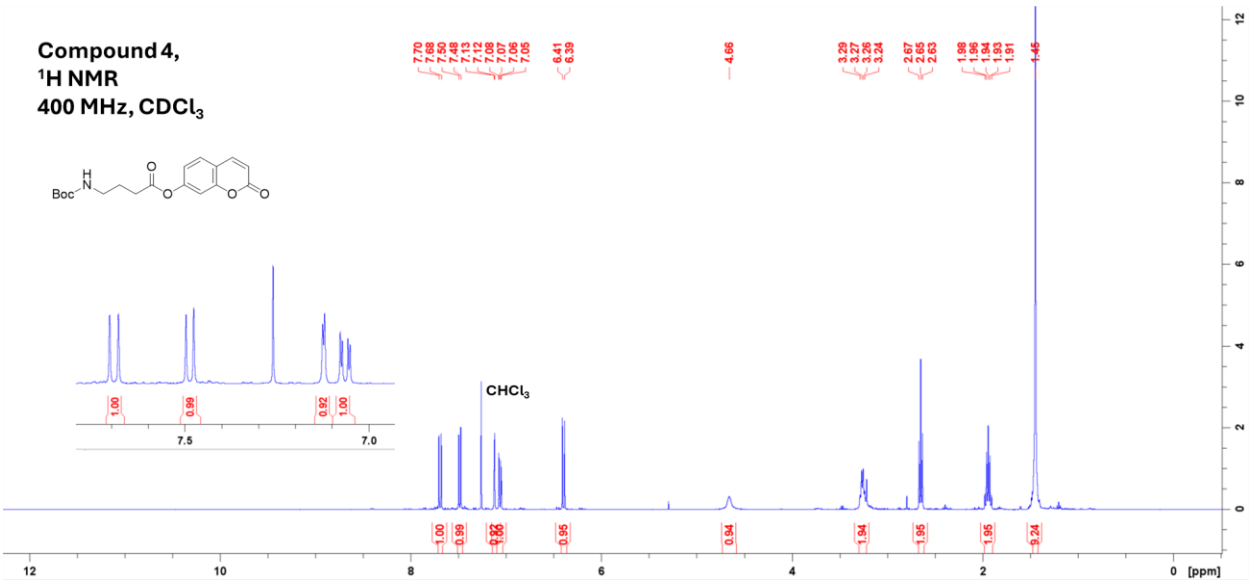

Figure A2.23. Compound **4** – ^{1}H NMR, 400 MHz, $CDCl_3$

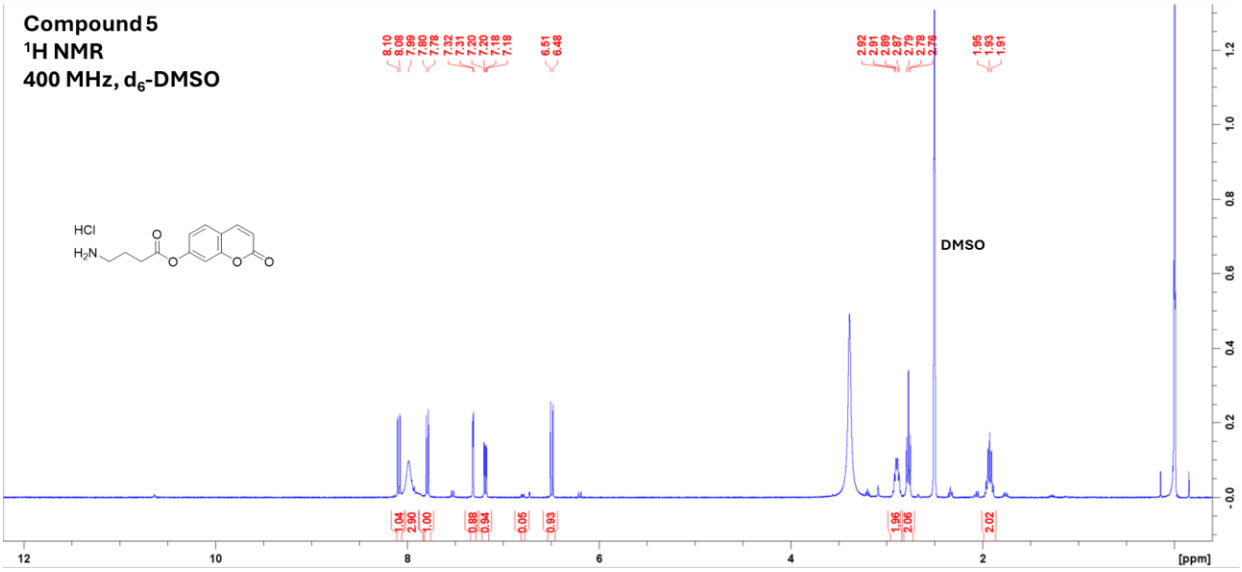

Figure A2.24. Compound **5** – ^{1}H NMR, 400 MHz, d_6-DMSO

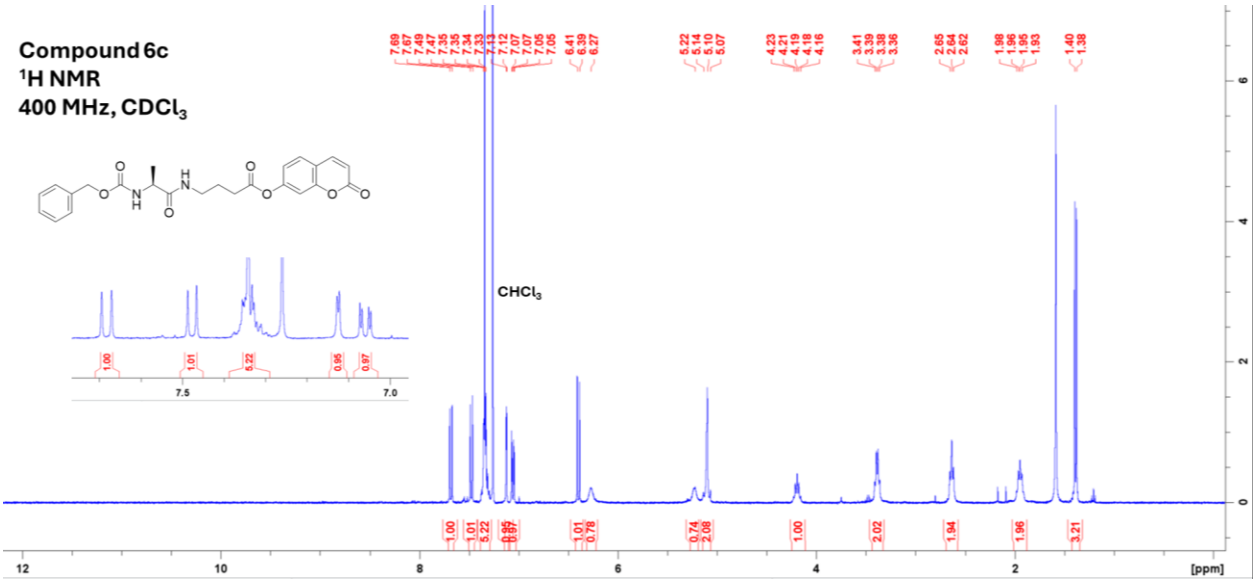

Figure A2.25. Compound **6c** – ^{1}H NMR, 400 MHz, $CDCl_3$

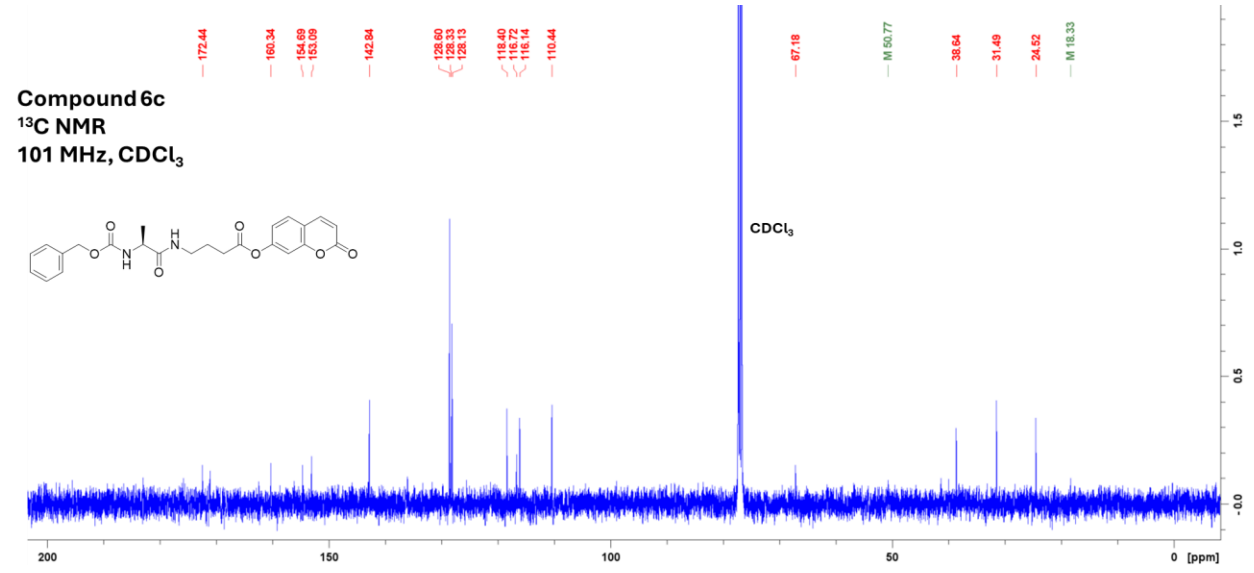

Figure A2.26. Compound **6c** – ^{13}C NMR, 101 MHz, $CDCl_3$

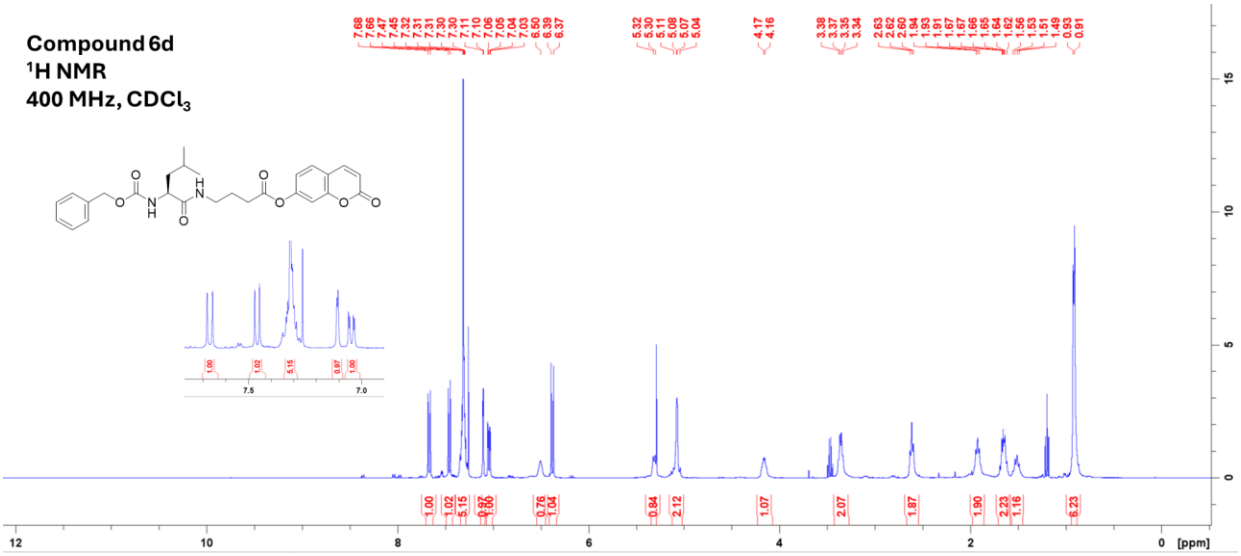

Figure A2.27. Compound **6d** – ^{1}H NMR, 400 MHz, $CDCl_3$

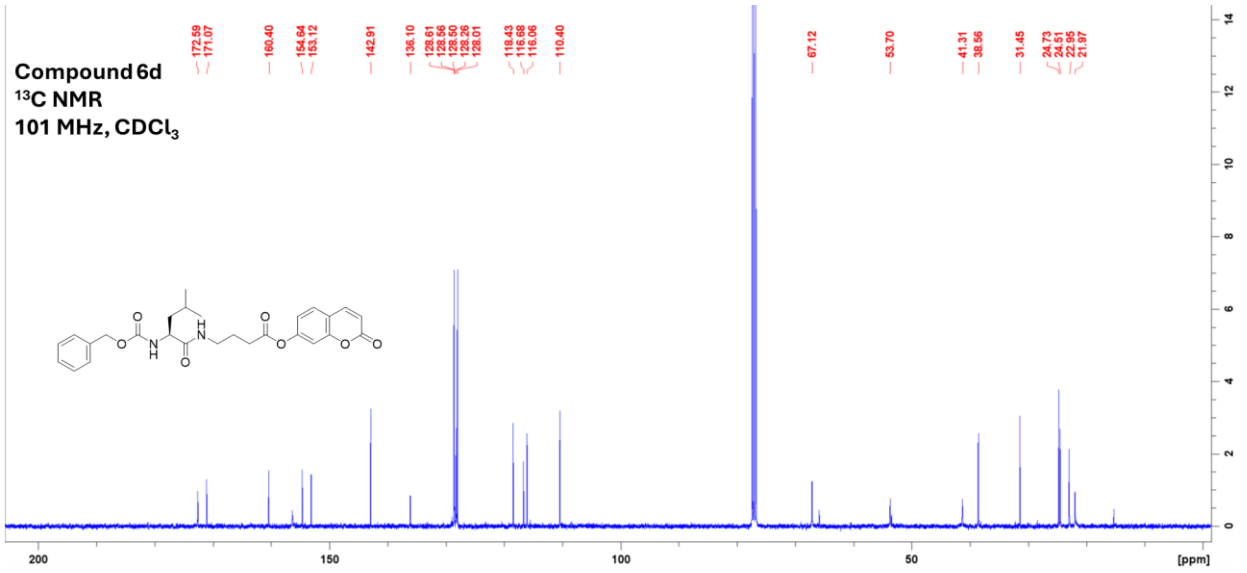

Figure A2.28. Compound **6d** – ^{13}C NMR, 101 MHz, $CDCl_3$

Appendix to Chapter 3

Table A3.1. k_{cat}/K_M data for all substrates screened (0-50 μM)

A3.1a) Aliphatic esters

Compound number	k_{cat}/K_M ($M^{-1}s^{-1}$) (Standard error)
7a	23.6 (1.5)
7b	41.5 (2.8)
7c	73.4 (2.9)
7d	130.2 (7.0)
7e	103.7 (14.3)

A3.1b) *N*-acetylated ω-amino esters

Compound number	k_{cat}/K_M ($M^{-1}s^{-1}$) (Standard error)
8a	29.2 (4.2)
8b	67.9 (2.1)
8c	220.9 (10.1)
8d	100.6 (0.8)
8e	97.6 (0.3)
8f	86.7 (3.2)
8g	84.9 (2.7)

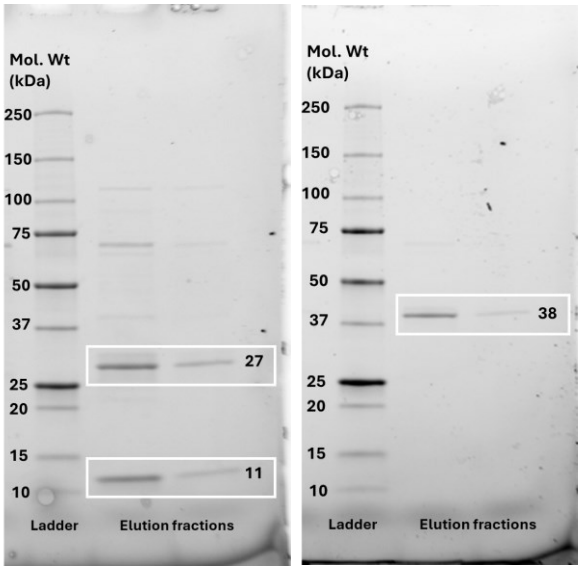

Figure A3.1. Left: elution fractions following Ni-affinity purification of $NylC_A$. Right: elution fractions following Ni-affinity purification of $NylC_A^{T276A}$. Protein standard ladder (Bio-Rad) ranges from 10-250 kDa.

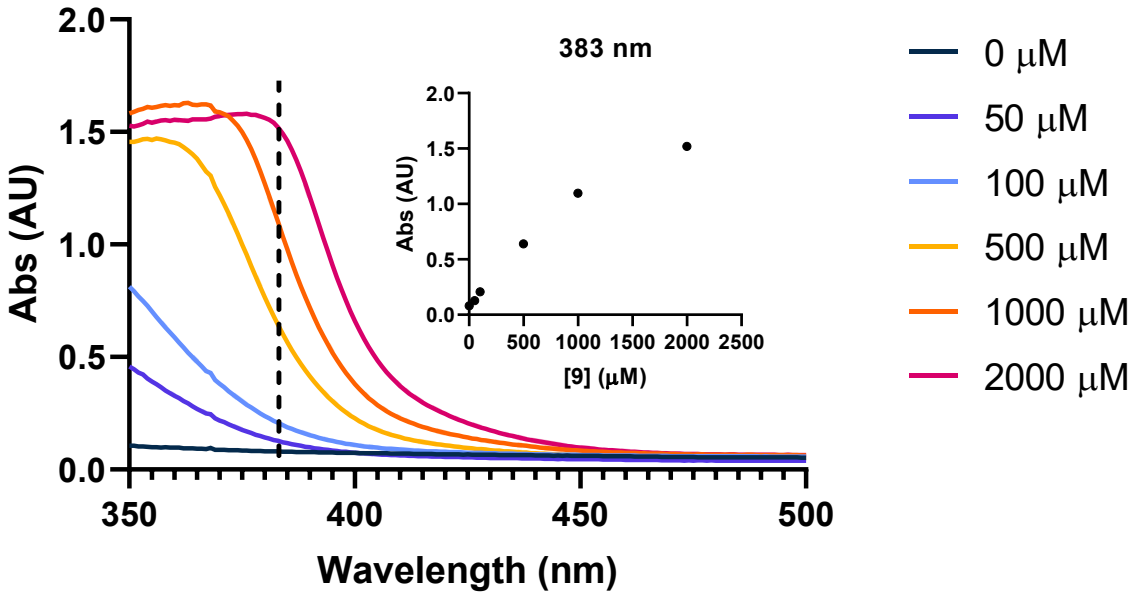

Figure A3.2 Absorbance spectra of **9** at varying concentrations**.** The absorbance was measured in the presence of 100 mM Tris buffer (pH 6.9) and 10% v/v DMSO. The vertical dashed line indicates 383 nm. Inset: the absorbance at 383 nm was plotted against concentration of **9**, demonstrating that absorbance is nonlinear with respect to concentration at concentrations higher than ~ 1000 μM of **9**.

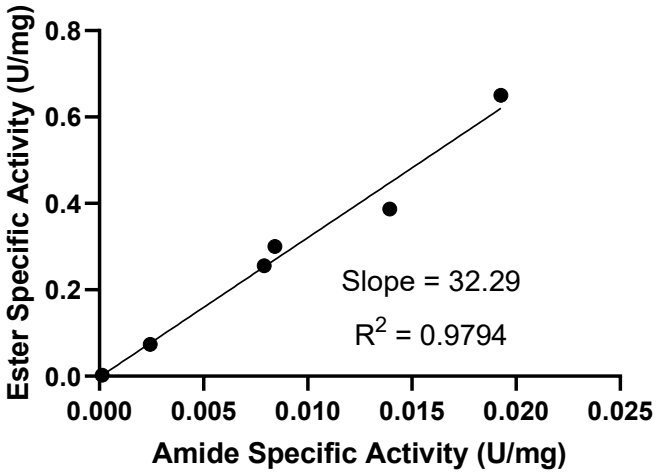

Figure A3.3. Hydrolysis activity of NylC towards ester substrate **8c** plotted against activity towards amide substrate **9**. Each datapoint represents activity demonstrated by a unique batch of enzyme. Values are reported as specific activity in units of substrate turned over per mg of enzyme (U/mg), and are averages of two replicates. Error bars are shown in both x- and y-dimensions, but are smaller than the corresponding data symbols.

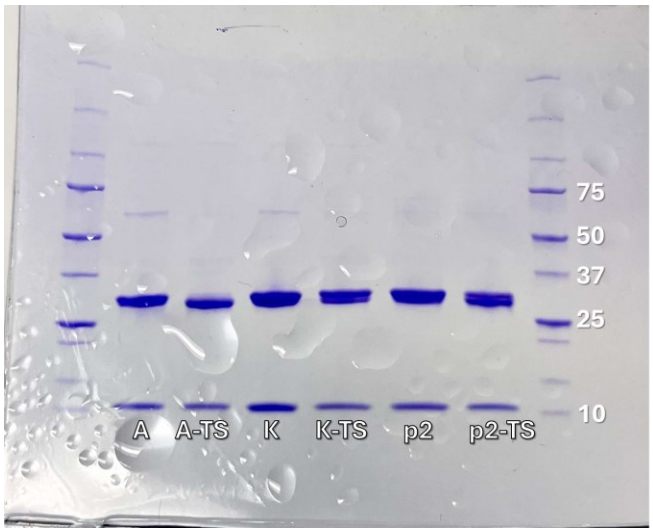

Figure A3.4. SDS-PAGE of NylC enzymes following overnight incubation at 37 °C, indicating full autoprocessing into two fragments (no visible band at 37 kDa indicating inactive protein).

Table A3.2. Sequences of primers used for site-directed mutagenesis by full-plasmid PCR

Primer	**Sequence**
pAR2-1-T267A-fwd	5′ – GCGACAATTAGCGCCATTGTTAC – 3′
pAR2-1-T267mut-fwd	5′ – ATTACCTGCTTCGGTAACCG – 3′

Table A3.3. Plasmids acquired from AddGene for the expression of NylC variants.

Enzyme	Plasmid Name	Addgene ID
NylC$_A$	NylCA_pET28a	215418
NylC$_A$-TS	NylCA-TS_pET28a	215419
NylC$_{p2}$	NylCp2_pET28a	215420
NylC$_{p2}$-TS	NylCp2-TS_pET28a	215421
NylC$_K$	NylCK_pET28a	215422
NylC$_K$-TS	NylCK-TS_pET28a	215423

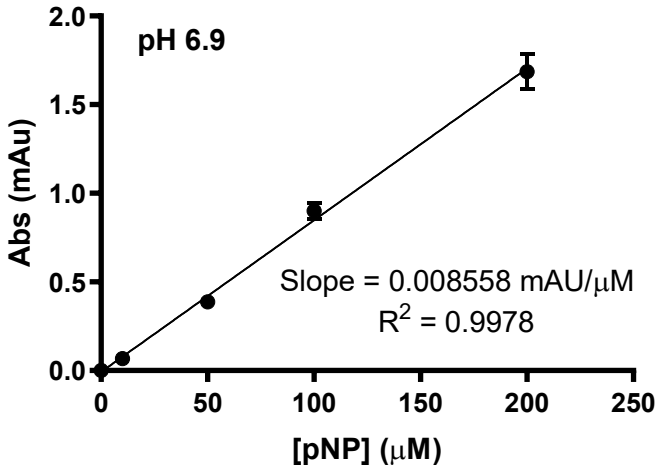

Figure A3.5. Standard curve of *p*-nitrophenol at 399 nm at pH 6.9. The absorbance of *p*-nitrophenol (pNP) was measured at pH 6.9 over a range of concentrations. All measurements were done in duplicate and the error bars represent the standard deviation between the replicates.

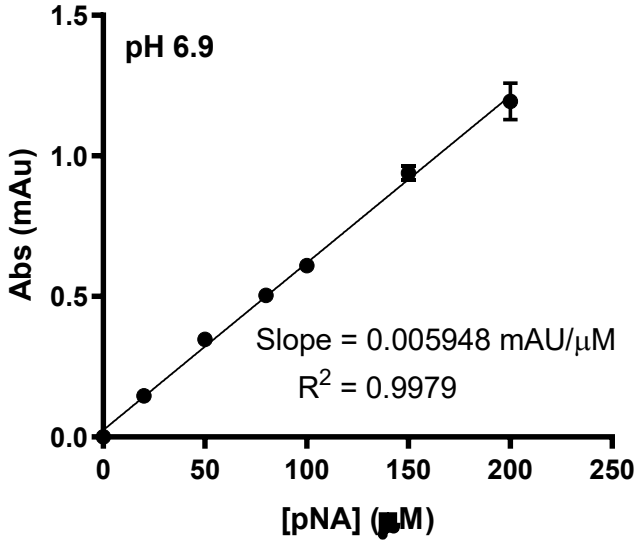

Figure A3.6. Standard curve of *p*-nitroaniline at 383 nm at pH 6.9. The absorbance of *p*-nitroaniline (pNA) at various concentrations was measured. All measurements were done in duplicate, and the error bars represent the standard deviation between the replicates.

Characterization data

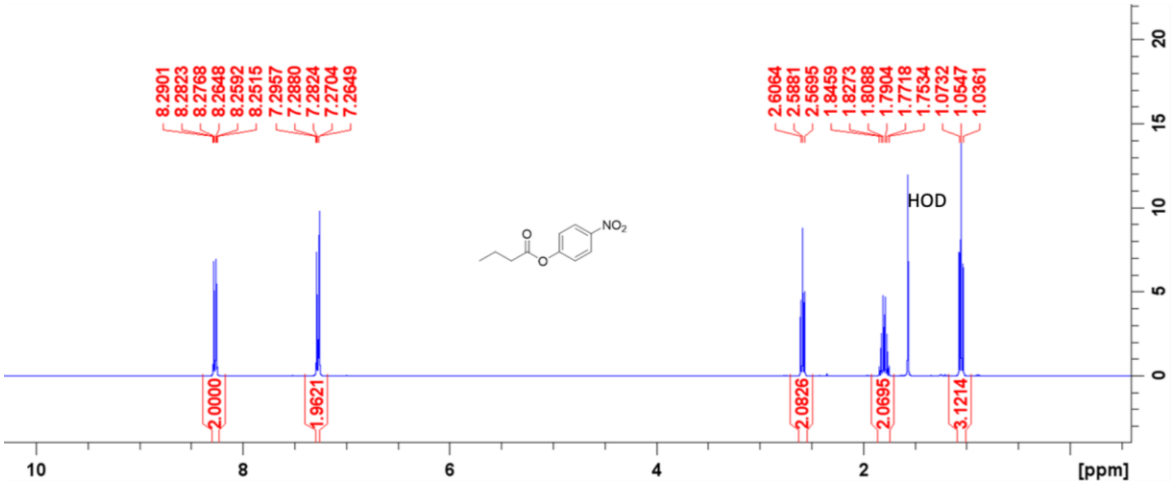

^{1}H NMR spectrum (400 MHz, $CDCl_3$) of 7a.

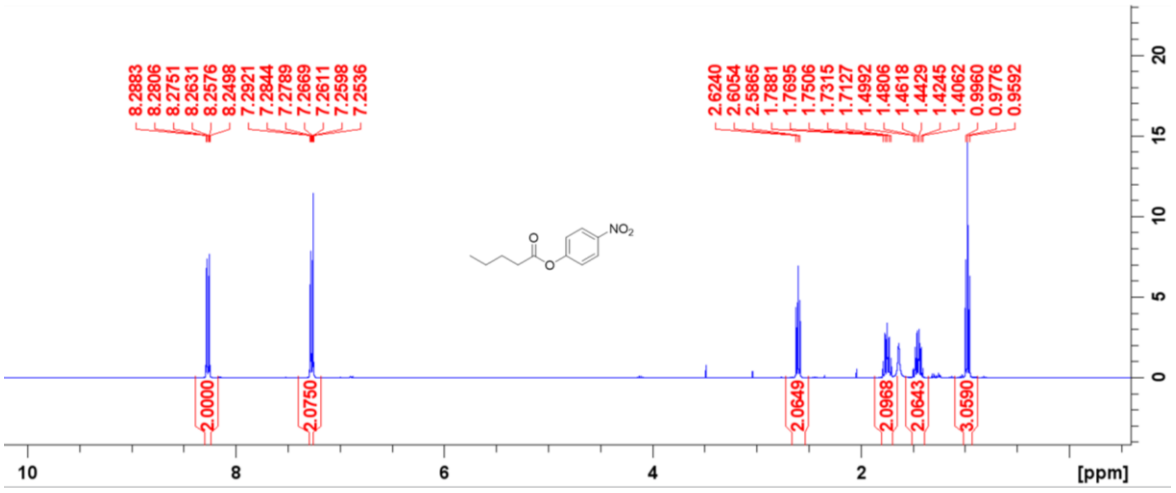

^{1}H NMR spectrum (400 MHz, $CDCl_3$) of 7b.

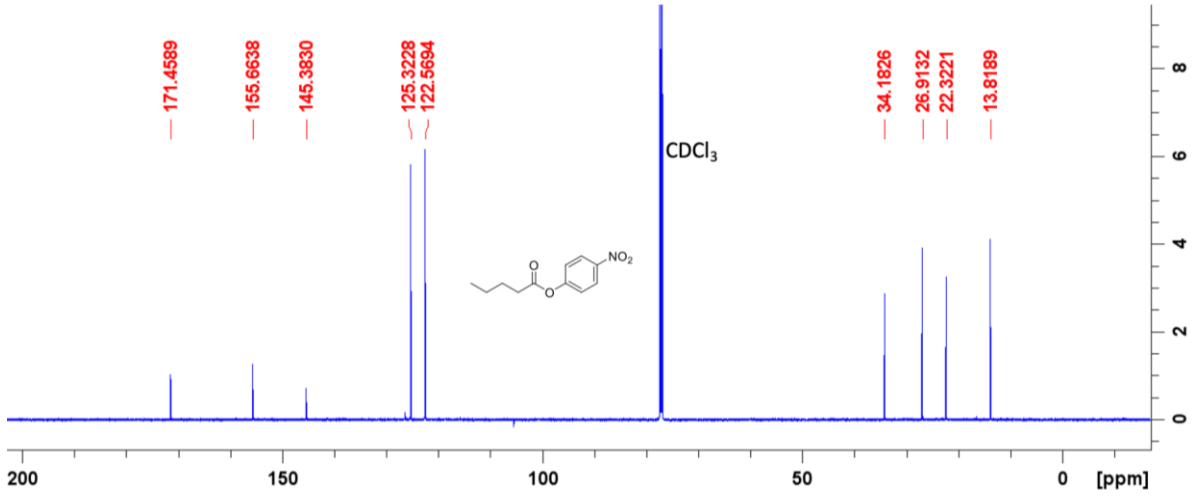

^{13}C NMR spectrum (151 MHz, $CDCl_3$) of 7b.

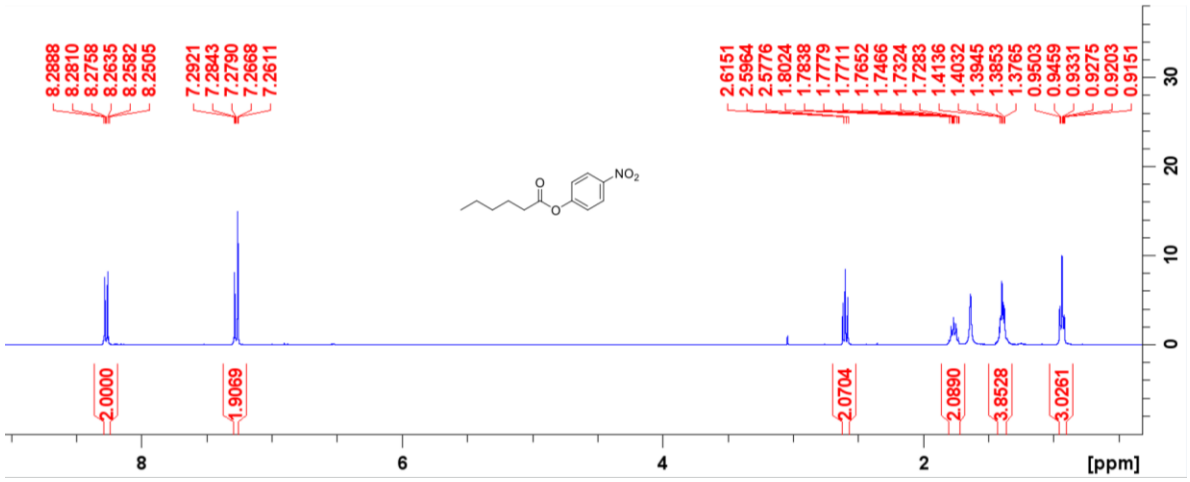

^{1}H NMR spectrum (400 MHz, $CDCl_3$) of 7c.

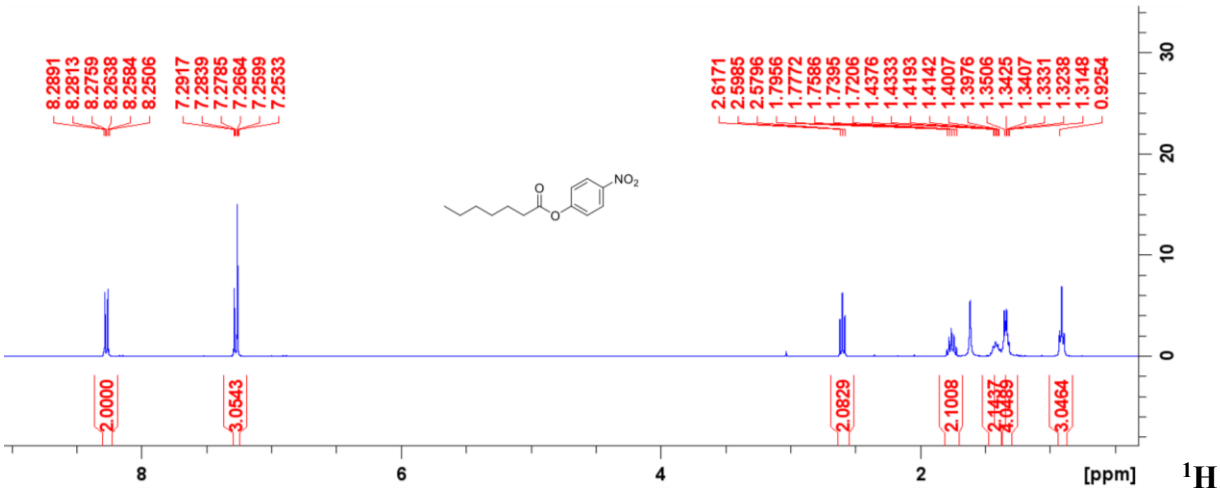

NMR spectrum (400 MHz, $CDCl_3$) of 7d.

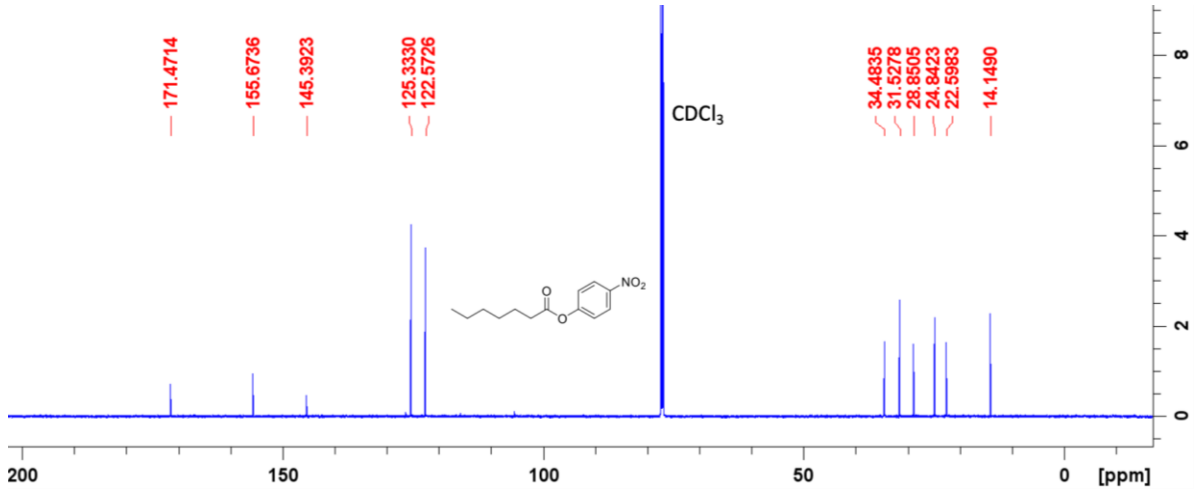

^{13}C NMR spectrum (151 MHz, $CDCl_3$) of 7d.

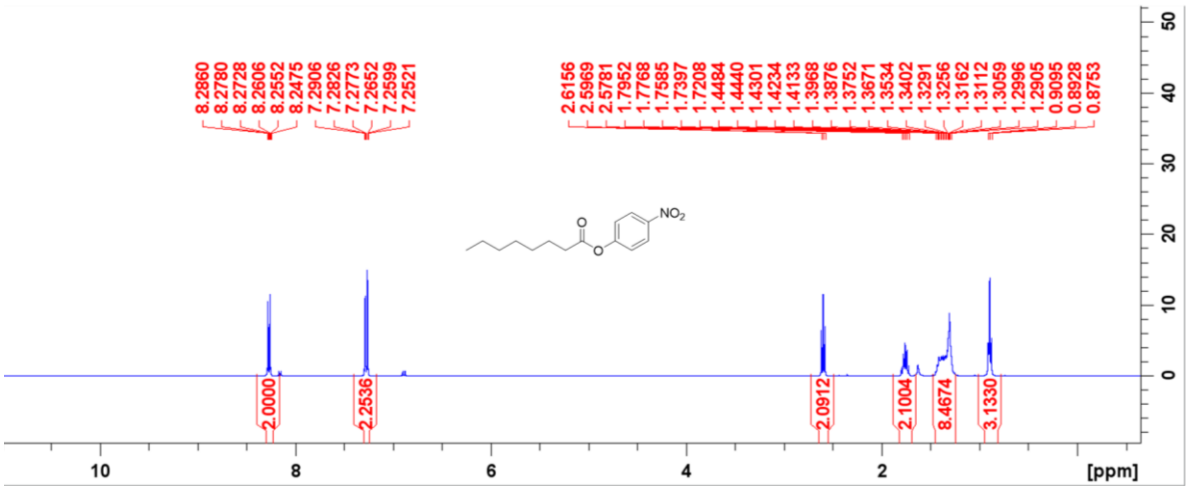

^{1}H NMR spectrum (400 MHz, $CDCl_3$) of 7e.

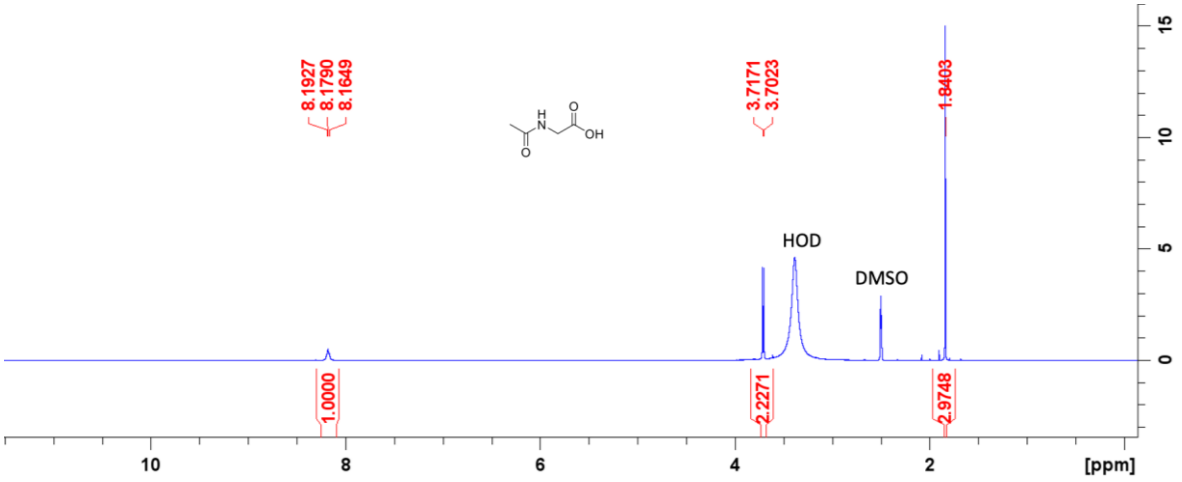

^{1}H NMR spectrum (400 MHz, DMSO-d_6) of 10a.

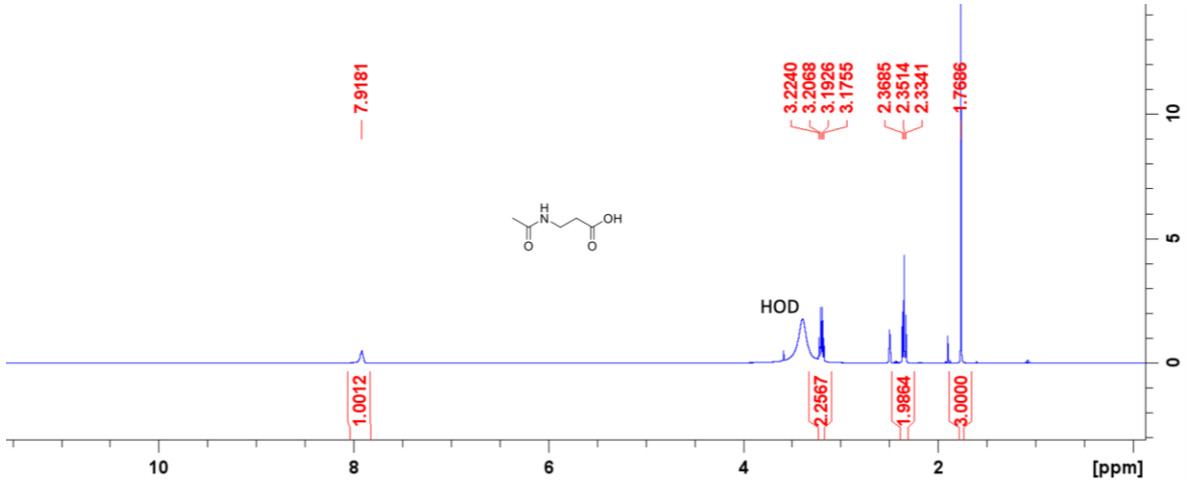

^{1}H NMR spectrum (400 MHz, DMSO-d$_6$) of 10b.

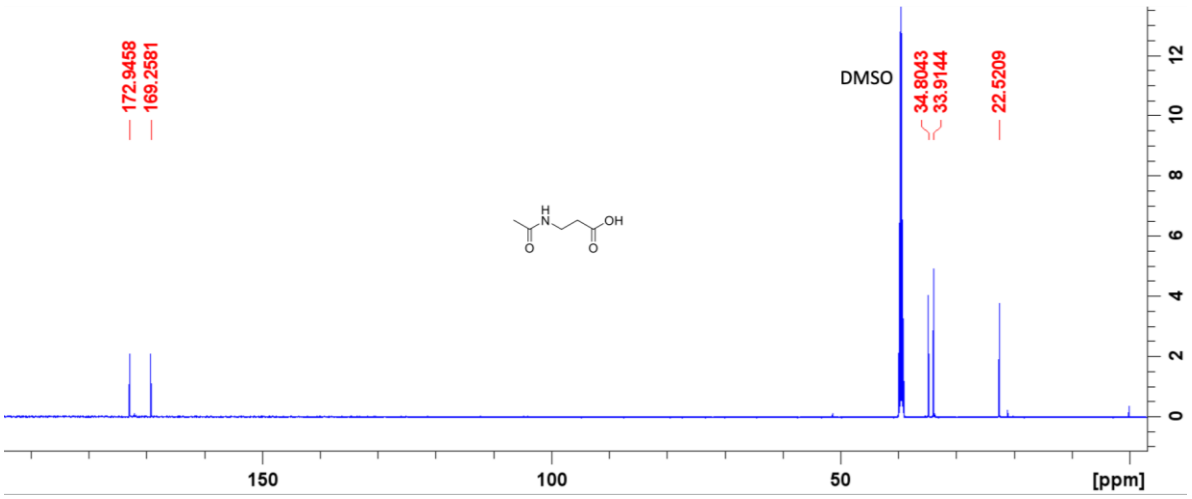

^{13}C NMR spectrum (151 MHz, DMSO-d$_6$) of 10b.

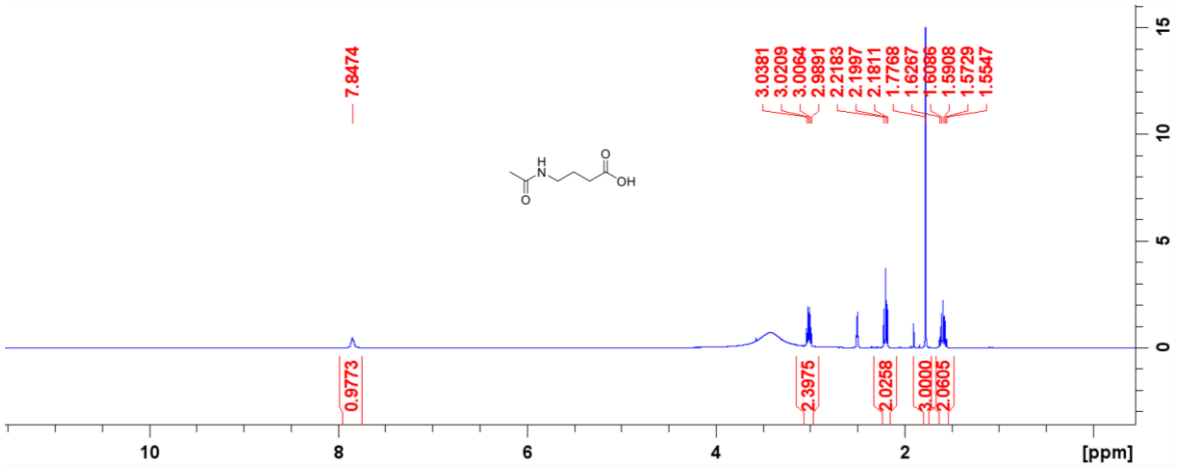

^{1}H NMR spectrum (400 MHz, DMSO-d$_6$) of 10c.

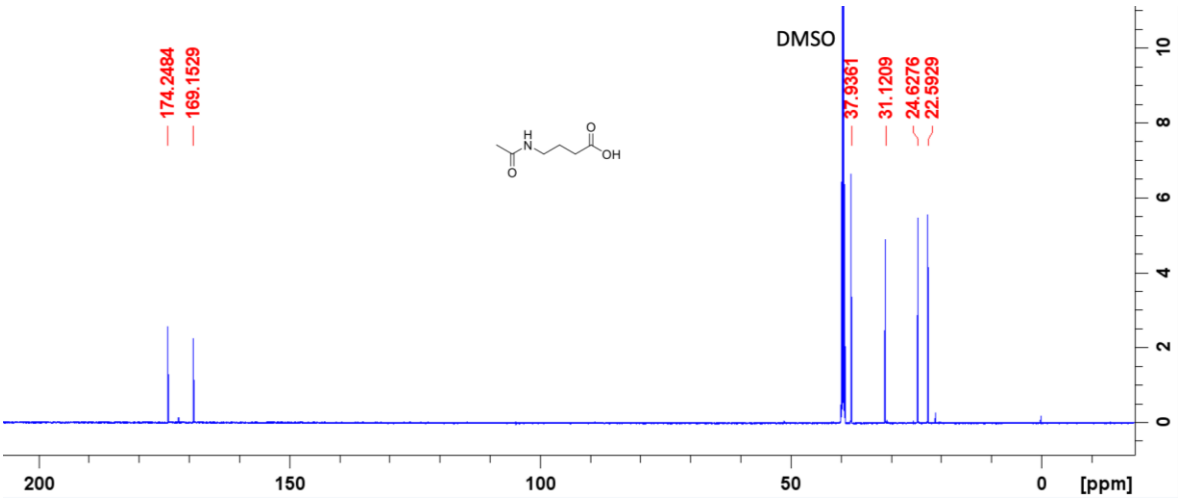

^{13}C NMR spectrum (151 MHz, DMSO-d$_6$) of 10c.

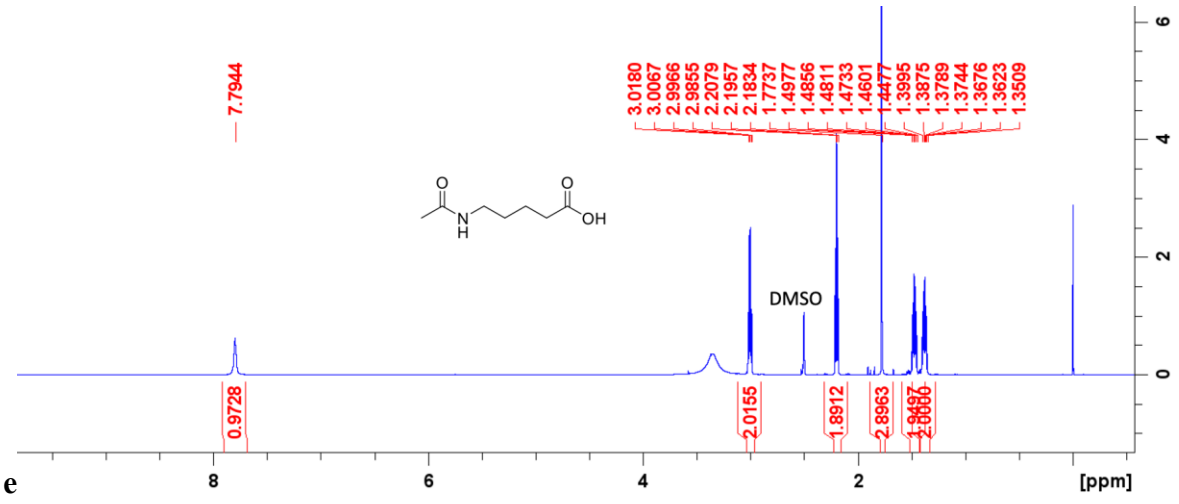

e

[1]H NMR spectrum (600 MHz, DMSO-d6) of 10d.

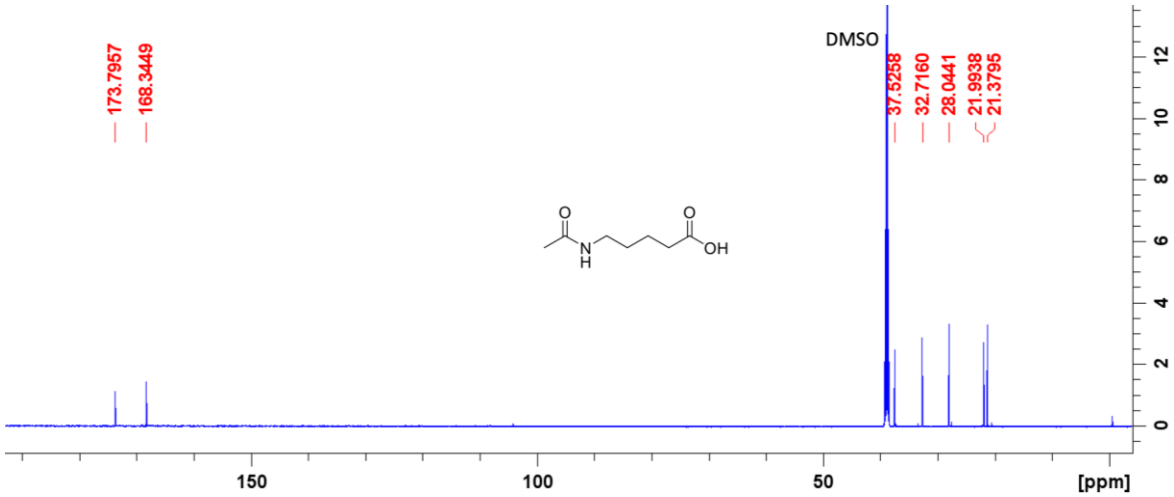

[13]C NMR spectrum (151 MHz, DMSO-d6) of 10d.

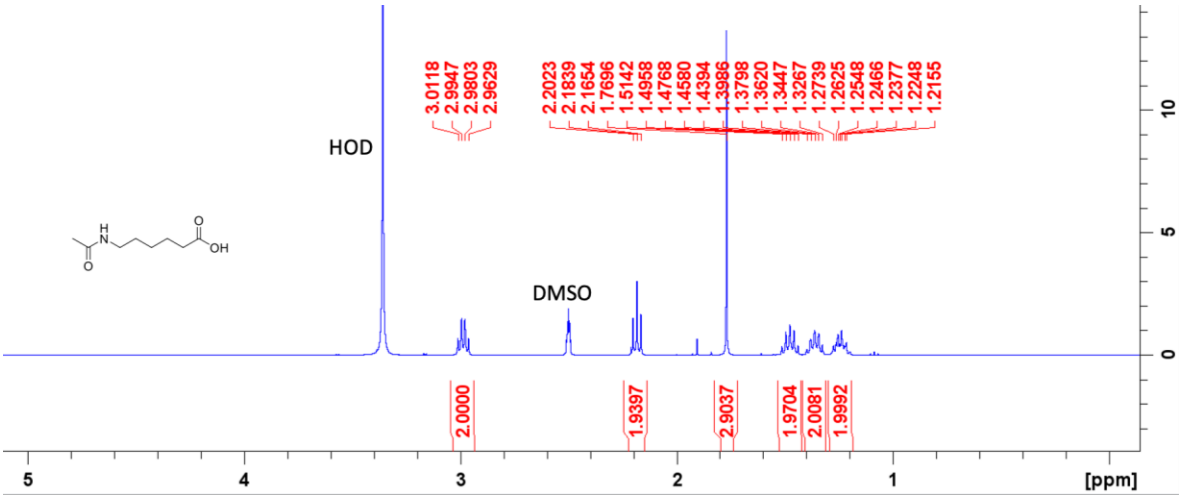

^{1}H NMR spectrum (400 MHz, DMSO-d_6) of 10e.

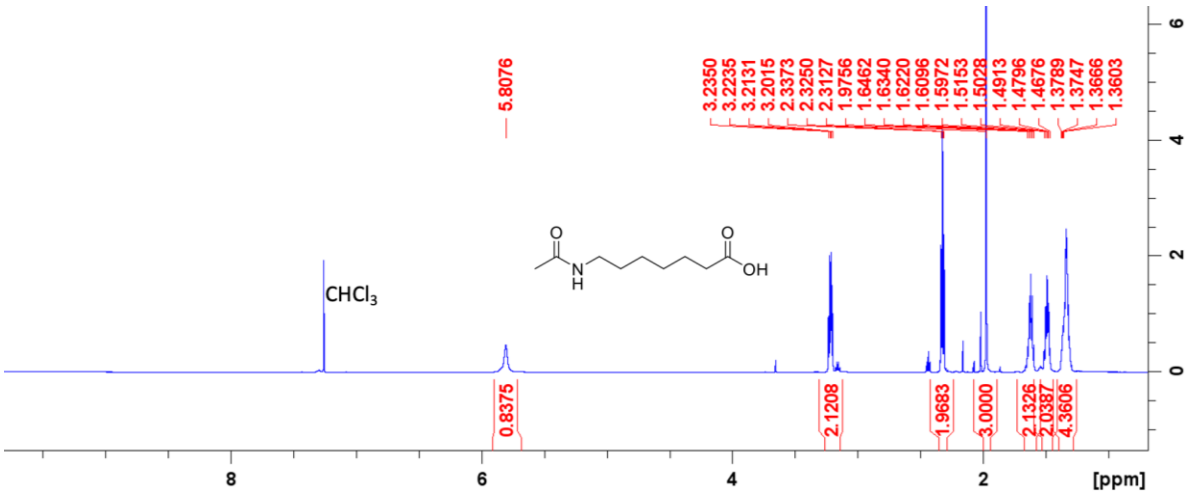

[1]H NMR spectrum (600 MHz, $CDCl_3$) of 10f.

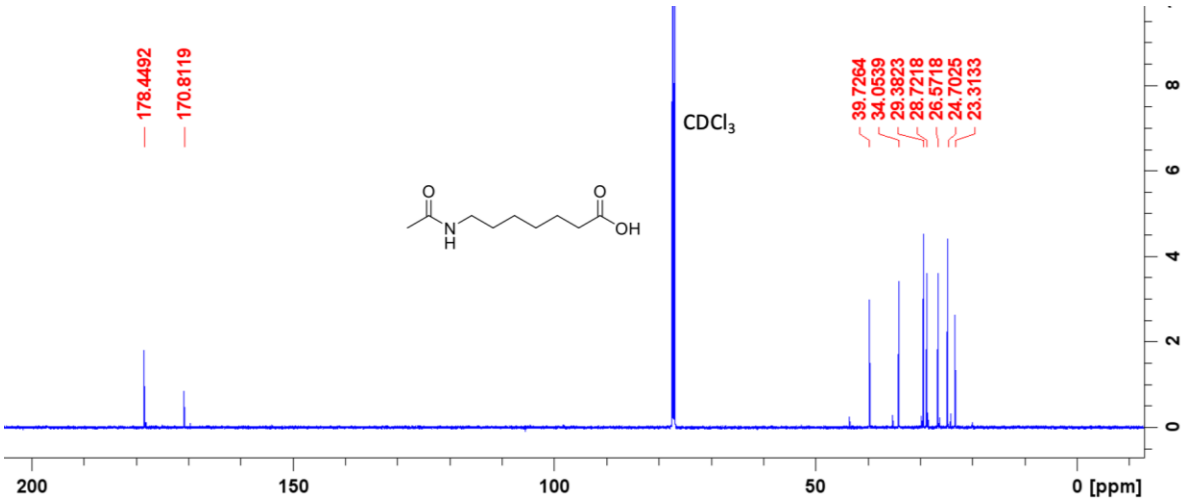

[13]C NMR spectrum (151 MHz, $CDCl_3$) of 10f.

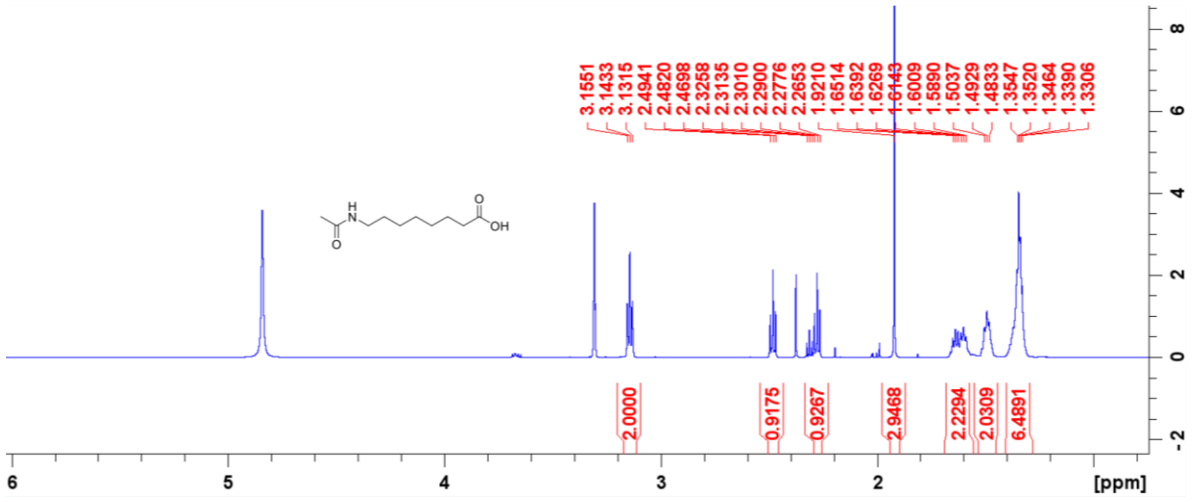

^{1}H NMR spectrum (600 MHz, CD_3OD) of 10g.

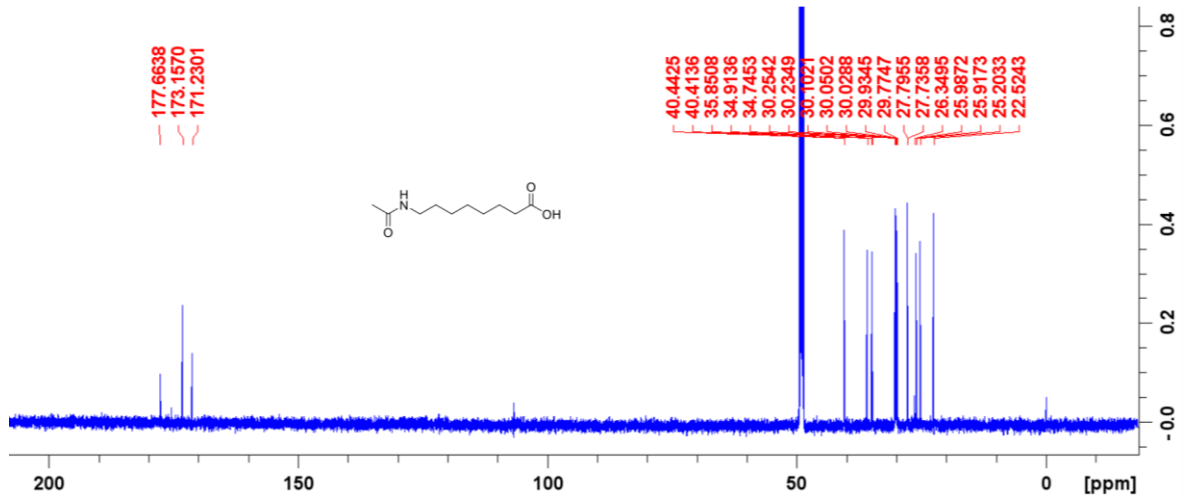

^{13}C NMR spectrum (151 MHz, CD_3OD) of 10g.

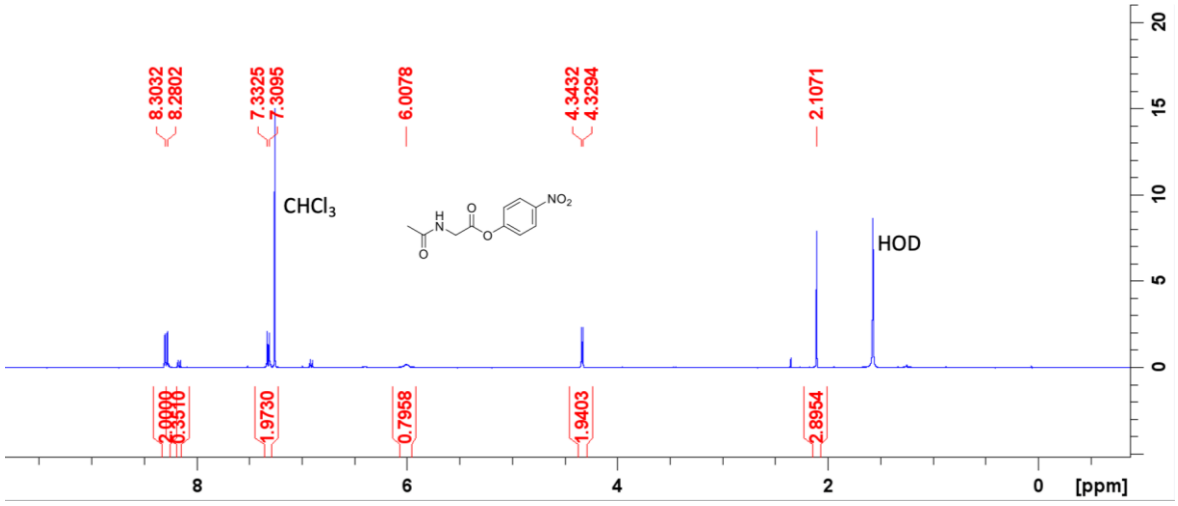

^{1}H NMR spectrum (400 MHz, $CDCl_3$) of 8a.

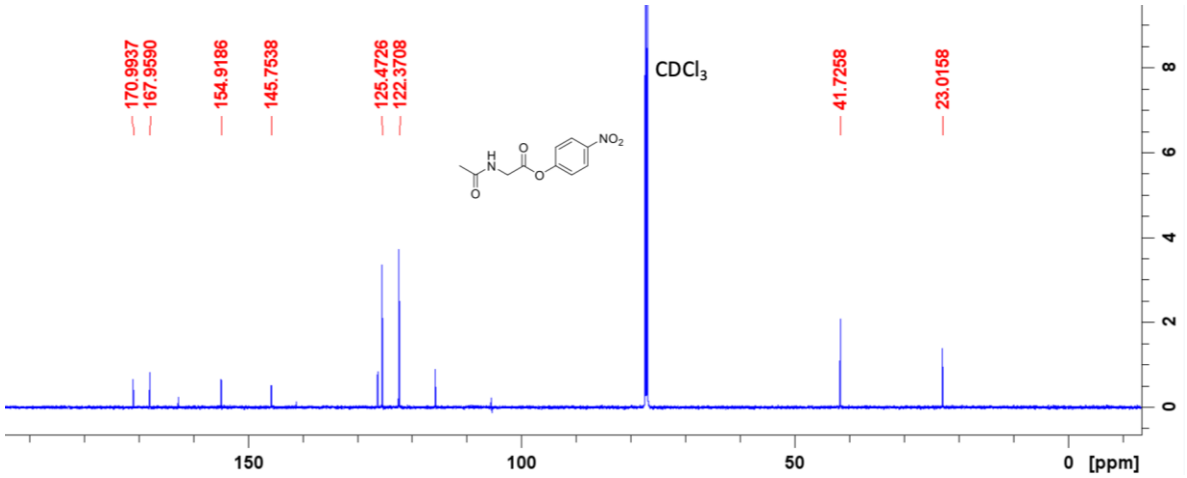

^{13}C NMR spectrum (151 MHz, $CDCl_3$) of 8a.

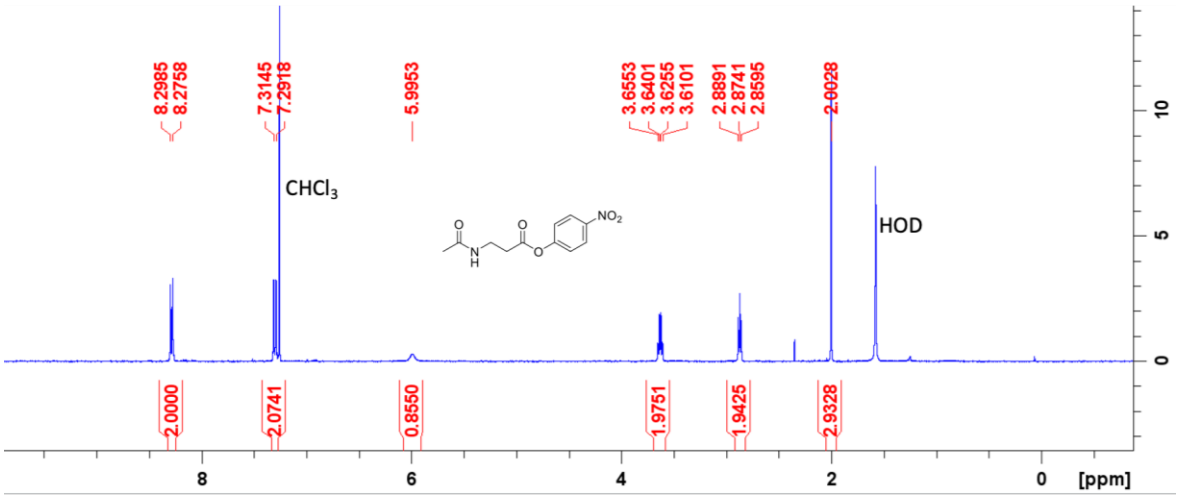

^{1}H NMR spectrum (400 MHz, $CDCl_3$) of 8b.

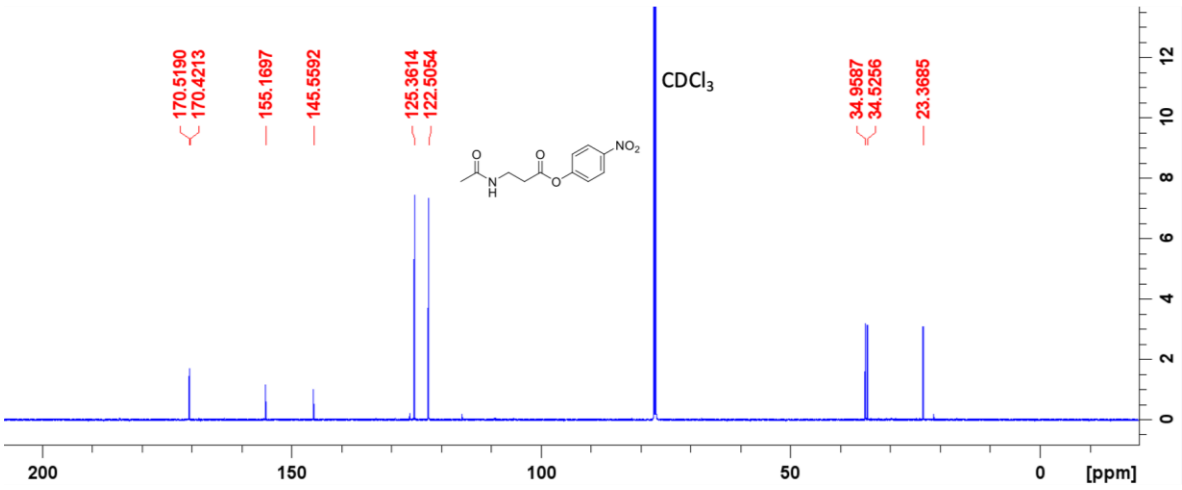

^{13}C NMR spectrum (151 MHz, $CDCl_3$) of 8b.

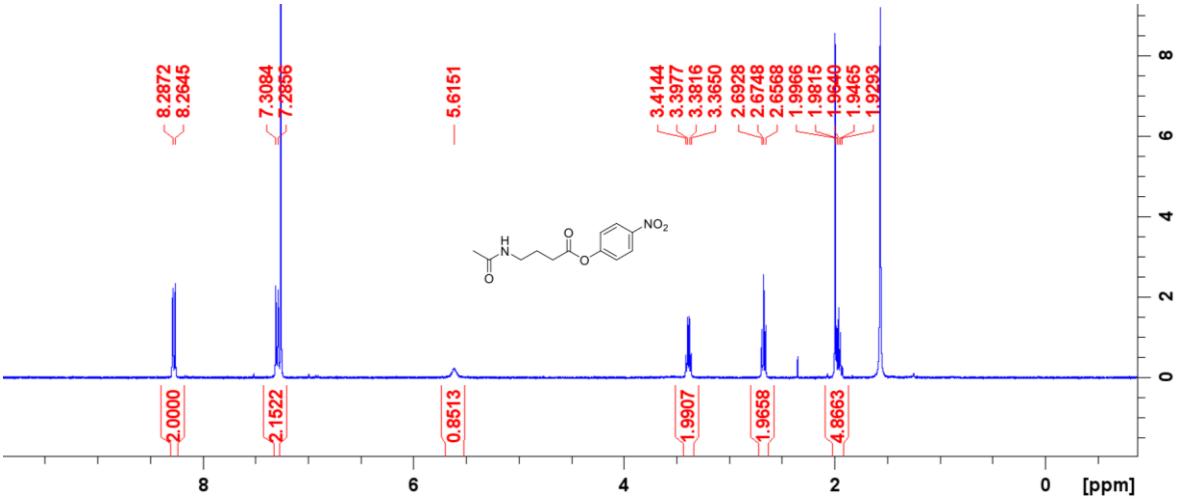

^{1}H NMR spectrum (400 MHz, $CDCl_3$) of 8c.

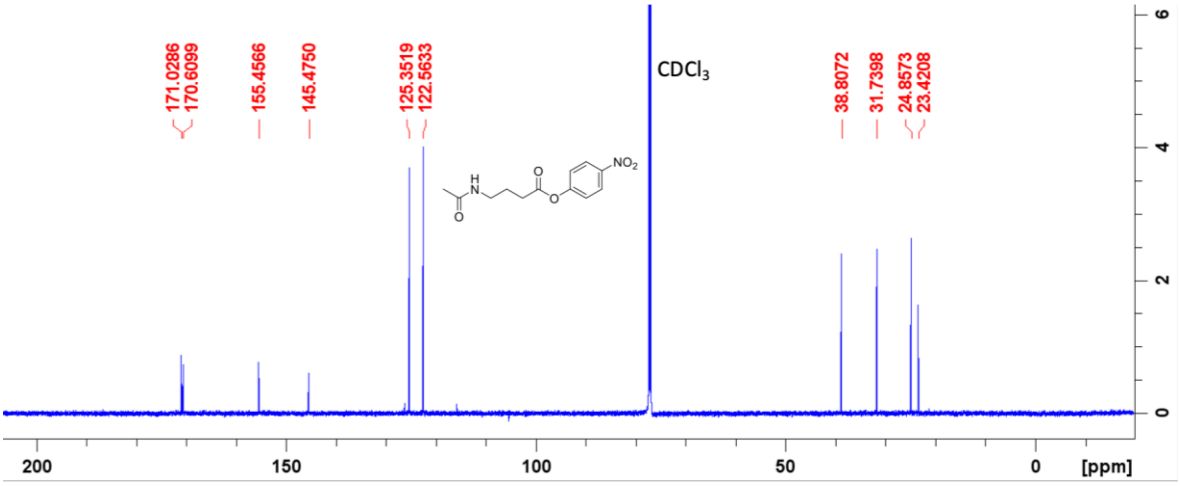

^{13}C NMR spectrum (151 MHz, $CDCl_3$) of 8c.

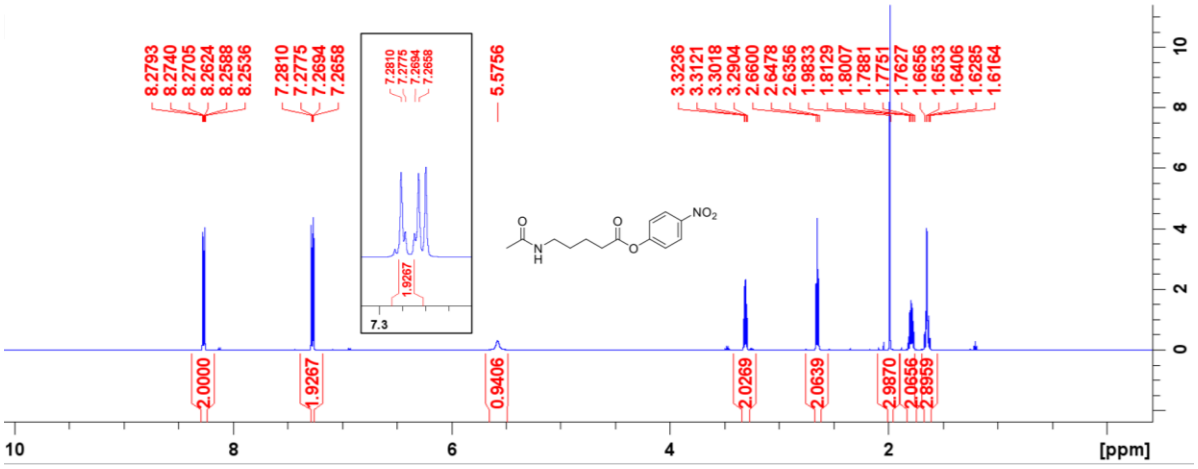

^{1}H NMR spectrum (600 MHz, $CDCl_3$) of 8d.

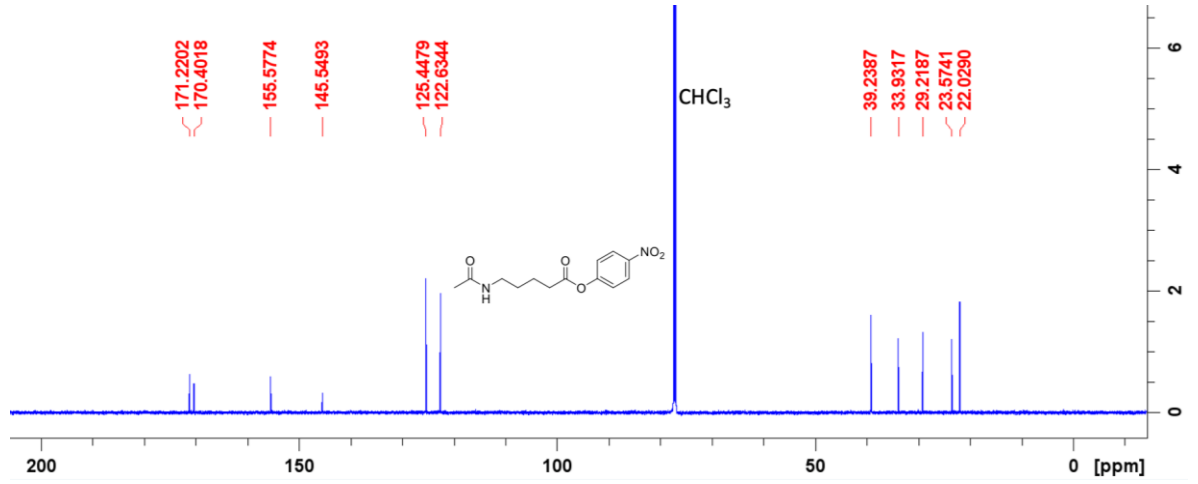

^{13}C NMR spectrum (151 MHz, $CDCl_3$) of 8d.

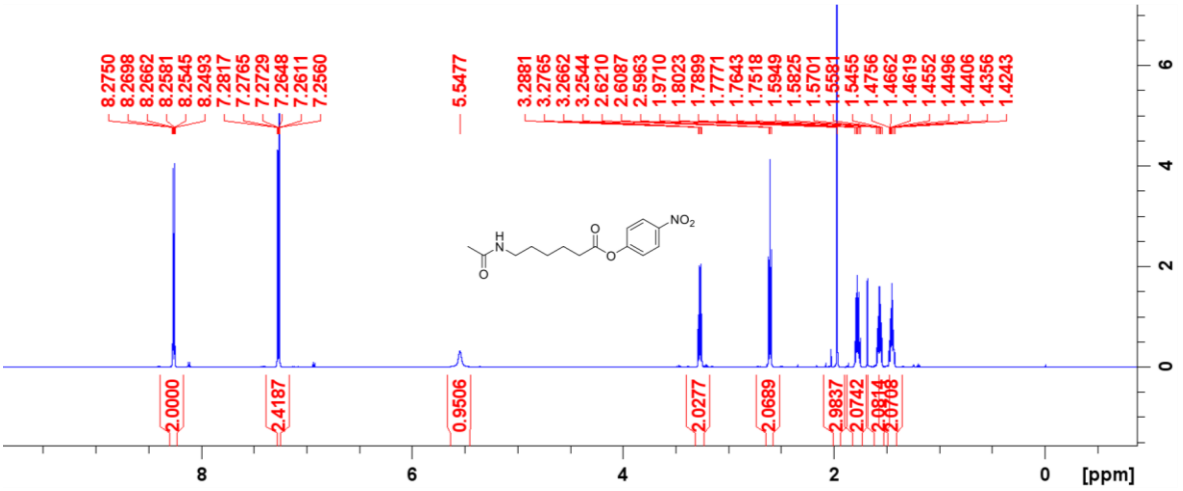

^{1}H NMR spectrum (600 MHz, $CDCl_3$) of 8e.

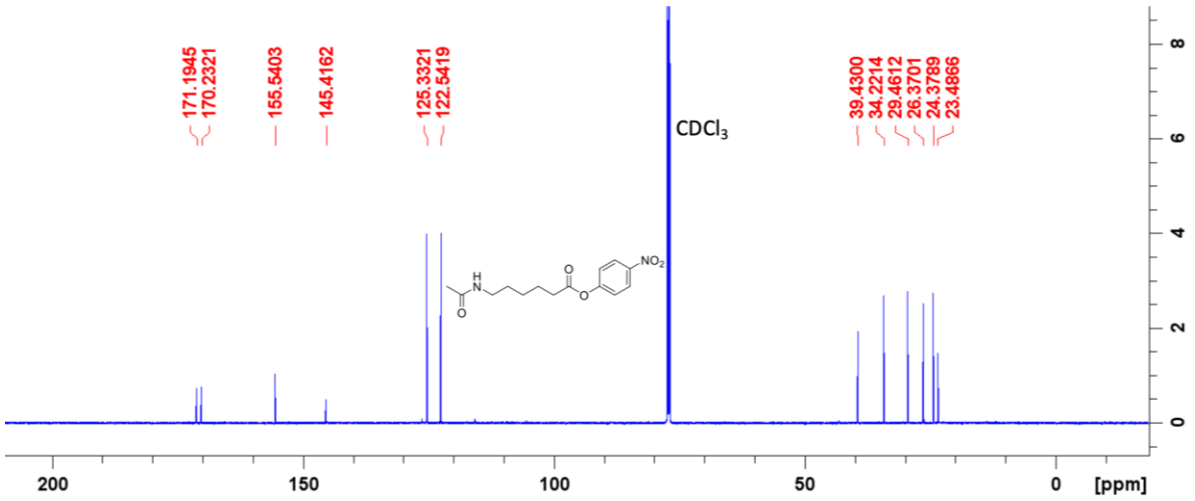

^{13}C NMR spectrum (151 MHz, $CDCl_3$) of 8e.

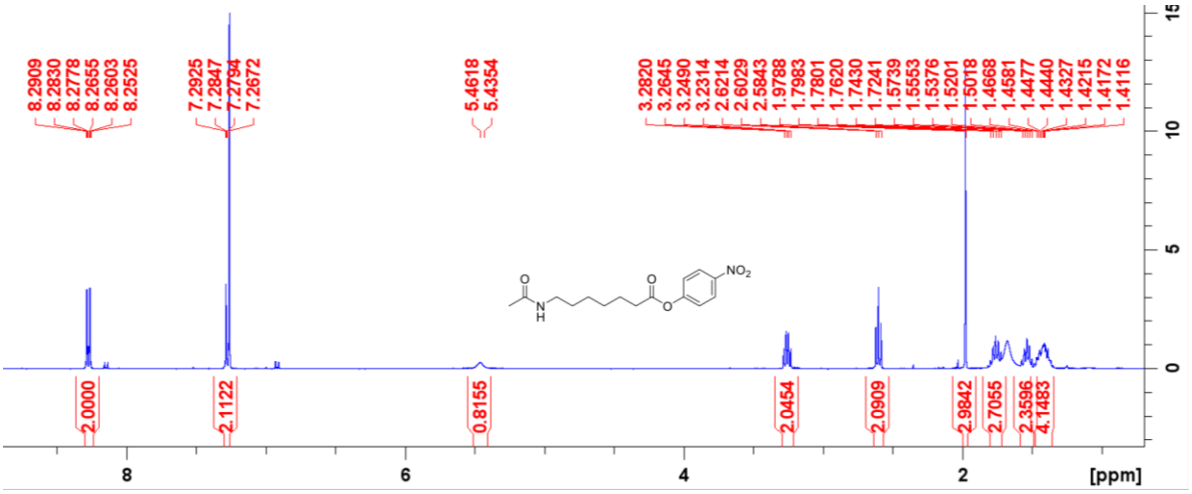

^{1}H NMR spectrum (400 MHz, $CDCl_3$) of 8f.

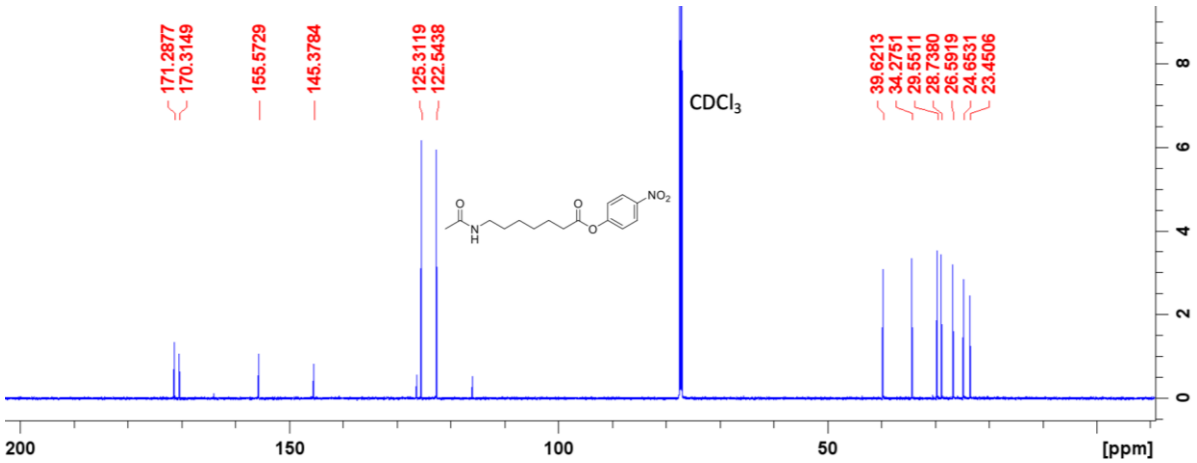

^{13}C NMR spectrum (151 MHz, $CDCl_3$) of 8f.

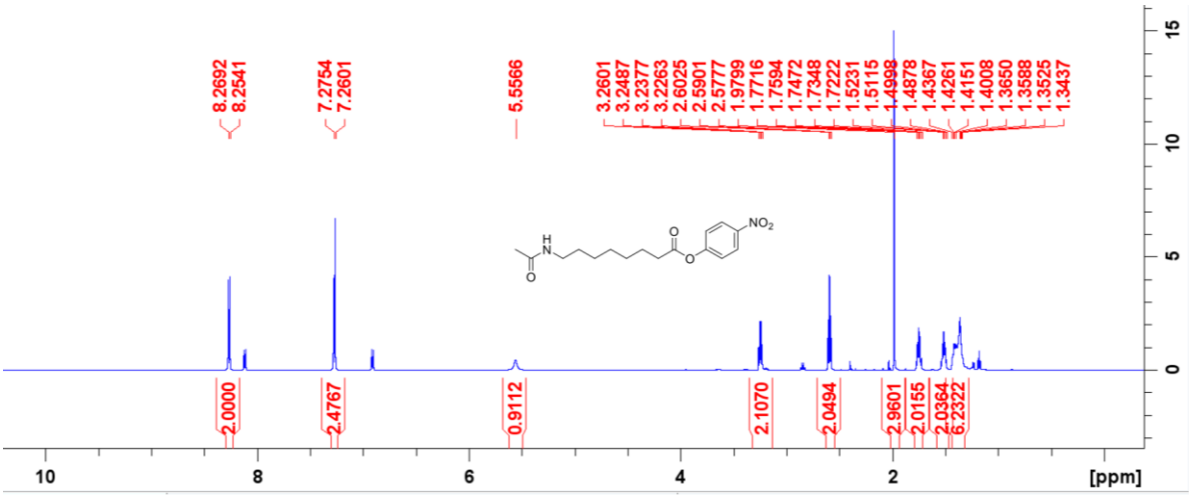

^{1}H NMR spectrum (600 MHz, $CDCl_3$) of 8g.

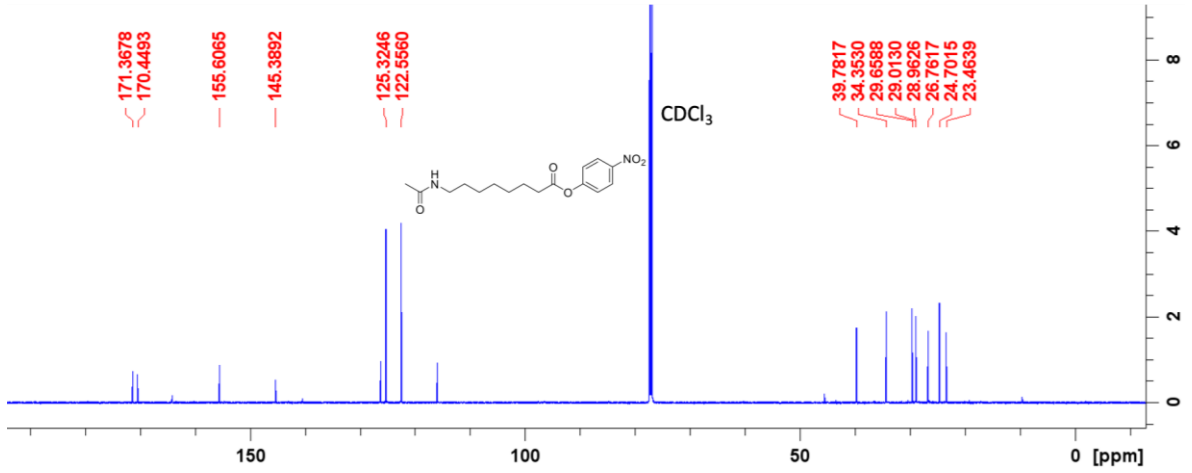

^{13}C NMR spectrum (151 MHz, $CDCl_3$) of 8g.

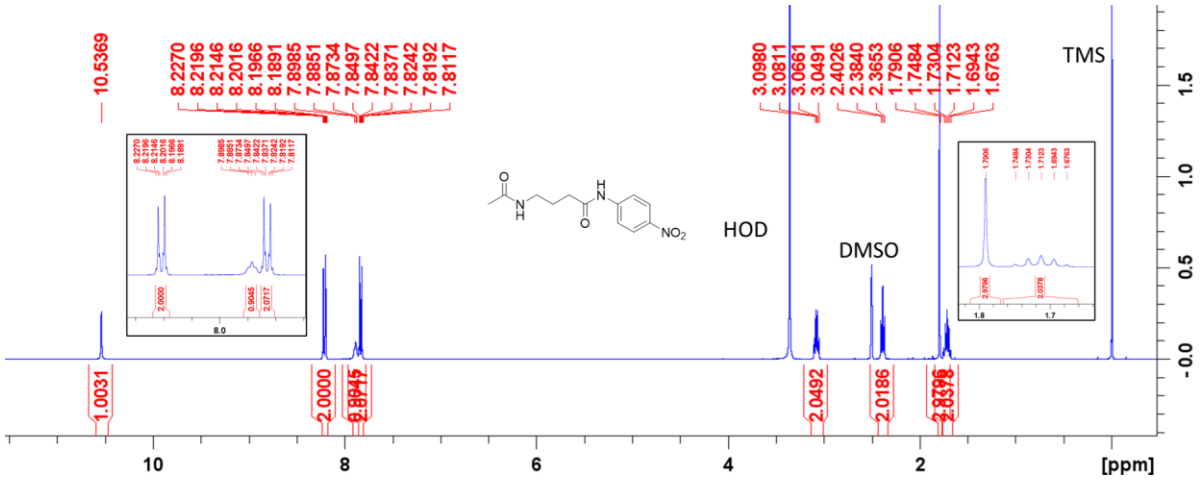

^{1}H NMR spectrum (400 MHz, d_6-DMSO) of 9.

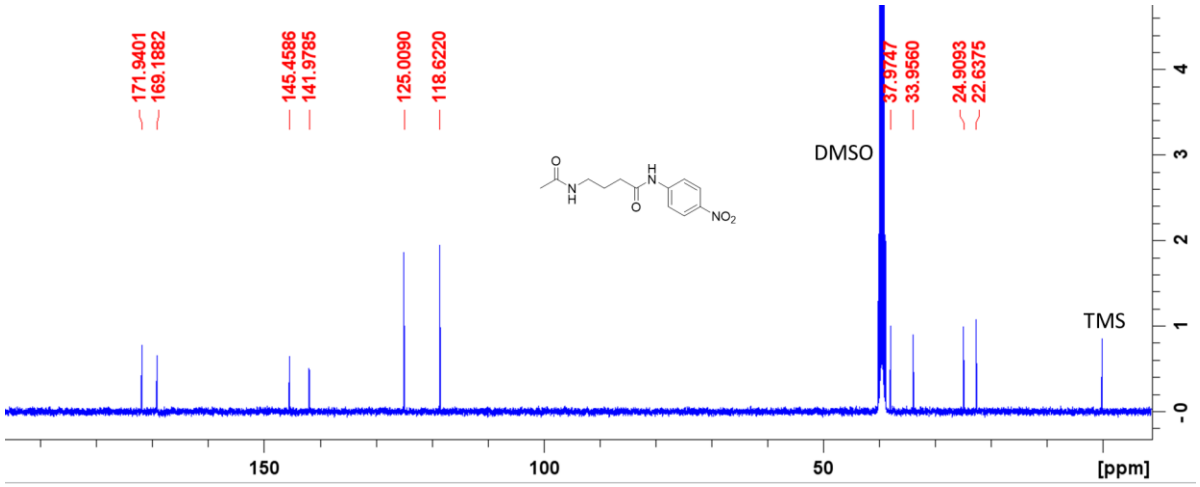

^{13}C NMR spectrum (101 MHz, d_6-DMSO) of 9.

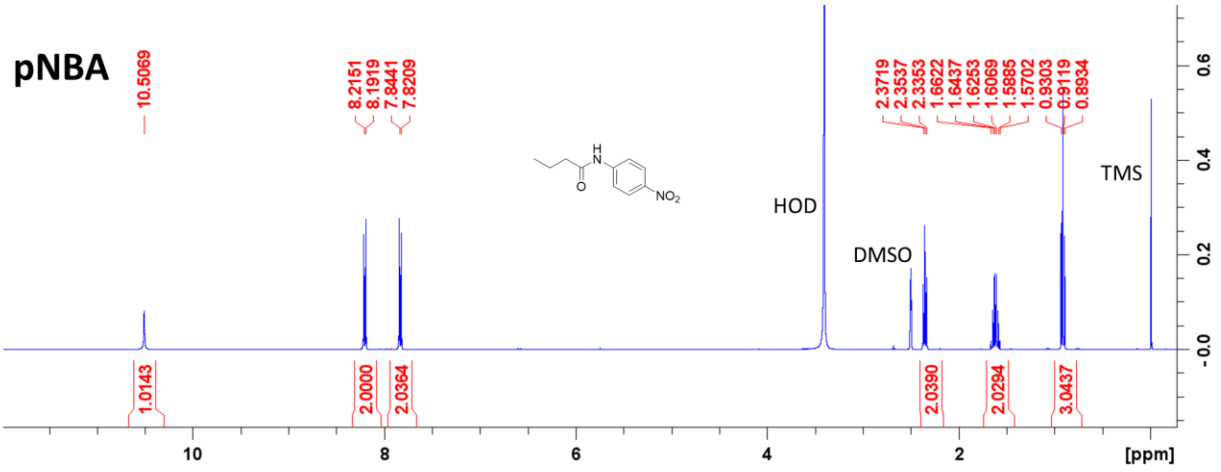

^{1}H NMR spectrum (400 MHz, d_6-DMSO) of 4-nitrobutyric acid (pNBA).

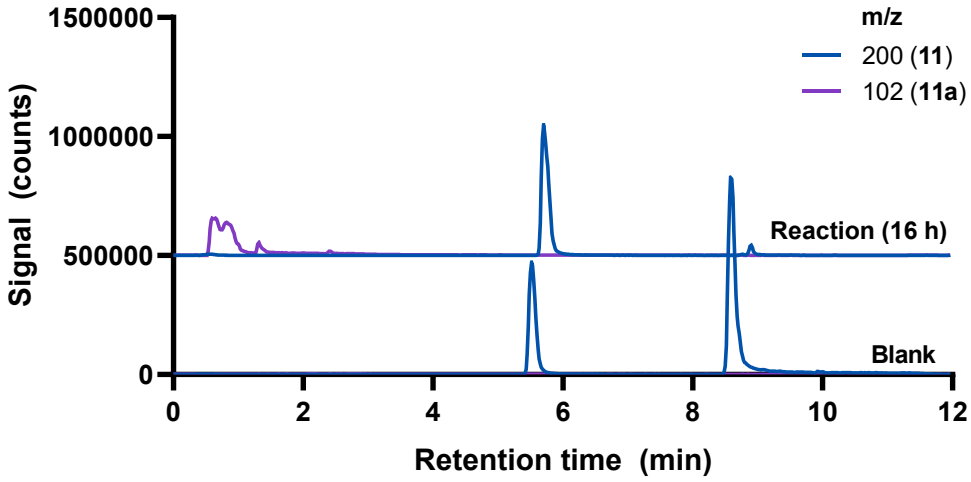

Figure A4.1. LCMS extracted ion chromatograms (EICs) for the reaction of $NylC_A$ with compound **11**. Each trace corresponds to $(M+H)^+$ for the starting material or possible reaction products (see Figure A4.3).

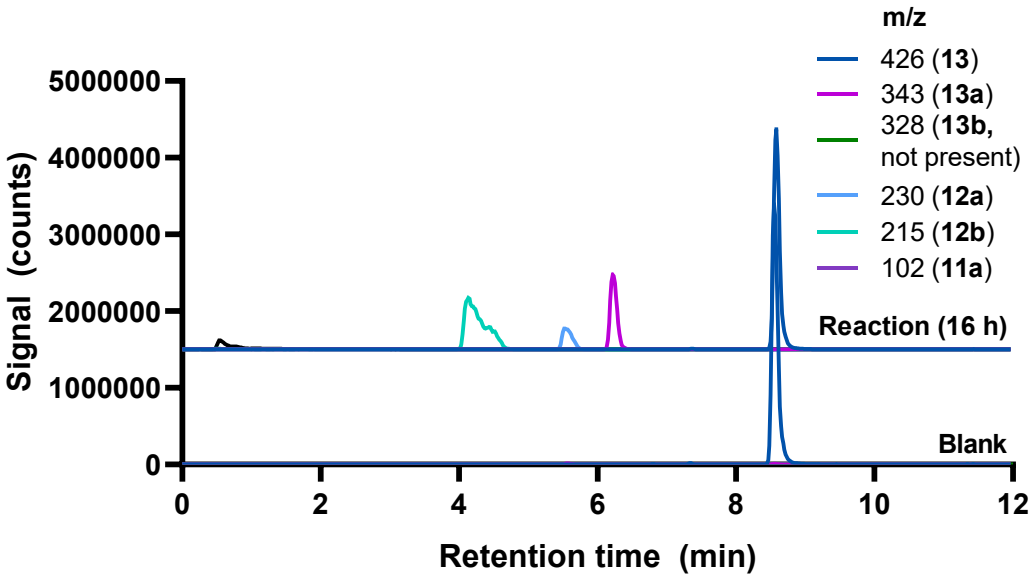

Figure A4.2. LCMS EICs for the reaction of $NylC_A$ with compound **13**. Each trace corresponds to $(M+H)^+$ for the starting material or possible reaction products (see Figure A4.3).

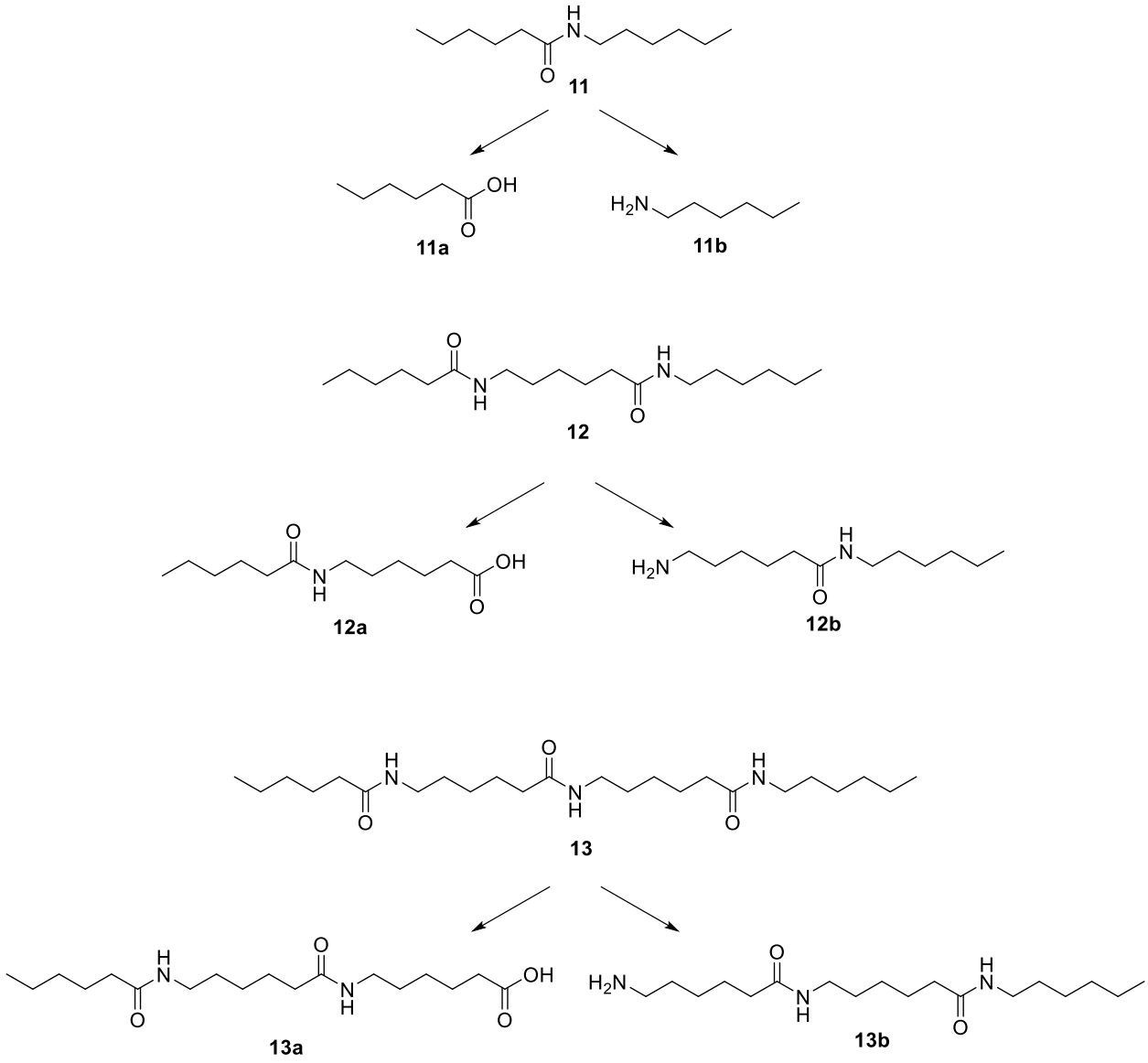

Figure A4.3. Hydrolysis of compounds **11-13** give products **11-13a-b**. Notably, hydrolysis of higher order oligomers also give the products shown above them in the scheme (i.e. compound **13** gives possible hydrolysis products **13a-b**, **12a-b, and 11a-b**.)

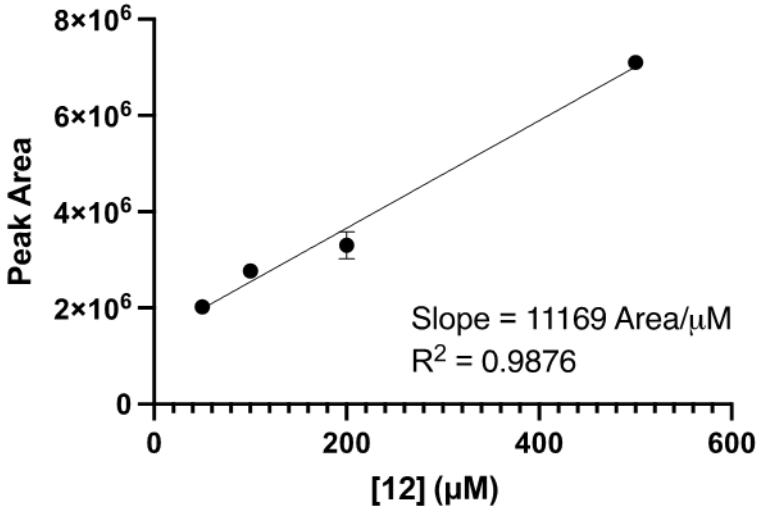

Figure A4.4. Standard curve of compound **12** obtained via LCMS. Concentrations of compound **12** ranging from 50 to 500 μM, were incubated in 20 mM potassium phosphate pH 7.3, 15% glycerol, 0.1 mg/mL of BSA and 5% of methanol at 25 °C. Aliquots were collected and prepared for LCMS analysis according to the sample preparation described in section 4.4.2. Samples were prepared in duplicates and error bars represent the standard deviation between them.

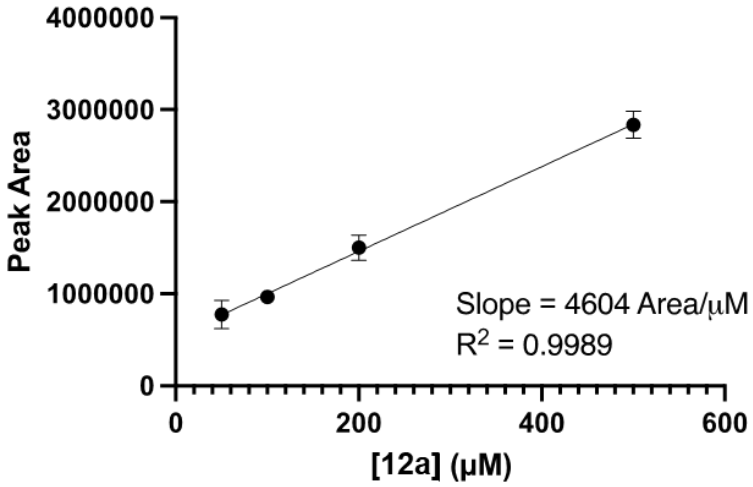

Figure A4.5. Standard curve of compound **12a** obtained via LCMS. Concentrations of compound **12a** ranging from 50 to 500 μM, were incubated in 20 mM potassium phosphate pH 7.3, 15% glycerol, 0.1 mg/mL of BSA and 5% of methanol at 25 °C. Aliquots were collected and prepared for LCMS analysis according to the sample preparation described in section 4.4.2. Samples were prepared in duplicates and error bars represent the standard deviation between them.

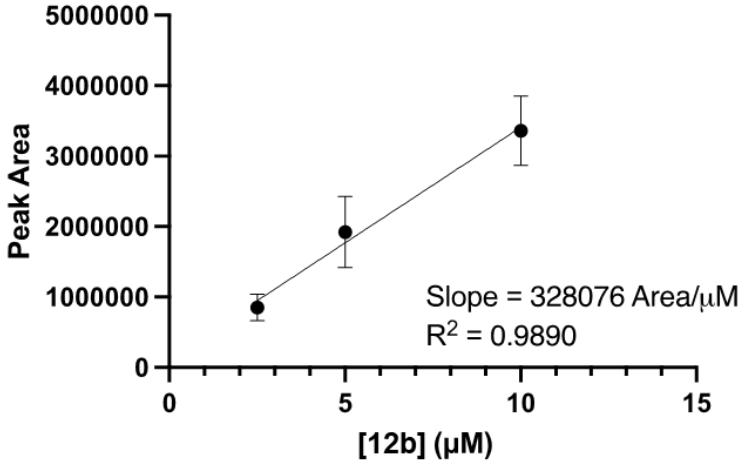

Figure A4.6. Standard curve of compound 12b obtained via LCMS. Concentrations of compound **12b** ranging from 2.5 to 10 μM, were incubated in 20 mM potassium phosphate pH 7.3, 15%

glycerol, 0.1 mg/mL of BSA and 5% of methanol at 25 °C. Aliquots were collected and prepared for LCMS analysis according to the sample preparation described in section 4.4.2 Samples were prepared in duplicates and error bars represent the standard deviation between them.

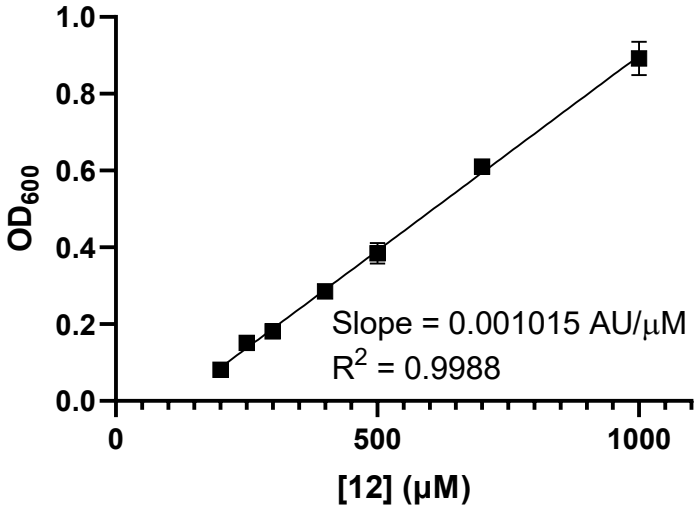

Figure A4.7. Calibration curve for varying concentrations of **12** measured at 600 nm on the Varian Cary 100 Bio spectrophotometer. Standard suspensions contain: substrate (200-1000 μM), potassium phosphate buffer (20 mM, pH 7.3), glycerol (15%), BSA (0.1 mg/mL), MeOH (5%). Data points are averages of two replicates, with error bars showing standard deviations.

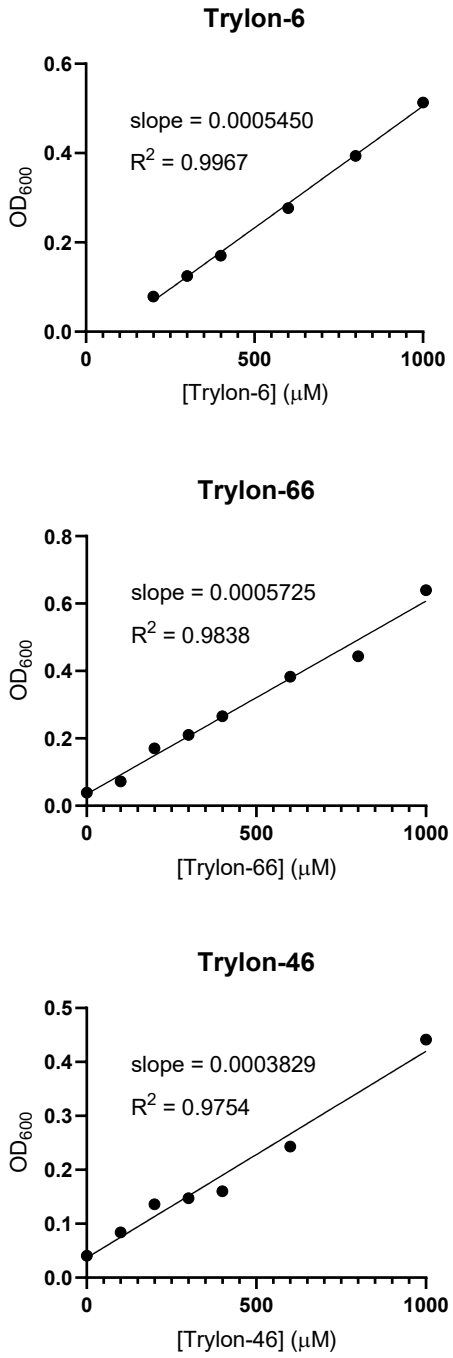

Figure A4.8. Calibration curve for varying concentrations of Trylon-6, Trylon-66 and Trylon-46 measured at 600 nm on a BioTek plate reader, at 25 °C. Standard suspensions contain: substrate (0-1000 μM), potassium phosphate buffer (20 mM, pH 7.3), glycerol (15%), BSA (0.1 mg/mL), MeOH (5%). Data points are averages of three replicates, and error bars show standard deviations, though they are smaller than the datapoints here.

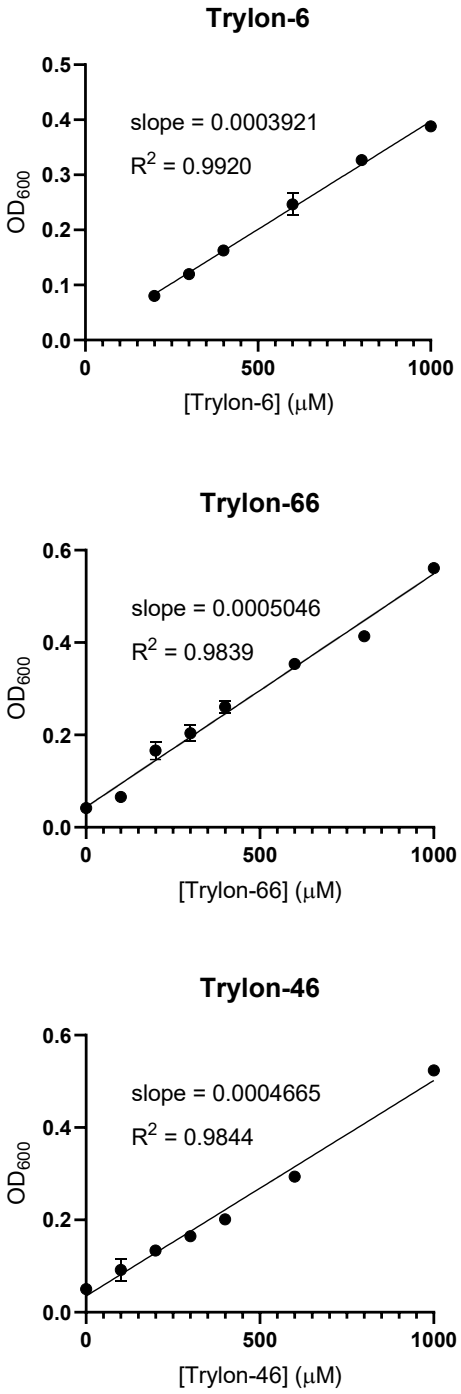

Figure A4.9. Calibration curve for varying concentrations of Trylon-6, Trylon-66 and Trylon-46 measured at 600 nm on a BioTek plate reader, at 50 °C. Standard suspensions contain: substrate (0-1000 μM), potassium phosphate buffer (20 mM, pH 7.3), glycerol (15%), BSA (0.1 mg/mL), MeOH (5%). Data points are averages of three replicates, and error bars show standard deviations.

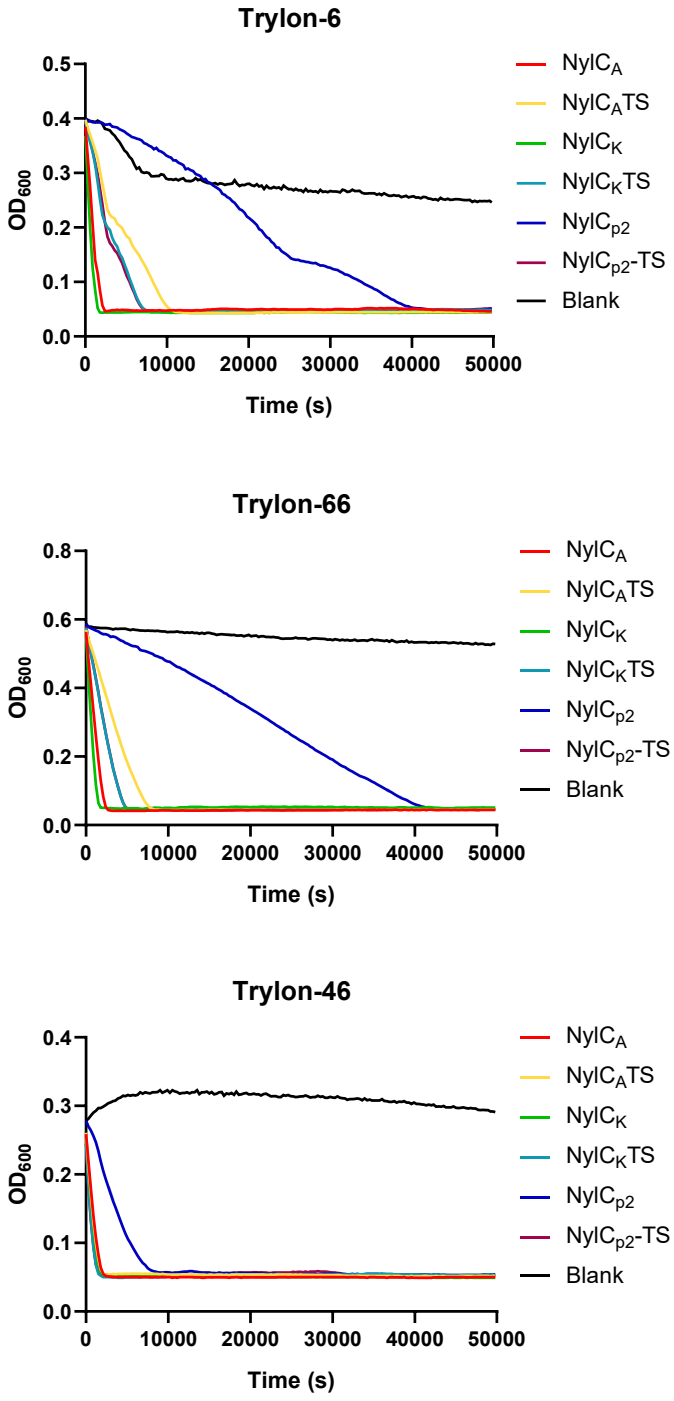

Figure A4.10. Hydrolysis of each substrate surrogate by each NylC enzyme, performed at 25 °C. Reaction conditions: Substrate (1 mM), enzyme (0.1 mg/mL), potassium phosphate buffer (20 mM, pH 7.3), glycerol (15%), BSA (0.1 mg/mL), MeOH (5%). Traces shown are an average of 3 replicates (error bars are not shown for clarity).

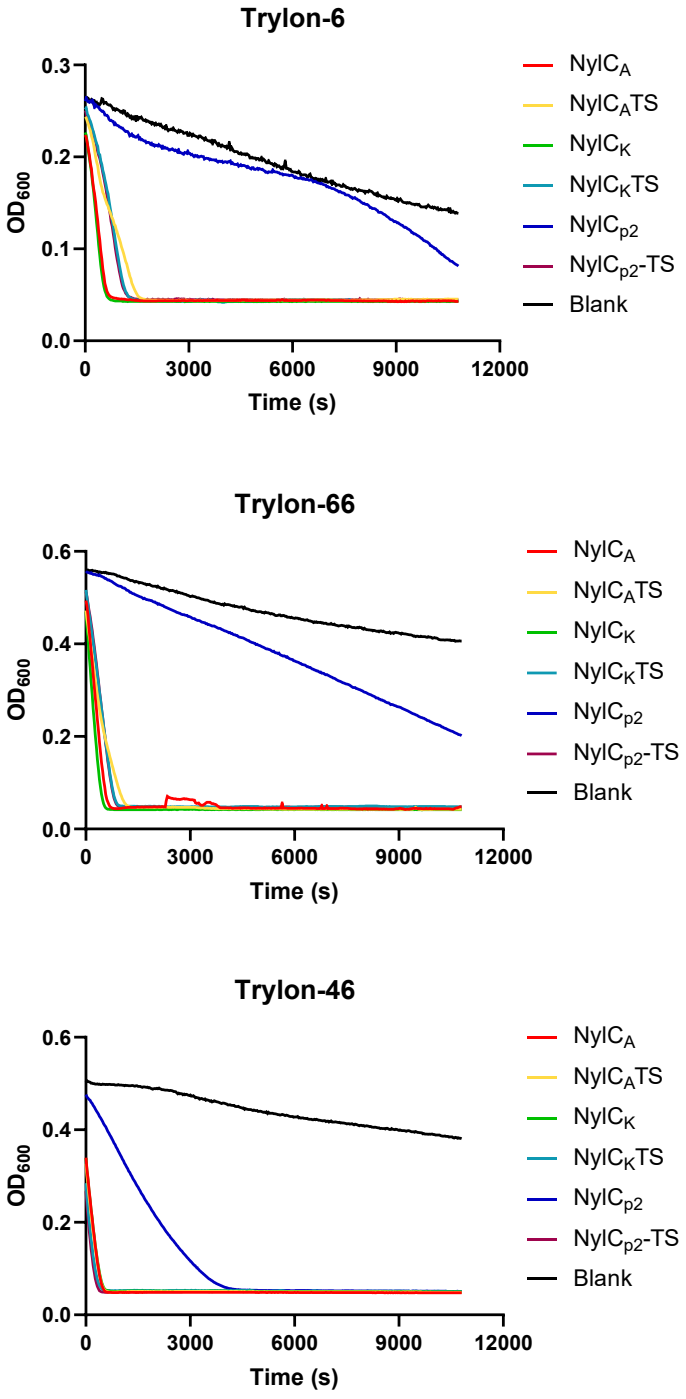

Figure A4.11. Hydrolysis of each substrate surrogate by each NylC enzyme, performed at 50 °C. Reaction conditions: Substrate (1 mM), enzyme (0.1 mg/mL), potassium phosphate buffer (20 mM, pH 7.3), glycerol (15%), BSA (0.1 mg/mL), MeOH (5%). Traces shown are an average of 3 replicates (error bars are not shown for clarity).

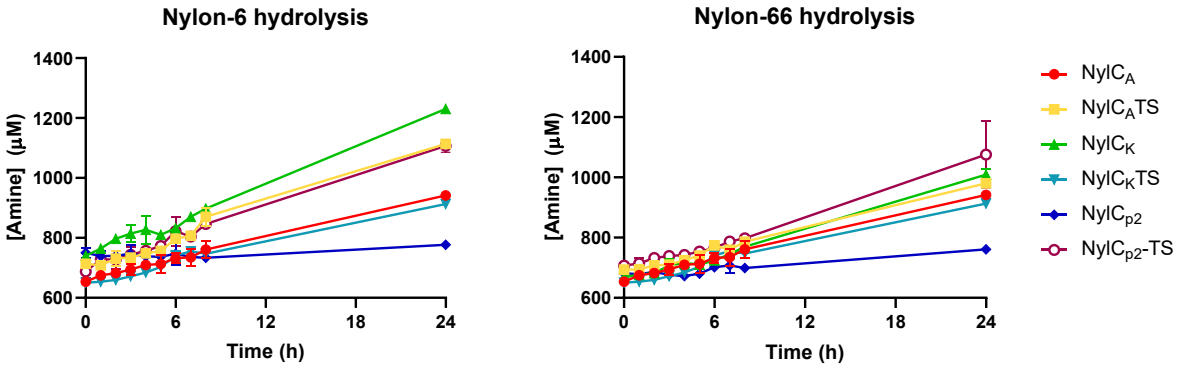

Figure A4.12. Concentration of amines produced over time, as quantified by TNBS, by reaction of each NylC enzyme with either Nylon-6 or Nylon-66 film. Reaction conditions: NylC (0.1 mg/mL), potassium phosphate buffer (20 mM, pH 7.3), nylon film (Nylon-6: 8.2 mg, Nylon-66: 18.1 mg), 50 °C. Values for nylon hydrolysis are averages of two replicates, with error bars showing standard deviations.

Table A4.1. Initial rates of Nylon-6 and Nylon-66 hydrolysis by NylC enzymes. Values are averages of duplicate experiments, with errors shown in parentheses.

Enzyme	Nylon-6 hydrolysis rate (µM/h)	Nylon-66 hydrolysis rate (µM/h)	Relative rate of Nylon-66 hydrolysis (% of Nylon-6 rate)
NylC$_A$	17.9 (2.2)	11.9 (0.6)	66
NylC$_A$TS	16.0 (0.7)	11.0 (0.9)	69
NylC$_K$	20.0 (0.8)	14.4 (1.2)	72
NylC$_K$TS	15.7 (0.9)	11.5 (0.4)	73
NylC$_{p2}$	1.3 (0.6)	3.6 (0.2)	290
NylC$_{p2}$TS	17.1 (2.3)	15.4 (5.1)	91

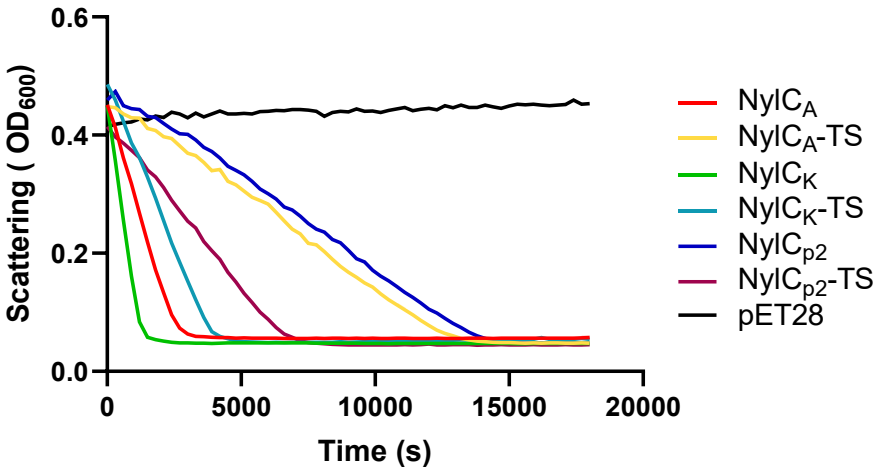

Figure A4.13. Hydrolysis of Trylon-6 by cell lysate at 25 °C. Reaction mixtures contained potassium phosphate buffer (20 mM, pH 7.3), glycerol (15%), BSA (0.1 mg/mL), substrate (1 mM), MeOH (5%) and cell lysate (10% v/v).

NMR spectra of all new synthesized compounds

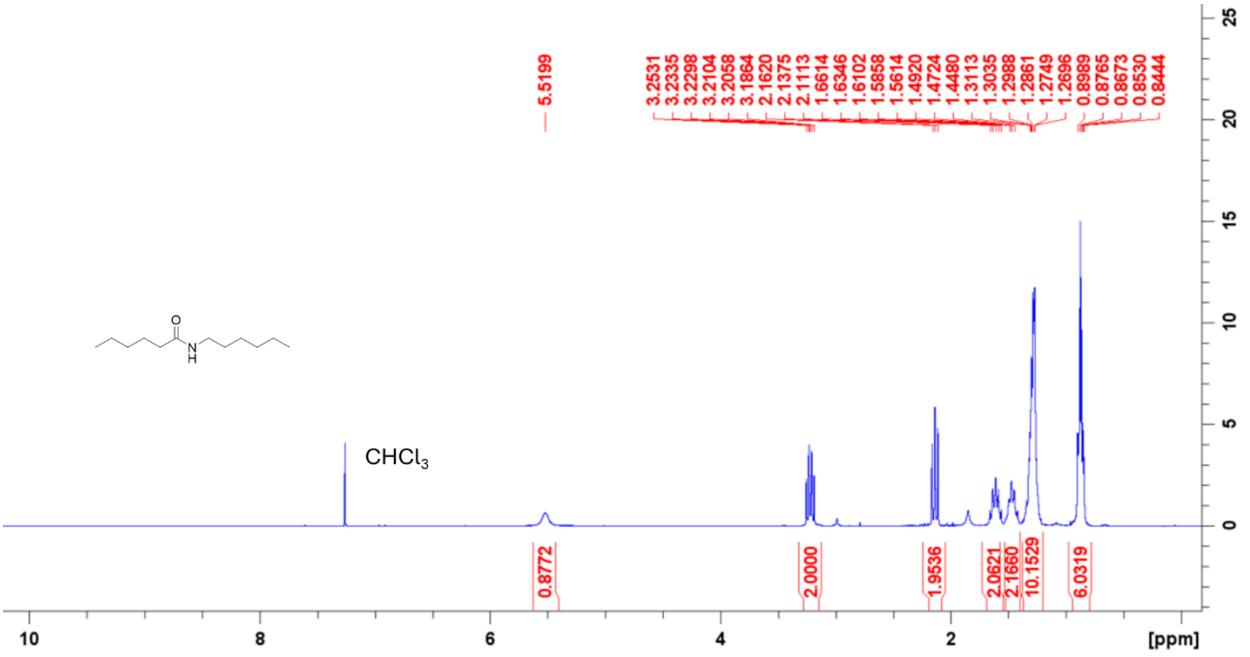

Figure S16. ^{1}H NMR spectrum (400 MHz, $CDCl_3$) of 11.

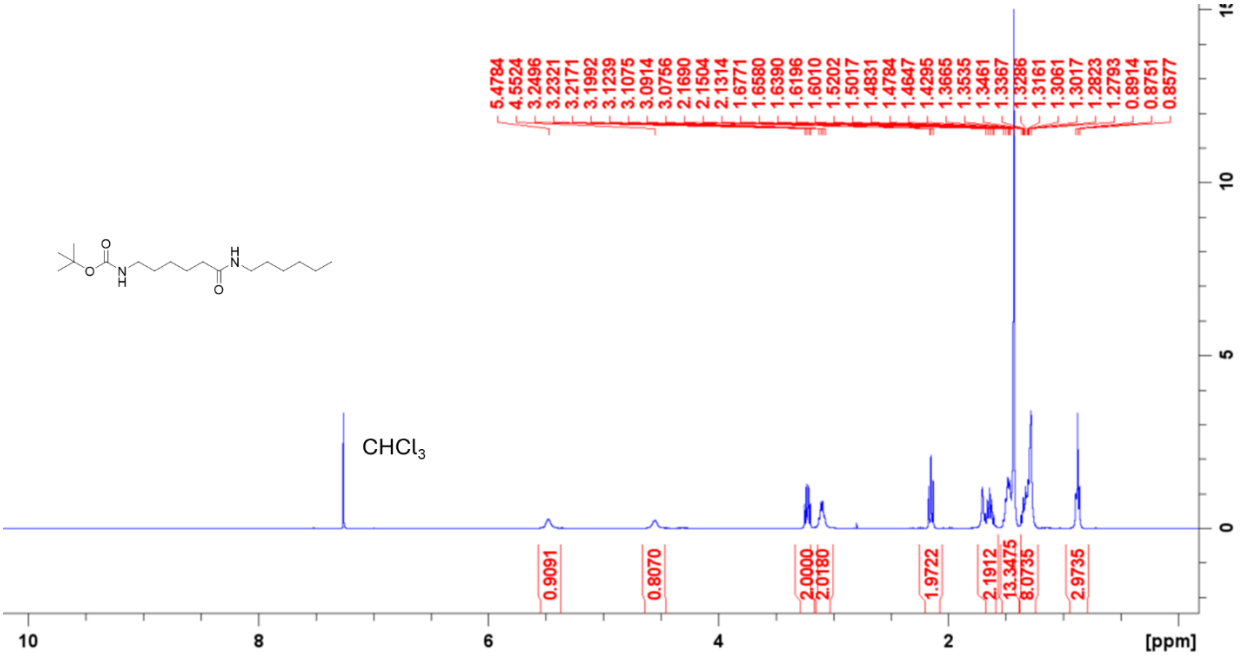

^{1}H NMR spectrum (400 MHz, $CDCl_3$) of 18.

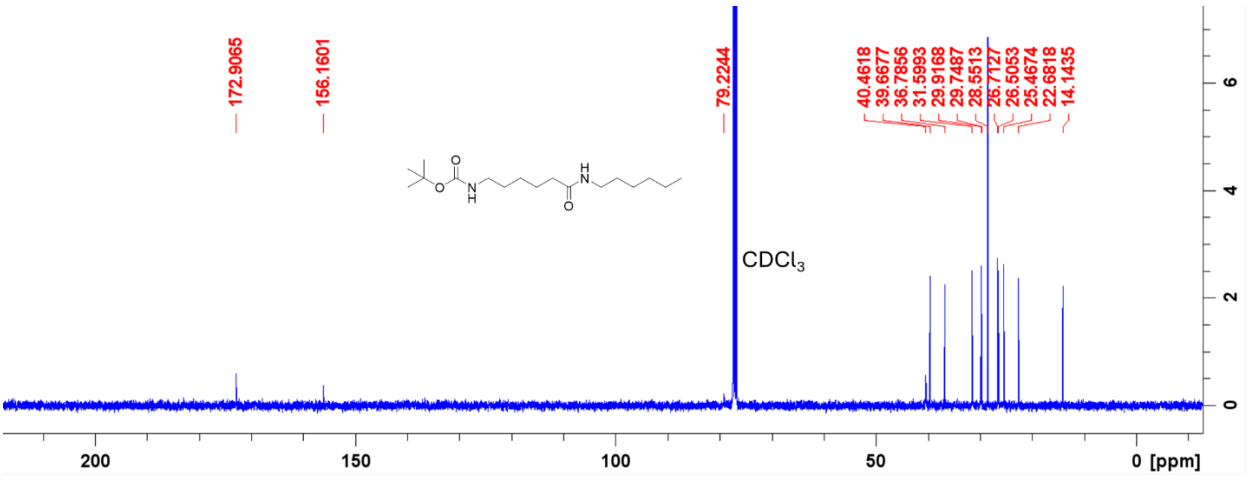

^{13}C NMR spectrum (101 MHz, $CDCl_3$) of 18.

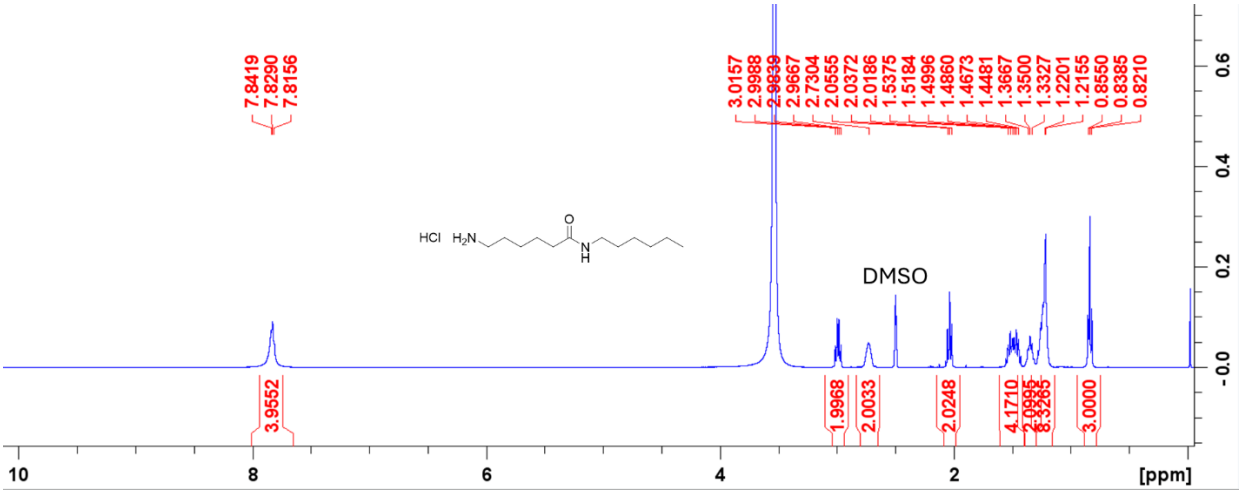

[1]H NMR spectrum (400 MHz, d6-DMSO) of 12b.

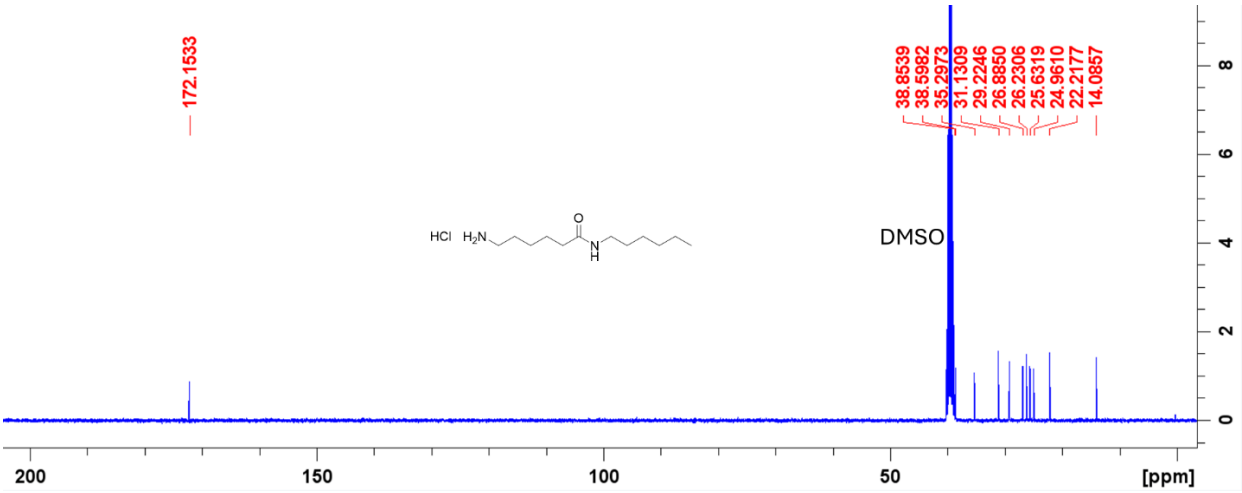

[13]C NMR spectrum (101 MHz, d6-DMSO) of 12b.

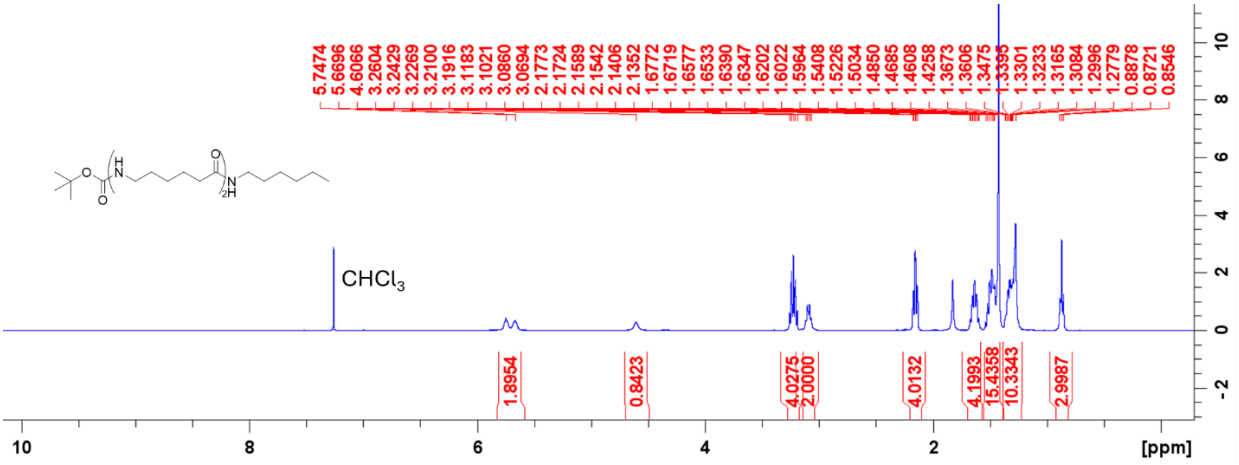

^{1}H NMR spectrum (400 MHz, $CDCl_3$) of 19.

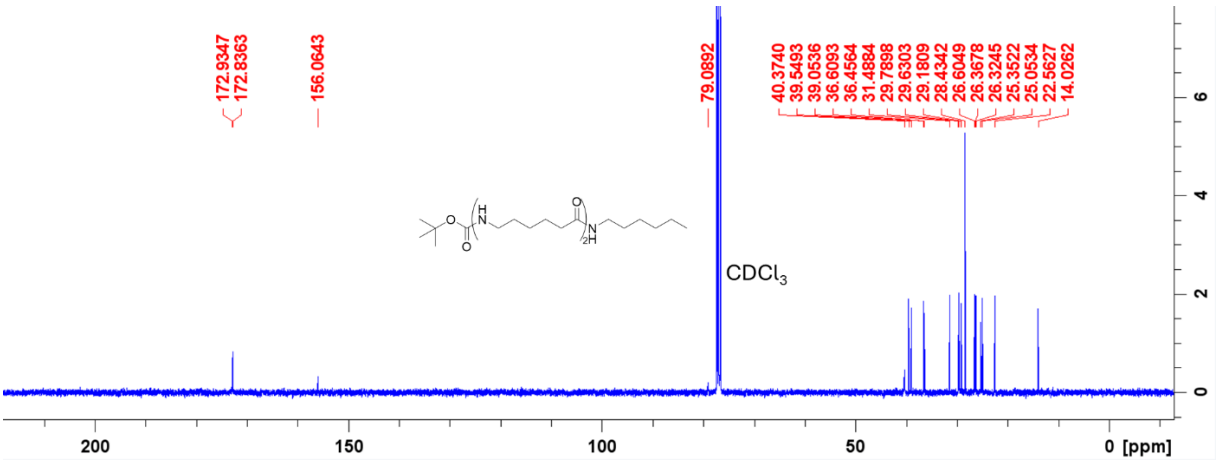

^{13}C NMR spectrum (101 MHz, $CDCl_3$) of 19.

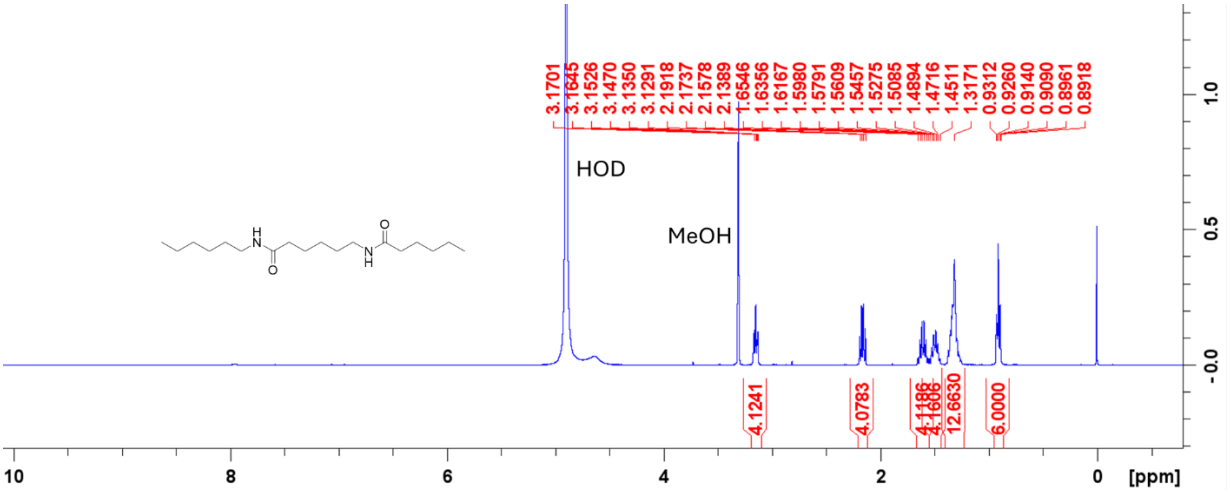

[1]H NMR spectrum (400 MHz, MeOD) of 12.

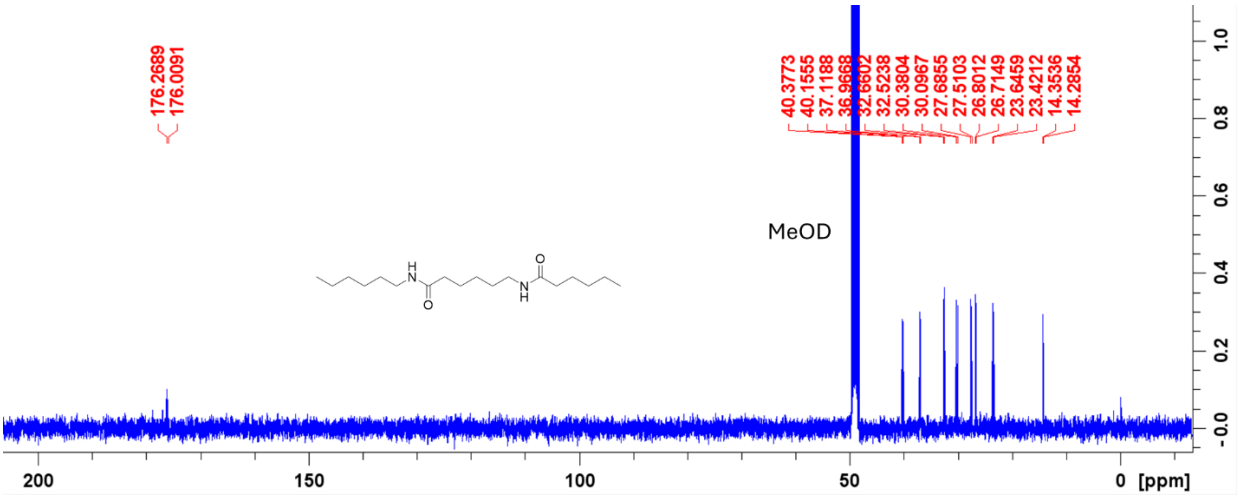

[13]C NMR spectrum (101 MHz, MeOD) of 12.

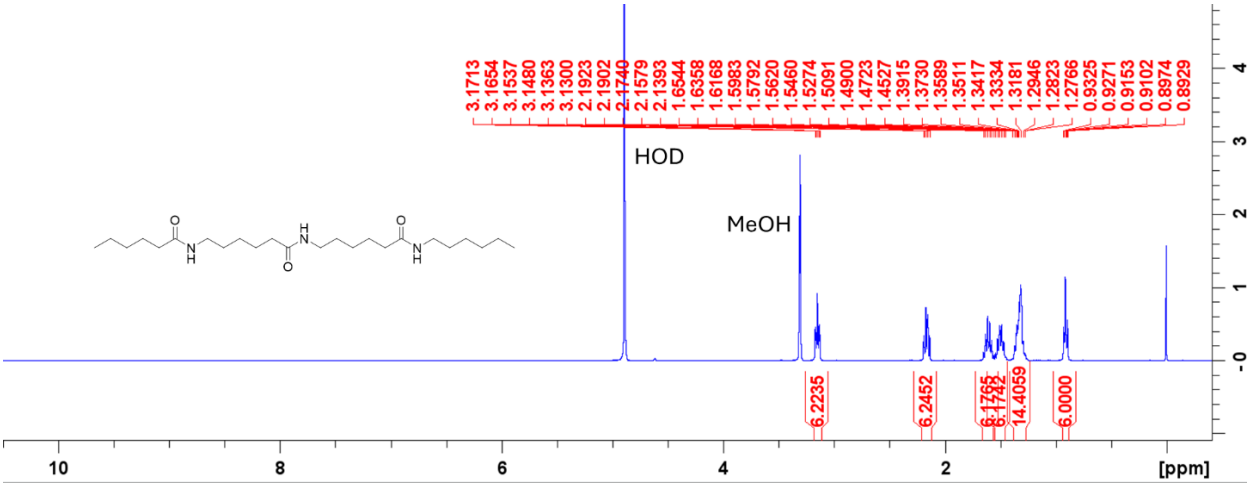

^{1}H NMR spectrum (400 MHz, MeOD) of 13.

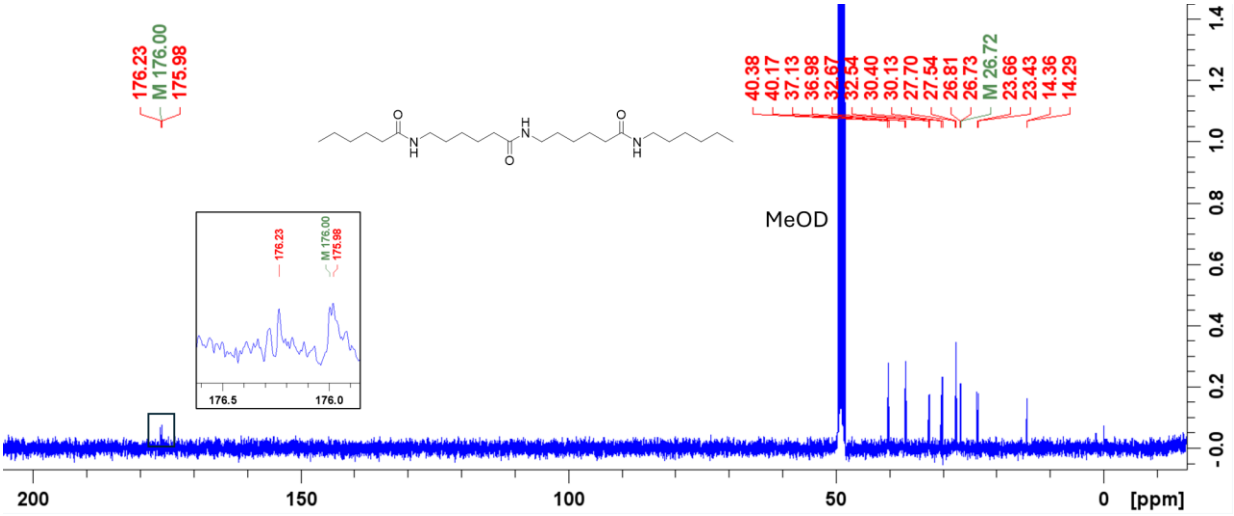

^{13}C NMR spectrum (101 MHz, MeOD) of 13.

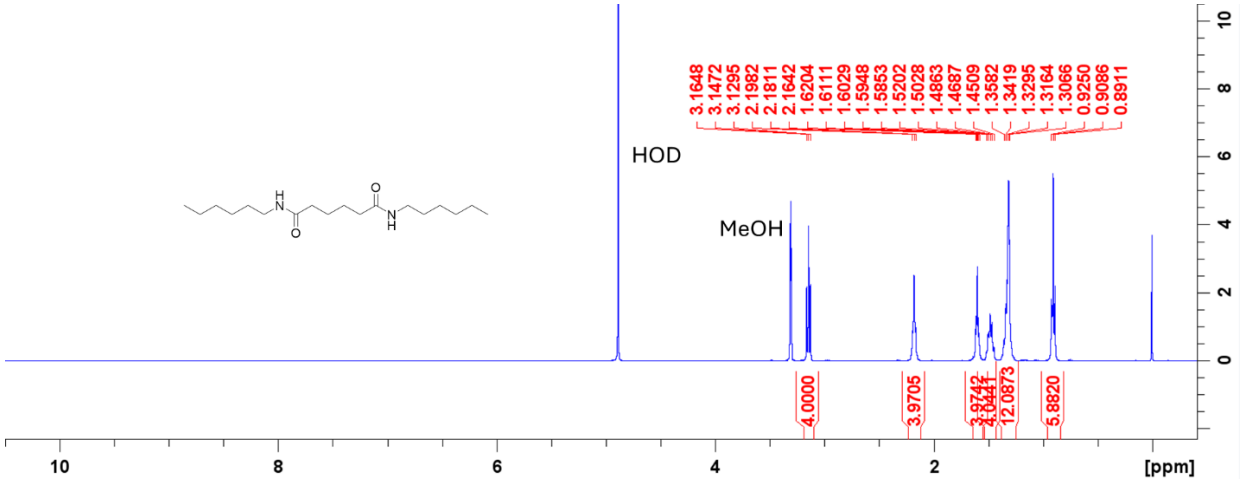

^{1}H NMR spectrum (400 MHz, MeOD) of 14.

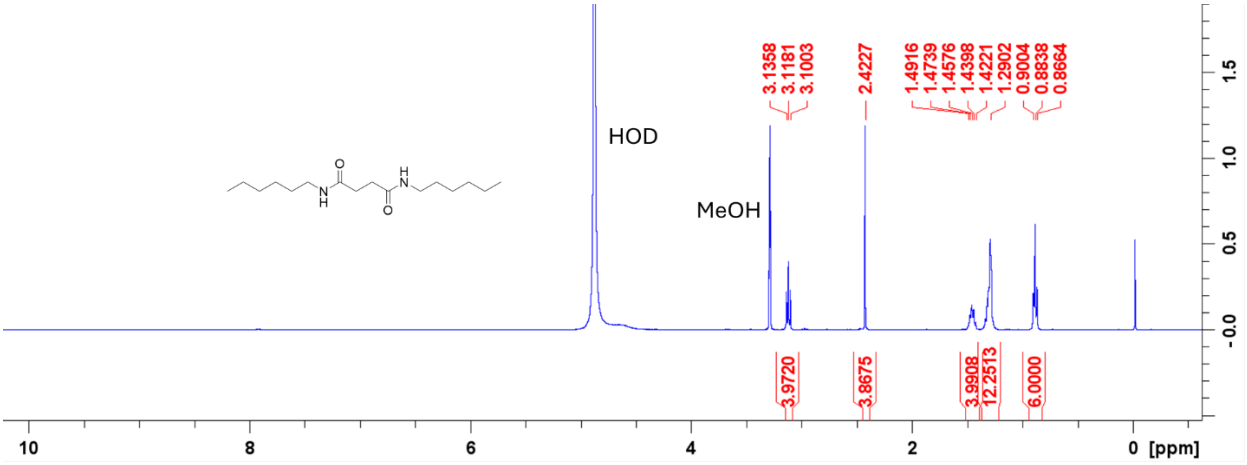

[1]H NMR spectrum (400 MHz, MeOD) of 15.

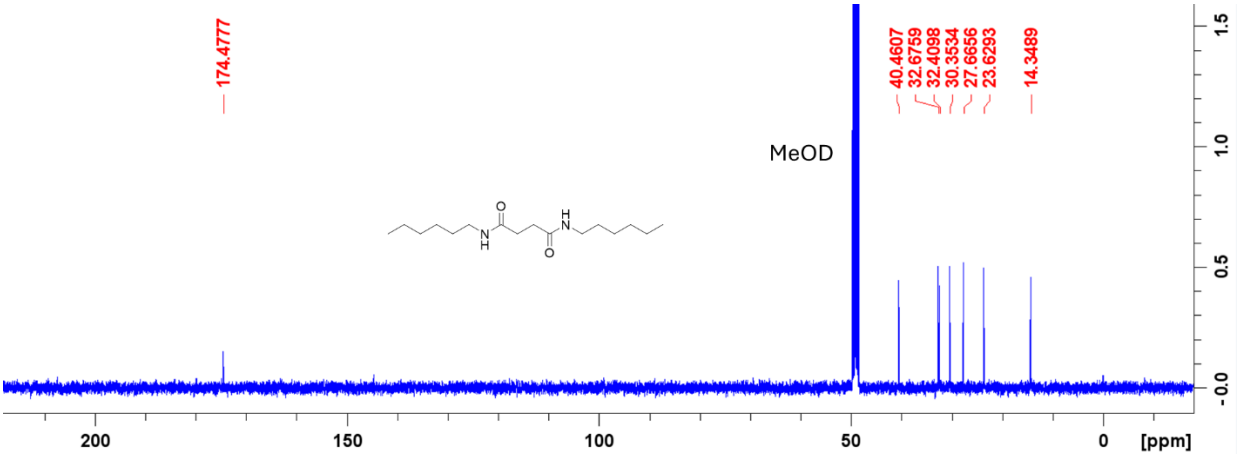

[13]C NMR spectrum (101 MHz, MeOD) of 15.

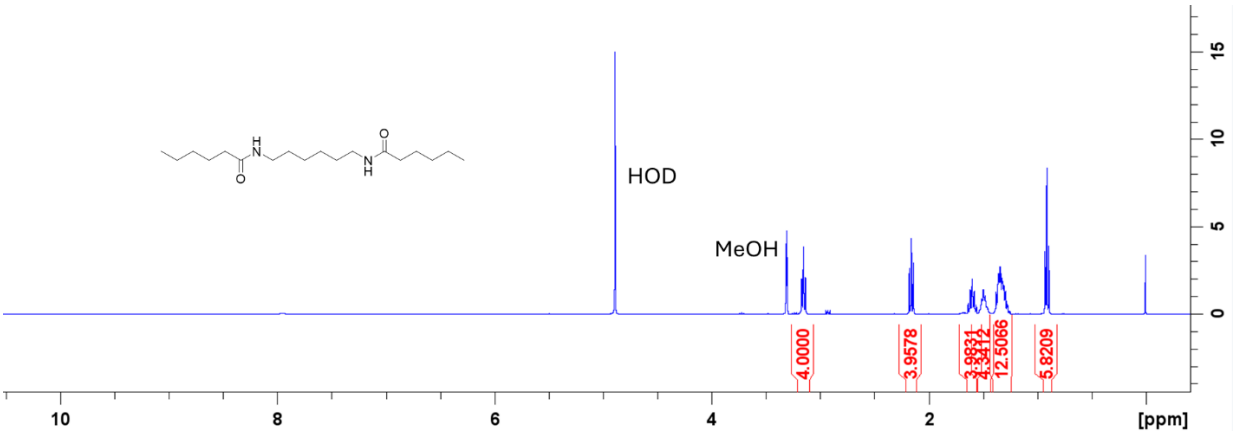

^{1}H NMR spectrum (400 MHz, MeOD) of 16.

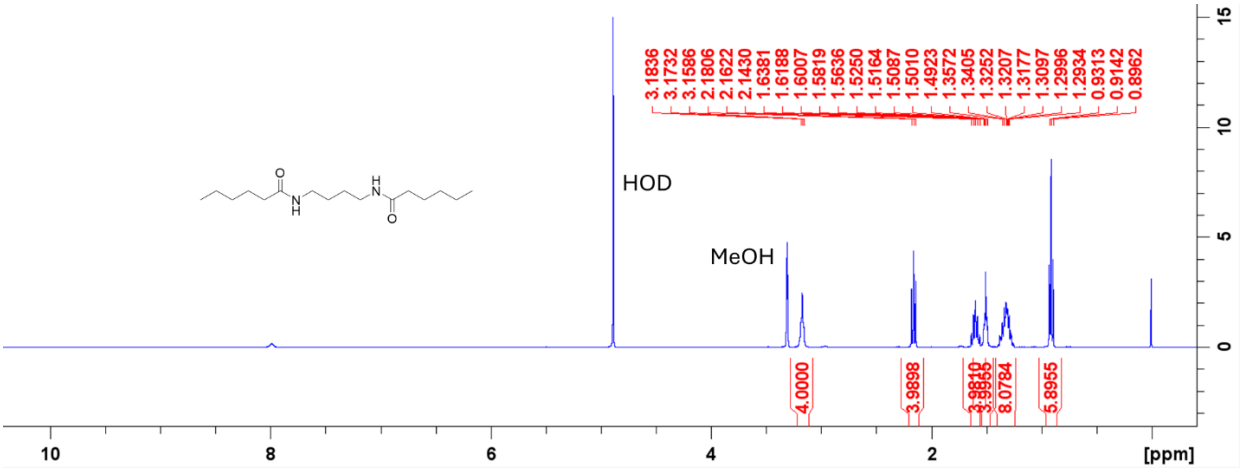

^{1}H NMR spectrum (400 MHz, MeOD) of 17.

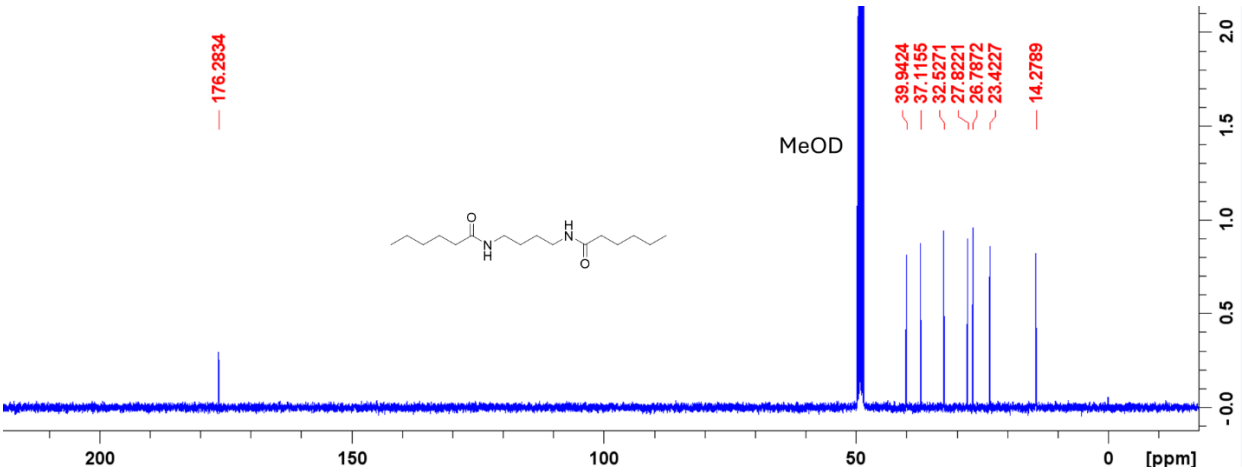

Figure S32. ^{13}C NMR spectrum (101 MHz, MeOD) of 7.

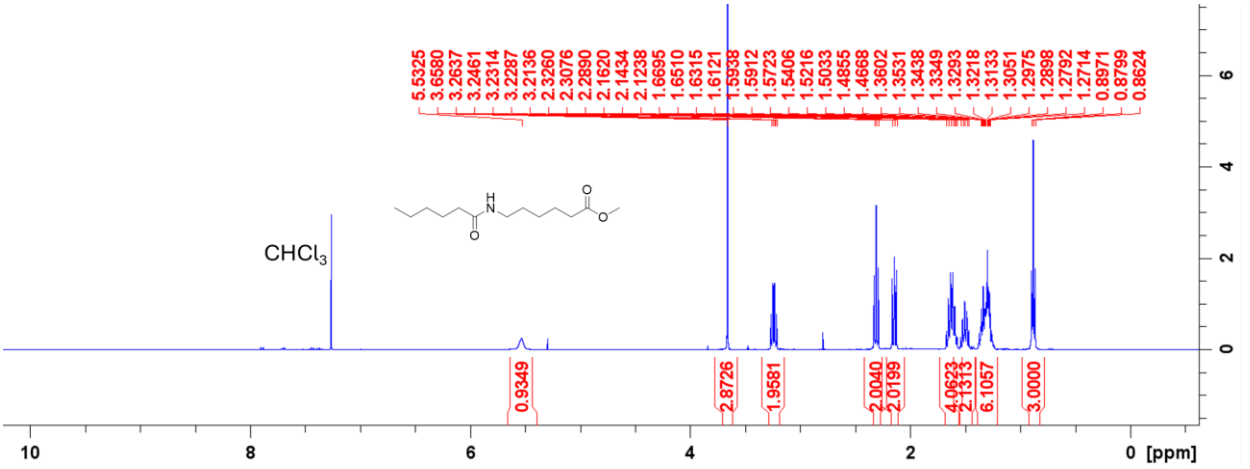

^{1}H NMR spectrum (400 MHz, $CDCl_3$) of 20.

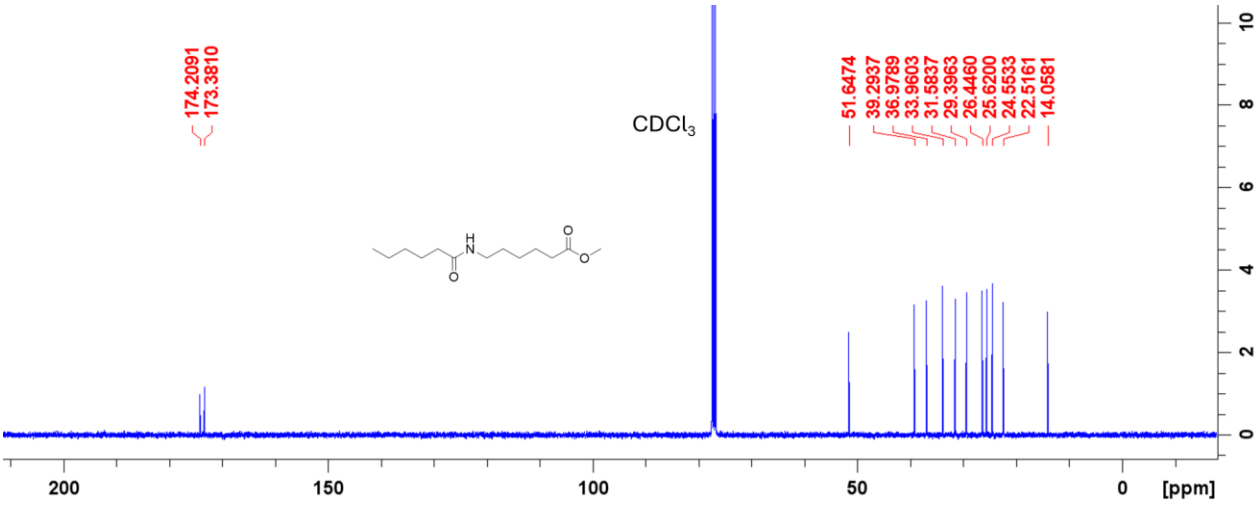

^{13}C NMR spectrum (101 MHz, $CDCl_3$) of 20.

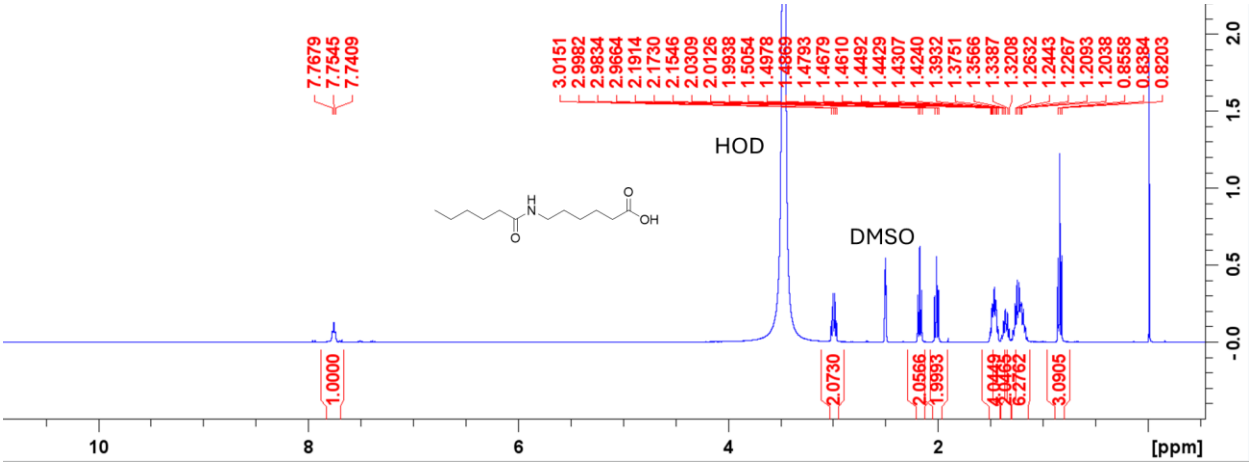

[1]H NMR spectrum (400 MHz, DMSO) of 12a.

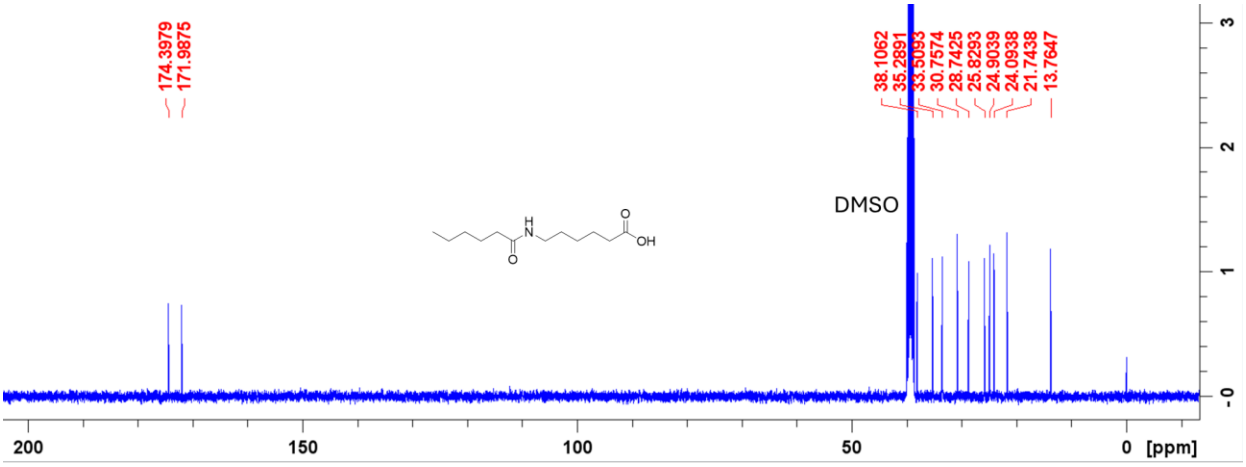

[13]C NMR spectrum (101 MHz, DMSO) of 12a.

Appendix to Chapter 5

Table A5.1. Primers used for site-saturation mutagenesis at positions 146, 192, 189, and 305. The letters F and R indicate the forward and reverse primers at each position.

Primer	Sequence
NylC_Y146X-F	5′ – NNKGACTTCTCTGCCCGTTCAAC – 3′
NylC_Y146X-R	5′ – GATTACTGCGGAAGACACCAGTTG – 3′
NylC_W192X_F	5′ – NNKGATCGTACCGAGATCACAGGT – 3′
NylC_W192X_R	5′ – ATCAACTTTGCCCGCGCTG – 3′
NylC_K189X_F	5′ – NNKGTTGATTGGGACCGTACCGAG – 3′
NylC_K189X_R	5′ – GCCTGCGCTTGCGCTCAT – 3′
NylC_M305X_F	5′ – NNKGACGGCGATACCCTGTTC – 3′
NylC_M305X_R	5′ – ATCGGTGTGAAATGGCTGGATACC – 3′

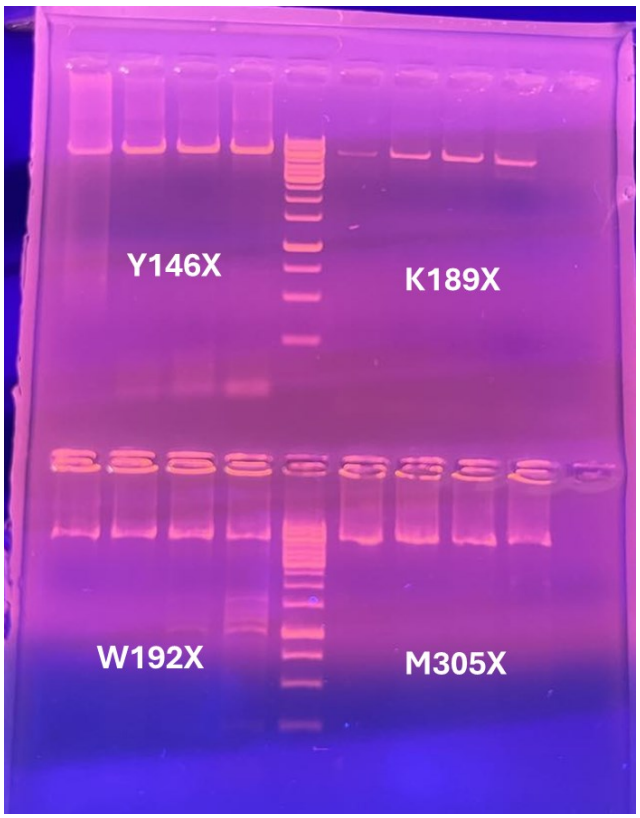

Figure A5.1. Analysis of PCR products for all 4 site-saturation mutagenesis libraries. PCR reactions were performed at 4 annealing temperatures, giving rise to 4 bands for each mutation here.

Figure A5.2a-d. Bitmaps for all screens showing OD_{600} vs time curves at each well. Sequencing results for selected wells are shown as one-letter codes superimposed on the corresponding well.

a) Y146X

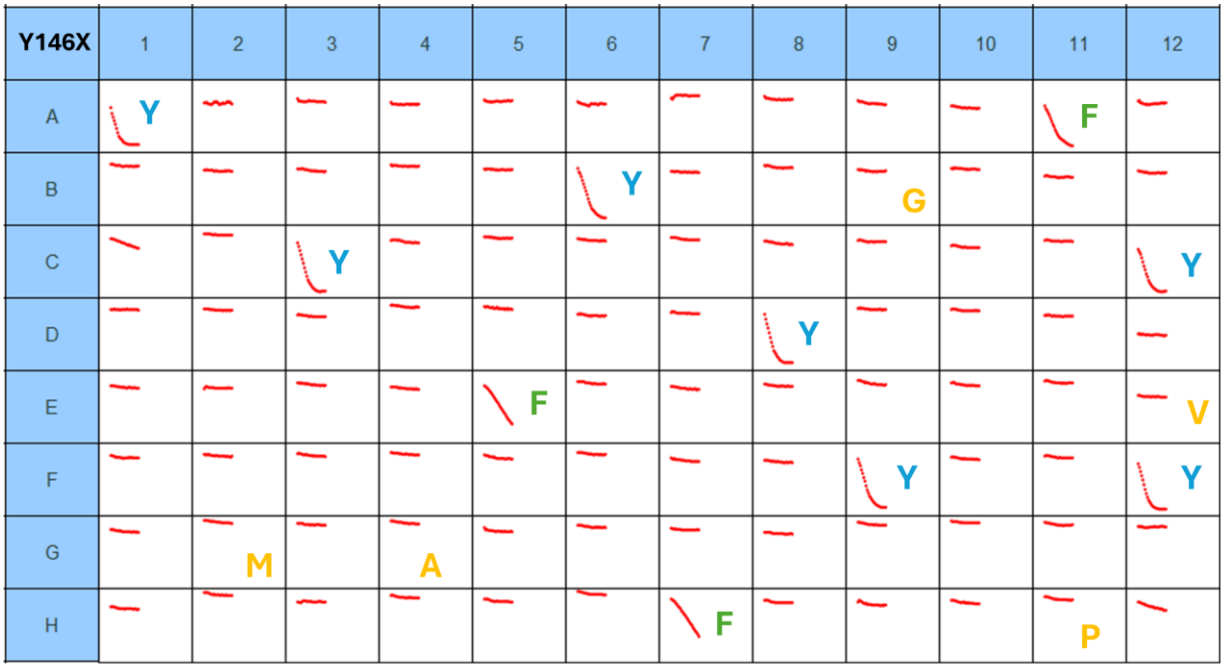

b) W192X. This plate was inoculated upside down: this image was rearranged to match the reference plate.

c) K189X.

K189X	1	2	3	4	5	6	7	8	9	10	11	12
A	K			R				K				
B										Y		
C		K					K					K
D					A							
E									K			
F	K											K
G								K				
H	G			K						K		

d) M305X.

M305X	1	2	3	4	5	6	7	8	9	10	11	12
A	M					L				M		
B			L									
C					T	L						
D	C							H				
E				G							L	L
F									Q			M
G		C				T						
H					V						R	

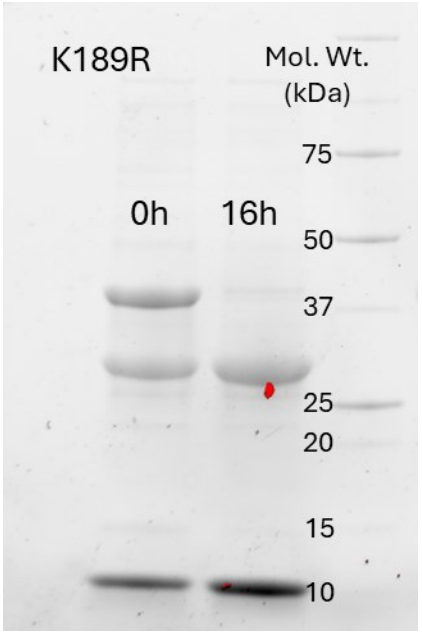

Figure A5.3. SDS-PAGE analysis of NylC$_K$TS^{K189R} before (0 h) and after (16 h) incubation at 37 °C.

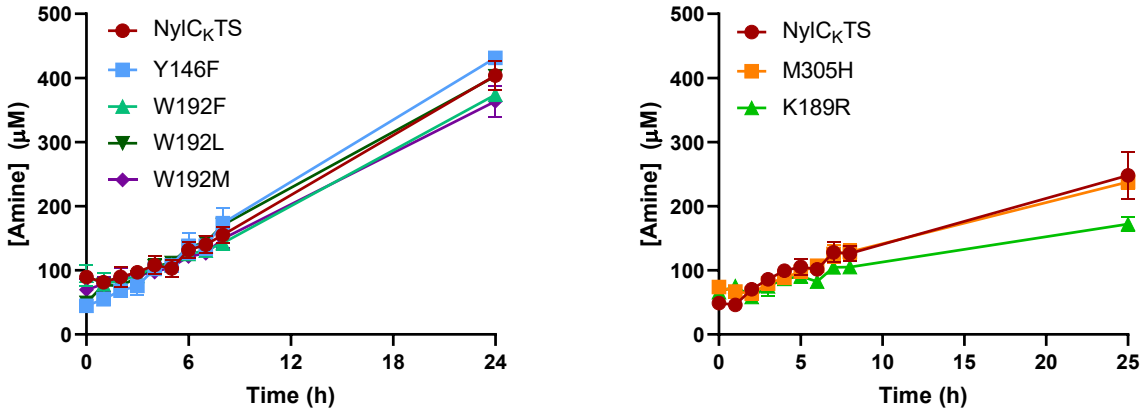

Figure A5.4. Nylon hydrolysis data for NylC$_K$TS mutants. Left: Batch 1; Right: Batch 2. Data are averages of three replicates, with error bars showing standard deviations.

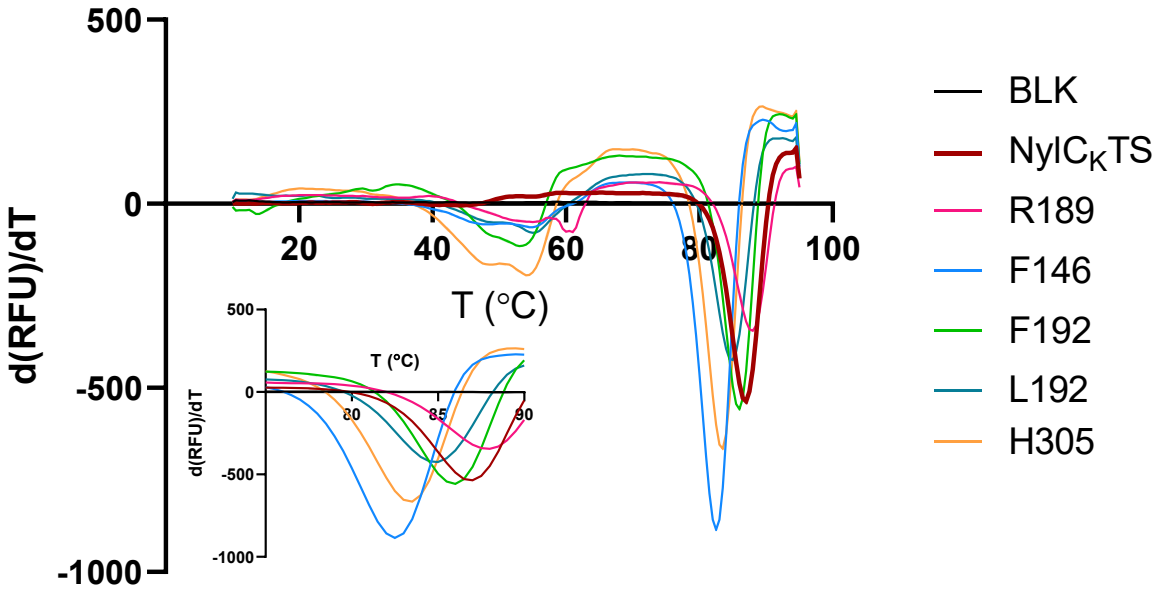

Figure A5.5. Differential scanning fluorimetry data (negative first derivative of fluorescence over time). Inset: 75-90 °C region. Data are averages of 3 replicates. Error bars are omitted for clarity.

Table A5.2. Summary of Nylon-6 hydrolysis rates and melting temperatures of NylC_KTS and mutant enzymes. *These values are corrected based on relative rates of the positive control, NylC_KTS.

Enzyme variant	Nylon-6 hydrolysis (rate of amine production, μM/h) (error)	Adjusted rate – Batch 2 (μM/h) (error)	T_M (°C) (error)
NylC_KTS (wild-type)	14.4 (0.7)	-	87.0 (0.0)
Y146F	16.4 (0.2)	-	82.5 (0.0)
W192F	13.4 (0.5)	-	85.8 (0.3)
W192L	14.8 (0.1)	-	85.0 (0.9)
W192M	13.5 (1.9)	-	Not measured
M305H*	7.7 (0.9)	13.7 (1.7)	83.5 (0.0)
K189R*	4.5 (0.6)	8.1 (1.1)	87.8 (0.8)